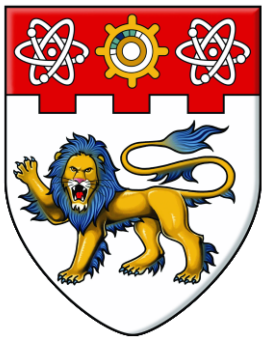

NANYANG TECHNOLOGICAL UNIVERSITY

FABRICATION OF HIGH PERFORMANCE GLUCOSE BIOSENSORS BASED ON NANOSTRUCTURED ELECTRODE MATERIALS

SI PENG

SCHOOL OF CHEMICAL AND BIOMEDICAL ENGINEERING

2014

FABRICATION OF HIGH PERFORMANCE GLUCOSE BIOSENSORS BASED ON NANOSTRUCTURED ELECTRODE MATERIALS

SI PENG

SCHOOL OF CHEMICAL AND BIOMEDICAL ENGINEERING

A thesis submitted to the Nanyang Technological University

in partial fulfilment of the requirement for the degree of

Doctor of Philosophy

2014

Acknowledgement

First of all, I would like to express my sincere appreciation to my Ph.D supervisor, Assistant Professor Kim Dong-Hwan, Richie, for his constant support, warm encouragement, patient guidance and inspiring advices on my research during the 4 years of my Ph.D life. His brilliant ideas fuelled my research interests and enabled me to progress quickly on my Ph.D research projects, and a free research environment offered by him provided me the opportunities to explore my own ideas and allowed me to fully develop my research potential. Prof Kim not only imparted me knowledge and guided my research, but also helped me to improve my skills on manuscript writing, funding proposal writing, manuscript review, communication, presentation, teaching and student guiding, which are important for the future development of my academic career.

Second, my acknowledgements are extended to all the previous and current lab members, for their kind suggestions and generous help on my research and life over the years. I treasure the great time spent together with them and the valuable friendship with them. Special thanks are given to Dr. Guo Longhua, Dr. Huang Youju, Dr. Palanisamy Kannan, Dr. Bai Zhenhua and Ms. Chen Hailan for imparting their rich knowledge, sharing their precious experience and spending their time to discuss with me.

Next, I would like to thank all the collaborators in my Ph.D study period for their great help on my thesis work. Special acknowledgements are given to Prof Lou Xiongwen (David), Prof Chen Peng, Dr. Ding Shujiang, Dr. Dong Xiaochen and Mr. Wang Xuewan.

Finally, I would like to give my deepest gratitude to my parents, for their selfless dedication in raising me, guiding me, supporting me, encouraging me and educating me throughout the twenty-seven years of my life.

Abstract

The thesis work is dedicated to developing novel nanostructured electrode materials with large specific surface areas, good conductivity, excellent biocompatibility and high electrocatalytic activity toward the fabrication of novel generation, high-performance glucose biosensors.

Multi-layered carbon nanotubes and gold nanoparticles hybrid structure were constructed on a gold electrode via a layer-by-layer self-assembly method. A second-generation glucose biosensor was fabricated by immobilizing glucose oxidase (GOx) on the multi-layered nanohybrid-modified electrode. The sensor achieved a high sensitivity of 19.27 μA mM^{-1} cm^{-2}, a wide linear range of 20 μM to 10 mM with a low detection limit of 2.3 μM (S/N=3) for amperometric detection of glucose in the presence of ferrocene mediator.

One-dimensional hierarchically structured TiO_2 (1DHS TiO_2) was synthesized by hydrothermal method with multi-walled carbon nanotube as a sacrificing template. The material exhibited a mesoporous structure with a large specific surface area of 218.4 m^2 g^{-1} and a uniform pore size distribution of 7~9 nm. GOx immobilized on 1DHS TiO_2 achieved direct electrochemistry with a fast electron transfer rate of 7.8 s^{-1}. A third generation-glucose biosensor was fabricated by modifying the biocomposite of GOx/1DHS TiO_2 on a glassy carbon electrode, which showed a high sensitivity of 9.9 μA mM^{-1} cm^{-2}, a linear range up to 1.5 mM and a low detection limit of 1.29 μM for mediatorless measurement of glucose concentrations.

Hierarchically structured MnO_2 spheres were further synthesized by the electrodeposition method for the immobilization of GOx. The synthesized MnO_2 mesoporous spheres also showed mesoporous morphology, exhibiting a surface area of 128.5 m^2 g^{-1} with pore sizes in the range of 5~12 nm. Direct electron transfer (DET) between the electrode and the immobilized GOx was observed, and the electrode modified with GOx/MnO_2 was also successfully demonstrated for glucose sensing in a mediator-free environment. The sensor exhibited a fast response within 3s, an

enhanced sensitivity of 31.6 μA mM^{-1} cm^{-2}, an improved linear range up to 3.15 mM and a low detection limit of 0.35 μM (S/N=3).

Moreover, uniquely structured carbon nanocages (CNCs) were synthesized by MgO template-assisted CVD method. CNCs exhibited a distinguished hollow interior, pronounced graphitic crystallinity and an extremely large surface area of 1651 m^2 g^{-1}, which is favourable for the enzyme immobilization and application as electrode materials. Fast DET was achieved between the immobilized GOx and the electrode, and mediatorless glucose detection was realized by modifying a GCE with the GOx/CNCs biocomposite material. The third-generation glucose sensor based on GOx/CNCs-GCE showed a significantly improved linear range up to 14 mM, with an excellent sensitivity of 19.18 μA mM cm^{-2} and a low detection limit of 0.33 μM.

Finally, a hierarchically structured nanocomposite material of Mn_3O_4/3D graphene was developed by hydrothermal growth followed by electrodeposition. The material showed an extremely high electrocatalytic activity toward the glucose oxidation in a high-pH solution. Due to the flexibility and mechanical strength of the composite, Mn_3O_4/3D graphene was employed as a free-standing and flexible electrode for non-enzymatic biosensing of glucose. The non-enzymatic glucose biosensor showed an ultrahigh sensitivity of 360 μA mM cm^{-2}, a wide linear range of 0.1 ~ 8 mM and a low detection limit of 10 μM. In addition, the non-enzymatic glucose biosensor also showed excellent selectivity for glucose.

The thesis works have deepened the understanding of DET and forwarded the research toward the development of third-generation glucose biosensors. In addition, the nanostructured electrode materials and biosensing platforms developed in present thesis work provided many new opportunities for the research of other electrochemical devices, such as supercapacitors and biofuel cells.

Table of Contents

Chapter 1-Introduction

1.1. Background

Diabetes is a major health problem marked by the inability of the body to properly manage the level of glucose in the blood, resulting from insulin deficiency and hyperglycemia. The disease is one of the leading causes of mortality and disability in the globe.[1] Diabetes is mainly presented as two forms: Type 1 and Type 2. Type 1 diabetics do not produce any insulin, the hormone that regulates the usage of sugar in a human body. Without strict control of blood glucose level, Type 1 diabetic individuals suffer from serious and chronic complications including blindness and tissue damage.[2] Type 1 diabetes affects approximately 10% of the diabetic population. Type 2 diabetes mellitus, constituting 90% of the diabetes cases results from insulin resistance and relative deficiency of insulin secretion. Type 2 diabetics may suffer from complications such as heart disease, stroke and kidney failure.[3] With careful management and stringent control of the blood glucose level, the complications arising from Type 1 and Type 2 diabetes could be greatly reduced, delayed or even prevented. [1, 4]

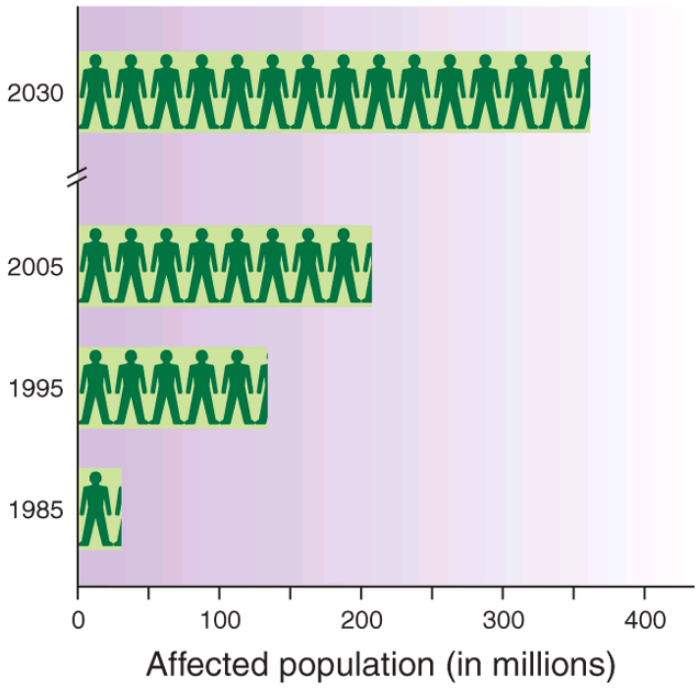

Figure 1-1. The diabetic population in the world (data collected from WHO).

World Health Organization (WHO) reports that 347 million people worldwide have diabetes in 2008,[5] and estimates that diabetes deaths will double between 2005 and 2030.[6] (Figure 1-1) In 2004, glucose biosensors occupied 85% of the entire biosensor market, which accounts for approximate US $5 million.[4] After accelerated growth during the last decade, the global market for glucose sensors and strips has expanded to US $11.5 million in 2012, according to the recent report by Global Industry Analysts, Inc.[7] The figure is expected to increase continually in the next few years.

1.2. Motivations

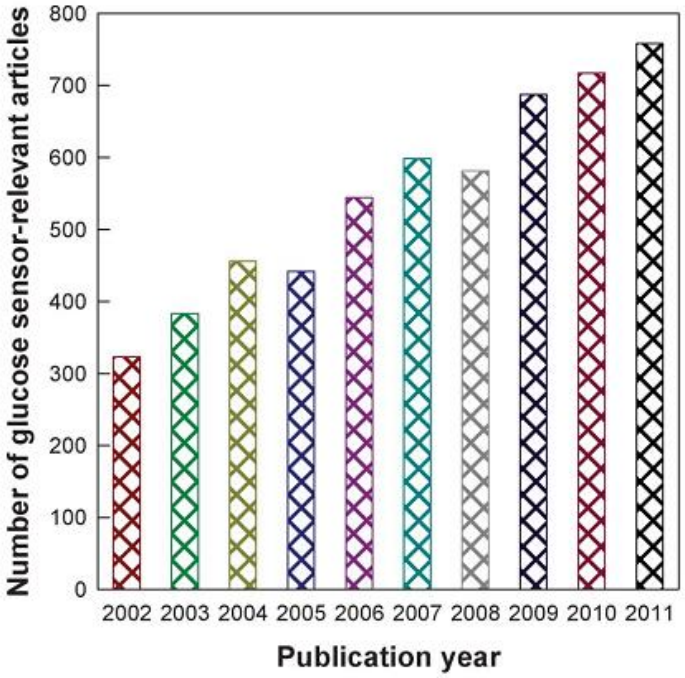

Figure 1-2. The number of articles related to glucose sensors published in the last decade (Reprinted with permission from reference 9).

Although the research of electrochemical glucose biosensors began 60 years ago when Clark and Lyons pioneered the first enzyme electrode for glucose monitoring[8], there is no sign of illness until today in this field. The number of publications pertaining to glucose biosensors has been gaining momentum in the last decade (Figure 1-2), according to Science Citation Index.[9] The significant activity in the field of glucose biosensors reflects the clinical importance of the topic. Enormous demand

for tight management of diabetes has led to continuous innovation of the biosensing technology for glucose monitoring. Accordingly, major fundamental advances and technological breakthrough have been witnessed during the past six decades to improve the reliability and enhance the accuracy of glucose measuring devices. Combination of elegant new research concepts with numerous technological innovations has opened the door for electrochemical glucose sensors for widespread applications. The innovation and revolution of glucose sensing technology has thus contributed to tremendous economic impact and fascinating research opportunities. The advance of glucose sensing technology has also promoted the development of other *in-vitro* and *in-vivo* biosensing devices for the detection of other biologically important molecules. Likewise, the concepts and materials initially employed for glucometers (i,e. mediators, membranes and catalysts) are now applied to improve the performance of a wide variety of biosensing devices.

Although impressive progress has been made during the past decades, the goal of effective management of diabetes is yet to be fully achieved. There are still many challenges and obstacles to be conquered before fulfilment of the promise toward blood glucose monitoring in a highly stable, reliable and real-time manner. Substantial improvement in tight diabetes management could be expected with continuous monitoring of the moment-to-moment changes of blood glucose level. Providing such tight control of diabetes thus has become the primary focus in the field of glucose biosensors and has fuelled enormous research activity. Obviously, success in this direction requires a detailed understanding of the underlying biochemistry, physiology, surface chemistry, materials chemistry and electrochemistry. However, commercial and regulatory considerations rather than scientific aspects are dominant for the ultimate implementation of the new biomedical devices.

As the field enters its sixth decade of intense research, the emergence and advances of nanotechnology have provided enormous opportunities for the development of new approaches for glucose biosensors. Since nanomaterials can be tailored to have the similar dimension as glucose oxidase (GOx), they are capable of reaching the ‘redox centre’ of the enzyme and improving the electrical contact between GOx and the

electrode supports. This could lead to the achievement of third-generation glucose biosensors and revolutionize the glycemic monitoring technology. In addition, nanotechnology also brings new inspirations for the development of innovative non-enzymatic biosensors. Nanostructured electrocatalysts are promising to solve the problems associated with non-enzymatic glucose biosensors, such as poor selectivity and surface fouling. Due to their large surface areas, nanomaterials based non-enzymatic electrochemical biosensors are also expected to show significantly higher sensitivities than those based on bulk electrode materials.

1.3. Research Objectives

The main objective of this thesis work is to develop novel nanostructured and nanocomposite materials for the fabrication of highly stable, reliable and sensitive electrochemical glucose biosensors toward tight diabetes management. Carbon nanomateirals including carbon nanotubes (CNTs) and graphene are mainly used as support for the development of novel nanocomposite materials due to their large specific surface areas. Metal oxides such as TiO_2 and MnO_2 are tailored to have mesoporous nanostructures in order to effectively immobilize the enzyme and interface the 'redox centre' of enzyme. Another metal oxide (Mn_3O_4) is synthesized as a nanostructured electrocatalyst for non-enzymatic glucose biosensors. Gold nanoparticles are employed not only to immobilize the proteins but also to improve the conductivity of fabricated glucose biosensor.

1.3.1. Assembly of Nanocomposite Electrode Materials for Highly Stable and Sensitive Mediator-based Glucose Sensing

Stability is the major issue of commercialized second-generation glucose biosensor. Gold nanoparticles (AuNPs), due to their small size and excellent biocompatibility, could provide a suitable microenvironment for the immobilization of GOx while retaining their bioactivities.[10, 11] Multi-walled carbon nanotubes (MWCNTs) are used as electrically conductive supports for the self-assembly of AuNPs. The research objective is to fabricate multilayered assembly of MWCNTs and AuNPs on an electrode surface to provide a biocompatible and stable matrix for enzyme

immobilization and improve the sensitivity of mediator-based glucose biosensors.

1.3.2. Development of Mesoporous Nanostructured Materials for Interfacing the Redox Centre of Enzyme toward the Fabrication of Third-Generation Glucose Sensors

It is generally very difficult for GOx to transfer electrons directly from its redox centre to the electrode surface, because the redox centre is surrounded by a thick protein insulating shell. Mesoporous nanomateirals with pore sizes similar to GOx are able to mediate the electron shuttling between the redox centre and electrode supports due to the greatly shortened electron transfer distance.[12, 13] In addition, mesoporous nanomaterials usually have large specific surface areas, which are beneficial for improving the sensitivity of glucose biosensor. The mesopores could also effectively immobilize a large amount of GOx. The research objective is to synthesize mesoporous metal oxides and carbon nanomaterials for GOx immobilization, explore the direct transfer between GOx and electrode, and fabricate third-generation biosensors for glucose sensing.

1.3.3. Synthesis of Nanostructured Electrocatalysts toward the Application of Non-enzymatic Glucose Biosensor

Nanostructured electrocatalysts promise to solve the problems related to bulk electrode materials based non-enzymatic glucose biosensors such as surface fouling and poor selectivity. In addition, the sensitivity of non-enzymatic glucose sensor could also be significantly enhanced as a result of the extremely high catalytic activity of nanostructured electrocatalysts. Three-dimensional graphene (3D graphene) was recently reported to have very large specific surface area and high conductivity while exhibiting excellent mechanical strength and flexibility.[14] The objective of this research is to fabricate a freestanding nonenzymatic glucose biosensor with nanocomposite material of 3D graphene and *in-situ* grown nanostructured Mn_3O_4. 3D graphene serves as an independent and flexible electrode support while Mn_3O_4 serves as the electrocatalysts.

1.4. Organization

In Chapter 1, a brief introduction is given to describe the background of my thesis work, and the motivations behind the objectives of my research. Chapter 2 overviews the literatures related to three generations of enzymatic glucose biosensors and nonenzymatic glucose biosensors, among which nanomaterials based electrochemical sensing is focused. Chapter 3 summarizes the methods used for nanomaterials synthesis, materials characterizations, electrode fabrication and electrochemical measurement. Chapter 4 describes a highly stable and sensitive glucose biosensor constructed by self-assembly of multi-layered MWCNTs, AuNPs and GOx on Au electrode. In Chapter 5, a uniquely structured nanomaterial, hierarchically structured one-dimensional TiO_2 (1DHS TiO_2), is introduced and its performance for enzyme immobilization, mediating direct electron transfer of GOx and glucose sensing, is discussed. Chapter 6 presents the synthesis and application of another hierarchically structured metal oxide, MnO_2 mesoporous sphere, for enzyme immobilization and glucose sensing. A new mesoporous nanomaterial, carbon nanocage, is explored for the fabrication of third-generation glucose biosensor in Chapter 7. In Chapter 8, the non-enzymatic glucose biosensor based on a nanocomposite material of 3D graphene/Mn_3O_4 is studied. Chapter 9 is the last chapter, which summarizes the thesis work and outlooks the future research prospects.

Reference

1. J. Wang, *Chemical Reviews*, 2008, **108**, 814-825.
2. K. G. M. M. Alberti and P. Zimmet, *Diabetic medicine*, 1998, **15**, 539-553.
3. C. M. Ripsin, H. Kang and R. J. Urban, *Am Fam Physician*, 2009, **79**, 29-36.
4. J. D. Newman and A. P. F. Turner, *Biosensors & Bioelectronics*, 2005, **20**, 2435-2453.
5. G. Danaei, M. M. Finucane, Y. Lu, G. M. Singh, M. J. Cowan, C. J. Paciorek, J. K. Lin, F. Farzadfar, Y.-H. Khang, G. A. Stevens, M. Rao, M. K. Ali, L. M. Riley, C. A. Robinson and M. Ezzati, *The Lancet*, **378**, 31-40.
6. S. Wild, G. Roglic, A. Green, R. Sicree and H. King, *Diabetes Care*, 2004, **27**, 1047-1053.
7. E. H. Yoo and S. Y. Lee, *Sensors*, 2010, **10**, 4558-4576.
8. L. C. Clark and C. Lyons, *Annals of the New York Academy of Sciences*, 1962, **102**, 29-&.
9. C. Chen, Q. Xie, D. Yang, H. Xiao, Y. Fu, Y. Tan and S. Yao, *RSC Advances*,

2013, **3**, 4473-4491.
10. M. C. Daniel and D. Astruc, *Chemical Reviews*, 2004, **104**, 293-346.
11. Y. Xiao, F. Patolsky, E. Katz, J. F. Hainfeld and I. Willner, *Science*, 2003, **299**, 1877-1881.
12. A. H. Liu, M. D. Wei, I. Honma and H. S. Zhou, *Analytical Chemistry*, 2005, **77**, 8068-8074.
13. K. J. McKenzie and F. Marken, *Langmuir*, 2003, **19**, 4327-4331.
14. Z. P. Chen, W. C. Ren, L. B. Gao, B. L. Liu, S. F. Pei and H. M. Cheng, *Nature Materials*, 2011, **10**, 424-428.

Chapter 2-Literature Review†

†Partially reprinted from [P. Si, *et al.* **RSC Adv,** 2013, 3 (11), 3487-3502] by permission from The Royal Society of Chemistry. Copyright 2013

2.1. Introduction of Glucose Biosensors

A biosensor is defined as a sensing device consisting of a biological recognition element (i.e, enzymes, proteins, antibodies, nucleic acids, cells, tissues or receptors) that selectively reacts with the target analyte in intimate contact with a suitable transducer, which is able to convert the biological recognition reaction or eventually the biocatalytic process into a measurable electronic signal.[1] The configuration of a biosensor is demonstrated in Figure 2-1. Biosensors offer many favourable analytical characteristics, such as high sensitivity, good selectivity, portability, high speed, low cost and potential for miniaturization, which create exciting opportunities for numerous decentralized analytical applications, and they are quickly becoming useful tools in medicine, food quality control, environmental monitoring and other practical fields.[2-4] In principle, biosensors can be tailored to match individual analytical demands for almost any target molecule or compound that interacts selectively with a biological system.[5]

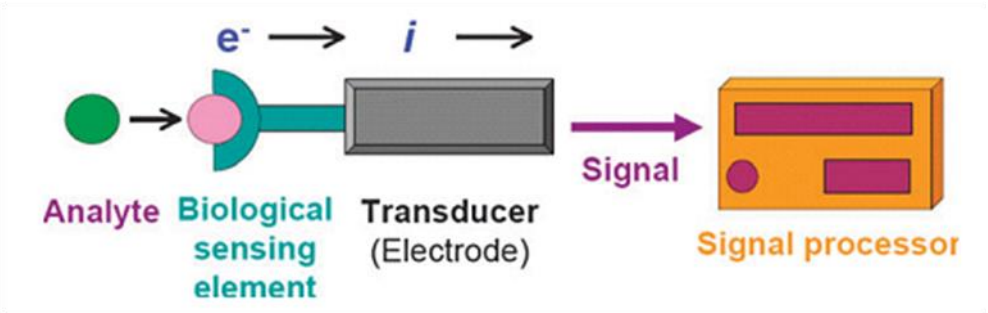

Figure 2- 1. Schematic illustration of the configuration of a biosensor.[6] (Reprinted with permission from Ref. 6. Copyright 2010 The Royal Society of Chemistry).

The sensing elements commonly used for glucose biosensors are enzymes, due to their high specificity and biocatalytic activity for glucose.[7] The most widely used two

families of enzymes are glucose oxidase (GOx) and glucose dehydrogenase (GDH) (Table 2-1), the wide type of which are originally derived from *Aspergillus niger* and *Acinetobacter calcoaceticus*, respectively.[8] GOx could directly catalyze the oxidation of analyte glucose in the presence of oxygen (Eqn 1):

$$\text{glucose} + O_2 \xrightarrow{\text{GOx}} \text{gluconic acid} + H_2O_2 \quad (1)$$

However, GDH requires cofactors and redox mediators for the oxidation of glucose. The cofactors could be nicotinamide adenine dinucleotide (NAD^+), pyrroloquinoline quinone (PQQ) and flavin adenine dinucleotide (FAD). In the presence of excess Ca^+, the PQQ cofactor is able to bind stably to the apoenzyme.[9] The mechanisms of glucose oxidation by glucose dehydrogenase are as follows (Eqn 2, 3):

$$\text{glucose} + NAD^+ \xrightarrow{\text{GDH}} \text{glucotactone} + NADH \quad (2)$$

$$\text{glucose} + PQQ(ox) \xrightarrow{\text{GDH}} \text{glucolactone} + PQQ(red) \quad (3)$$

PQQ-GDH is the most widely used dehydrogenase system for glucose sensing due to its efficient catalytic efficiency and rapid electron transfer rate.[10] However, the use of PQQ-GDH is limited by its stability and poor selectivity, because PQQ-GDH not only catalyzes the oxidation of glucose, but also other sugars.[8, 11]

Table 2-1. The enzyme system used in commercialized glucose biosensors

Manufacturer	Brand	Enzyme system
AgaMatrix	WaveSense KeyNote	GOx
Bionime	Rightest GM300	GOx
Diabestic Supply of Suncoast	Advocate Redi-Code	GOx
Diagnostic Devices	Prodigy Autocode	GOx
LifeScan	OneTouch UltraLink	GOx
Nova Biomedical	NovaMax	GOx
Abbott	FreeStyle Freedom Lite	PQQ-GDH
Roche	Accu-Chek Aviva	PQQ-GDH
Bayer	Ascensia Contour	FAD-GDH

According to the monitoring methods, glucometers can be classified as intermittent sensors or continuous sensors (Figure 2-2). Intermittent sensors include clinical stand-alone instruments and near patient (point-of-care) devices, which probably occupy the largest biosensor market.[12] Continuous sensors are further assorted into 3 types, which are invasive, minimally invasive and non-invasive glucose monitors. [13] The ultimate goal of the implantable continuous glucose sensor is the creation of an 'artificial pancreas', which releases insulin into the blood stream automatically once triggered by the signal of a high blood glucose level.

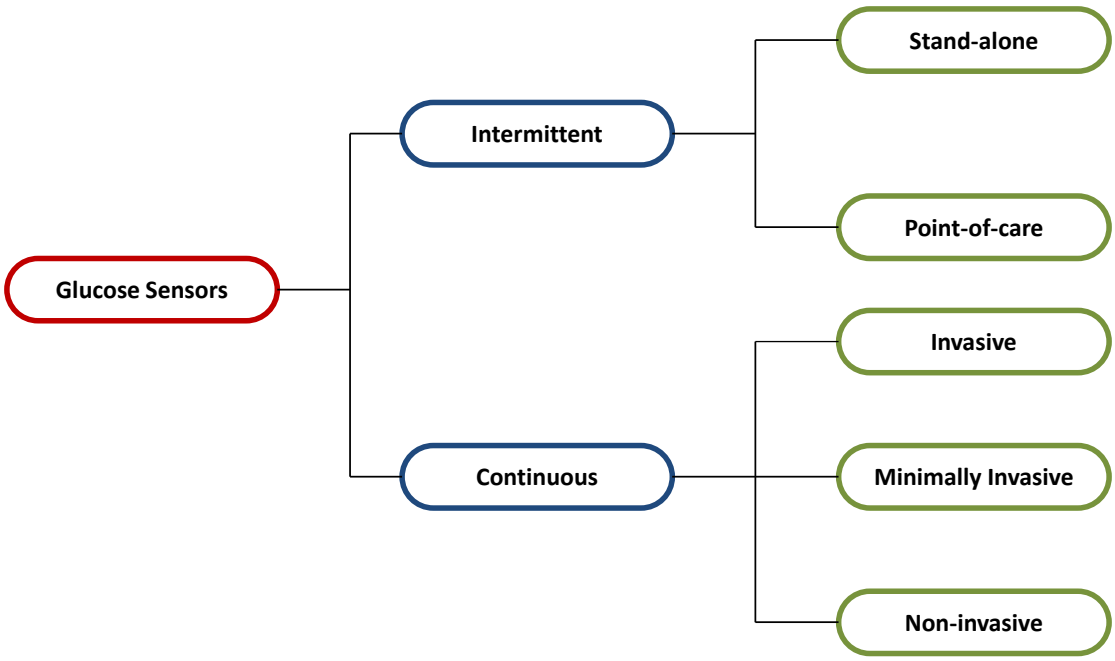

Figure 2-2. Classification of glucose sensors according to the detection approaches.

According to the type of transducers, glucose monitoring devices could be divided into electrochemical glucose biosensors and optical glucose biosensors. The electrochemical method is a well-established technique widely used in most commercially successful glucose biosensors. The glucose biosensor market is well covered by electrochemical sensors,[8] mainly in the form of stand-alone instruments in clinical labs and homecare testing strips. In contrast, optical methods rely on the measurement of photons, rather than electrons. Although optical glucose sensors have not attained the success of the electrochemical glucose monitors, they are undergoing

highly active research and have several advantages. For example, optical glucose sensors are especially useful when the patients are wearing heart pacemakers or under radiotherapy for cancer, as the electromagnetic field would affect electrochemical sensing, but not optical sensing. Optical fibers enable the sensing of glucose in the deeper tissue or less accessible regions of body. In addition, since optical schemes do not require a reference electrode, they are especially beneficial for continuous sensing and non-invasive sensing of glucose. Absorptiometry (reflectometry), fluorescence and surface plasmon resonance (SPR) are the most successful optical methods to date. Among them, fluorescent and SPR methods are capable of continuous monitoring. Although the reflectometric or interferometric method has been described for glucose detection in plain water, it cannot sense glucose continuously in blood sample. Chemi- and bioluminescence-based optical sensors are not suitable for continuous monitoring either.[12]

2.1.1. Clinical High-throughput Instrumentation

Multiparametric instrumentation is widely used in hospitals in clinics for sensing glucose along with other interferential compounds in the blood such as Na^+, K^+, Cl^-, ascorbic acid, urea, lactate, O_2, etc. The instrument performs electrochemical-based assays capable of determining glucose concentrations in multiple blood samples simultaneously in a high-throughput manner. With the assistance of microfluidic or other flow systems, the instrument could produce readings within 1~2 min with a sample volume as small as 30~100 μL. The sensors in such instrumentation must be reusable or fully reversible. After each round of test, the sensor surface is regenerated by chemical means, and the sensors are recalibrated before the introduction of subsequent samples; this, however, compromises the frequency of assays.

2.1.2. Point-of-care Personal Glucose Meters

Near patient or point-of-care glucometers, on the other hand, are portable, disposable, low-cost and calibration free. Such devices do not have the requirements of biocompatibility, maintainability, reversibility, long operational lifetime or long

shelf time. With millions of testing strips consumed every year, the homecare devices obviously dominate the whole glucose sensor market.[14] The mediator-based electrochemical glucose meter enables the users to test their blood glucose daily at home, with a small sample loading volume of 1~10 μL and a result waiting time as short as 30 s. To date, majority of the homecare glucose testing strips in the market rely on enzyme based screen printed electrodes,[10, 15] which could be mass produced by rapid microfabrication technology or vapor deposition process.[16, 17]Screen-printing is a thick film process, which has been employed for the production of robust, low-cost and miniaturized electronic circuits since 1980s. A small laboratory-scale screen printer, as shown in Figure 2-3A, is capable of producing thousands of sensors per day. Larger ones could far exceed this figure. For example, Abbott Inc. produces over 1 billion biosensor strips every year. The screen-printing technology could contribute largely to the commercial success of electrochemical glucose personal sensors. Screen-printing functions by fabricating the patterns of conductors and insulators onto the surface of planer supporting substrates (usually ceramic or plastic) based on squeezing the ink suspension through a patterned mask. The inks for the printing of biosensor strip circuits are usually carbon and metals. [10, 17]Each printed strip comprises the counter-reference, fill detection and working electrode, which is immobilized with necessary reagents such as the enzyme, mediator, stabilizer, surfactant, membrane and binding agents. Figure 2-3B shows the inner architecture of a representative electrochemical test-strip, composed of seven major components. The bottom plastic substrate (1) is screen printed with the working electrode (2), which is immobilized with enzyme, mediators, etc. (3). The counter-reference and fill detection electrodes (4) are screen-printed on top plastic layer (5) and are separated from the working electrode by an adhesive layer (6). A small capillary chamber (7) is constructed on the adhesive material and over the electrodes, enabling the sensor to detect glucose with a blood sample volume as small as 1 μL.[8] By employing the aforementioned techniques, such a single-use device not only eliminates the problems

of carry over, cross contamination or drift, but also has the advantages of low cost, capability of mass production and high clinical accuracy.

Typically, diabetic patients need to prick their finger, place one small droplet of their blood on the testing strip, which is inserted into the control device to obtain to blood glucose concentration. The control devices are pocket sized, light and battery controlled. Most of them provide glucose concentration readings within 5~30 s. Although there are more than 50 different brands of testing strips and pocket-sized monitors available in the market, 90% of them are manufactured by four major companies: Bayer, Lifer Scan, Abbott and Roche Diagnostics.[18, 19] Figure 2-3C shows the top-selling personal glucose meter of Roche Diagnostics, the Accu-Chek Advantage ™, which is one of the fastest glucose sensors commercially available, displaying the results as fast as 5 s. The side-fill capillary configuration allows for easy drop and collection of blood sample into the strip and requires a sample volume as small as 1 μL. Overall, the attractive performance and elaborate features of near patient glucose monitor could be contributed to the significant scientific developments and major technological advances in past decades. Nevertheless, drawbacks of personal monitoring devices, including low and irregular testing frequency, inadequate interpretation of results by patient and liability issues, are expected to be overcome in the near future by more integrated devices, which provide multifunctional capability, enhanced interface with physicians and easy tracking of blood glucose level fluctuation.[10]

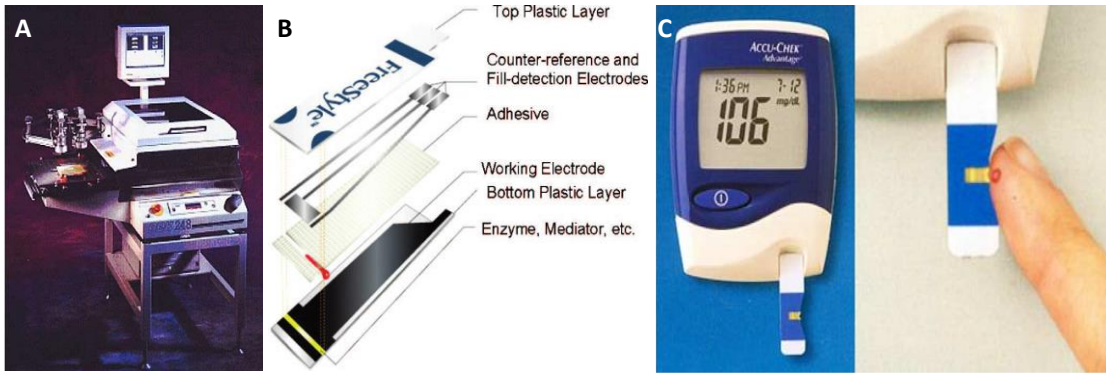

Figure 2-3. (A) Pilot-scale screen-printing machine. (B) Expanded view of a typical electrochemical test-strip, with blood droplet partially filled in the capillary chamber. More

than 1 billion of such strips are produced every year. (C) Accu-Chek Advantage™ personal glucose monitor manufactured by Roche Diagnostics. (Reprinted with permission from Ref. 8 and 10. Copyright 2005 Elsevier. Copyright 2008 American Chemical Society)

2.1.3. Implantable Long-term Glucose Monitors

Despite the big success of test-strip based personal glucose meters, the inconvenience of finger pricking associated with such sensors prevents the patients from frequently measuring their blood glucose level, especially during the night, resulting in poor approximation of blood glucose fluctuations. Tight diabetes management could be achieved by more frequent measurement or continuous monitoring, which provides greater information about the blood glucose fluctuation throughout the day, such as overall direction, magnitude, trend, pattern, duration and frequency of such variations. Sharp changes in blood glucose level could automatically trigger the alarms, warning of hypo- and hyperglycemic conditions.

In order to achieve fast and optimal therapeutic interventions, an 'artificial pancreas', which could deliver insulin timely in case of abnormal blood glucose levels, is highly desirable.[20] Such a 'holy grail' requires a closed-loop glycemic control system in which an implantable glucose monitor is the key component. The 'sense and release' concept is expected to revolutionize the means for glucose monitoring and have significant impact on diabetes management and treatment.[21] Generally, implantable glucose monitors are classified into three categories: subcutaneous, intravenous and microdialysis systems.[13]

Unfortunately, the development of an *in vivo* glucose monitoring system is not straightforward. Several major challenges have to be taken into consideration. For intravenous implantable devices, the main problem arises from the severe surface fouling of electrode by proteins and coagulation factors, which suppresses glucose response and increases the risk and thrombus formation. Therefore, the majority of the implantable glucose monitors have been developed to alternatively measure the glucose in the interstitial fluid of the subcutaneous tissue, where the glucose concentration reflects the blood glucose level.[22-27] Nevertheless, the wound site

generated by subcutaneous implantation would induce a serious local inflammatory response, which is associated with scar formation and accompanied by bacteria and macrophage adhesion, resulting in distortion of the glucose concentration near the sensor area (Figure 2-4A). The extent of inflammatory reaction varies according to size, shape, stiffness, physical and chemical properties of the sensor.[28]

The first subcutaneous implantation of needle-type glucose monitor was demonstrated by Shichiri *et al.* in 1982.[29] In the following 20 years, subcutaneous implantable glucose sensors moved gradually from the experimental stage to commercial products.[30, 31] After a long research program, MiniMed (Sylmar, CA, USA) marketed the first needle-type subcutaneous glucose monitor (Figure 2-4B) in 2002. The continuous glucose monitoring system (CGMS) allows for the measurement of glucose every 5 minutes, with nearly 300 readings per day and data storage in the monitor's memory. However, the MiniMed's device restricts patients' access to real-time data, which could only be downloaded by the physician. [30] Similar FDA-approved devices include Guardian REAL-Time system by Medtronic (Minneapolis, MN, USA), SEVEN by Dexcom (San Diego, CA, USA) and Freestyle Navigator by Abbott (Abbott Park, IL, USA), which are all flexible sensors with sub 1 mm diameter, containing a GOx-immobilized working electrode and a Ag/AgCl counter-reference electrode under the skin (Figure 2-4C). The needle-type sensor is inserted in the subcutaneous fat, usually 5-10 mm below the skin by a hollow, retractable sharp needle. The amperometric measurements of glucose are typically conducted at intervals of 1~5 minutes by the implantable sensor, which is connected to a small on-skin potentiostat that transmits signals wirelessly to the displaying device. The disposable needle-type sensors could be implanted up to seven days before replacement.[32] TheraSense (Alameda CA, USA, now Abbott) developed a new generation of subcutaneous glucose monitors with a miniaturized needle 10% shorter than MiniMed's system that could be painlessly replaced by patients. The system is based on the enzyme wiring technology developed by Heller and Feldman.[31] In

addition, the signal transduction between the sensor and monitor is based on a wireless system, making the device easy to carry and user-friendly. MiniMed (Sylmar CA, USA) has also developed an artificial insulin pump, which is able to regulate the insulin release automatically with the design of a “closed-loop”, which enables the direct communication between the implanted glucose sensor and the insulin pump. The updated version Model 2007 was approved by Europe in 2000 and is projected to have a 10-year battery life. Animas (Frazer, PA, USA) aims to develop a long-term subcutaneous glucose monitor which could be used for more than 5 years without replacement. The Animas sensor measures glucose concentration by an optical method, near-infrared adsorption of blood. The device is designed to have implantation across a vein with readings transmitted to wrist-wearing display unit by radio wave telemetry. However, spectroscopic determination of blood glucose is proved to be difficult since the glucose concentration is low in blood and its spectra overlaps with other components in the blood such as urea, uric acid, water, hemoglobin and other proteins. Most attempts to measure glucose through the skin or mucous membranes failed due to the loss of light energy in intervening tissues or the difficulty of discerning blood spectra from tissues.[10]

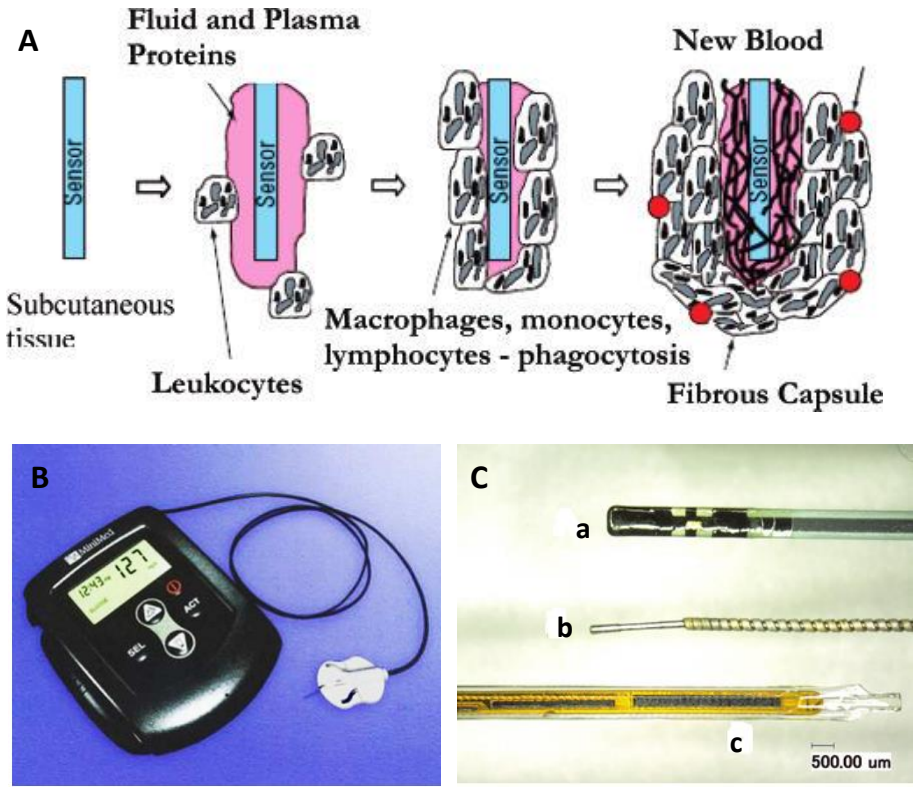

Figure 2-4. (A) Schematic illustration of protein fouling and inflammatory response at the surface of implantable glucose sensor. (B) The first commercial implantable glucose monitor launched by MiniMed™. (C) Commercially available needle-type subcutaneous sensors: (a) Abbott's FreeStyle Navigator, (b) Dexcom STS, and (c) Medtronic's Guardian RT. (Reprinted with permission from Ref 8, 10 and 11. Copyright 2005 Elsevier. Copyright 2008 American Chemical Society)

The alternative approach for implanted glucose biosensors is microdialysis sampling, which enables continuous subcutaneous glucose monitoring without direct contact between the transducer and the interstitial fluid.[33, 34] Typically a hollow dialysis fiber is implanted in the subcutaneous tissue and perfused with isotonic fluid. Glucose is diffused from tissue into the fiber and pumped toward the enzymatic biosensor. Microdialysis based glucose sensors have been extensively studied in recent years[35-56] and portable systems have been developed by several groups for continuous glucose monitoring.[44, 57-61] For example, Vering *et al* developed a wearable *in-vivo* continuous monitoring system based on a biocompatible microdialysis needle.[44] Langerman *et al.* applied microdialysis systems for glucose and lactate sensing in the brain tissue of injured critical care patients.[57] Commercial microdialysis-based systems include GlucoDay (Menarini, Florence, Italy)[48, 49, 62] and

SCGM1 (Roche, Mannheim, Germany)[63]. The microdialysis fibers of both devices are implanted in the abdominal adipose tissue, with interstitial fluid flowing to an external amperometric electrode immobilized with GOx. The results of GlucoDay show good consistency with the measurement of blood glucose level of 70 diabetes patients.[48] The SCGM1 is a non-enzymatic system based on monitoring glucose-induced changes in the viscosity associated with binding to the lectin concanavalin.[58] The readings of SCGM1 lag by 30 minutes behind the actual blood-glycemia.[63] Although microdialysis techniques based implantable glucose monitors provide more clinical accuracy and less signal drift than needle-type sensors,[52, 64] the many issues such as biocompatibility, lagging measurement, calibration, long-term stability, specificity, linearity and miniaturization of the sensor still remain as challenges. The lifetime of a microdialysis-based system is mainly limited by surface fouling and bacterial contamination of the sensor. The extent of the lag in measurement is determined by equilibration, flow rate and volume of the sensor compartment.[48, 50, 52] A novel microdialyzer that adds constant glucose concentration to the perfusate and operates in a pulsatile flow mode would eliminate the need for calibration.[47]

2.1.4. Minimally Invasive Glucose Sensors

In order to alleviate the pain and discomfort associated with regular finger-pricking and to avoid the problems pertaining to *in vivo* monitoring devices, some workers have proposed the method of minimally invasive measurement, which aims to avoid traditional blood sampling by drawing fluid through the skin without conventional puncture.

LifeGuide™ developed by Integ (St. Pau, MN, USA) enables the user to collect 1 μL interstitial fluid by a 1.4 mm small needle. The sample is then analyzed by infrared spectroscopy. The approach is less painful than traditional pricking method by Lancet. However, spectroscopy-based detection lacks sufficient accuracy compared to the enzyme electrode-based electrochemical method. SpectRx™ (Norcross, GA, USA) conducts the measurements by collecting interstitial fluid through an array of

microscopic holes created with a laser in stratum corneum. Kumetrix (Union City, CA, USA) have developed an interesting sampling system based on silicon micro-needles that mimic the dimension of human hair. By penetrating the skin, the micro-needles draw a very small volume of blood (~100 nL), which is then loaded in a disposable element where the glucose concentration is measured.

2.1.5. Non-invasive Glucose Monitoring Systems

Non-invasive glucose monitoring is another trend in the development of glucose sensing technology, which has attracted tremendous research efforts. Reverse-iontophoretic, impedimetric and optical approaches are the most commonly employed methods.[13, 65]

The GlucoWatch developed by Cygnus Inc. (Redwood City, CA, USA) extracts glucose from interstitial fluid by reverse iontophoresis and transports fluid across the skin to an externally worn monitor for glucose measurement.[66, 67] GlucoWatch G2 Biographer (GW2B) was sold by Animas Technologies Inc. (now part of Johnson & Johnson). The detection of glucose is based on enzyme-based electrooxidation at 0.42 V with Ag/AgCl as the reference electrode. GW2B provides 36 readings within a 12 h period after a single calibration, showing the trends, tracking patterns in glucose levels and alarming hypoglycemic and hyperglycemic events. A study[68] of 89 pediatric patients suggests that the mean relative absolute difference between GW2B results and laboratory serum values is 22%, which is similar to that of subcutaneous implanted devices.[69] Unfortunately, GW2B was discontinued in 2008 due to skin irritation induced by iontophoresis and missed readings in periods of perspiration.[70] Some other considerable issues such as long warm up time, false alarms, fingerstick calibration and change of skin temperature also limited the utility of the device.

The Pendra™ developed by Pendragon (Zurich, Switzerland) utilizes impedance spectroscopy for non-invasive continuous glucose monitoring. The wrist watch-like device measures glucose-related effects by detecting the impedimetric changes of the skin and underlying tissue. It is claimed that the device is suitable for both Type 1 and

Type 2 diabetics. Nevertheless, Type 1 diabetics need to conduct a fingerstick test following a warning from the device, as is the case for Cygnus and MiniMed glucose sensors. Two-point calibration is required by the device to provide users with absolute offset data and ratios between impedance variations and glucose changes.[10]

The optical methods used for non-invasive glucose detection are numerous, including polarimetry,[71] Raman spectroscopy,[72] near infrared (NIR) absorption spectroscopy,[73] photoacoustics,[74] optical coherence tomography (OCT),[75] etc. In spite of the difficulties involving continuous glucose monitoring with NIR, the approach has been pursued and intensively researched by several companies. Although they have claimed that the problems have been overcome already, up to now there have been no commercially available non-invasive glucose sensors based on optical detection; the clinical utility and reliability of these devices have yet to be accepted by the market.

2.2. Electrochemical Glucose Biosensors

2.2.1. Electrochemical Biosensing Techniques

As is introduced above, most commercial glucose biosensors are based on electrochemical transducers because of their low cost, portability, reliability and simplicity of construction.[76, 77] The electrochemical reaction typically generates a measurable current, charge accumulation or change in conductivity, which could be detected by amperometry, potentiometry and conductometry, respectively.[7] Furthermore, impedance spectroscopy is commonly used for monitoring resistance and reactance at the electrode/electrolyte interface.[7]

Electrochemistry is a surface technique which requires very small sample volumes for measurement.[78] In addition, electrochemical sensing is not interfered by compounds such as flurophores, chromophores and particles that affect optical detection. Thus the electrochemical technique is quite suitable for sensing coloured or turbid samples such as whole blood, which is rich in blood cells, fat globules, bilirubin and haemoglobin that have strong optical absorbance.[79, 80]

Electrochemical biosensors mainly measure three types of signals: current, potential and impedance. Current measurement can be achieved by voltammetry or amperometry, which are the most commonly used electrochemical techniques in glucose biosensors. Voltammetric and amperometric techniques function by applying a potential to the working electrode *versus* a reference electrode and measuring the current, which is a result of electrochemical oxidation or reduction at the working electrode surface. The electrolysis current is limited by the mass transport rate of molecules to the electrode.[81]

Voltammetry is characterized as a potential scanned over a potential range. The current response is a peak or plateau that is proportional to the analyte concentration. Voltammetric technique includes a variety of methods, including cyclic voltammetry (CV), differential pulse voltammetry (DPV), square-wave voltammetry, hydrodynamic voltammetry, ac voltammetry, polarography, and stripping voltammetry.

Amperometry is a technique where the change of current *versus* time is monitored during an electrochemical reaction while the potential applied at the working electrode remains constant against the reference electrode.[82] Amperometric biosensors have the advantage of good selectivity since the detection is performed at the potential where the analyte species are oxidized or reduced. In addition, due to its high sensitivity and low limit of detection (LOD), the technique is widely used in biocatalytic biosensors such as glucose sensors.[6] The high sensitivity could contribute to the applied fixed potential, which generates negligible charging current and minimizes the background signal that adversely affects the LOD. Hydrodynamic amperometry provides additional advantages such as enhanced mass transport to the electrode surface[83] in the condition that the working electrode rotates or vibrates with respect to the electrolyte,[84, 85] or in a flowing system where a sample solution passes through a working electrode.[86, 87]

Electrochemical biosensors are typically in a configuration of three-electrode or

two-electrode system. A three-electrode system (Figure 2-5A) consists of a working electrode made of chemically inert materials such as gold, platinum or carbon (i,e. graphite, glassy carbon, carbon paste), a counter or auxiliary electrode made of platinum wire, and a reference electrode including silver chloride (Ag/AgCl) and saturated calomel electrode (SCE). In order to maintain a known and stable reference potential, the reference electrode is usually removed from electrochemical cell where the redox reaction occurs[7] (Figure 2-5B). This setup could prevent the reference electrode from changing its half-cell potential since the charge only passes through the counter electrode during the electrochemical reaction. A two-electrode system contains only a working electrode and a reference electrode. It is usually employed when the current density is below 1 μA cm^{-2}, which could be carried by the reference electrode without adverse effects.[82] In addition, the two-electrode system is preferred for disposable sensors which do not require long-term stability of the reference electrode and target low fabrication cost.

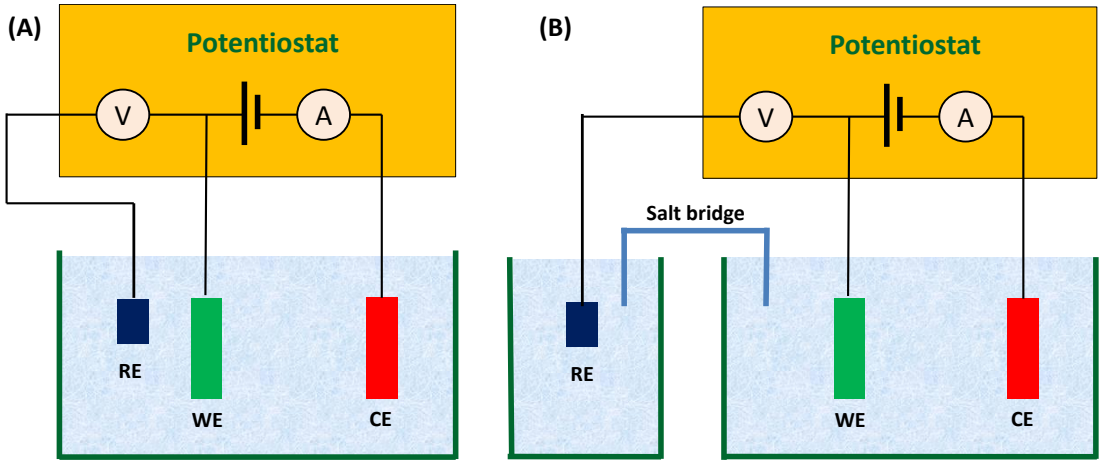

Figure 2-5. There electrode system with (A) and without (B) reference electrode in the redox reaction cell.

Electrochemical impedance spectroscopy (EIS), first described by Lorenz and Schulze in 1975,[88] is a powerful technique to probe the interface properties of surface modified electrodes.[89, 90] EIS measures the resistive and capacitive properties of materials upon perturbation of a system by a small amplitude sinusoidal ac excitation signal typically of 2–10 mV.[91] The frequency is varied over a wide range to obtain the

impedance spectrum. The technique enables sampling of mass transfer at low frequency and electron transfer at high frequency range. Impedimetric detection is especially useful for investigating biomolecule immobilization, immunological reaction between antibody (Ab)-antigen (Ag) and hybridization between DNA molecules in biocatalytic and affinity sensors.[92]

2.2.2. Three Generations of Enzymatic Glucose Biosensors

The glucose biosensors based on glucose oxidase (GOx) have dominated the glucose sensor industry for more than 30 years primarily due to their advantages of excellent selectivity, high clinical accuracy and stability. The key component of GOx is flavin adenine dinucleotide (FAD), which is the redox centre of the enzyme that catalyses the glucose oxidation reaction. However, the centre is deeply buried in the insulating protein shell, which limits the electron transfer to the electrode surface and causes complex electron transfer mechanisms. To date, three approaches have been developed to mediate the electron transfer between the redox centre of enzyme and the electrode surface. According to the various electron transfer mechanisms behind different approaches, the enzymatic glucose sensors are generally divided into three generations which appear sequentially in the history.[93] The working mechanisms of three generations of enzymatic glucose biosensors are schematically illustrated in Figure 2-6.

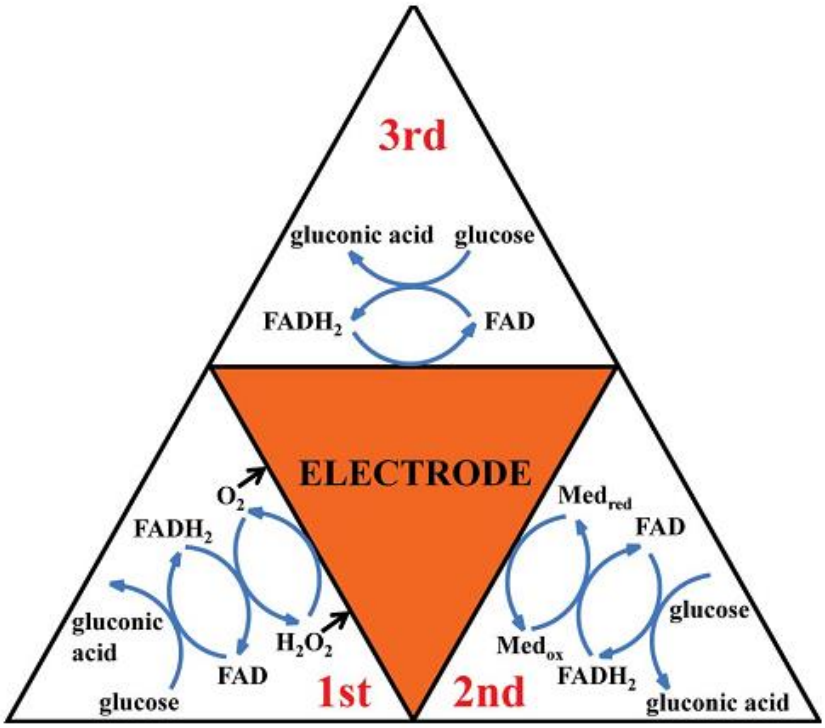

Figure 2-6. Summary of the glucose oxidation mechanisms in first, second and third generation glucose biosensors. (Reprinted with permission from Ref. 102, Copyright 2013 The Royal Society of Chemistry.)

The first-generation glucose sensors were pioneered by Clark and Lyons in 1950s and 1960s.[94] Their device relied on a thin layer of glucose oxidase (GOx) enzyme, immobilized over an oxygen electrode (via a semipermeable dialysis membrane), and monitored the amount of oxygen consumed by the enzyme-catalyzed reaction by electrochemical method.[95] The reaction could be explained by the following equation[95]:

$$\text{glucose} + O_2 \xrightarrow{\text{GOx}} \text{gluconic acid} + H_2O_2 \qquad (2\text{-}1)$$

A negative potential was applied to the platinum cathode for a reductive detection of the oxygen consumption:

$$O_2 + 4H^+ + 4e^- \rightarrow 2H_2O \qquad (2\text{-}2)$$

The technique was further developed by Updike and Hicks[96] who employed an additional oxygen working electrode (without enzyme) and measured the differential current between two working electrodes to correct for the oxygen background

variation in samples. Subsequently, Guilbault and Lubrano[97] introduced another enzyme electrode for blood glucose measurement based on amperometric monitoring of the hydrogen peroxide as a product:

$$H_2O_2 \rightarrow O_2 + 2H^+ + 2e^- \quad (2\text{-}3)$$

The drawbacks of first-generation glucose sensor are the strong dependence of ambient oxygen and too high applied potentials for reduction of oxygen or oxidation of H_2O_2. Both the high negative and positive potentials may cause serious interfering reactions of electroactive compounds (e.g., ascorbate, urate and paracetamol) in the blood if a size-selective membrane is not present.

The second-generation glucose sensors based on mediators were introduced in the 1980s.[98, 99] Mediators are small, soluble redox active molecules (e.g., ferrocene derivates, ferrocyanide, conducting organic salts and quinones) capable of undergoing rapid and reversible redox reactions, shuttling the electrons between the redox center at the active site of enzyme and the electrode surface. The mechanism of the second-generation biosensors could be understood by the following equations:

$$\text{glucose} + \text{GOx(FAD)} \rightarrow \text{gluconic acid} + \text{GOx(FADH}_2\text{)} \quad (2\text{-}4)$$

$$\text{GOx(FADH}_2\text{)} + 2\text{M(ox)} \rightarrow \text{GOx(FAD)} + 2\text{M(red)} + 2\text{H}^+ \quad (2\text{-}5)$$

$$2\text{M(red)} \rightarrow 2\text{M(ox)} + 2\text{e}^- \quad (2\text{-}6)$$

where M(ox) and M(red) are the oxidized and reduced forms of the mediator. Mediators have replaced O_2 molecules as the electron shuttle to react with the redox active center of enzyme (Eqn 5) and M(red) are re-oxidized at relatively low potentials which generates a current when they come in contact with the working electrode (Eqn 6). Incorporation of mediators in the glucose sensor alleviates the influence of interferential molecules and eliminates oxygen dependence for glucose sensing. By taking advantage of the high specificity and reliability of second-generation glucose sensor, the first personal glucose meter was commercialized by Medisense Inc. in 1987.[11] Various other companies including

Roche Diagnostics, LifeScan, Abbott and Bayer thereafter launched different types of glucose sensors with lower sample loading volumes and more advanced functions, but the basic concept of glucose sensor design has remained largely unchanged. Although the practicability of second-generation glucose biosensors has been successfully achieved by the commercialization of a series of home-use, disposable devices based on screen printed strips, the soluble nature of most mediators leads to short operation time and irreproducible results, and the potential biotoxicity of mediators prevent the second-generation biosensor from being applied for *in vivo* glucose testing.

The ultimate goal of glucose sensing is to eliminate the usage of a mediator, or even an enzyme to lower the fabrication cost and complexity while increasing glucose sensor durability. The third-generation glucose sensor enables direct electron transfer between the redox center of enzyme and the electrode, leading to a very high sensitivity and reproducibility without using mediators. The system could be operated at a low potential close to the physiological enzyme redox potential of ~0.44V[100]. The mechanism of the third-generation of glucose biosensor can be explained by following reactions [101, 102]:

$$\text{glucose} + \text{GOx(FAD)} \rightarrow \text{gluconic acid} + \text{GOx(FADH}_2\text{)} \qquad (2\text{-}7)$$

$$\text{GOx(FADH}_2\text{)} + 2e^- \rightarrow \text{GOx(FAD)} + 2H^+ \qquad (2\text{-}8)$$

Due to a significantly lowered operating potential, the interferential responses of electroactive species are also greatly diminished. The third-generation glucose sensor is well suited for the *in vivo* monitoring of blood sugar due to its stability and biocompatibility. However, it suffers from relatively smaller linear range compared to the first- and second-generation glucose sensors. Therefore, the implantable glucose monitors on the market currently are still based on the concept of first-generation ones. Further effort is needed to improve the performance of the third-generation of glucose sensor in order to meet the commercialization criteria.

Some historical hallmarks in the development of electrochemical enzyme glucose biosensors are listed in table 2-2.

Table 2-2. Some defining events in the evolution history of electrochemical enzymatic glucose biosensors.

Year	Event
1916	First report on the protein immobilization:
1956	Invention of the oxygen electrode (Clark)
1962	First description of enzyme electrode for amperometric glucose sensing (Clark and Lyons)
1967	First practical enzyme electrode based on oxygen detection (Updik and Hicks)
1973	Enzyme electrode for blood glucose sensing based on hydrogen peroxide detection (Guilbault and Lubrano)
1975	Launch of the first commercial glucose biosensor YSI analyser (Yellow Springs Instruments)
1976	First bedside artificial pancreas (Miles Biostator)
1982	First needle-type enzyme electrode for subcutaneous implantation (Shichiri)
1984	First ferrocene mediated amperometric glucose biosensor (Cass *et al.*)
1987	Launch of the ExacTech blood glucose biosensor (MediSense Inc.)
1992	Launch of hand-held blood analyser (i-STAT)
1996	Glucocard launched
1996	Abbott acquires MediSense for $867 million
1998	FastTake blood glucose biosensor launched (LifeScan Inc.)
1999	Launch of a commercial *in vivo* glucose sensor (MiniMed Inc.)
2000	Introduction of wearable non-invasive glucose monitor GlucoWatch™ (Cygnus Inc.)
2001	LifeScan purchases Inverness Medical's glucose testing busi-ness for $1.3 billion
2003	Abbott acquires i-STAT for $392 million
2004	Abbott acquires TheraSense for $1.2 billion

2.2.3. The Enzyme Immobilization Methods

Enzyme immobilization is one of the most important features in designing and fabricating glucose biosensors. The way in which proteins are immobilized on the electrode is critical for the performance of glucose monitoring devices. Improper immobilization of proteins can lead to partial or complete loss their bioactivities[103, 104]. In order to retain the biological activities, proteins should be immobilized without affecting their conformations. Thousands of protocols have been reported for effective

immobilization of enzymes.[105-110] A suitable immobilization approach should be determined by the physicochemical and chemical properties of both protein and electrode materials. As is shown in Figure 2-7, enzyme immobilization methods can be mainly classified into four categories: adsorption, covalent conjugation, entrapment and cross-linking.[111-114]

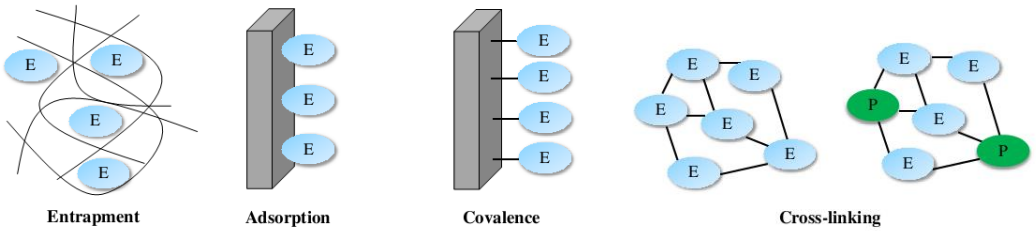

Figure 2-7. Schematic illustration of four major enzyme immobilization methods. 'E' indicates enzyme, 'P' indicates inactive protein. (Reprinted with permission from Ref. 114. Copyright 2012 Elsevier.)

2.2.3.1 Adsorption

Enzymes can absorb onto nanomaterials by physical adsorption via intermolecular forces such as hydrophobic interaction, polar effect and ionic bonds. This method is very simple and theoretically, it can be used for any protein immobilization on nanomaterials[115]. For this process, generally, there are two steps, contact step and washing step. In the contact step, proteins in the buffer solution will adsorb onto nanomaterials via intermolecular forces. The molecules loosely bonded will be removed by washing with the buffer.

Using this approach, many kinds of proteins have been successfully immobilized on nanomaterials with various compositions and structures with typical examples being carbon nanotubes, Au nanoparticles, mesoporous TiO_2 and macroporous Au film[116-121]. For example, mesoporous TiO_2 with a specific surface area as high as 343 m^2 g^{-1} and a uniform porous distribution of 7.8 nm was used for protein GOx adsorption. The pore size matched the dimension of the protein molecules used (7.0 nm × 5.5 nm × 8.0 nm).[121] As expected, after adsorption, GOx loading amount could reach as high as 39.3 wt % (10 mg/ml in solution). The adsorbed GOx showed fast direct electron transfer with its host matrix.

This method, however is not perfect[115]; one drawback is that adsorbed proteins may be removed by buffer solution during the measurement process. Another drawback is that it might suffer from susceptibility to changes in pH, ionic strength and temperature. In spite of these drawbacks, the physical adsorption approach for many successful protein immobilizations have been demonstrated, thus still opening promising avenues for further development.

Layer-by-layer (LBL) assembly is a relatively new method by which enzyme can be immobilized on the electrode via electrostatic adsorption. LBL is achieved by sequential adsorption of positive or negative charged species by alternatively dipping into the solutions and rinsing the excess after each adsorption step[122, 123]. There are numerous advantages of LBL including simplicity and thickness control in nanoscale. Further LBL can use the variety of species and components available and this has led to an exceptional growth in the research field and applications of LBL nanocomposites[124, 125].

Many proteins show a polyelectrolyte nature in buffer solution and this nature opens the door for their immobilization on electrode surface by LBL assembly. Sometimes, the process of LBL assembly for protein immobilization can be tuned by pH values. As we know, in a neutral pH both GOx (isoelectric point of 4.2 for GOx from *Aspergillus niger*) and acid-treated SWCNT have negative charge; they will repel each other when they co-exist in a neutral pH buffer. Conducting in 0.1 M acetate buffer solution with pH 3.8, Zhang et al. successfully immobilized GOx on the electrode surface via LBL by using acid-treated SWCNT as counterion because GOx has positive charge and carboxylic groups of SWCNT have a negative charge in the above pH buffer solution[126]. The LBL assembled electrode showed two pairs of well-defined redox peaks with midpoint potentials of -0.09 V and -0.46 V corresponding to the redox reaction of carboxylic groups on SWCNT and active centers of GOx, respectively. GOx in this LBL assembly electrode involved a two electrons and two protons redox process, confirmed by its voltammetric behavior

influenced by pH.

Compared with the method of direct utilization of protein as one electrolyte mentioned above, the polyelectrolyte LBL film itself can also be used to immobilize proteins. This method may be better in retaining the conformation and bioactivity of proteins since it can avoid the direct contact of the proteins with acid or base aqueous solution (for tuning pH), organic solvent, and the loading process is spontaneous. Wang et al. applied this method to entrap Mb by developing four different kinds of LBL films using polyelectrodes and inorganic nanoparticles as a hosting matrix[127]. Mb in all four types of LBL films gave well-defined quasi-reversible reaction peak pairs at around -0.34 V (vs SCE reference electrode). They also found that Mb immobilized onto PDDA/$(ZrO_2)_n$ gave the best electrochemical and electrocatalytic activity because of its better porosity.

2.2.3.2. Covalent conjugation

With its assembled functional unit of amino acids, proteins can be covalently bound to surface of nanomaterials through accessible functional groups. Compared with other immobilization methods, two of the major advantages of covalent bonding are that it is widely applicable and it can also provide a much more stable immobilization. This method involves three basic steps: (1) activation of nanomaterials via functionalization, (2) coupling protein, and (3) removal of loosely bound proteins[128, 129]. There is no optimal experimental condition for each step, which has to be determined by the properties of the nanomaterials and proteins. The functional groups available in proteins for immobilization and the functionalities of the required surfaces of nanomaterials are summarized in Table 2-3.

Table 2- 3. Functional groups in proteins and the required functionalities of nanomaterial surface. The table is from reference.[115]

Amino acids	Functional side group	Required surfaces
Asp, Glu	-COOH	amine
Ser, Thr	-OH	epoxy

Lys, hydroxyl-Lys	$-NH_2$	carboxylic acid, active ester (NHS), epoxy, aldehyde
Cys	-SH	maleimide, pyridyil disulfidevinyl sulfone

Two famous examples of these interactions are amine and thiol chemistry. It is well known that lysine residues with amine groups are the most commonly used amino acids in protein because they are always present on the exterior of the protein surface.[130-132] Aldehyde and N-Hydroxysuccinimide (NHS) are two most commonly used agents for coupling with amine groups, forming stable labile Schiff's bases and amide bonds, respectively. Another amino acid, cysteine, contains the unique functional group thiol, which is originally designed for the stability of the protein (secondary structure of protein) by creating internal disulfide bonds[133, 134]. Maleimide can react rapidly with thiol group to form stable thioether bonds in a specific pH range (usually 6.5-7.5). One example is the work reported by Kong et al about protein horseradish peroxidase (HRP) immobilized on one kind of conducting polymer, 5,2′:5′,2″-terthiophene-3′-carboxylic acid (TCAP)[135]. Using 1-Ethyl-3-(3-dimethylamino-propyl)carbodiimide (EDC) as an activating agent, HRP was successfully immobilized by forming peptide bonds between the amine groups of the HRP (from lysine residues in the peptide chain of protein) and the carboxylic acid groups of the conducting polymer TCAP. Direct electron transfer of HRP covalently immobilized on TCAP with a pair of redox peaks was observed and the electrode displayed an excellent electrocatalytical response to the reduction of hydrogen peroxide with high sensitivity.

Though this approach is widely used in protein immobilization, there are solely reports on their applications in direct electron transfer based study and applications. One reason might be that covalent bonding will decrease or even cause total loss of the bonded protein's bioactivity.

2.2.3.3. Polymer (gel) entrapment

The entrapment method for protein immobilization is a simple approach with the ability to imprison proteins on electrode surfaces while at the same time promoting the substrates to diffuse through membrane-like structure freely. It offers other advantages such as requiring only a small amount of enzyme, preserving the integrity of the enzyme and being easy to prepare[136].

Membrane-like structures constructed by the sol-gel method for immobilizing proteins has drawn great interest in recent years due to its simple preparation, chemical inertness, tunable porosity, low-temperature encapsulation and swelling behavior[137-140]. Among various sol-gel based methods, silicate sol-gel matrix might be the most famous because of its two significant advantages: (1) it can maintain a large content of water in the membrane which makes the entrapped proteins stable over a long term and (2) the preparation process can be performed at room temperature. For example, Wang et al. first prepared a silica sol-gel solution by hydrolyzing an alkoxide precursor, tetraethylorthosilicate (TEOS) at room temperature at suitable pH value[141]. After Hb was spread onto the electrode surface and dried, a small amount of as-prepared silica sol-gel solution was pipetted to cover the Hb electrode. A porous matrix of silica was formed on electrode surface by the partial hydrolysis of the TEOS, at the same time supporting an aqueous microenvironment for entrapping Hb. The silica sol-gel entrapped Hb showed nearly reversible cyclic voltammetric peaks corresponding to the Hb Fe(III)/Fe(II) redox couple. After calibration they found that the formal potential varied linearly with the increase of pH in the range of 5.0-10.0 with a slope of 49.44 mV/pH, suggesting that a proton transfer was accompanied with each electron transfer in the electrochemical reaction of the encapsulated Hb in silica sol-gel.

Specific surfactants with a polar (or charged head group) and at least a non-polar tail (usually long hydrocarbon chains) can form stable biomembrane-like films when they are casted on an electrode that can provide proteins with a natural-like environment[142, 143]. Surfactants fulfilling the above requirements should have ionic

headgroups and at least two hydrocarbon tails with more than twelve carbons. For example, Munge et al. prepared a lipid bilayer structure on an electrode with protein entrapped inside by casting the mixture of dimyristoylphosphatidylcholine (DMPC) vesicle and protein spinach photosystem I onto the electrode[142]. The entrapped proteins retained their native conformation in the lipid film, and for the first time, the direct and reversible electron transfer of the entrapped proteins was obtained in the lipid bilayer film.

Some CPs such as polypyrrole and its derivatives can be electro-synthesized in biocompatible conditions and have interesting chemical and physical properties derived from their unique conjugated π-electron systems[144-146]. More importantly, some properties, like the conductivity of the CPs, can be adjusted by their doping process. Nanoscaled protein molecules can be used as doping agents of CPs. The protein could be simultaneously entrapped by the CP during the electropolymerization process and immobilized on electrode surface together with the CP[147].

Ramanavicius et al. used in-situ polymerization of the conducting polymer Ppy by using protein quino-hemoprotein alcohol dehydrogenase (QH-ADH) as the dopant. Briefly, they prepared the polymerization solution first by adding 270 μL of pyrrole solution (100 mM pyrrole in 100 mM KCl) and 30 μL of enzyme solution (7.6 mg L^{-1}). The in-situ polymerization was carried out by applying 30 potential pulses between 950 (1 s) and 350 mV (for 10 s), which allowed the enzyme and the monomer to equilibrate in the neighborhood of the electrode. They also observed that the Ppy entrapped enzyme QH-ADH could go through the fast direct electron transfer pathway via the conducting polymer chains[148].

2.2.3.4. Cross-linking

Another well-known approach for enzyme immobilization is cross-linking proteins with glutaraldehyde or other bifunctional agents such as glyoxal or hexamethylenediamine. The enzyme can be either cross-linked together with each other or in the presence of an inactive protein, bovine serum albumin (BSA). The

advantages of this method are the strong chemical binding between the molecules and the simplicity, but one major concern is the possible loss of enzyme activity due to the change of enzyme conformation and alternation of the enzyme active center in the process of chemical treatment.

Pei and colleagues[149] immobilized GOx onto a cantilever surface by cross-linking the enzyme with glutaraldehyde and BSA. The gravimetric biosensor was able detect glucose selectively in blood. Kong and coworkers[150] developed an amperometric glucose biosensor by immobilizing GOx onto ZnO nanotubes via cross-linking. The biosensor achieved a low detection limit of 1 μM, long-term stability of 2 months and excellent anti-interference performance. By cross-linking GOx and BSA with glutaraldehyde, Yonemori *et al*[151] developed an implantable needle-type biosensor which is employed for continuous glucose monitoring in the eyeball scleral interstitial fluid of fish. The biosensor showed a satisfied linear range of 3.9 mM ~ 23 mM.

2.2.4. Non-enzymatic Glucose Biosensors

Nonenzymatic glucose biosensors are based on the glucose oxidation reaction catalysed by a variety of electrocatalyts, including metals (Au, Pt, Pd), metal oxides (Co_3O_4, CuO, RuO_2), alloys (PtPb, PtRu), complexes (cobalt phthalocyanine tetrasulfonate, nickel hexacyanoferrate) and carbon (carbon nanotubes, boron doped diamond). Except for the last category, all other catalysts listed above contain a transition metal center. There are generally two widely accepted theories that explain the electrooxidation of glucose by transition-metal containing electrocatalysts. Pletcher proposed the activated chemisorption model[152] which suggests that the electrocatalyic oxidation of glucose occurs via a concentrated step, i.e. the adsorption of glucose molecule on the surface of metal-containing electrocatalyst followed by the abstraction of hemiactalic hydrogen atom**.** The adsorption process presumably involves the formation of suitable bonds between the adsorbate and the transition-metal substrate with d-electrons and d-orbitals. The hydrogen removal process is deemed as the rate-determining step in most glucose electrooxidation

experiments and is generally considered to occur simultaneously with the chemisorption of anaytes. Hence, the adjacent metal active center is occupied by a single absorbate each time, implying well-spaced adsorption sites on the surface of electrocatalysts with suitable geometry could contribute to the kinetic enhancement of the glucose oxidation process. Another model, namely 'Incipient Hydrous Oxide Adatom Mediator' (IHOAM), was proposed by Burke,[153] who discussed the role of hydroxyl radicals in the electrocatalytic process. IHOAM was based on the observation that 'active' metal surface atoms undergo a premonolyaer oxidation step that forms an incipient hydrous oxide layer of OH_{ads}, which mediates the electrooxiation of glucose and many other organic molecules and inhibits many kinetically slow reduction process. The 'active' atoms on the electrode surface are considered to have a low lattice co-ordination value and lack normal lattice stabilization energy. Polycrystalline surfaces at discontinuous areas such as grain boundaries and edges, are usually exposed to the solution more directly than the bulk crystal surface, thus they are more probable to undergo premonolayer oxidation at lower potentials. According to the IHOAM model, the electrocatalytic oxidation of glucose is initiated by the formation of hydrous species on the electrode surface followed by the chemisorption of glucose molecules. After that, the hydrous premonolayer could mediate the electrooxidation of absorbed glucose at significantly low potentials, with the regeneration of metal surface. The surface of the 'active' metal is then oxidized again by the oxygen species at a certain potential and glucose is continuously oxidized during the repetitive cycling process. Both the activated chemisorption model and IHOAM model will be discussed in the following sections with respect to different electrode materials. IHOAM model explains the enhancement of electrocatalytic performance of most noble metal-based materials. The hydroxyl group also plays important role in the electroctatlytic process of nickel- and copper-based electrodes. However, in these cases, the incipient hydrous premonolayer is formed not to induce catalysis, but rather to change the oxidation state of the metal

hydroxide.

2.3. Nanomaterials for Electrochemical Enzymatic Glucose Biosensors

2.3.1 Metallic Nanomaterials

Metal nanocrystals are ideal electrode materials for electrochemical biosensing applications since noble metals exhibit unique physical, chemical and catalytic properties at nanoscale dimensions. [154-159]

Among all metal nanomaterials, gold (Au) nanostructures are the most intensively studied for protein immobilization and direct electron transfer.[160] Gold nanoparticles (AuNPs) can provide a suitable microenvironment, which is similar to the redox centre of a native protein, to immobilize enzyme and retain their bioactivities.[161] Besides, AuNPs allow a variety of functional groups, such as –SH, -NH_2 and –CN to bind covalently on their surfaces, which is favorable for the stable immobilization of biomolecules.[162, 163] In addition, AuNPs can greatly reduce the charge transfer resistance at electrode interfaces and provide a highly conducting pathway to facilitate the electron transport.[164] Other characteristics of AuNPs such as its high surface-to-volume ratio, small size, tailored structure and high biocompatibility have also been claimed as important factors to promote DET between the redox proteins and the electrode.[165] AuNPs are also able to catalyse small molecules involved in many significant biochemical reactions, such as H_2O_2, O_2 and NADH.[166] Taking these advantages into account, AuNPs were extensively explored to construct glucose biosensors either alone or combined with other materials.[167-169] The direct electrical communication between GOx and electrode via the link of AuNP was achieved by Willner's group,[102, 170] who developed the wiring strategy to covalently attach the co-factor FAD on an AuNP-modified Au electrode, followed by reassembling the apo-enzyme on FAD (Figure 2-8). Recently, Holland et al[171] reported a genetic modification approach to expose free thiol groups near the active site of GOx, which enables the site specific attachment of AuNPs to the enzyme and facilitates the direct

electrical communication between the conjugated enzyme and electrode (Figure 2-9). The DET of GOx was also achieved by immobilizing GOx and colloidal AuNPs in Nafion film on GCE.[172] The formal redox potential of the modified electrode was observed at -0.434 V in pH 7.0 PBS buffer solution. Other Au nanostructures have also been explored for DET; one example is the glucose sensor based on DET of GOx immobilized onto nanostructured Au thin films, which was fabricated by electrodeposition and galvanic replacement technology.[173] CV of the modified electrode indicated that the immobilized GOx displayed a direct, reversible and surfaxe-confined redox reaction in the PBS buffer. The sensor based on GOx/nanoAu thin film exhibited two linear ranges, which are 2.5~32.5 μM and 60~130 μM, respectively with a detection limit of 0.32 μM (S/N=3).

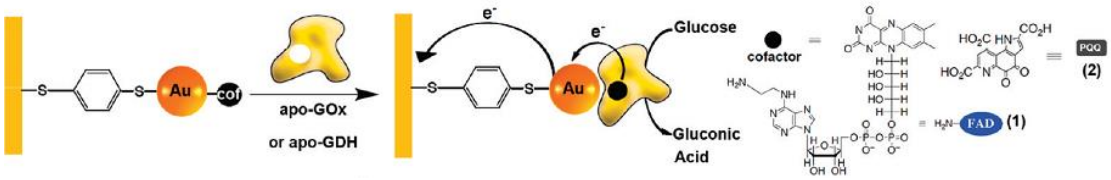

Figure 2-8. Scheme showing that the direct electrical communication between GOx and electrode could be achieved by 'wiring' the cofactor with AuNPs followed by re-assembly of the apo-enzyme. Reprinted with permission from Ref. 170. Copyright 2010 American Chemical Society.

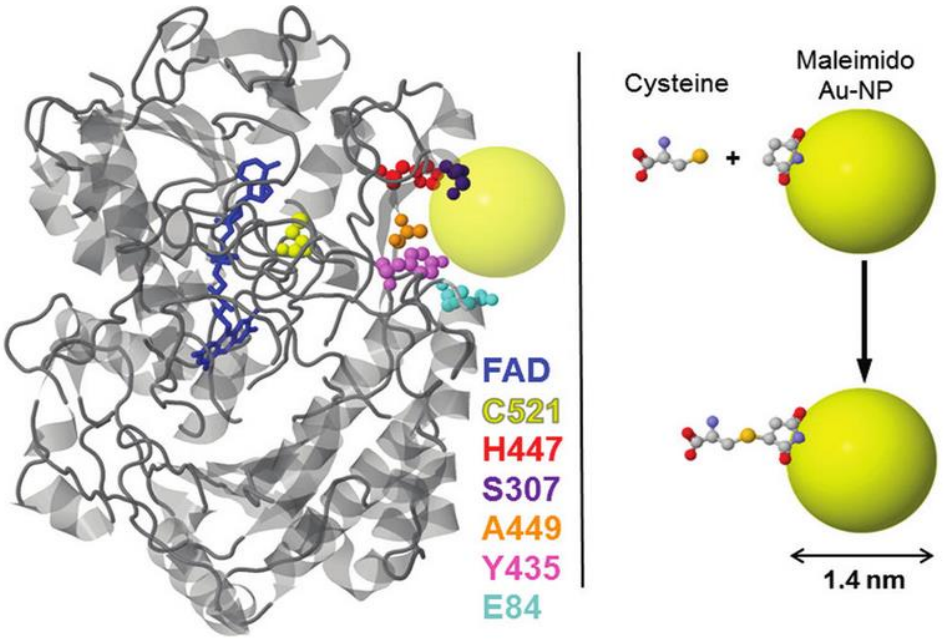

Figure 2-9. Left: The genetic modification strategy enables GOx to display a free thiol group

near its redox centre and site-specifically attach maleimide-modifed AuNP to the enzyme. Right: Schematic drawing of the covalent binding chemistry of cysteine to a maleimide-modified AuNP. Reprinted with permission from Ref. 171. Copyright 2011 American Chemical Society.

2.3.2 Nanostructured Metal Oxides

Nanostructured metal oxides have been intensively studied as electrode materials for biosensor fabrication due to their interesting properties such as tailored structure, high electrocatalytic activity, large surface area, high mechanical strength, and good biocompatibility. Therefore, they promise to immobilize a high quantity of enzymes, facilitate the direct electron transfer, lower the electrochemical overpotential and improve the sensitivity and selectivity of fabricated biosensor. [174, 175]

Titanium dioxide (TiO_2) is one of the most widely used oxide materials in dye-sensitized solar cells,[176, 177] hydrolysis catalysts,[178, 179] electrochromic devices[180, 181] and lithium-ion batteries,[182, 183] exhibiting excellent electron transfer behavior and superior photocatalytic capability.[184] It also shows excellent electrocatalytic activity towards a variety of molecules such as H_2O_2, ascorbic acid, guanine, L-tyrosine, acetaminophen, and β-NADH.[185] Nanocrystalline TiO_2 films have recently been introduced to improve the catalytic activity of enzymes in the applications of gas sensors[186-188] and biosensors.[189-191] Due to its tailored structure, high surface area, biocompatibility and hydrophilic nature[121, 176, 177, 192-194], nanostructured TiO_2 could also facilitate direct electron transfer of immobilized enzymes such as glucose oxidase (GOx),[121] HRP,[189] or hemoglobin,[195] which makes it a suitable material for the fabrication of third-generation biosensors.[196] The electrochemical properties of TiO_2-based devices are not only influenced by the crystalline form of the TiO_2, but also by the textural properties of the TiO_2 such as dimension, geometry, porosity and surface area.[121, 197] A high specific surface area and a uniform distribution of pore size of the electrode material are especially favorable for enzyme immobilization, fast and direct electron exchange between enzyme and electrode, and accessibility of electrolyte and target molecules at the medium/electrode interface.[197] A variety of

TiO_2 nanostructures have been developed to immobilize GOx and facilitate its direct electron transfer on the electrode surface.[121, 191, 195, 198-200] Cao et al.[191] developed 3D macroporous TiO_2 inverse opals which were successfully employed for the immobilization of GOx. The TiO_2 inverse opals were synthesized by the sol-gel method using polystyrene colloidal crystals as sacrificing templates. GOx immobilized on the 3D TiO_2 modified indium tin oxide (ITO) electrode showed direct electron transfer in the absence of glucose indicated by a pair of stable and well defined redox peaks on the cyclic voltammetry. At the detection potential of 0.3 V vs. SCE, the amperometric glucose sensor showed a high sensitivity of 151 μA mM cm^{-2} with a low detection limit of 0.02 μM (S/N=3). Viticoli and co-workers[200] showed that GOx immobilized on nanostructured TiO_2 thin film on a Si substrate could also achieve the direct voltammetric responses with electron transfer rate (k_s) as fast as 50 ±5 s. The biosensor based on GOx/TiO_2 thin film modified Si electrode was successfully employed for glucose detection without the use of any mediators, showing a fast response time of 7 s, low LOD of ~ 1 μM and linear range of 5~550 μM. Bao and colleagues[121] reported a mediator-free glucose biosensor by immobilizing GOx on anatase TiO_2 with uniformly mesoporous structure. The novel mesoporous TiO_2 synthesized by CNT template-assisted hydrothermal method exhibited a large specific surface area of 343 m^2 g^{-1} with a uniform pore-size distribution of 6-9 nm. GOx immobilized on the material achieved facile direct electrochemistry, as shown by a pair of well-defined redox peaks at the formal potential of FAD/$FADH_2$ and excellent electrocatalytic performance toward glucose without any mediators.

In addition to nanostructured TiO_2, the direct electron transfer of GOx on electrode surface could also be achieved by a few other oxide nanomaterials with unique structures. For example, Salimi et al reported that the DET of GOx could be achieved by co-deposition of the enzyme on NiO nanoparticles at the surface of glassy carbon electrode (GCE).[201] GOx immobilized on NiO nanoparticles displayed a pair of

well-defined and nearly reversible peaks at the formal potential of -0.42 V (vs. Ag/AgCl), with a heterogeneous electron transfer rate constant (k_s) of 25.2 ±0.5 s. The biosensor displayed a fast response time within 3 s upon the addition of glucose, with a sensitivity of 446.2 nA mM^{-1}, a LOD of 24 μM and a wide linear range from 30 μM to 5 mM. NiO hollow nanospheres were developed by Li et al. and adopted to construct a novel glucose biosensor by immobilizing GOx on their surfaces by a chitosan-assisted cross-linking technique.[202] Due to the high electrocatalytic activity and large amount of active sites on the NiO hollow nanospheres, the sensor exhibited a high sensitivity of 3.43 μA mM^{-1} and an estimated detection limit of 47 μM (S/N=3). The direct electron transfer feature of GOx was also observed by entrapping the enzyme and SWCNTs together in biologically derived silica, which provided a high electroactive surface area.[203] The voltammetry of the composite electrode displayed oxidation and reduction peaks at an optimal potential close to that of the $FAD/FADH_2$ co-factor. The immobilized enzyme could stably maintain its catalytic activity for glucose oxidation for a storage period of up to one month. A nanocomposite material of MWCNTs@SnO_2-Au was developed and demonstrated to immobilize GOx by Niu and co-workers.[204] The DET process was successfully achieved on the GOx/ MWCNTs@SnO_2-Au modified glassy carbon electrode. The constructed glucose sensor exhibited a wide linear range of 4.0~12.0 mM, which is quite suitable for clinical analysis of glucose concentration in human blood samples. ZnO nanoparticles electrodeposited on MWCNT have also been reported to facilitate the DET of immobilized GOx.[205]

2.3.3 Nanostructured Conducting Polymers

In the last few decades, conducting polymers, a kind of organic polymer possessing π-conjugated extended systems with low energy band gaps (the energy gap between LOMO and HOMO state) have attracted great attention due to their intrinsically conducting nature in a doped form and a potential substitution of traditional metallic and semiconducting materials[206-208]. These π-conjugated organic polymers, grown

electrochemically or chemically from their suitable monomers, have been intensively synthesized and successfully applied in various fields such as sensors, batteries, actuators and processing of electronic circuit boards.[209-214]

Among many conducting polymers studied, much attention has been paid to conducting polymers with low band gap and high conductivity. One typical example of such conducting polymers is polypyrrole (PPy), which is intensively applied for the design of bioelectronic devices due to its biocompatibility, chemical stability and ease of preparation.[215, 216] Such properties make PPy a suitable matrix to immobilize and facilitate direct electron transfer of redox proteins.[217-222] Aizawa[223] and Koopal[224] suggested the direct electron communication between GOx and PPy and developed mediatorless glucose sensors based on the GOx/PPy systems (Figure 2-10). However, the relatively high overpotential of the FAD/$FADH_2$ redox process indicates that the electron transfer was probably mediated by the oligometric pyrroles present on the polymer surface.[11] Guo et al reported the direct electron transfer of GOx and biosensing of glucose by using another conducting polymer, poly (3,4-ethylenedioxythiophene) (PEDOT) coated NiO hollow spheres.[225] The k_s of GOx immobilized on nanostructured PEDOT/NiO composite was calculated to be 6.5 s^{-1}, much larger than the 3.12 s^{-1} achieved by GOx on pure NiO hollow spheres. The sensor demonstrated the capability of mediatorless detection of glucose in nitrogen-saturated PBS, showing a linear range of up to 5 mM. In addition, when the modified electrode was employed for glucose measurement in air-saturated PBS, it exhibited a high sensitivity of 16.9 μA mM^{-1} cm^{-2}. Moreover, Cai and co-workers developed an amperometric glucose biosensor based on the DET of GOx by electrochemically entrapping GOx onto the inner wall of highly ordered polyaniline nanotubes (nanoPANi),[226] which were synthesized by using anodic aluminium oxide (AAO) as a template (Figure 2-11). CV study revealed that GOx immobilized on nanoPANi presented a pair of well-defined and nearly symmetric redox peaks at the formal potential of -0.405 V with an apparent electron transfer constant of 5.8 ± 1.6

s^{-1}, clearly indicating that GOx immobilized on nanoPANi underwent direct electron transfer reaction. Such mediatorless glucose sensors based on nanoPANi provided an ultrafast response time of ~3 s, a low LOD of 0.3±0.1 μM, a linear range of up to 5.5 mM and an extremely high sensitivity of 97.18±4.62 μA mM^{-1} cm^{-2}. In addition, due to the very low detection potential of -0.3 V, the biosensor exhibited excellent anti-interference performance for glucose detection in the presence of a variety of interfering molecules such as ascorbic acid (AA), uric acid (UA) and 4-acetamidophenol.

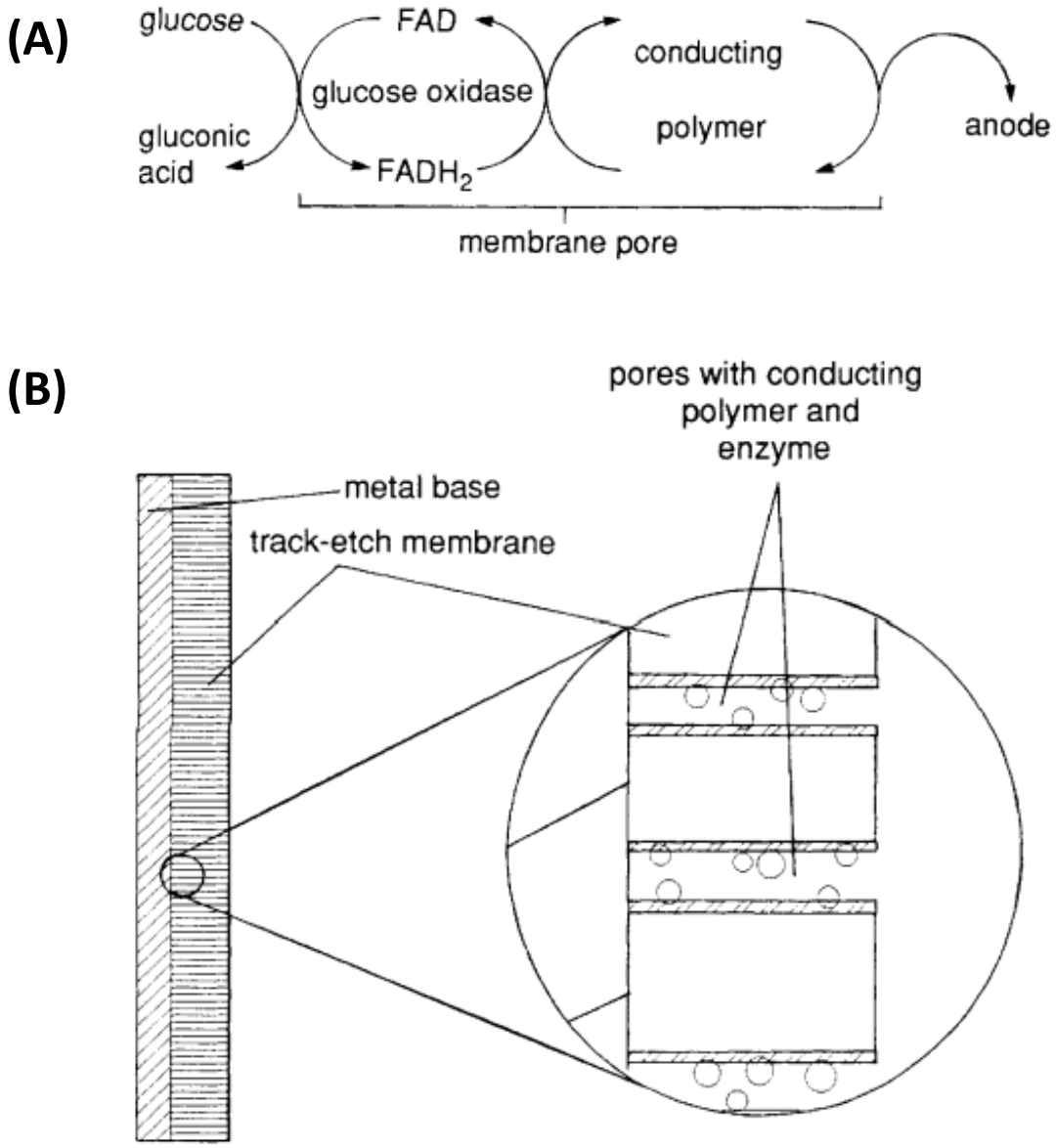

Figure 2-10. (A) Scheme showing the mechanism of DET between FAD and electrode via a conducting polymer. (B) Schematic representation of a microporous membrane/conducting

polymer based glucose biosensor. Ref. 224. Reprinted by permission of The Royal Society of Chemistry.

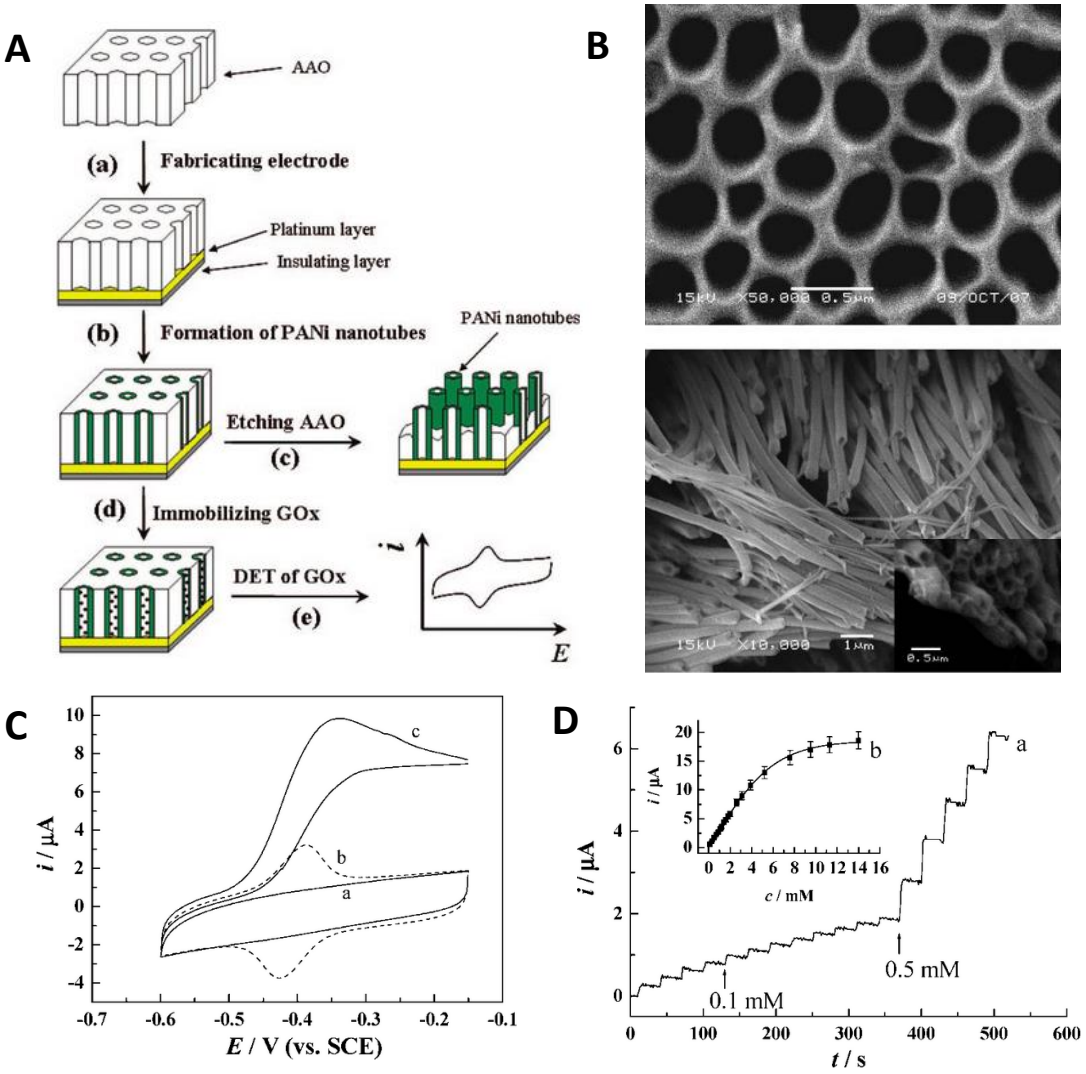

Figure 2-11. (A) Schematic diagram showing the process of synthesizing ordered PANi nanotubes with AAO as a template and electrochemically entrapping GOx in nanoPANi. (B) SEM images of AAO and obtained PANi nanotubes. (C) CVs of GOx/PANi-Pt electrode before and after addition of 5 mM glucose. (D) Amperometric performance and calibration curve (inset) of the glucose biosensor based on nanoPANi. Reprinted with permission from Ref. 226. Copyright 2009 American Chemical Society.

2.3.4 Carbon Nanomaterials

Carbon nanomaterials play significant roles in development of novel biosensing devices. This significance arises as they can help address some of the key issues: designing the biosensing interface so that the analyte selectively interacts with the biosensing surface; achieving efficient transduction of the biorecognition event;

increasing in the sensitivity and selectivity of the biosensor; and improving the response times in very sensitive systems. More specific challenges include: making biosensors compatible with biological matrices, so that they can be used in complex biological samples or even in vivo; fabricating viable biosensors that can operate within confined environments such as inside cells; and multiplexing biosensors so multiple analytes can be detected on one device.

Carbon nanotubes (CNTs), the all carbon hollow graphitic tubes, represent one of the best studied carbon nanomaterials[227, 228]. Generally, according to their structure, CNTs can be classified into two types: single-wall carbon nanotubes (SWCNT) and multi-wall carbon nanotubes (MWCNT). With a unique and fascinating one dimensional nanostructure, CNTs have high aspect ratios, high mechanical strength, high surface areas, ultra-light weight, excellent chemical and thermal stability, and rich electronic and optical properties [229]. The above amazing properties make CNTs important transducer materials in bioelectronic devices [230-234]. A large number of reports have shown that they could greatly promote the electron transfer of a number of proteins and enhance the electrochemical sensing performance of various of biomolecules.[235, 236] For example, Guiseppi-Elie et al. [237] reported on the direct electron transfer between SWCNT and the redox center of adsorbed GOx. Both FAD and GOx were found to spontaneously adsorb to annealed CNT that were cast onto the glassy-carbon surface to display quasi-reversible one-electron transfer. It was assumed that the tubular fibrils became positioned within a tunneling distance of the cofactors with little consequence to denaturation. Willner's group [238] demonstrated that aligned reconstituted GOx on the edge of SWCNT can be linked to an electrode surface. Such enzyme reconstitution on the end of CNT represents an extremely efficient approach for 'plugging' an electrode into GOx. Luong et al. [239] reported on the promoted electron transfer of GOx at a MWCNT-modified glassy-carbon electrode. Gooding [235] and Rusling [236] reported that aligned CNT 'forests' can act as molecular wires to allow electrical communication between the underlying electrode

and redox proteins (covalently attached to the ends of the SWCNT). Very recently, Stevenson and co-workers[240] studied the interfacial electron transfer of GOx at CNT and nitrogen-doped CNT (N-CNT). DET was observed for GOx absorbed on both CNT and N-CNT (Figure 2-12). Glucose biosensing was successfully conducted when an appropriate artificial redox mediator was placed in a buffer solution, or the natural redox mediator, oxygen, was used. Unfortunately, mediatorless glucose detection could not be achieved on GOx absorbed CNT/N-CNT electrodes.

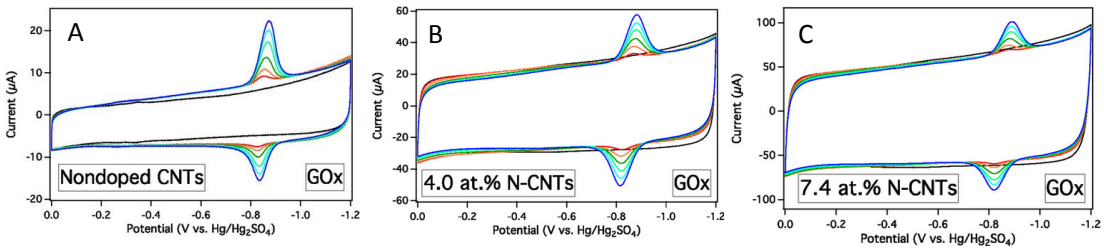

Figure 2-12. The direct electrochemistry of GOx observed on CNTs (A), 4.0 at.% nitrogen-doped CNTs (B) and 7.4 at.% nitrogen-doped CNTs (C). Reprinted with permission from Ref 240. Copyright 2013 The American Chemical Society.

Recently, graphene has attracted strong scientific and technological interest.[241-243] It has shown great promise in biosensor applications due to its unique physicochemical properties: high surface area (theoretically 2630 m^2 /g for single-layer graphene) [242, 243], excellent thermal conductivity [244] and electric conductivity [245], and strong mechanical strength [246]. Graphene-based electrodes have shown superior performance in terms of electrocatalytic activity [247] and macroscopic scale conductivity [248] compared to carbon nanotube-based ones. Graphene exhibits excellent electron transfer promoting ability for some enzymes and excellent catalytic behavior toward small biomolecules such as H_2O_2, NADH, which makes graphene extremely attractive for enzyme-based biosensors, e.g. glucose biosensors and ethanol biosensors. Shan et al. [249] and Kang et al. [250] reported the direct electrochemistry of glucose oxidase (GOx) on graphene. Shan et al. [249] reported the first graphene-based glucose biosensor with a graphene/polyethylenimine-functionalized ionic liquid nanocomposites modified electrode which exhibits wide linear glucose response (2 to 14 mM, R=0.994), good reproducibility (relative standard deviation of the current response to 6 mM glucose at

0.5 V was 3.2% for 10 successive measurements), and high stability (response current +4.9% after 1 week). Zhou et al. [251] reported a glucose biosensor based on chemically reduced graphene oxide (CR-GO). Graphene (CR-GO)-based biosensors exhibit substantially enhanced amperometric signals for sensing glucose: wide linear range (0.01 – 10 mM), high sensitivity (20.21 μA mM^{-1} cm^{-2}) and low detection limit of 2.00 mM (S/N=3). The response at the GOx/CR-GO/GC electrode to glucose is very fast (9 s to steady-state response) and highly stable (91% signal retention for 5 h), which makes the GOx/CR-GO/GC electrode a potentially fast and highly stable biosensor to continuously measure the plasma glucose level for the diagnosis of diabetes. Kang et al [250] employed biocompatible chitosan to disperse graphene and construct glucose biosensors. It was found that chitosan helped to form a well-dispersed graphene suspension and immobilize the enzyme molecules, and the graphene-based enzyme sensor exhibited excellent sensitivity (37.93 μA mM^{-1} cm^{-2}) and long-term stability for measuring glucose.

Outside of CNT and graphene, other kinds of carbon materials such as mesoporous carbon,[252-254] carbon black[255-258], carbon fiber[259, 260], and fullerenes[261] with good conductivities and large surface areas have also been used as functional electrode materials to immobilize enzymes. For example, Ma et al. used cetyltrimethylammonium bromide (CTAB) dispersed-carbon black powders as electrode materials to immobilize Hb and obtained a direct quasi-reversible electrochemical reaction with one-electron-reaction process coupled one-proton-transfer.[258]

2.4. Nanomaterials for Electrochemical Non-enzymatic Glucose Biosensors

2.4.1. Transition metals

Transition metals are known to be good electrocatalysts due to their ability to adopt multiple oxidation states and absorb other species on their surfaces to form intermediate and activate them in the reaction process. The advantages of

nanostructured metallic materials are their unique physical, chemical, optical and electrical properties[262-268] such as high surface-to-volume ratio, high index facets, large specific surface area, good electrical conductivity, tunable optical property and high electrocatalytic activity. Therefore, transition metal nanomaterials could serve as effective catalysts due to their high ratio of surface atoms with free valences to the cluster of total atoms and the resulting enhanced mass transport property. A wide range of transition metal nanomaterials have been studied in recent years for the electrocatalytic biosensing. According to the literatures, gold (Au), platinum (Pt), palladium (Pd), Copper (Cu) and Nickel (Ni) are the most intensively studied nanomaterials for non-enzymatic catalysis of glucose oxidation.

2.4.2. Metal oxides

2.4.2.1. Cobalt oxide

Cobaltous oxide (CoO), cobaltic oxide (Co_2O_3) and cobaltosic oxide (Co_3O_4) are three well known polymorphs of cobalt oxide. Cobalt oxide had not been explored for non-enzymatic electrochemical biosensing until the first study by Ding et al,[269] who investigated the mechanism of electrospun Co_3O_4 nanofibers (Co_3O_4 NF) toward electrocatalytic oxidation of glucose and employed Co_3O_4 NF/Nafion modified GCE for sensitive and selective glucose detection. Ding proposed that the catalytic property of as-synthesized Co_3O_4 NF towards glucose oxidation in alkaline solution was due to the redox reaction of $CoOOH/CoO_2$ at 0.59 V vs Ag/AgCl, and the mechanism of glucose electrochemical oxidation could be explained by the following equation:

$$2CoO_2 + C_6H_{12}O_6 \text{ (glucose)} \rightarrow 2CoOOH + C_6H_{10}O_6 \text{ (gluconolactone)} \quad (9)$$

The Co_3O_4 NF-based glucose sensor showed a fast response within 7 s, a high sensitivity of 36.25 μA mM^{-1} cm^{-2}, a detection limit of 0.97 μM with a linear range of up to 2.04 mM. Followed by this Co_3O_4 study, Kung et al[270] reported an acicular cobalt oxide nanorod (CoONRs) synthesized by chemical bath deposition for the non-enzymatic detection of glucose. The study claimed that CoONRs-modified electrode could selectively detect glucose without the casting of Nafion, a negatively

charged membrane capable of excluding negatively charged interferential molecules. The sensitivity and LOD of CoONRs-based glucose sensor are 571 .8 μA mM^{-1} cm^{-2} and 0.058 μM, which is 15 times higher and 10 times lower, respectively, than Ding's electrode. In addition, the biosensor also exhibited a wider linear range up to 3.5 mM and lower detection potential of 0.5 V than Ding's sensor. Simultaneously, Dong et al[271] reported a composite material of 3D graphene-cobalt oxide (Co_3O_4) nanowire as a freestanding electrode for non-enzymatic glucose sensing. The biosensor achieved a sensitivity of 3.39 mA mM cm^{-2} and a LOD of 25 nM, which are respectively nearly 6 times higher and 2 times lower than those of CoONRs-modified electrode in Kung's study. However, the up to 80 μM linear range of 3D graphene/Co_3O_4 nanowire electrode is much smaller than those of both Ding's and Kung's biosensors. Very recently, a graphene/cobalt oxide-based needle electrode has been reported by the same group of Dong.[272] The biosensor showed a capability for glucose detection in micro-droplets within the linear concentration range of 50 ~ 300 μM.

2.4.2.2 Copper oxide

Copper oxide seems to have been the most extensively studied metal oxide for non-enzymatic glucose biosensing in recent years.[273-286] The mechanism of glucose electrochemical oxidation on copper oxide electrodes is similar to that on Cu electrodes. Zhuang et al[287] fabricated a non-enzymatic glucose sensor based on CuO nanowires modified Cu electrode, which exhibited a substantially lower overpotential than bare Cu electrode toward glucose oxidation. At an applied potential of 0.33 V vs. Ag/AgCl, the biosensor showed a sensitivity of 490 μA mM, with a linear response over the concentration range from 0.4 μM to 2 mM, and LOD of 49 nM (σ=3). Similarly, Zhang et al[285] reported CuO nanowires and Wang et al[282] reported the CuO/Cu nanowire composite modified GCE for enzymeless glucose sensing. The former electrode achieved a fast response (<2s) with a low detection limit of 45 nM, while the latter biosensor exhibited a wide linear range from 0.1 to 12 mM for glucose detection. An enzymeless biosensor based on a flower-like Cu_xO modified Cu

electrode was investigated by Li.[277] The sensor achieved a high sensitivity of 1.62 mA mM cm^{-2} over the linear concentration range of up to 4 mM. Except for the nanowire structure, CuO nanofibers (CuO NF)[288] and CuO nanospherers[289] have also been investigated for the glucose electrocatalysis. However, it seems that the biosensing performance of CuO nanowire-modified electrodes outperform others. Additionally, Cu_2O nanoparticles (Cu_2O NPs) were decorated on MWCNTs to improve the sensitivity of copper oxide based biosensors.[286] In a study by Jiang,[290] CuO NPs modified-MWCNTs array electrode exhibited an extremely high sensitivity of 2.596 μA mM cm^{-2} over the concentration range up of up to 1.2 mM with a LOD of 0.2 μM. The CuO NP/MWCNT electrode also achieved a very fast response within 1 s upon the addition of 0.1 mM glucose.

2.4.2.3. Nickel oxide

The electrochemical glucose oxidation on NiO-modified electrode is based on the redox couple of $Ni(OH)_2$/NiOOH derived from NiO,[291] similar to that of Ni-based electrode. The reaction mechanism is indicated by the following equations:

$$NiO + OH^- \rightarrow Ni(OH)_2 \quad (10)$$

$$Ni(OH)_2 + OH^- \leftrightarrow NiOOH + H_2O + e^- \quad (11)$$

$$NiOOH + glucose \leftrightarrow Ni(OH)_2 + glucolactone \quad (12)$$

A variety of NiO nanomaterials have been reported in recent years by a number of groups for the study of nonenzymetic glucose sensing performance.[292-298] Mu and colleagues[291] have investigated the electrochemical properties and electroanalytical performance of nano-NiO modified CPE toward the oxidation of glucose. The biosensor showed a quick response to the glucose within 5 s and a calibration plot in the concentration range of 1 ~ 110 μM, with a sensitivity of 43.9 nA μM^{-1} and a LOD of 0.16 μM. NiO/MWCNT nanocomposite-based enzymeless glucose biosensors have been reported by Shamsipur[297] and Zhang[298]. MWCNT was found to remarkably improve the reactivity of NiO for glucose oxidation. Shamsipur's electrode showed a wide linear range of 0.2 mM ~ 20 mM with a LOD of 0.16 mM, while Zhang's

biosensor exhibited a high sensitivity of 1.77 mA mM cm^{-2} with linear range up to 7 mM and a LOD of 2 μM.

2.4.3 Alloys

A wide variety of alloy nanomaterials, including Pt-Pb,[299-302] Pt-Ru,[303, 304] Pt-Ir,[305] Pt-Ni,[306-308] Pt-Pd,[309] Au-Pt,[310-315] Au-Ag,[316] Au-Ru,[317] Au-Cu[318, 319] and Ni-Cu[320, 321] have been reported in recent years for non-enzymatic biosensing. Among them, Pt based alloy nanomaterials are most popular since they exhibit the highest catalytic activity toward the electrooxidation of small organic compounds.[322] Sun et al[300] compared alloys with different combinations of Pt, Pb, Au, Pd and Rh, and concluded that Pt and Pb comprise the best composition (i.e., Pt_2Pb) and achieved the highest catalytic activity for glucose oxidation. In addition to its higher sensitivity, Pt_2Pb also exhibited excellent selectivity because it could catalyse the oxidation of glucose at negative potentials, where most of the interferences including AA, UA and AP are not responsive. However, the Pt_2Pb electrode did not alleviate the problem of surface poisoning by chloride ions, which remains a critical challenge for non-enzymatic glucose sensors. The performance of Pt-Pb alloy based non-enzymatic glucose sensor was improved by Wang et al[301], who reported that the PtPb nanoporous network modified Ti electrode was highly resistant to the poisoning of chloride ions. In addition, the biosensor also exhibited excellent anti-interference properties since the nanoporous PtPb electrode was capable of amperometric sensing glucose at a remarkably low potential, ca. -80 mM (vs. Ag/AgCl) in PBS solution (pH 7.4). Similarly, Bai et al[299] synthesized PtPb nanowire for the non-enzymatic detection of glucose. The biosensor achieved a high sensitivity of 11.25 μA mM^{-1} cm^{-2} with a linear range of up to 11 mM and detection limit down to 8 μM (σ=3). The nonenzyamtic glucose sensor based on hybrid material of PtPb alloy nanoparticles and MWCNTs has also been reported.[302] Although the nanocomposite modified electrode achieved a slightly improved sensitivity of 18 μA mM^{-1} cm^{-2}, it was compromised with a shorter linear range of up to 5 mM. Interestingly, Xiao et al[304]

compared the non-enzymatic glucose sensing performance of PtM (M= Ru, Pd and Au) nanoparticles on the composite film of MWCNT/ionic liquid (IL) and found that PtRu (1:1)/MWCNT/IL modified GCE exhibited the strongest electrocatalytic activity toward glucose oxidation in neutral media. The biosensor achieved a linear range of up to 15 mM, with a sensitivity of 10.7 μA mM^{-1} cm^{-2} and LOD of 50 μM. The non-enzymatic glucose biosensor based on CNTs-supported PtRu alloy nanoparticles has also been investigated by Li and colleagues,[303] who reported a similar linear range to Xiao's work, but with a higher sensitivity of 28.26 μA mM^{-1} cm^{-2} and a lower LOD of 0.25 μM. On the other hand, the catalytic performances of Cu-based alloys of Ni, Fe and Mn have been investigated by Yeo.[320] It was observed that the anodic response of Mn_5Cu_{95} to glucose in 0.1 M NaOH solution is larger than other electrodes possibly due to the preadsorption of glucose molecules on Mn sites. A NiCu alloy based non-enzymatic glucose biosensor was also reported by Jafarian et al.[321] Unfortunately, the above mentioned Cu alloyed nanomaterials are not able to determine the glucose concentration in blood since they could not catalyse the glucose oxidation under physiological conditions. The recently reported 3D Au@nanoporous Cu (Au@NPC) core-shell composite material[319] promises to solve the biosensing problem associated with Cu-alloyed nanomaterials. As was observed, the Au@NPC alloy showed a strong oxidation peak of glucose in 0.1 M PBS (pH 7.4) and the nanocomposite modified GCE achieved a linear response for glucose oxidation in the range of 3 ~ 8 mM in PBS. Nevertheless, the previously reported Au-Cu nanoparticle alloy modified carbon electrode[318] did not show the feature of glucose sensing in neutral pH solution.

Reference

1. D. Thevenot, K. Toth and R. Durst, *Biosensors & Bioelectronics*, 2001, **16**, 121-131.
2. J. Wang, *Journal of Pharmaceutical and Biomedical Analysis*, 1999, **19**, 47-53.
3. B. M. Cullum, J. Mobley, J. S. Bogard, M. Moscovitch, G. W. Phillips and T. Vo-Dinh, *Analytical Chemistry*, 2000, **72**, 5612-5617.

4. S. S. Rosatto, R. S. Freire, N. Duran and L. T. Kubota, *Quimica Nova*, 2001, **24**, 77-86.
5. W. H. Scouten, J. H. T. Luong and R. S. Brown, *Trends in Biotechnology*, 1995, **13**, 178-185.
6. N. J. Ronkainen, H. B. Halsall and W. R. Heineman, *Chemical Society Reviews*, 2010, **39**, 1747-1763.
7. D. Grieshaber, R. MacKenzie, J. Voros and E. Reimhult, *Sensors*, 2008, **8**, 1400-1458.
8. A. Heller and B. Feldman, *Chemical Reviews*, 2008, **108**, 2482-2505.
9. A. Sato, K. Takagi, K. Kano, N. Kato, J. A. Duine and T. Ikeda, *Biochemical Journal*, 2001, **357**, 893-898.
10. J. D. Newman and A. P. F. Turner, *Biosensors & Bioelectronics*, 2005, **20**, 2435-2453.
11. J. Wang, *Chemical Reviews*, 2008, **108**, 814-825.
12. M. S. Steiner, A. Duerkop and O. S. Wolfbeis, *Chemical Society Reviews*, 2011, **40**, 4805-4839.
13. N. S. Oliver, C. Toumazou, A. E. G. Cass and D. G. Johnston, *Diabetic medicine*, 2009, **26**, 197-210.
14. V. V. Tuchin, *Handbook of Optical Sensing of Glucose in Biological Fluids and Tissues*, Taylor & Francis, 2010.
15. A. P. F. Turner, B. N. Chen and S. A. Piletsky, *Clinical Chemistry*, 1999, **45**, 1596-1601.
16. J. Wang, J. Liu, L. Chen and F. Lu, *Analytical Chemistry*, 1994, **66**, 3600-3603.
17. J. D. Newman, S. F. White, I. E. Tothill and A. P. F. Turner, *Analytical Chemistry*, 1995, **67**, 4594-4599.
18. J. K. Kirk and C. C. Rheney, *Journal of the American Pharmaceutical Association*, 1998, **38**, 210-219.
19. A. Heller, *Aiche Journal*, 2005, **51**, 1054-1066.
20. G. S. Wilson and R. Gifford, *Biosensors & Bioelectronics*, 2005, **20**, 2388-2403.
21. S. Deo, E. Moschou, S. Peteu, P. Eisenhardt, L. Bachas, M. Madou and S. Daunert, *Analytical Chemistry*, 2003, **75**, 207a-213a.
22. D. S. Bindra, Y. N. Zhang, G. S. Wilson, R. Sternberg, D. R. Thevenot, D. Moatti and G. Reach, *Analytical Chemistry*, 1991, **63**, 1692-1696.
23. E. Csoregi, D. W. Schmidtke and A. Heller, *Analytical Chemistry*, 1995, **67**, 1240-1244.
24. C. Henry, *Analytical Chemistry*, 1998, **70**, 594a-598a.
25. J. G. Wagner, D. W. Schmidtke, C. P. Quinn, T. F. Fleming, B. Bernacky and A. Heller, *Proceedings of the National Academy of Sciences of the United States of America*, 1998, **95**, 6379-6382.
26. D. W. Schmidtke, A. C. Freeland, A. Heller and R. T. Bonnecaze, *Proceedings of the National Academy of Sciences of the United States of America*, 1998, **95**, 294-299.
27. K. Rebrin and G. M. Steil, *Diabetes Technol Ther*, 2000, **2**, 461-472.

28. G. Reach and G. S. Wilson, *Analytical Chemistry*, 1992, **64**, A381-A386.
29. M. Shichiri, R. Kawamori, Y. Yamasaki, N. Hakui and H. Abe, *Lancet*, 1982, **2**, 1129-1131.
30. T. M. Gross, B. W. Bode, D. Einhorn, D. M. Kayne, J. H. Reed, N. H. White and J. J. Mastrototaro, *Diabetes Technol Ther*, 2000, **2**, 49-56.
31. B. Feldman, R. Brazg, S. Schwartz and R. Weinstein, *Diabetes Technol Ther*, 2003, **5**, 769-779.
32. M. Cox, *Journal of Pediatric Health Care*, 2009, **23**, 344-347.
33. Y. Hashiguchi, T. Uemura, M. Sakakida, K. Kajiwara, K. Nishida and M. Shichiri, *Diabetes Care*, 1994, **17**, 387-396.
34. A. Poscia, M. Mascini, D. Moscone, M. Luzzana, G. Caramenti, P. Cremonesi, F. Valgimigli, C. Bongiovanni and M. Varalli, *Biosensors & Bioelectronics*, 2003, **18**, 891-898.
35. E. Csöregi, T. Laurell, I. Katakis, A. Heller and L. Gorton, *Microchimica Acta*, 1995, **121**, 31-40.
36. F. J. Schmidt, W. J. Sluiter and A. J. Schoonen, *Diabetes Care*, 1993, **16**, 695-700.
37. F. J. Schmidt, A. L. Aalders, A. J. Schoonen and H. Doorenbos, *Int J Artif Organs*, 1992, **15**, 55-61.
38. M. Mascini, D. Moscone and L. Bernardi, *Sensors and Actuators B: Chemical*, 1992, **6**, 143-145.
39. D. Moscone, M. Pasini and M. Mascini, *Talanta*, 1992, **39**, 1039-1044.
40. C. Meyerhoff, F. Bischof, F. J. Mennel, F. Sternberg and E. F. Pfeiffer, *Int J Artif Organs*, 1993, **16**, 268-275.
41. F. Palmisano, D. Centonze, A. Guerrieri and P. G. Zambonin, *Biosensors and Bioelectronics*, 1993, **8**, 393-399.
42. Y. Hashiguchi, M. Sakakida, K. Nishida, T. Uemura, K. Kajiwara and M. Shichiri, *Diabetes Care*, 1994, **17**, 387-396.
43. B. C. Towe and V. B. Pizziconi, *Biosensors and Bioelectronics*, 1997, **12**, 893-899.
44. T. Vering, S. Adam, H. Drewer, C. Dumschat, R. Steinkuhl, M. Knoll, A. Schulze and E. G. Siegel, *Analyst*, 1998, **123**, 1605-1609.
45. L. K. Summers, M. L. Clark, S. M. Humphreys, J. Bugler and K. N. Frayn, *Horm Metab Res*, 1999, **31**, 424-428.
46. H. L. Lutgers, L. M. Hullegie, K. Hoogenberg, W. J. Sluiter, R. P. Dullaart, K. J. Wientjes and A. J. Schoonen, *Neth J Med*, 2000, **57**, 7-12.
47. U. Hoss, B. Kalatz, R. Gessler, H. J. Pfleiderer, E. Andreis, M. Rutschmann, H. Rinne, M. Schoemaker, C. Haug and R. D. Fussgaenger, *Diabetes Technol Ther*, 2001, **3**, 237-243.
48. A. Maran, C. Crepaldi, A. Tiengo, G. Grassi, E. Vitali, G. Pagano, S. Bistoni, G. Calabrese, F. Santeusanio, F. Leonetti, M. Ribaudo, U. Di Mario, G. Annuzzi, S. Genovese, G. Riccardi, M. Previti, D. Cucinotta, F. Giorgino, A. Bellomo, R. Giorgino, A. Poscia and M. Varalli, *Diabetes Care*, 2002, **25**, 347-352.
49. A. Poscia, M. Mascini, D. Moscone, M. Luzzana, G. Caramenti, P. Cremonesi, F.

Valgimigli, C. Bongiovanni and M. Varalli, *Biosensors and Bioelectronics*, 2003, **18**, 891-898.
50. K. J. Wientjes, U. Grob, A. Hattemer, K. Hoogenberg, K. Jungheim, C. Kapitza and A. J. Schoonen, *Diabetes Technol Ther*, 2003, **5**, 615-620.
51. F. Ricci, D. Moscone, C. S. Tuta, G. Palleschi, A. Amine, A. Poscia, F. Valgimigli and D. Messeri, *Biosensors & Bioelectronics*, 2005, **20**, 1993-2000.
52. I. M. Wentholt, M. A. Vollebregt, A. A. Hart, J. B. Hoekstra and J. H. DeVries, *Diabetes Care*, 2005, **28**, 2871-2876.
53. C. Fayolle, J. F. Brun, J. Bringer, J. Mercier and E. Renard, *Diabetes Metab*, 2006, **32**, 313-320.
54. T. Kubiak, B. Worle, B. Kuhr, I. Nied, G. Glasner, N. Hermanns, B. Kulzer and T. Haak, *Diabetes Technol Ther*, 2006, **8**, 570-575.
55. P. Rossetti, F. Porcellati, C. G. Fanelli and G. B. Bolli, *Diabetes Technol Ther*, 2006, **8**, 326-337.
56. F. Ricci, F. Caprio, A. Poscia, F. Valgimigli, D. Messeri, E. Lepori, G. Dall'Oglio, G. Palleschi and D. Moscone, *Biosensors & Bioelectronics*, 2007, **22**, 2032-2039.
57. H. Langemann, A. Mendelowitsch, H. Landolt, B. Alessandri and O. Gratzl, *Clinical Neurology and Neurosurgery*, 1995, **97**, 149-155.
58. U. Beyer, D. Schäfer, A. Thomas, H. Aulich, U. Haueter, B. Reihl and R. Ehwald, *Diabetologia*, 2001, **44**, 416-423.
59. G. Freckmann, B. Kalatz, B. Pfeiffer, U. Hoss and C. Haug, *Exp Clin Endocrinol Diabetes*, 2001, **109**, S347-S357.
60. R. M. Rhemrev-Boom, R. G. Tiessen, A. A. Jonker, K. Venema, P. Vadgama and J. Korf, *Clinica Chimica Acta*, 2002, **316**, 1-10.
61. A. Maran, C. Crepaldi, A. Tiengo, G. Grassi, E. Vitali, G. Pagano, S. Bistoni, G. Calabrese, F. Santeusanio, F. Leonetti, M. Ribaudo, U. Di Mario, G. Annuzzi, S. Genovese, G. Riccardi, M. Previti, D. Cucinotta, F. Giorgino, A. Bellomo, R. Giorgino, A. Poscia and M. Varalli, *Diabetes Care*, 2002, **25**, 347-352.
62. G. Sparacino, F. Zanderigo, S. Corazza, A. Maran, A. Facchinetti and C. Cobelli, *IEEE Trans Biomed Eng*, 2007, **54**, 931-937.
63. M. Schoemaker, E. Andreis, J. Roper, R. Kotulla, V. Lodwig, K. Obermaier, P. Stephan, W. Reuschling, M. Rutschmann, R. Schwaninger, U. Wittmann, H. Rinne, H. Kontschieder and W. Strohmeier, *Diabetes Technol Ther*, 2003, **5**, 599-608.
64. J. K. Nielsen, G. Freckmann, C. Kapitza, G. Ocvirk, K. H. Koelker, U. Kamecke, R. Gillen, I. Amann-Zalan, N. Jendrike, J. S. Christiansen, T. Koschinsky and L. Heinemann, *Diabetic medicine*, 2009, **26**, 714-721.
65. D. C. Klonoff, *Diabetes Care*, 1997, **20**, 433-437.
66. M. J. Tierney, H. L. Kim, M. D. Burns, J. A. Tamada and R. O. Potts, *Electroanalysis*, 2000, **12**, 666-671.
67. R. T. Kurnik, B. Berner, J. Tamada and R. O. Potts, *Journal of The Electrochemical Society*, 1998, **145**, 4119-4125.
68. *Diabetes Technol Ther*, 2003, **5**, 791-800.

69. *Diabetes Technol Ther*, 2003, **5**, 781-789.
70. H. P. Chase, R. Beck, W. Tamborlane, B. Buckingham, N. Mauras, E. Tsalikian, T. Wysocki, S. Weinzimer, C. Kollman, K. Ruedy and D. Xing, *Diabetes Care*, 2005, **28**, 1101-1106.
71. S. Boeckle, R. R. Ansari, L. Rovati, J. F. King and K. I. Suh, *Investigative Ophthalmology & Visual Science*, 2004, **45**, U494-U494.
72. M. J. Goetz, G. L. Cote, R. Erckens, W. March and M. Motamedi, *Ieee Transactions on Biomedical Engineering*, 1995, **42**, 728-731.
73. I. Gabriely, R. Wozniak, M. Mevorach, J. Kaplan, Y. Aharon and H. Shamoon, *Diabetes Care*, 1999, **22**, 2026-2032.
74. H. A. MacKenzie, H. S. Ashton, S. Spiers, Y. C. Shen, S. S. Freeborn, J. Hannigan, J. Lindberg and P. Rae, *Clinical Chemistry*, 1999, **45**, 1587-1595.
75. K. V. Larin, M. S. Eledrisi, M. Motamedi and R. O. Esenaliev, *Diabetes Care*, 2002, **25**, 2263-2267.
76. B. R. Eggins, *Chemical sensors and biosensors*, Wiley, 2008.
77. J. Wang, *Analytical electrochemistry*, Wiley-VCH, 2006.
78. N. J. Ronkainen-Matsuno, J. H. Thomas, H. B. Halsall and W. R. Heineman, *TrAC Trends in Analytical Chemistry*, 2002, **21**, 213-225.
79. A. Brajter-Toth and J. Chambers, *Electroanalytical Methods of Biological Materials*, CRC Press, 2002.
80. H. Yao, S. H. Jenkins, A. J. Pesce, H. B. Halsall and W. R. Heineman, *Clinical Chemistry*, 1993, **39**, 1432-1434.
81. P. T. Kissinger and W. R. Heineman, *Laboratory techniques in electroanalytical chemistry*, CRC press, 1996.
82. P. N. Bartlett, *Bioelectrochemistry: fundamentals, experimental techniques and applications*, Wiley, 2008.
83. M. Trojanowicz, M. Szewczynska and M. Wcislo, *Electroanalysis*, 2003, **15**, 347-365.
84. C. A. Wijayawardhana, H. B. Halsall and W. R. Heineman, *Analytica Chimica Acta*, 1999, **399**, 3-11.
85. C. A. Wijayawardhana, S. Purushothama, M. A. Cousino, H. B. Halsall and W. R. Heineman, *Journal of Electroanalytical Chemistry*, 1999, **468**, 2-8.
86. R. Puchades and A. Maquieira, *Critical Reviews in Analytical Chemistry*, 1996, **26**, 195-218.
87. T. Jiang, H. B. Halsall, W. R. Heineman, T. Giersch and B. Hock, *Journal of Agricultural and Food Chemistry*, 1995, **43**, 1098-1104.
88. W. Lorenz and K. D. Schulze, *Journal of Electroanalytical Chemistry and Interfacial Electrochemistry*, 1975, **65**, 141-153.
89. E. A. H. Hall, N. G. Skinner, C. Jung and S. Szunerits, *Electroanalysis*, 1995, **7**, 830-837.
90. F. Patolsky, M. Zayats, E. Katz and I. Willner, *Analytical Chemistry*, 1999, **71**, 3171-3180.

91. I. I. Suni, *TrAC Trends in Analytical Chemistry*, 2008, **27**, 604-611.
92. E. Katz and I. Willner, *Electroanalysis*, 2003, **15**, 913-947.
93. C. Chen, Q. Xie, D. Yang, H. Xiao, Y. Fu, Y. Tan and S. Yao, *RSC Advances*, 2013, **3**, 4473-4491.
94. L. C. Clark Jr and C. Lyons, *Annals of the New York Academy of Sciences*, 1962, **102**, 29-45.
95. S. R. Mikkelsen and E. Cortón, *Bioanalytical chemistry*, LibreDigital, 2004.
96. S. J. Updike and G. P. Hicks, *Nature*, 1967, **214**, 986-988.
97. Guilbaul.Gg and G. J. Lubrano, *Analytica Chimica Acta*, 1973, **64**, 439-455.
98. A. E. G. Cass, G. Davis, G. D. Francis, H. A. O. Hill, W. J. Aston, I. J. Higgins, E. V. Plotkin, L. D. L. Scott and A. P. F. Turner, *Analytical Chemistry*, 1984, **56**, 667-671.
99. P. D. Hale, T. Inagaki, H. I. Karan, Y. Okamoto and T. A. Skotheim, *Journal of the American Chemical Society*, 1989, **111**, 3482-3484.
100. J. Wang, *Chemical Reviews*, 2007, **108**, 814-825.
101. J. P. Liu, C. X. Guo, C. M. Li, Y. Y. Li, Q. B. Chi, X. T. Huang, L. Liao and T. Yu, *Electrochemistry Communications*, 2009, **11**, 202-205.
102. Y. Xiao, F. Patolsky, E. Katz, J. F. Hainfeld and I. Willner, *Science*, 2003, **299**, 1877-1881.
103. J. A. Camarero, *Biopolymers*, 2008, **90**, 450-458.
104. E. Barendrecht, *Journal of Applied Electrochemistry*, 1990, **20**, 175-185.
105. R. J. Chen, Y. G. Zhang, D. W. Wang and H. J. Dai, *Journal of the American Chemical Society*, 2001, **123**, 3838-3839.
106. D. G. Castner and B. D. Ratner, *Surface Science*, 2002, **500**, 28-60.
107. A. Bernard, E. Delamarche, H. Schmid, B. Michel, H. R. Bosshard and H. Biebuyck, *Langmuir*, 1998, **14**, 2225-2229.
108. A. S. Blawas and W. M. Reichert, *Biomaterials*, 1998, **19**, 595-609.
109. T. Kodadek, *Chemistry & Biology*, 2001, **8**, 105-115.
110. J. Lahiri, E. Ostuni and G. M. Whitesides, *Langmuir*, 1999, **15**, 2055-2060.
111. S. Andreescu and J. L. Marty, *Biomolecular Engineering*, 2006, **23**, 1-15.
112. S. K. Arya, M. Datta and B. D. Malhotra, *Biosensors and Bioelectronics*, 2008, **23**, 1083-1100.
113. M. M. F. Choi, *Microchimica Acta*, 2004, **148**, 107-132.
114. A. Sassolas, L. J. Blum and B. D. Leca-Bouvier, *Biotechnology Advances*, 2012, **30**, 489-511.
115. F. Rusmini, Z. Y. Zhong and J. Feijen, *Biomacromolecules*, 2007, **8**, 1775-1789.
116. M. A. Rahman, H. B. Noh and Y. B. Shim, *Analytical Chemistry*, 2008, **80**, 8020-8027.
117. A. Zabet-Khosousi and A. A. Dhirani, *Chemical Reviews*, 2008, **108**, 4072-4124.
118. M. E. Aubin-Tam and K. Hamad-Schifferli, *Biomedical Materials*, 2008, **3**.
119. A. F. Loftus, K. P. Reighard, S. A. Kapourales and M. C. Leopold, *Journal of the American Chemical Society*, 2008, **130**, 1649-1661.
120. Y. Liu, S. Wu, H. X. Ju and L. Xu, *Electroanalysis*, 2007, **19**, 986-992.

121. S. J. Bao, C. M. Li, J. F. Zang, X. Q. Cui, Y. Qiao and J. Guo, *Advanced Functional Materials*, 2008, **18**, 591-599.
122. Z. Y. Tang, Y. Wang, P. Podsiadlo and N. A. Kotov, *Advanced Materials*, 2006, **18**, 3203-3224.
123. Y. Lvov, K. Ariga and T. Kunitake, *Chemistry Letters*, 1994, 2323-2326.
124. X. P. Jiang and P. T. Hammond, *Langmuir*, 2000, **16**, 8501-8509.
125. R. J. Pei, X. Q. Cui, X. R. Yang and E. K. Wang, *Biomacromolecules*, 2001, **2**, 463-468.
126. J. Zhang, M. Feng and H. Tachikawa, *Biosensors & Bioelectronics*, 2007, **22**, 3036-3041.
127. G. X. Wang, Y. Liu and N. F. Hu, *Electrochimica Acta*, 2007, **53**, 2071-2079.
128. N. Kobko, L. Paraskevas, E. del Rio and J. J. Dannenberg, *Journal of the American Chemical Society*, 2001, **123**, 4348-4349.
129. Y. Osawa and L. R. Pohl, *Chemical Research in Toxicology*, 1989, **2**, 131-141.
130. J. H. Gu, C. M. Yam, S. Li and C. Z. Cai, *Journal of the American Chemical Society*, 2004, **126**, 8098-8099.
131. D. Barriet, C. M. Yam, O. E. Shmakova, A. C. Jamison and T. R. Lee, *Langmuir*, 2007, **23**, 8866-8875.
132. K. Y. Jiang, L. S. Schadler, R. W. Siegel, X. J. Zhang, H. F. Zhang and M. Terrones, *Journal of Materials Chemistry*, 2004, **14**, 37-39.
133. M. P. Lutolf and J. A. Hubbell, *Biomacromolecules*, 2003, **4**, 713-722.
134. S. C. Rizzi and J. A. Hubbell, *Biomacromolecules*, 2005, **6**, 1226-1238.
135. Y. T. Kong, M. Boopathi and Y. B. Shim, *Biosensors & Bioelectronics*, 2003, **19**, 227-232.
136. Y. H. Wu and S. S. Hu, *Microchimica Acta*, 2007, **159**, 1-17.
137. L. M. Ellerby, C. R. Nishida, F. Nishida, S. A. Yamanaka, B. Dunn, J. S. Valentine and J. I. Zink, *Science*, 1992, **255**, 1113-1115.
138. B. C. Dave, B. Dunn, J. S. Valentine and J. I. Zink, *Analytical Chemistry*, 1994, **66**, A1120-A1127.
139. T. K. Das, I. Khan, D. L. Rousseau and J. M. Friedman, *Journal of the American Chemical Society*, 1998, **120**, 10268-10269.
140. Q. L. Wang, G. X. Lu and B. J. Yang, *Langmuir*, 2004, **20**, 1342-1347.
141. Q. L. Wang, G. X. Lu and B. J. Yang, *Biosensors & Bioelectronics*, 2004, **19**, 1269-1275.
142. B. Munge, S. K. Das, R. Ilagan, Z. Pendon, J. Yang, H. A. Frank and J. F. Rusling, *Journal of the American Chemical Society*, 2003, **125**, 12457-12463.
143. A. E. F. Nassar, W. S. Willis and J. F. Rusling, *Analytical Chemistry*, 1995, **67**, 2386-2392.
144. U. Lange, N. V. Roznyatouskaya and V. M. Mirsky, *Analytica Chimica Acta*, 2008, **614**, 1-26.
145. J. G. Bokria, A. Kumar, V. Seshadri, A. Tran and G. A. Sotzing, *Advanced Materials*, 2008, **20**, 1175-+.

146. B. V. C. Martins, G. Brunetto, F. Sato, V. R. Coluci and D. S. Galvao, *Chemical Physics Letters*, 2008, **453**, 290-295.
147. Q. Lu and C. M. Li, *Biosensors & Bioelectronics*, 2008, **24**, 767-772.
148. A. Ramanavicius, A. Kausaite and A. Ramanaviciene, *Biosensors & Bioelectronics*, 2005, **20**, 1962-1967.
149. J. H. Pei, F. Tian and T. Thundat, *Analytical Chemistry*, 2004, **76**, 292-297.
150. T. Kong, Y. Chen, Y. P. Ye, K. Zhang, Z. X. Wang and X. P. Wang, *Sensors and Actuators B-Chemical*, 2009, **138**, 344-350.
151. Y. Yonemori, E. Takahashi, H. F. Ren, T. Hayashi and H. Endo, *Analytica Chimica Acta*, 2009, **633**, 90-96.
152. D. Pletcher, *Journal of Applied Electrochemistry*, 1984, **14**, 403-415.
153. L. D. Burke, *Electrochimica Acta*, 1994, **39**, 1841-1848.
154. M. C. Daniel and D. Astruc, *Chemical Reviews*, 2004, **104**, 293-346.
155. M. A. El-Sayed, *Accounts of Chemical Research*, 2001, **34**, 257-264.
156. Y. G. Sun and Y. N. Xia, *Science*, 2002, **298**, 2176-2179.
157. B. Wiley, Y. G. Sun, B. Mayers and Y. N. Xia, *Chemistry-a European Journal*, 2005, **11**, 454-463.
158. Y. G. Sun and Y. N. Xia, *Analyst*, 2003, **128**, 686-691.
159. J. Y. Chen, B. J. Wiley and Y. N. Xia, *Langmuir*, 2007, **23**, 4120-4129.
160. X. G. Hu and S. J. Dong, *Journal of Materials Chemistry*, 2008, **18**, 1279-1295.
161. J. Zhao, R. W. Henkens, J. Stonehuerner, J. P. O'Daly and A. L. Crumbliss, *Journal of Electroanalytical Chemistry*, 1992, **327**, 109-119.
162. R. G. Freeman, K. C. Grabar, K. J. Allison, R. M. Bright, J. A. Davis, A. P. Guthrie, M. B. Hommer, M. A. Jackson, P. C. Smith, D. G. Walter and M. J. Natan, *Science*, 1995, **267**, 1629-1632.
163. K. C. Grabar, R. G. Freeman, M. B. Hommer and M. J. Natan, *Analytical Chemistry*, 1995, **67**, 735-743.
164. J. M. Pingarrón, P. Yáñez-Sedeño and A. González-Cortés, *Electrochimica Acta*, 2008, **53**, 5848-5866.
165. S. Q. Liu, D. Leech and H. X. Ju, *Analytical Letters*, 2003, **36**, 1-19.
166. M. H. Rashid, R. R. Bhattacharjee, A. Kotal and T. K. Mandal, *Langmuir*, 2006, **22**, 7141-7143.
167. F. Li, Z. Wang, C. Shan, J. Song, D. Han and L. Niu, *Biosensors and Bioelectronics*, 2009, **24**, 1765-1770.
168. D. Ragupathy, A. I. Gopalan and K.-P. Lee, *Electrochemistry Communications*, 2009, **11**, 397-401.
169. S. X. Zhang, N. Wang, Y. M. Niu and C. Q. Sun, *Sensors and Actuators B-Chemical*, 2005, **109**, 367-374.
170. I. Willner and B. Willner, *Nano Letters*, 2010, **10**, 3805-3815.
171. J. T. Holland, C. Lau, S. Brozik, P. Atanassov and S. Banta, *Journal of the American Chemical Society*, 2011, **133**, 19262-19265.

172. S. Zhao, K. Zhang, Y. Bai, W. W. Yang and C. Q. Sun, *Bioelectrochemistry*, 2006, **69**, 158-163.
173. C. C. Qiu, X. Wang, X. Y. Liu, S. F. Hou and H. Y. Ma, *Electrochimica Acta*, 2012, **67**, 140-146.
174. R. Khan and M. Dhayal, *Electrochemistry Communications*, 2008, **10**, 263-267.
175. Y. F. Li, Z. M. Liu, Y. L. Liu, Y. H. Yang, G. L. Shen and R. Q. Yu, *Analytical Biochemistry*, 2006, **349**, 33-40.
176. U. Bach, D. Lupo, P. Comte, J. E. Moser, F. Weissortel, J. Salbeck, H. Spreitzer and M. Gratzel, *Nature*, 1998, **395**, 583-585.
177. B. Oregan and M. Gratzel, *Nature*, 1991, **353**, 737-740.
178. A. Fujishima and K. Honda, *Nature*, 1972, **238**, 37-38.
179. G. K. Mor, K. Shankar, M. Paulose, O. K. Varghese and C. A. Grimes, *Nano Letters*, 2005, **5**, 191-195.
180. M. Gratzel, *Nature*, 2001, **409**, 575-576.
181. A. Hagfeldt and M. Gratzel, *Chemical Reviews*, 1995, **95**, 49-68.
182. J. S. Chen, Y. L. Tan, C. M. Li, Y. L. Cheah, D. Luan, S. Madhavi, F. Y. C. Boey, L. A. Archer and X. W. Lou, *Journal of the American Chemical Society*, 2010, **132**, 6124-6130.
183. S. J. Ding, J. S. Chen, D. Y. Luan, F. Y. C. Boey, S. Madhavi and X. W. Lou, *Chemical Communications*, 2011, **47**, 5780-5782.
184. H. Zhou, L. Liu, K. Yin, S. L. Liu and G. X. Li, *Electrochemistry Communications*, 2006, **8**, 1168-1172.
185. A. Curulli, E. Valentini, G. Padeletti, A. Viticoli, D. Caschera and G. Palleschi, *Sensors and Actuators B-Chemical*, 2005, **111**, 441-449.
186. O. K. Varghese, D. W. Gong, M. Paulose, K. G. Ong, E. C. Dickey and C. A. Grimes, *Advanced Materials*, 2003, **15**, 624-627.
187. C. A. Grimes, K. G. Ong, O. K. Varghese, X. P. Yang, G. Mor, M. Paulose, E. C. Dickey, C. M. Ruan, M. V. Pishko, J. W. Kendig and A. J. Mason, *Sensors*, 2003, **3**, 69-82.
188. H. Miyazaki, T. Hyodo, Y. Shimizu and M. Egashira, *Sensors and Actuators B-Chemical*, 2005, **108**, 467-472.
189. S. Q. Liu and A. C. Chen, *Langmuir*, 2005, **21**, 8409-8413.
190. E. Topoglidis, C. J. Campbell, A. E. G. Cass and J. R. Durrant, *Langmuir*, 2001, **17**, 7899-7906.
191. H. M. Cao, Y. H. Zhu, L. H. Tang, X. L. Yang and C. Z. Li, *Electroanalysis*, 2008, **20**, 2223-2228.
192. S. U. M. Khan, M. Al-Shahry and W. B. Ingler, *Science*, 2002, **297**, 2243-2245.
193. J. C. Yu, J. G. Yu, W. K. Ho, Z. T. Jiang and L. Z. Zhang, *Chemistry of Materials*, 2002, **14**, 3808-3816.
194. E. L. Crepaldi, G. Soler-Illia, D. Grosso, F. Cagnol, F. Ribot and C. Sanchez,

Journal of the American Chemical Society, 2003, **125**, 9770-9786.
195. H. Zhou, X. Gan, J. Wang, X. L. Zhu and G. X. Li, *Analytical Chemistry*, 2005, **77**, 6102-6104.
196. H. Song, G. Q. Wu, Z. G. Zhang, Z. Huang and Z. J. Ruan, *Materials Letters*, 2006, **60**, 3385-3389.
197. X. Chen and S. S. Mao, *Chemical Reviews*, 2007, **107**, 2891-2959.
198. D. E. MacDonald, N. Deo, B. Markovic, M. Stranick and P. Somasundaran, *Biomaterials*, 2002, **23**, 1269-1279.
199. P. Si, S. J. Ding, J. Yuan, X. W. Lou and D. H. Kim, *ACS Nano*, 2011, **5**, 7617-7626.
200. A. Viticoli, A. Curulli, A. Cusma, S. Kaciulis, S. Nunziante, L. Pandolfi, F. Valentini and G. Padeletti, *Materials Science & Engineering C-Biomimetic and Supramolecular Systems*, 2006, **26**, 947-951.
201. A. Salimi, E. Sharifi, A. Noorbakhsh and S. Soltanian, *Biosensors & Bioelectronics*, 2007, **22**, 3146-3153.
202. C. C. Li, Y. L. Liu, L. M. Li, Z. F. Du, S. J. Xu, M. Zhang, X. M. Yin and T. H. Wang, *Talanta*, 2008, **77**, 455-459.
203. D. Ivnitski, K. Artyushkova, R. A. Rincon, P. Atanassov, H. R. Luckarift and G. R. Johnson, *Small*, 2008, **4**, 357-364.
204. F. H. Li, J. X. Song, F. Li, X. D. Wang, Q. X. Zhang, D. X. Han, A. Ivaska and L. Niu, *Biosensors & Bioelectronics*, 2009, **25**, 883-888.
205. F. X. Hu, S. H. Chen, C. Y. Wang, R. Yuan, Y. Q. Chai, Y. Xiang and C. Wang, *Journal of Molecular Catalysis B-Enzymatic*, 2011, **72**, 298-304.
206. A. J. Heeger, S. Kivelson, J. R. Schrieffer and W. P. Su, *Reviews of Modern Physics*, 1988, **60**, 781-850.
207. A. O. Patil, A. J. Heeger and F. Wudl, *Chemical Reviews*, 1988, **88**, 183-200.
208. G. Inzelt, M. Pineri, J. W. Schultze and M. A. Vorotyntsev, *Electrochimica Acta*, 2000, **45**, 2403-2421.
209. M. Gerard, A. Chaubey and B. D. Malhotra, *Biosensors & Bioelectronics*, 2002, **17**, 345-359.
210. J. Janata and M. Josowicz, *Nature Materials*, 2003, **2**, 19-24.
211.V. Saxena and B. D. Malhotra, *Current Applied Physics*, 2003, **3**, 293-305.
212. S. V. Frolov, A. Fujii, D. Chinn, Z. V. Vardeny, K. Yoshino and R. V. Gregory, *Applied Physics Letters*, 1998, **72**, 2811-2813.
213. T. F. Otero and J. M. Sansinena, *Advanced Materials*, 1998, **10**, 491-+.
214. M. Kryszewski and J. K. Jeszka, *Synthetic Metals*, 1998, **94**, 99-104.
215. H. KorriYoussoufi, F. Garnier, P. Srivastava, P. Godillot and A. Yassar, *Journal of the American Chemical Society*, 1997, **119**, 7388-7389.
216. T. A. Skotheim, H. S. Lee, P. D. Hale, H. I. Karan, Y. Okamoto, L. Samuelson and S. Tripathy, *Synthetic Metals*, 1991, **42**, 1433-1437.
217. Z. Q. Tong, R. Yuan, Y. Q. Chai, Y. Xie and S. H. Chen, *Journal of Biotechnology*, 2007, **128**, 567-575.

218. J. Haccoun, B. Piro, V. Noel and M. C. Pham, *Bioelectrochemistry*, 2006, **68**, 218-226.
219. V. Laurinavicius, J. Razumiene, A. Ramanavicius and A. D. Ryabov, *Biosensors & Bioelectronics*, 2004, **20**, 1217-1222.
220. J. C. Vidal, E. Garcia-Ruiz and J. R. Castillo, *Microchimica Acta*, 2003, **143**, 93-111.
221. W. Schuhmann, H. Zimmermann, K. V. Habermuller and V. Laurinavicius, *Faraday Discussions*, 2000, **116**, 245-255.
222. A. Ramanavicius, K. Habermuller, E. Csoregi, V. Laurinavicius and W. Schuhmann, *Analytical Chemistry*, 1999, **71**, 3581-3586.
223. S.-i. Yabuki, H. Shinohara and M. Aizawa, *Journal of the Chemical Society, Chemical Communications*, 1989, **0**, 945-946.
224. C. G. J. Koopal, B. de Ruiter and R. J. M. Nolte, *Journal of the Chemical Society, Chemical Communications*, 1991, **0**, 1691-1692.
225. C. X. Guo and C. M. Li, *Physical Chemistry Chemical Physics*, 2010, **12**, 12153-12159.
226. Z. Y. Wang, S. N. Liu, P. Wu and C. X. Cai, *Analytical Chemistry*, 2009, **81**, 1638-1645.
227. A. Galano, *Chemical Physics*, 2006, **327**, 159-170.
228. G. Pagona and N. Tagmatarchis, *Current Medicinal Chemistry*, 2006, **13**, 1789-1798.
229. D. Tasis, N. Tagmatarchis, A. Bianco and M. Prato, *Chemical Reviews*, 2006, **106**, 1105-1136.
230. X. B. Ji, C. E. Banks, G. Hu, A. Crossley and R. G. Compton, *Electroanalysis*, 2006, **18**, 2141-2147.
231. X. Dai, G. G. Wildgoose, C. Salter, A. Crossley and R. G. Compton, *Analytical Chemistry*, 2006, **78**, 6102-6108.
232. Y. C. Tsai and J. D. Huang, *Electrochemistry Communications*, 2006, **8**, 956-960.
233. G. G. Wildgoose, C. E. Banks, H. C. Leventis and R. G. Compton, *Microchimica Acta*, 2006, **152**, 187-214.
234. C. E. Banks and R. G. Compton, *Analyst*, 2006, **131**, 15-21.
235. J. J. Gooding, R. Wibowo, J. Q. Liu, W. R. Yang, D. Losic, S. Orbons, F. J. Mearns, J. G. Shapter and D. B. Hibbert, *Journal of the American Chemical Society*, 2003, **125**, 9006-9007.
236. X. Yu, D. Chattopadhyay, I. Galeska, F. Papadimitrakopoulos and J. F. Rusling, *Electrochemistry Communications*, 2003, **5**, 408-411.
237. A. Guiseppi-Elie, C. H. Lei and R. H. Baughman, *Nanotechnology*, 2002, **13**, 559-564.
238. F. Patolsky, Y. Weizmann and I. Willner, *Angewandte Chemie-International Edition*, 2004, **43**, 2113-2117.
239. J. H. T. Luong, S. Hrapovic, D. Wang, F. Bensebaa and B. Simard,

Electroanalysis, 2004, **16**, 132-139.
240. J. M. Goran, S. M. Mantilla and K. J. Stevenson, *Analytical Chemistry*, 2013, **85**, 1571-1581.
241. J. C. Meyer, A. K. Geim, M. I. Katsnelson, K. S. Novoselov, T. J. Booth and S. Roth, *Nature*, 2007, **446**, 60-63.
242. A. K. Geim, *Science*, 2009, **324**, 1530-1534.
243. S. Park and R. S. Ruoff, *Nature Nanotechnology*, 2009, **4**, 217-224.
244. A. A. Balandin, S. Ghosh, W. Z. Bao, I. Calizo, D. Teweldebrhan, F. Miao and C. N. Lau, *Nano Letters*, 2008, **8**, 902-907.
245. R. F. Service, *Science*, 2009, **324**, 875-877.
246. C. Lee, X. D. Wei, J. W. Kysar and J. Hone, *Science*, 2008, **321**, 385-388.
247. Y. Wang, Y. M. Li, L. H. Tang, J. Lu and J. H. Li, *Electrochemistry Communications*, 2009, **11**, 889-892.
248. S. Alwarappan, A. Erdem, C. Liu and C. Z. Li, *Journal of Physical Chemistry C*, 2009, **113**, 8853-8857.
249. C. S. Shan, H. F. Yang, J. F. Song, D. X. Han, A. Ivaska and L. Niu, *Analytical Chemistry*, 2009, **81**, 2378-2382.
250. X. H. Kang, J. Wang, H. Wu, I. A. Aksay, J. Liu and Y. H. Lin, *Biosensors & Bioelectronics*, 2009, **25**, 901-905.
251. M. Zhou, Y. M. Zhai and S. J. Dong, *Analytical Chemistry*, 2009, **81**, 5603-5613.
252. C. P. You, X. W. Yan, J. L. Kong, D. Y. Zhao and B. H. Liu, *Electrochemistry Communications*, 2008, **10**, 1864-1867.
253. G. X. Ma, Y. G. Wang, C. X. Wang, T. H. Lu and Y. Y. Xia, *Electrochimica Acta*, 2008, **53**, 4748-4753.
254. J. J. Feng, J. J. Xu and H. Y. Chen, *Biosensors & Bioelectronics*, 2007, **22**, 1618-1624.
255. J. Razumiene, J. Barkauskas, V. Kubilius, R. Meskys and V. Laurinavicius, *Talanta*, 2005, **67**, 783-790.
256. M. Tominaga, M. Otani, M. Kishikawa and I. Taniguchi, *Chemistry Letters*, 2006, **35**, 1174-1175.
257. G. X. Ma, H. Zhong, T. H. Lu and Y. Y. Xia, *Acta Physico-Chimica Sinica*, 2007, **23**, 1053-1058.
258. G. X. Ma, T. H. Lu and Y. Y. Xia, *Bioelectrochemistry*, 2007, **71**, 180-185.
259. Y. Tian, L. Q. Mao, T. Okajima and T. Ohsaka, *Biosensors & Bioelectronics*, 2005, **21**, 557-564.
260. M. A. Hayes and W. G. Kuhr, *Analytical Chemistry*, 1999, **71**, 1720-1727.
261. H. Zhang, L. Z. Fan and S. H. Yang, *Chemistry-a European Journal*, 2006, **12**, 7161-7166.
262. Y. Huang and D. H. Kim, *Langmuir*, 2011, **27**, 13861-13867.
263. Y. Huang and D. H. Kim, *Nanoscale*, 2011, **3**, 3228-3232.
264. Y. Huang and D. H. Kim, *Nanoscale*, 2012, **4** 6312 - 6317.

265. L. Wei, Y. J. Fan, H. H. Wang, N. Tian, Z. Y. Zhou and S. G. Sun, *Electrochimica Acta*, 2012, **76**, 468-474.
266. L. Wei, Y. J. Fan, N. Tian, Z. Y. Zhou, X. Q. Zhao, B. W. Mao and S. G. Sun, *Journal of Physical Chemistry C*, 2012, **116**, 2040-2044.
267. J. H. Zeng, *Journal of Materials Chemistry*, 2012, **22**, 3170-3176.
268. Z. L. Xiao, C. Y. Han, W. K. Kwok, H. W. Wang, U. Welp, J. Wang and G. W. Crabtree, *Journal of the American Chemical Society*, 2004, **126**, 2316-2317.
269. Y. Ding, Y. Wang, L. Su, M. Bellagamba, H. Zhang and Y. Lei, *Biosensors and Bioelectronics*, 2010, **26**, 542-548.
270. C. W. Kung, C. Y. Lin, Y. H. Lai, R. Vittal and K. C. Ho, *Biosensors & Bioelectronics*, 2011, **27**, 125-131.
271. X. C. Dong, H. Xu, X. W. Wang, Y. X. Huang, M. B. Chan-Park, H. Zhang, L. H. Wang, W. Huang and P. Chen, *ACS Nano*, 2012, **6**, 3206-3213.
272. X. W. Wang, X. C. Dong, Y. Q. Wen, C. M. Li, Q. H. Xiong and P. Chen, *Chemical Communications*, 2012, **48**, 6490-6492.
273. S. Cherevko and C. H. Chung, *Talanta*, 2010, **80**, 1371-1377.
274. N. A. Choudhry, D. K. Kampouris, R. O. Kadara, N. Jenkinson and C. E. Banks, *Analytical Methods*, 2009, **1**, 183-187.
275. K. M. El Khatib and R. M. A. Hameed, *Biosensors & Bioelectronics*, 2011, **26**, 3542-3548.
276. K. K. Lee, P. Y. Loh, C. H. Sow and W. S. Chin, *Electrochemistry Communications*, 2012, **20**, 128-132.
277. C. L. Li, Y. Su, S. W. Zhang, X. Y. Lv, H. L. Xia and Y. J. Wang, *Biosensors & Bioelectronics*, 2010, **26**, 903-907.
278. S. L. Luo, F. Su, C. B. Liu, J. X. Li, R. H. Liu, Y. Xiao, Y. Li, X. N. Liu and Q. Y. Cai, *Talanta*, 2011, **86**, 157-163.
279. M. U. A. Prathap, B. Kaur and R. Srivastava, *Journal of Colloid and Interface Science*, 2012, **370**, 144-154.
280. S. Priya and S. Berchmans, *Journal of the Electrochemical Society*, 2012, **159**, F73-F80.
281. A. J. Wang, J. J. Feng, Z. H. Li, Q. C. Liao, Z. Z. Wang and J. R. Chen, *Crystengcomm*, 2012, **14**, 1289-1295.
282. G. Wang, Y. Wei, W. Zhang, X. Zhang, B. Fang and L. Wang, *Microchimica Acta*, 2010, **168**, 87-92.
283. J. Yang, L. C. Jiang, W. D. Zhang and S. Gunasekaran, *Talanta*, 2010, **82**, 25-33.
284. Y. J. Yang, W. K. Li and X. H. Chen, *Journal of Solid State Electrochemistry*, 2012, **16**, 2877-2881.
285. P. Zhang, L. Zhang, G. C. Zhao and F. Feng, *Microchimica Acta*, 2012, **176**, 411-417.
286. X. J. Zhang, G. F. Wang, W. Zhang, Y. Wei and B. Fang, *Biosensors & Bioelectronics*, 2009, **24**, 3395-3398.

287. Z. J. Zhuang, X. D. Su, H. Y. Yuan, Q. Sun, D. Xiao and M. M. F. Choi, *Analyst*, 2008, **133**, 126-132.
288. W. Wang, L. L. Zhang, S. F. Tong, X. Li and W. B. Song, *Biosensors & Bioelectronics*, 2009, **25**, 708-714.
289. E. Reitz, W. Z. Jia, M. Gentile, Y. Wang and Y. Lei, *Electroanalysis*, 2008, **20**, 2482-2486.
290. L. C. Jiang and W. D. Zhang, *Biosensors & Bioelectronics*, 2010, **25**, 1402-1407.
291. Y. Mu, D. L. Jia, Y. Y. He, Y. Q. Miao and H. L. Wu, *Biosensors & Bioelectronics*, 2011, **26**, 2948-2952.
292. Y. Zhang, F. G. Xu, Y. J. Sun, Y. Shi, Z. W. Wen and Z. Li, *Journal of Materials Chemistry*, 2011, **21**, 16949-16954.
293. W. Lv, F. M. Jin, Q. G. Guo, Q. H. Yang and F. Y. Kang, *Electrochimica Acta*, 2012, **73**, 129-135.
294. G. M. Wang, X. H. Lu, T. Zhai, Y. C. Ling, H. Y. Wang, Y. X. Tong and Y. Li, *Nanoscale*, 2012, **4**, 3123-3127.
295. W. Wang, Z. Y. Li, W. Zheng, B. Dong, S. Y. Li and C. Wang, *Journal of Nanoscience and Nanotechnology*, 2010, **10**, 7537-7540.
296. Y. Ding, Y. Wang, L. C. Zhang, H. Zhang and Y. Lei, *Journal of Materials Chemistry*, 2012, **22**, 980-986.
297. M. Shamsipur, M. Najafi and M.-R. M. Hosseini, *Bioelectrochemistry*, 2010, **77**, 120-124.
298. W. D. Zhang, J. Chen, L. C. Jiang, Y. X. Yu and J. Q. Zhang, *Microchimica Acta*, 2010, **168**, 259-265.
299. Y. Bai, Y. Y. Sun and C. Q. Sun, *Biosensors & Bioelectronics*, 2008, **24**, 579-585.
300. Y. P. Sun, H. Buck and T. E. Mallouk, *Analytical Chemistry*, 2001, **73**, 1599-1604.
301. J. Wang, D. F. Thomas and A. Chen, *Analytical Chemistry*, 2008, **80**, 997-1004.
302. H. F. Cui, J. S. Ye, W. D. Zhang, C. M. Li, J. H. T. Luong and F. S. Sheu, *Analytica Chimica Acta*, 2007, **594**, 175-183.
303. L. H. Li, W. D. Zhang and J. S. Ye, *Electroanalysis*, 2008, **20**, 2212-2216.
304. F. Xiao, F. Q. Zhao, D. P. Mei, Z. R. Mo and B. Z. Zeng, *Biosensors & Bioelectronics*, 2009, **24**, 3481-3486.
305. P. Holt-Hindle, S. Nigro, M. Asmussen and A. C. Chen, *Electrochemistry Communications*, 2008, **10**, 1438-1441.
306. H. C. Gao, F. Xiao, C. B. Ching and H. W. Duan, *ACS Applied Materials & Interfaces*, 2011, **3**, 3049-3057.
307. S. S. Mahshid, S. Mahshid, A. Dolati, M. Ghorbani, L. X. Yang, S. L. Luo and Q. Y. Cai, *Electrochimica Acta*, 2011, **58**, 551-555.
308. S. S. Mahshid, S. L. Luo, L. X. Yang, S. Mahshid, A. Dolati, M. Ghorbani and

Q. Y. Cai, *Sensor Letters*, 2011, **9**, 1598-1605.
309. B. Lim, M. J. Jiang, P. H. C. Camargo, E. C. Cho, J. Tao, X. M. Lu, Y. M. Zhu and Y. N. Xia, *Science*, 2009, **324**, 1302-1305.
310. M. Khalid, N. Wasio, T. Chase and K. Bandyopadhyay, *Nanoscale Research Letters*, 2010, **5**, 61-67.
311.S. J. Guo, L. Wang, S. J. Dong and E. K. Wang, *Journal of Physical Chemistry C*, 2008, **112**, 13510-13515.
312. F. Xiao, Z. R. Mo, F. Q. Zhao and B. Z. Zeng, *Electrochemistry Communications*, 2008, **10**, 1740-1743.
313. F. Xiao, F. Q. Zhao, Y. F. Zhang, G. P. Guo and B. Z. Zeng, *Journal of Physical Chemistry C*, 2009, **113**, 849-855.
314. J. Ryu, K. Kim, H. S. Kim, H. T. Hahn and D. Lashmore, *Biosensors & Bioelectronics*, 2010, **26**, 602-607.
315. B. Singh, F. Laffir, T. McCormac and E. Dempsey, *Sensors and Actuators B-Chemical*, 2010, **150**, 80-92.
316. M. Tominaga, T. Shimazoe, M. Nagashima and I. Taniguchi, *Journal of Electroanalytical Chemistry*, 2008, **615**, 51-61.
317. Q. F. Yi, W. Q. Yu and F. J. Niu, *Electroanalysis*, 2010, **22**, 556-563.
318. M. Tominaga, Y. Taema and I. Taniguchi, *Journal of Electroanalytical Chemistry*, 2008, **624**, 1-8.
319. L. Y. Chen, T. Fujita, Y. Ding and M. W. Chen, *Advanced Functional Materials*, 2010, **20**, 2279-2285.
320. I. H. Yeo and D. C. Johnson, *Journal of Electroanalytical Chemistry*, 2000, **484**, 157-163.
321. M. Jafarian, F. Forouzandeh, I. Danaee, F. Gobal and M. G. Mahjani, *Journal of Solid State Electrochemistry*, 2009, **13**, 1171-1179.
322. Y. B. Vassilyev, O. A. Khazova and N. N. Nikolaeva, *Journal of Electroanalytical Chemistry*, 1985, **196**, 127-144.

Chapter 3-Experimental Section

3.1 Materials Synthesis

3.1.1. Preparation of Au Nanoparticles

The 13 nm gold nanospheres were prepared according to the previously reported sodium citrate reduction methods[1, 2] with slight modifications. Briefly, all glassware was washed thoroughly with aqua regia (3:1 HCl/HNO_3), rinsed repeatedly with double distilled water and then dried in an oven. 40 μL of 2.5 M $HAuCl_4$ and 100 mL of water were added to a two-neck flask, with one neck connected to a condenser and the other capped with a stopper. The flask was placed on a hot plate to reflux with stirring. When the reflux began, the stopper was removed and 10 mL of 38.8 mM sodium citrate was quickly injected. The stopper was then put back and the flask continued to flux for 20 min before the system was cooled down to room temperature under stirring. The gold nanoparticles (AuNPs) were then filtered with 0.45 μm acetate filters and stored at room temperature before use.

3.1.2. Functionalization of MWCNTs

MWCNT-COOH (OD ~50 nm, length ~20 μm, -COOH 1.23 wt %, purity 95 wt %) were purchased from Chengdu Organic Chemicals Co. Ltd, China. MWCNT-COOH was purified by sonication in the presence of 5 M HCl for 4 h at room temperature to remove metal catalysts. The purified MWCNT-COOH was filtered, washed with double distilled water and dried in vacuum. Then, 15 mg of MWCNT-COOH was refluxed with 30 ml of 10% (3-Mercaptopropyl)triethoxysilane (MPTS) in ethanol at 70 ℃ for 3 h under constant stirring. The entire reaction proceeded in a nitrogen atmosphere to prevent the oxidation of thiol groups present in the MPTS. The product MWCNT-Si-SH was collected and separated by centrifugation at 4,500 rpm for 15 min, and then washed with ethanol three times to remove excess MPTS and dried in vacuum at 60 ℃ for 3 h.

3.1.3. Synthesis of One Dimensional Hierarchical Structured TiO_2

The CNT-TiO_2 composite was synthesized by a simple hydrothermal method.[3] Briefly, 50 mg of acid-treated MWCNTs was dispersed in 40 mL of isopropyl alcohol (IPA) by sonication for 10 minutes, and then 0.03 mL of DETA was added. After gently stirring for 2 minutes, 1.8 mL of TIP was added. The solution was then transferred into a 60 mL Teflon-lined stainless steel autoclave and kept in an electric oven at 200 ^{o}C for 24 h. The autoclave was then taken out of the oven and left to cool down to room temperature. The black precipitate was collected by centrifugation, washed thoroughly with ethanol and dried at 60 ^{o}C overnight. To obtain the one dimensional hierarchical structured TiO_2 (1DHS TiO_2), the as-prepared composite was subjected to calcination at 550 ^{o}C for 2 h to remove the MWCNT template and obtain the hierarchically structured 1D TiO_2.

3.1.4. Synthesis of Hierarchically Structured MnO_2 Spheres

The hierarchically structured MnO_2 spheres were synthesized on an indium tin oxide (ITO) substrate by electrodeposition, which was conducted in a three-electrode electrochemical cell. ITO glass with the dimension of 1.5 cm $\times$ 1 cm was used as the working electrode; platinum foil and Ag/AgCl were used as the counter electrode and reference electrode, respectively. 10 mM manganese acetate aqueous solution was used as the electrolyte throughout the experiment. Thin film of hierarchically structured MnO_2 spheres could be obtained by electrodepositing manganese acetate at 1.5 V for 300 s under room temperature. The obtained materials were then scraped from the ITO surface by scalpel and dispersed in double distilled water by ultrasonication. The powder of hierarchically structured MnO_2 spheres was collected by centrifugation followed by drying in vacuum at 80 ℃ for 6 h.

3.1.5. Synthesis of Carbon Nanocages

Carbon nanocages (CNCs) were synthesized by the chemical vapour deposition (CVD) method[4] with MgO as template and ethanol as the carbon source. Specifically, 2 g magnesium carbonate ($4MgCO_3\,Mg(OH)_2\,5H_2O$) was spread uniformly in centre

of a quartz tube which was placed in a horizontal furnace. After the tube was purged by argon (Ar) flow for 30 min, the temperature was ramped to 800 ℃ by furnace with the protection of Ar gas. Then, ethanol was injected at a constant rate of 0.06 mL min^{-1} by a syringe pump. After 30 min of reaction, the syringe pump was switched off and the quartz tube was allowed to cool down to room temperature in the flow of Ar gas. The CNCs were obtained by treating the as-synthesized product in 6 M HCl with stirring to remove the MgO template followed by repeated washing with double distilled water until the pH became neutral. Finally, the CNCs powder was collected by centrifugation and drying at 60 ℃ in vacuum for 12 h.

3.1.6. Growth of Three-Dimensional Graphene

The three-dimensional graphene foam (3DGF) was synthesized using a template-based ethanol-CVD method previously reported by us.[5, 6] Briefly, the nickel foam (thickness of ~0.5mm, purchased from Alantum Advanced Technology Materials, China) was placed in the center of a quartz tube furnace and heated up to 1000 ℃ at a rate of 50 ℃/min. The temperature was maintained at 1000 ℃ for 10 min under ambient pressure with a gas flow of Ar (50 sccm) and H_2 (25 sccm) in order to remove the oxide layer on the surface of nickel foam. Ethanol was then bubbled into the furnace as carbon source by Ar flow. The concentration of ethanol was controlled by the flow rate of Ar. After 20 minutes of growth, the sample was taken out from the furnace and rapidly cooled down to room temperature at cooling rate of 100 ℃/min under the protection of Ar/H_2 flow (Ar: H_2= 50: 25). In order to remove the nickel foam template, the as-prepared 3DGF was first dipped into the solution of 4.5 % poly(methyl methacrylate) (PMMA with molecular weight of 996, 000) for several seconds, followed by drying at 90 ℃ for 1h. After that, the PMMA coated 3DGF networks were immersed into 3 M HCl at 80 ℃ to etch away the nickel substrate. Finally, the PMMA layer was removed by hot acetone vapor followed by annealing at 450 ℃ under Ar/H_2 flow.

3.1.7. Fabrication of Hierarchically Structured Mn_3O_4/3DGF Nanocomposite

The hierarchically structured Mn_3O_4 network was grown on the surface of 3DGF by an electrochemical deposition method. The electrodepositon was performed using electrochemical workstation (CHI 760D, CH instrument Inc, USA) in a conventional three-electrode system, with 3DGF as working electrode, Pt foil as counter electrode and Ag/AgCl as reference electrode. Under room temperature, a constant potential of 0.5 V was applied in an aqueous solution of 0.01 mol/L manganese acetate for 600 s to achieve the uniform coating of MnO_x on the skeleton of 3DGF. The product was then washed with double-distilled water for several times and dried by ultrapure nitrogen flow. Finally, the sample was calcinated at 400 ℃ in vacuum for 3h to obtain the highly crystalline Mn_3O_4 on 3DGF. The composite was then affixed to a flexible PET substrate by silicon rubber to use as a freestanding electrode and flexible biosensor.

3.2 Materials Characterizations

The surface morphology and microstructure of synthesized products were characterized by field-emission scanning electron microscopy (FESEM; JEOL, JSM-6700F, 5 kV) and transmission electron microscopy (TEM; JEOL, JEM-2100F, 200 kV). The TEM sample was prepared by sonicating the composite material in ethanol for 3 min followed by casting one drop of the obtained dispersion on TEM copper grid. The elemental compositions of the samples were analyzed with energy-dispersive X-ray spectroscopy (EDX) attached to the FESEM instrument. The crystallographic information of the samples was obtained by X-ray powder diffraction (XRD; The Bruker, D8 Advance X-ray diffractometer, Cu Kα, λ = 1.5406 Å). The specific surface area and pore size distribution of the products were measured by a BET analyzer (Quantachrome Instruments, Autosorb AS-6B) at 77 K. Protein immobilization was investigated by Fourier transform infrared spectroscopy (FTIR, Bruker EQUINOX 55 DuroscopeTM). The samples were dried in vacuum and pressed into pellets together with potassium bromide (KBr) for FTIR measurements. The UV spectra were recorded with Shimadzu UV-3600 UV-vis spectrophotometer

(Japan). The Raman spectra were obtained with a WITeck CRM200 confocal microscopy Raman system (488 nm laser wavelength, 2.54 eV, WITeck, Germany). Thermogravimetric analysis (TGA) was conducted on a TA Instrument 2960 from 100 ℃ to 1000 ℃ under air flow at a heating rate of 10 ℃ min^{-1}.

3.3 Electrochemical Measurements

The electrochemical experiments were conducted using a CHI 660C or CHI760D electrochemical workstations (CH Instrument, USA) with a conventional three-electrode system, including a working electrode, a platinum wire counter electrode and a saturated calomel electrode (SCE) or Ag/AgCl electrode as the reference electrode. Cyclic voltammetry (CV) studies were performed either in deoxygenated or air-satureated 0.1 M PBS buffer (pH 7.4). Deoxygenated buffer was prepared by bubbling the PBS solution with ultrapure nitrogen gas for 20 min before the experiment. Amperometric sensing experiments were performed in ambient condition with a three-electrode electrochemical cell under continuous stirring, which is provided by a magnetic stirrer. Electrochemical impedance spectroscopy (EIS) measurement was performed in the mixture of 5 mM $K_3[Fe(CN)_6]/K_4[Fe(CN)_6]$ (1:1) solution in the frequency range between 0.1 to 100,000 Hz at E =0.21 V, which is the formal potential of the system. The amplitude of the alternative voltage of the system was 10 mV.

Reference

1. G. Frens, *Nature*, 1973, **241**, 20-22.
2. J. Liu and Y. Lu, *Nature Protocols*, 2006, **1**, 246-252.
3. S. J. Ding, J. S. Chen and X. W. Lou, *Advanced Functional Materials*, 2011, **21**, 4120-4125.
4. K. Xie, X. T. Qin, X. Z. Wang, Y. N. Wang, H. S. Tao, Q. Wu, L. J. Yang and Z. Hu, *Advanced Materials*, 2012, **24**, 347-+.
5. X.-C. Dong, H. Xu, X.-W. Wang, Y.-X. Huang, M. B. Chan-Park, H. Zhang, L.-H. Wang, W. Huang and P. Chen, *ACS Nano*, 2012, **6**, 3206-3213.
6. Y.-C. Yong, X.-C. Dong, M. B. Chan-Park, H. Song and P. Chen, *ACS Nano*, 2012, **6**, 2394-2400.

Chapter 4-Self-Assembly of Multilayered Carbon Nanotubes Decorated with High Density of Gold Nanoparticles on Electrode for Highly Sensitive Glucose Detection†

†Reproduced from [**P. Si,** P. Kannan, L. Guo, H. Son and D. H. Kim, ***Biosensors and Bioelectronics***, *2011, 26 (9), 3845-3851*] by permission from Elsevier. Copyright 2011.

4.1. Introduction

Diabetes mellitus is a worldwide public disease resulting from insulin deficiency and hyperglycemia, reflected by blood glucose levels higher or lower than the normal range of 80-120 mg/dL (4.4-6.6 mM).[1] The complications caused by diabetes include higher risks of heart disease, kidney failure, blindness, etc.[2] Such complications can be greatly reduced through stringent personal control of blood glucose. The development of a highly stable and sensitive glucose biosensor is therefore of critical importance for the diagnosis and keen observation of blood glucose levels. In addition, the accurate detection of glucose is also of great interest in industrial applications such as food industry and bio-fermentation process.[3] Much effort has been devoted so far on developing suitable techniques for precisely monitoring the glucose level with high sensitivity, good selectivity, high reliability and faster response.

Since the concept of enzyme electrode was first introduced by Clark and Lyons about 50 years ago,[4] glucose oxidase (GOx) based enzyme sensors have been widely employed to fabricate glucose biosensors. However, simple and efficient immobilization of high content of GOx on the electrode still remains a challenge for improving the performance of glucose biosensors. In the past years, a variety of nanomaterials have been used to structurally-modify the electrodes and immobilize GOx.[5-11] Among them, gold nanoparticles (AuNPs) have drawn considerable attention because of their unique size, shape dependent physical, chemical and electronic

properties when compared to the bulk gold.[12, 13] It has been reported that, AuNPs can provide a suitable microenvironment, which is similar to the redox center of a native protein, to immobilize enzyme and retain their bioactivities. Besides, owing to their special chemical properties, AuNPs allow a variety of functional groups, including –SH, -NH_2 and –CN, to bind to their surface covalently, which is favorable for the stable immobilization of biomolecules.[14, 15] In addition, due to their high conductivity, AuNPs can easily minimize the impedance on electrode interface and provide a necessary conduction pathway to facilitate the electron transfer between the immobilized enzyme and electrode surface.[16] Taking account of these advantages, AuNPs were extensively used to construct glucose biosensors either alone or combined with other materials.[17-19] However, it is difficult to attach a high density of AuNPs on the electrode surface due to the limited binding sites and low adsorption rate of AuNPs, which is not favorable for the immobilization of a large quantity of enzyme on the electrode. Consequently, the biosensor may result in low sensitivity and narrow linear range.

Layer-by-layer (LBL) is a simple and efficient method to immobilize high volume of enzyme on the electrode. Because of the simplicity of fabrication procedure, wide choice of materials and tailorable control of thickness, LBL based on electrostatic interaction has attracted tremendous interest in recent years.[20, 21] Wu and coworkers reported the amperometric glucose biosensor based on multilayered AuNPs, chitosan and GOx.[22] Yan et al., fabricated a glucose biosensor via LBL self-assembly of MWCNT, PDDA and GOx.[23] Deng and colleagues constructed a glucose biosensor by assembling multilayered GOx and polyelectrolyte on MWCNTs.[24] Komathi et al., proposed a glucose biosensor based on LBL assembly of MWCNT, conducting polymer, AuNPs and GOx.[25] However, the biosensors constructed via electrostatic adsorption have some major drawbacks such as instability in high ionic solution, film leaching over long time storage and long response time, which limited their application.[23] While covalent binding of GOx to CNTs or AuNPs usually requires

pretreatment for quite a long time with strong acid (e.g. H_2SO_4 and HNO_3) or HIO_4,[26] which are harmful to the environment and human health. In addition, long time treatment is not favorable for industrial production. Thus, the optimal approach for construction of glucose biosenosrs should be a mild condition which can offer both high stability and high efficiency to immobilize large quantities of enzyme.

In the present study, we report a three dimensional (3-D) assembly of high density AuNPs architecture, which is constructed by LBL covalent attachment of (3-mercaptopropyl) triethoxysilane (MPTS) functionalized MWCNTs and AuNPs. This nanohybrid material can act as a suitable matrix to immobilize GOx for the fabrication of glucose biosensor. The proposed biosensor successfully overcame the problems mentioned above, which provides a stable biosensing interface, mild enzyme immobilizing environment and efficient fabrication process. MWCNTs were used in the present work to construct the 3-D structure due to their high mechanical strength, chemical stability, large surface area, and biocompatibility.[27] In addition, MWCNTs can also facilitate the shuttling of electrons between the enzyme and the electrode surface.[28] However, the poor solubility of MWCNT in most solvents is a major barrier for constructing MWCNT-based structure on electrode. In this study, MPTS was employed to covalently functionalize MWNCTs, the high density of –SH groups presented on the side walls of MWCNT not only can stabilize the MWCNT dispersion, but also provide a large amount of AuNP binding sites. The surface coverage of AuNP on electrode was found to be 90 %. To the best of our knowledge, such high density of AuNPs covalently assembled on electrode surface was achieved for the first time. The resulting biosensor has achieved a remarkably enhanced sensitivity, which is much superior to multi-layered GOx/MWCNT or GOx/AuNPs-based electrodes.

4.2 Electrode Modification and Biosensor Fabrication

The Au electrode was thoroughly polished with alumina powder, followed by etching with 1:3 (v/v) H_2O_2/H_2SO_4 for 3 min and then sonication in double distilled

water for 4 min.. The pre-treated Au electrode was then alternately dipped in 0.5 mg/mL MWCNT-Si-SH and AuNPs solutions each for 2.5 h to form self-assembled multilayers of AuNPs/MWCNT on the Au electrode surface. After the each dipping step, the modified electrode was carefully rinsed with double distilled water and dried with high purity nitrogen stream to remove the non-specifically assembled species. As control experiment, monolayer of AuNPs modified electrode was fabricated according to the previous literature.[29] Afterwards, 5 μL of GOx solution (10 mg/mL) was dropped onto the center of the as-prepared electrode, which was then covered by a small Eppendorf tube and dried at 4 ℃ overnight to immobilize the enzyme on the surface of the hierarchically assembled AuNP structures. Finally, the electrode was thoroughly rinsed with water and stored in PBS (pH 7.4) at 4 ℃ before use. Figure 4-1 shows the stepwise fabrication process of the glucose biosensor.

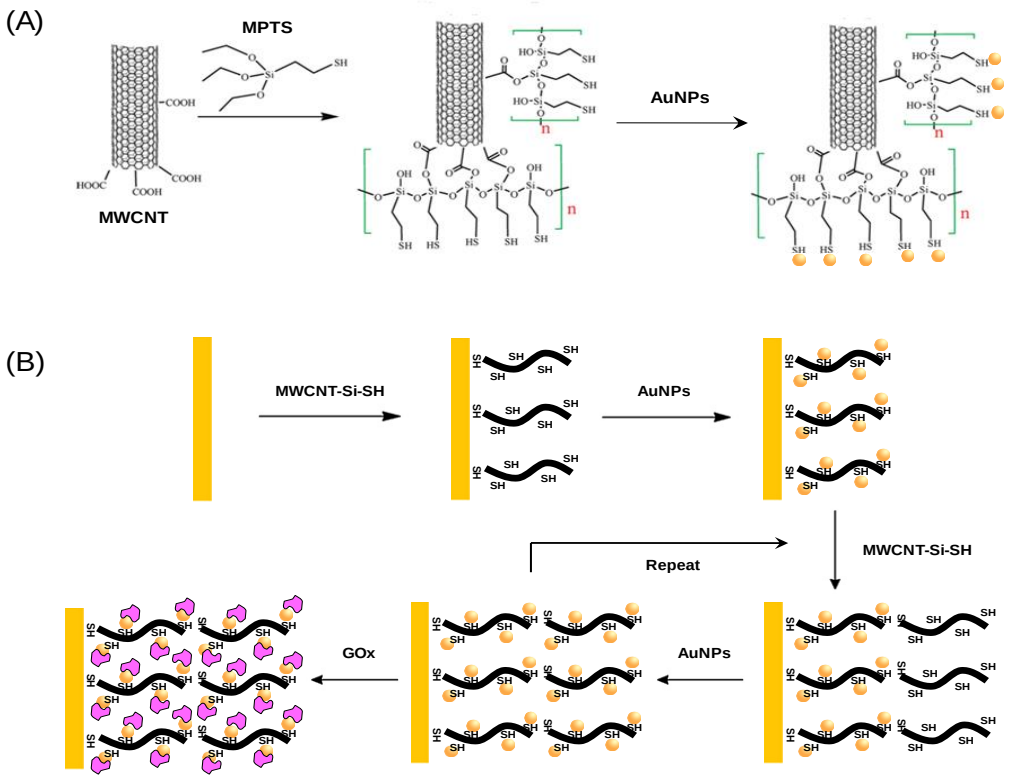

Figure 4-1. (A) Illustration of MWCNTs functionalized by MPTS followed by self-assembly of AuNPs. (B) The schematic diagram of self-assembling multilayered AuNPs/MWCNT on Au electrode surface followed by immobilization of GOx on the AuNPs/MWCNT matrix.

4.3. Results and Discussion

4.3.1. Characterizations of the Self-Assembly

In this study, MWCNTs were first functionalized by MPTS through hydroxyl-carboxyl dehydrate reaction.[30] The attached MPTS can expose large arrays of -SH groups on the end and side walls of MWCNTs through hydrolysis followed by self-polymerization (Figure 4-1A). Then, MWCNT-Si-SH can easily absorb on the surface of Au electrode and AuNPs through the S-H bond cleavage.[31] Figure 4-2A shows one layer of MWCNTs self-assembled on the Au electrode surface through gold-thiol interaction. As can be observed, the MWCNTs were uniformly distributed on the electrode surface. Afterwards, significant amount of AuNPs could easily absorbed both on the end and side walls of MWCNTs via the same mechanism. As a result, one layer of the AuNPs/MWNCNT nanocomposite film was formed on the electrode surface (Figure 4-2B). The AuNPs tethered on MWCNTs further provided the binding sites of MWCNT-Si-SH, which allowed for the self-assembly of subsequent layers. The high density of multilayered AuNPs/MWNCNT hybrid structure was obtained on the Au electrode surface by repeating the modification process for several times. Figure 4-2C shows the electrode modified with five layers of AuNPs/MWNCNT nanocomposite architectures. As is observed, the coverage of AuNPs/MWNCNT on the electrode surface increased significantly compared with Figure 4-2B. In addition, the multilayered hybrid film shows a large surface area and nanoporous structure, which allows for further immobilization of GOx and provides high accessibility to the target molecules.

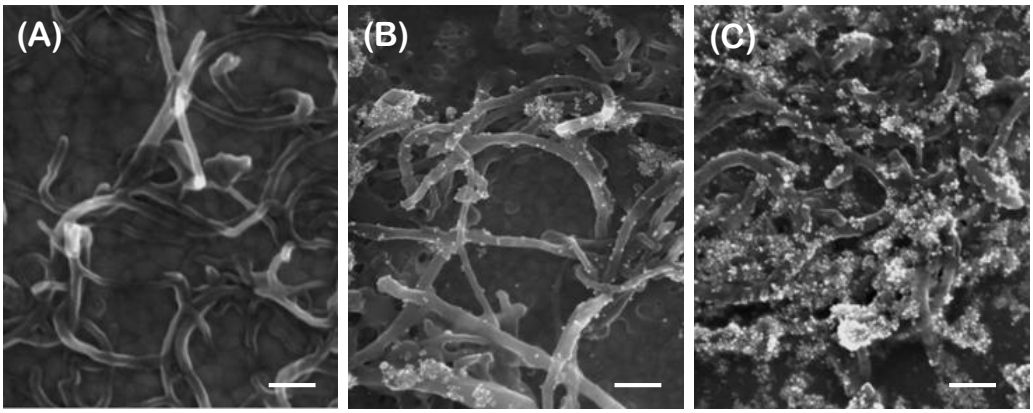

Figure 4-2. FESEM images of (A) one layer of MWCNTs self-assembled on Au substrate, (B) one layer of AuNPs/MWNCNT hybrid film on Au substrate, (C) five layers of AuNPs/MWNCNT modified Au substrates. The scale bar is 100 nm.

4.3.2. Surface Coverage of AuNPs

The AuNPs coverage on the electrode surface was studied by scanning cyclic voltammograms (CV) between -0.6 and 0.7 V in 0.1 M NaOH.[32] Figure.4-3A shows the CVs of 1~5 layers of AuNPs/MWCNTs nanocomposite modified electrodes. The particle coverage (θ_p) is defined as the ratio between the electrochemically accessible AuNPs area and the geometric area of the Au electrode in contact with the electrolyte solution. The particle area was calculated by using the charge involved in the reduction of the electrochemically formed Au oxide. Assuming the charge density for the reduction of the Au oxide is 723 μC/cm^2, the particle coverage could be calculated by the following equation:[33]

$$\theta_p = \frac{\text{Au oxide reduction charge } (\mu\text{C}) / 723\,(\mu\text{C/cm}^2)}{\text{Electrode geometric area } (\text{cm}^2)} \times 100\% \qquad 4\text{-}1$$

The particle coverage of 1~5 layers of AuNPs/MWNCNT modified Au electrodes were calculated to be 39, 65, 78, 87 and 90 % respectively. The five layered AuNPs/MWNCNT habrid architecture shows much superior surface particle coverage compared to the previous reports, which are 10 %,[34] 25~30 %[35] and 50 %[32] respectively. In the present case of modification, such high surface coverage of AuNPs is achieved for the first time. Figure 4-3B compares the surface particle coverage of the electrodes modified with 1~10 layers of the AuNPs/MWCNT hybride structure. As can be seen, after 5 layers of modification of AuNPs/MWCNT nanocomposites, the surface coverage of AuNPs reached saturation. This could be a result that when more MWCNTs assembled on the electrode, the surface area of AuNPs was increasingly covered. Thus, five layers of AuNPs/MWNCNT were used throughout the experiment to modify the electrode and immobilize the enzyme.

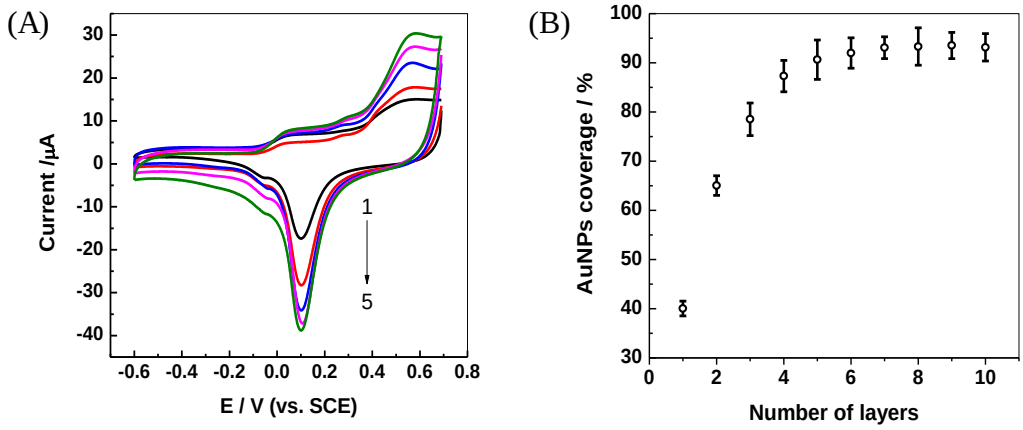

Figure 4-3. (A) CVs obtained for 1~5 layers of AuNPs/MWNCNT film modified Au electrode in 0.1 M NaOH. Scan rate: 50mV/s. (B) the AuNPs coverage on Au electrode modified with 1~10 layers of MWNCT/AuNPs.

4.3.3. Immobilization of GOx

The immobilization of GOx on multilayered AuNPs/MWNCNT was examined by electrochemical impedance spectroscopy (EIS), which is a sensitive technique to study the surface modification of electrodes.[36-38] It is reported that the GOx could be chemisorbed onto the surface of AuNPs though their amino groups.[39, 40] Figure 4-4 shows the typical Nyquist plot obtained for bare Au electrode, $(AuNPs/MWNCNT)_5$/Au electrode and GOx/$(AuNPs/MWNCNT)_5$/Au electrode. The bare Au electrode (Figure 4-4a) presents a small semicircle followed by a linear tail. The semicircle portion illustrates an electron transfer limited process while the linear tail suggests a diffusion controlled electrochemical behavior. The diameter of the semicircle is proportional to the electron transfer resistance (R_{et}) on the electrode surface. When five layers of AuNPs/MWNCNT were modified on the electrode, an increase of the impedance was observed as shown in Figure 4-4b, which was possibly caused by the electron transfer barrier formed by the bi-functional MPTS sol-gel conjugated on MWCNTs, However, the impedance was lowered by about 50 % compared with monolayer of AuNPs/MWNCNT modified electrode, which could contribute the good conductivity of highly assembled AuNPs. When GOx were immobilized on the multilayered matrix of AuNPs/MWNCNT, the R_{et} was increased

by nearly 4 times (Figure 4-4c). It is reported that GOx can generate an insulating layer on the electrode surface which blocked the electron transfer of $[Fe(CN)_6]^{3-/4-}$ therefore increasing the impedance of the electrode.[41] The surface coverage of GOx (θ_E) on the electrode was calculated to be 72.4 % according to the equation $\theta_E = (1 - R_{ct} / R_{ct}^{GOD}) \times 100\%$,[42] indicating the multilayered AuNPs structure has the capability to immobilize large quantities of enzyme on the electrode surface efficiently.

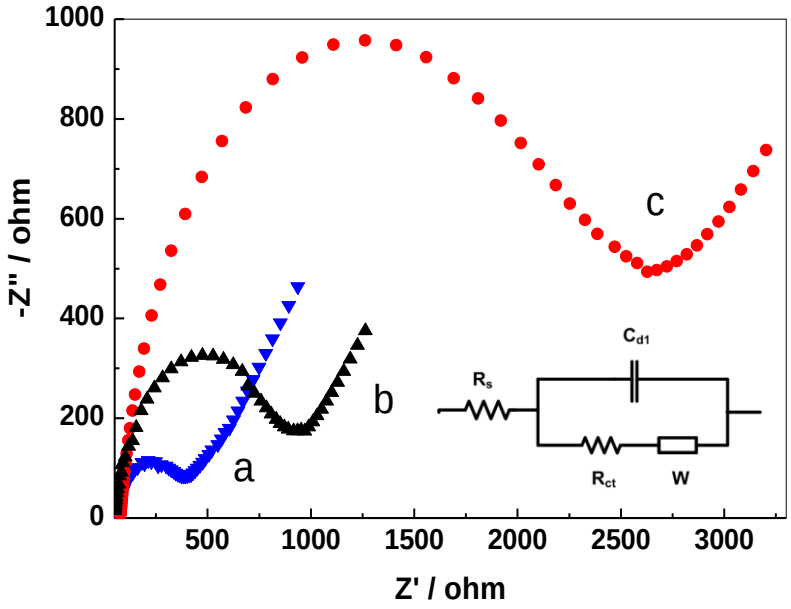

Figure 4-4. Nyquist plots of bare Au electrode (a), $(AuNPs/MWNCNT)_5$/Au electrode (b) and GOx/$(AuNPs/MWNCNT)_5$/Au electrode (c) obtained in 0.1M KCl solution containing 5 mM $[Fe(CN)_6]^{4-/3-}$.

4.4.4. Performance of the Biosensor

The electrochemical behaviors of the modified electrodes were investigated by CV. Figure 4-5A shows the cyclic voltammetric responses for 20 mM glucose recorded at GOx/MWCNT/Au electrode, GOx/AuNPs/Au electrode, GOx/AuNPs/MWNCT/Au electrode and GOx/$(AuNPs/MWNCNT)_5$/Au electrode in pH 7.4 PBS containing 0.1 mM ferrocenemethanol as redox mediator. The anodic currents could be observed when the scanning potential exceeds 100 mV, which is a result of the electrocatalytic

oxidation of glucose by the immobilized GOx on the multilayered film modified electrode. The oxidation of glucose can be described as the following mechanism:[43]

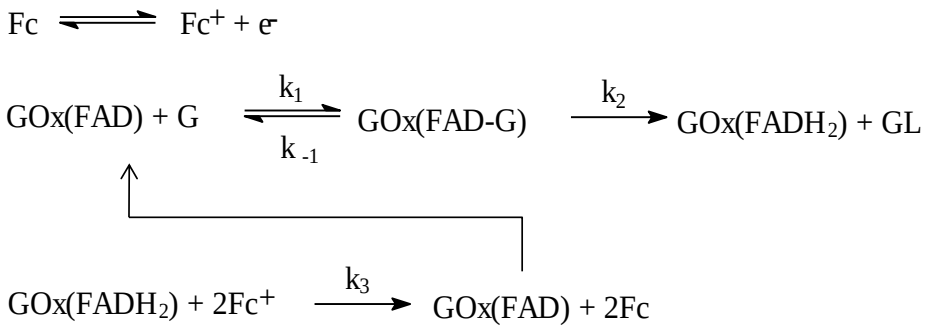

where GOx ($FADH_2$) and GOx(FAD) represent reduced and oxidized form of GOx, Fc and Fc^+ are the reduced and oxidized form of ferrocenemethanol mediator, and G and GL are β-D-glucose and glucose-D-lactone, respectively.

The direct immobilization of GOx on monolayer of MWCNT or AuNPs showed poor oxidation current for glucose as can be observed in Figure 4-5A (a and b). While the biosensor with GOx immobilized on one layer of AuNPs/MWCNT showed notably increased current response (Figure 4-5A(c)), which is even higher than the summation of a and b, indicating the GOx immobilized on AuNPs/MWCNT hybrid has much superior electrocatalytic activity for glucose oxidation. The result is consistent with the previous report in which the electrode was modified with Pt nanoparticles and MWCNT.[44] Surprisingly, the Au electrode modified with 5 layers of AuNPs/MWCNT and GOx showed a response current of 21.5 mA, which is more than 5 times higher than the single layer hybrid modified electrode. The observed result indicates that the multilayered construction of AuNPs/MWCNT significantly improved the sensitivity of the glucose biosensor, which might contribute to both the increased surface area and the enzyme loading on the electrode. As is observed in Figure 4-5A inset, the bare Au electrode (dashed curve) displayed a couple of poor redox peaks at the scan rate of 50 mV s^{-1} in 0.1 M PBS. After modification with 5 layers of AuNPs/MWNCNT and GOx, redox peak currents notably enhanced and shifted to the less positive potential side (solid curve), indicating the favorable electron transfer behavior of the multilayered AuNPs/MWNCNT hybrids. The current

response of the resulting glucose biosensor modified with 1~10 layers of AuNPs/MWCNT and GOx for 20 mM glucose are compared in Figure 4-5B. We found that the current response rises with the increase of modified AuNPs/MWCNT layers for the first five layers, while a plateau current was observed from the sixth layer. This result conforms well to the surface coverage of AuNPs, implying AuNPs play an essential role for the immobilization of GOx. Interestingly, a decreasing current was observed after the eighth layer. This could result from the diffusion blockage of target molecules and mediators on the electrode surface for high density of MWCNT structure would make the electrode less porous and inaccessible to small molecules.

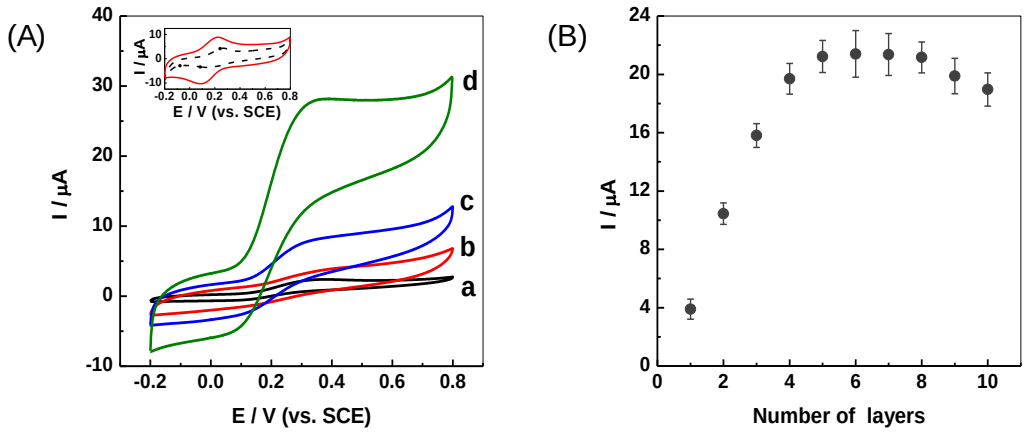

Figure 4-5. (A) CVs of GOx/AuNPs/Au electrode (a), GOx/MWCNT/Au electrode (b), GOx/AuNPs/MWCNT/Au electrode (c) and GOx/(AuNPs/MWCNT)$_5$/Au electrode (d) for 20 mM glucose in 0.1 M PBS containing 0.1 mM ferrocenemethanol. Inset: CVs of bare Au electrode (dashed) and GOx/(AuNPs/MWCNT)$_5$/Au electrode (solid) in 0.1 M PBS containing 0.1 mM ferrocenemethanol. (B) The current response for 20 mM glucose on Au electrode modified with 1~10 layers of AuNPs/MWCNT and GOx.

Figure 4-6A shows the CVs of the GOx/(AuNPs/MWNCNT)$_5$/Au electrode in PBS containing 0.1 mM ferrocenemethanol at different scan rates. The anodic and cathodic peak currents were linear against the square root of the scan rates ranging from 20 to 300 mV s^{-1}, as the calibration plot shown in Figure 4-6B. This result illustrates that the electrochemical process on the electrode surface was diffusion controlled, and the self-assembled multilayer structure on the electrode was highly

accessible to the redox mediator.

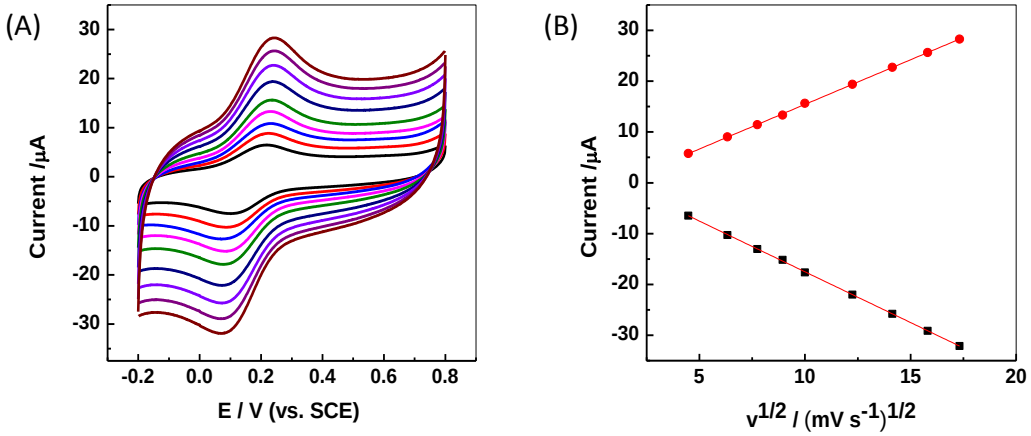

Figure 4-6. (A) CVs obtained for the GOx/(AuNPs/MWNCNT)$_5$/Au electrode in 0.1 M PBS (pH 7.4) containing 0.1 mM ferrocenemethanol at different scan rates. From inside to outside: 20, 40, 60, 80, 100, 150, 200, 250, 300 mV/s. (B) The relationship of the anodic and cationic peak current vs. the square root of the scan rate.

4.4.5. Amperometric sensing of glucose

Amperometric method was used to examine the sensitivity of the resulting GOx/(AuNPs/MWNCNT)$_5$/Au electrode towards the detection of glucose. Figure 4-7A shows the amperometric response of the present glucose biosensor upon successive addition of different concentrations of glucose in a homogeneously stirred PBS at an applied potential of 0.3 V (vs. SCE) until the glucose level in the solution reached 1 mM. The resulting biosensor exhibited rapid and sensitive responses to the addition of glucose, which reached 95 % of the steady state current within 3s. Two aspects might contribute to the fast response. On one hand, the highly porous structure of multilayered AuNPs/MWCNT allows for rapid diffusion of glucose and mediator from bulk solution to the enzyme. On the other hand, the highly assembled AuNPs yields a good conduction pathway which facilitates the electron transfer between the mediator and the electrode surface. Figure 4-7B shows the amperogram of the GOx/(AuNPs/MWNCNT)$_5$/Au electrode upon successive addition of 1mM glucose operating at the same conditions as Figure 4-7A. When the glucose reached a high concentration, a plateau current can be observed, showing the typical characteristic

features of Michaelis-Menten kinetics.[45] The plotted calibration curve (Figure 4-7C) obtained from amperometry results (Figure 4-7A and Figure 4-7B) shows that the present glucose biosensor has a linear range of 20 μM to 10 mM, with a sensitivity of 19.27±0.5 μA mM^{-1} cm^{-2} and the detection limit of 2.3 μM (S/N=3). The sensitivity of the present electrode is approximate three times higher than multilayered GOx/AuNPs modified electrode [46] and two times higher than multilayed GOx/MWCNTs-based electrode.[23]

The apparent Michaelis-Menten constant was calculated from the electrochemical version of the Lineweaver-Burk plot:[47]

$$\frac{1}{i_{ss}} = \frac{K_m^{app}}{i_{\max}} \frac{1}{C} + \frac{1}{i_{\max}} \qquad 4\text{-}2$$

where i_{ss} is the steady-state current after addition of glucose, $i_{\max}$ is the maximum current measured under saturated substrate condition, and C is the bulk concentration of the substrate. The K_m^{app} was determined by analysis of the slope and intercept of the double-reciprocal plot of the steady-state current vs. glucose concentration as shown in Figure 4-7D. The K_m^{app} was calculated to be 6.7 mM. which is much smaller than previously reported values in the literatures (10.5mM,[39] 14.9 mM [48] and 20 mM[10] respectively). The smaller K_m^{app} value means that the immobilized GOx well retained their catalytic activity and the biosensor has high strong affinity for the analyte glucose.

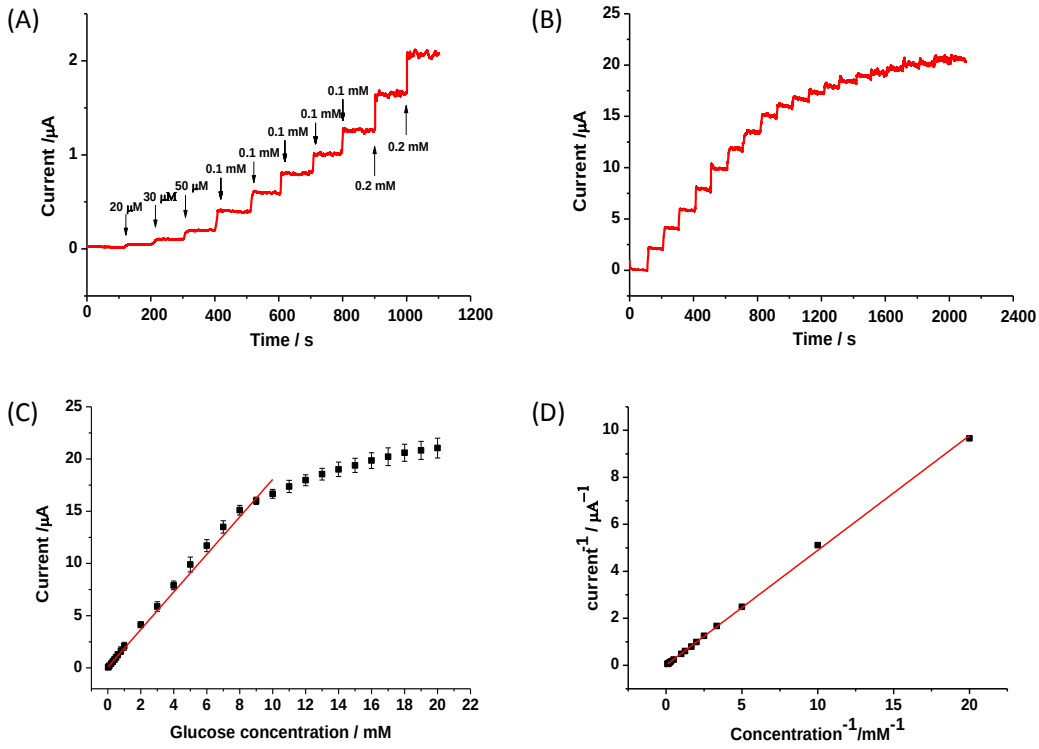

Figure 4-7. (A) Amperometric response of the GOx/(AuNPs/MWNCNT)$_5$/Au electrode to successive addition of different concentrations of glucose at applied potential of 0.3 V (vs. SCE) in PBS containing 0.1 mM ferrocenemethanol. (B) Amperometric response of the above electrode to successive addition of 1 mM glucose at applied potential of 0.3 V (vs. SCE) in PBS containing 0.1 mM ferrocenemethanol.. (C) The calibration curve of present glucose biosensor obtained from (A) and (B). (D) Lineweaver-Burk plot of the above glucose biosensor for the determination of K_m^{app}.

4.4.6. Studies of interferences and stability

We have also studied the determination of glucose in the presence of common physiological interferents such as ascorbic acid (AA), uric acid (UA) and acetaminophen (AP) by amperometric method. Figure 4-8 shows the amperometric *i-t* curve responses of the GOx/(AuNPs/MWCNT)$_5$/Au electrode for 0.5 mM of AA, 0.5 mM AP, 1 mM UA and 0.5 mM glucose in a homogeneously stirred 0.1 M PBS (pH=7.4) at a constant applied potential of 0.30 V. The initial addition of 0.5 mM each AA, AP and 1 mM UA with a sample interval of 100 s into the homogeneously stirred PBS yields an insignificant change of amperometric current, while the addition of 0.5 mM glucose evoked the rapid response of higher amprometric current. The current

responses of the interferents are negligible compared to that induced by the glucose, indicating the present glucose biosensor is feasible for the determination of glucose in the presence of common interfering compounds.

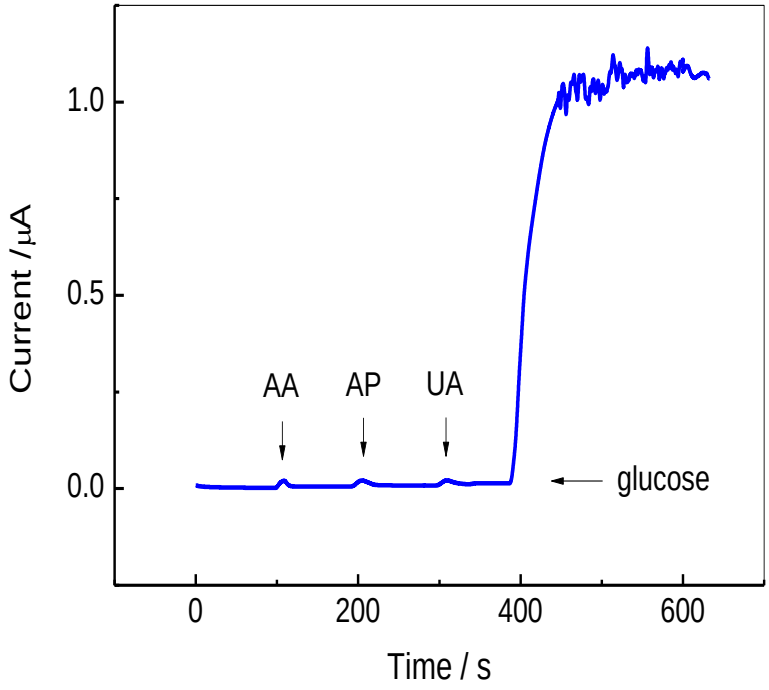

Figure 4-8. Amperometric response of 0.5 mM AA, 0.5 mM AP, 1 mM UA and 0.5 mM glucose on the GOx/$(AuNPs/MWCNT)_5$/Au electrode recorded at 0.3V vs. SCE in 0.1 M PBS containing 0.1 mM ferrocenemethanol.

The operating stability of our five layers of AuNPs/MWCNT nanocomposite electrode toward the voltammetric detection has been evaluated. The voltammetric oxidation current was tested by potential cycling from -0.2 to 0.8 V in the presence of 10 mM glucose at a scan rate of 50 mV/s. No obvious anodic current decrease was observed during 30 cycles of measurement. The storage stability was examined by measuring the amperometric response of the resulting biosensor to 10 mM glucose every day and keeping the modified electrode at 4°C in 0.1 M PBS after use. The biosensor remained 95.4 % of its initial current intensity after one week (Fig. S5). The long-term storage stability reflects the excellent durability of the self-assembled multilayer films and good biocompatibility of the multilayered AuNPs/MWCNT matrix toward immobilizing GOx.

4.4.7. Determination of glucose in human blood serum

The GOx/(AuNPs/MWCNT)$_5$/Au electrode was further employed to detect glucose levels in healthy human blood serum sample by using the calibration curve obtained above. The original glucose concentration in the serum was determined to be 3.52 mM, the corresponding results after addition of standard glucose solution were listed in Table 4-1. A small relative standard deviation (R.S.D) value (less than 4.2 %) was obtained from 6 parallel modified electrodes, indicating that the good reproducibility of the present fabrication method, while high recovery values (96~102 %) showed the capability of the biosensor for real sample detection. These results demonstrate that the proposed biosensor is reliable and effective.

Table 4-1. Determination of glucose in human blood serum sample using GOx/(AuNPs/MWCNT)$_5$/Au electrode.

Sample	Found (mM)	Added (mM)	Found (mM)	R.S.D. (%)	Recovery (%)
1	3.52	2.00	5. 63	4.2	102
2	3.52	4.00	7.89	2.9	105
3	3.52	6.00	9.14	3.7	96

4.4. Conclusion

In summary, we successfully fabricated a glucose biosensor by immobilizing large quantities of GOx on a high density AuNPs matrix, which composed of multilayered AuNPs/MWCNT nanohybrid structure. A high surface coverage of AuNPs was achieved by the multilayered AuNPs/MWCNT nanohybrid architecture, which effectively facilitated the electron transfer, lowered the charge transfer resistance and enhanced the enzyme loading capability of the electrode. The covalent assembly of multilayered AuNPs and MWCNT provides a highly stable biosensing interface which effectively improves the durability of the electrode for long time storage. The five layers of AuNPs/MWCNT composites and GOx exhibited an excellent electrocatalytic activity towards oxidation of glucose, which presents a wide liner

range from 20 μM to 10 mM, with a sensitivity of 19.27 μA mM^{-1} cm^{-2} and a detection limit of 2.3 μM (S/N=3). The resulting glucose biosensor (GOx/(AuNPs/MWCNT)5/Au electrode) showed much superior sensitivity than the multilayered GOx/MWCNT- or multilayered GOx/AuNPs- based electrodes. In addition, the proposed biosensor electrode exhibited satisfied recovery results when employed to determine glucose levels in human blood serum sample. The many advantages of multilayered AuNPs/MWCNT nanostructure reported in our present study can provide great potentials for development of other enzyme-based biosensors.

Reference

1. J. Wang, *Chemical Reviews*, 2008, **108**, 814-825.
2. J. Wang, *Electroanalysis*, 2001, **13**, 983-988.
3. S. G. Wang, Q. Zhang, R. Wang, S. F. Yoon, J. Ahn, D. J. Yang, J. Z. Tian, J. Q. Li and Q. Zhou, *Electrochemistry Communications*, 2003, **5**, 800-803.
4. L. C. Clark Jr and C. Lyons, *Annals of the New York Academy of Sciences*, 1962, **102**, 29-45.
5. Z. Cheng, E. Wang and X. Yang, *Biosensors and Bioelectronics*, 2001, **16**, 179-185.
6. S. Deng, G. Jian, J. Lei, Z. Hu and H. Ju, *Biosensors and Bioelectronics*, 2009, **25**, 373-377.
7. D. J. Guo and H. L. Li, *Carbon*, 2005, **43**, 1259-1264.
8. S. R. Lee, Y. T. Lee, K. Sawada, H. Takao and M. Ishida, *Biosensors and Bioelectronics*, 2008, **24**, 410-414.
9. A. Salimi, R. G. Compton and R. Hallaj, *Analytical Biochemistry*, 2004, **333**, 49-56.
10. S. Sampath and O. Lev, *Analytical Chemistry*, 1996, **68**, 2015-2021.
11. Z. Wang, S. Liu, P. Wu and C. Cai, *Analytical Chemistry*, 2009, **81**, 1638-1645.
12. M. C. Daniel and D. Astruc, *Chemical Reviews*, 2004, **104**, 293-346.
13. Y. Xiao, F. Patolsky, E. Katz, J. F. Hainfeld and I. Willner, *Science*, 2003, **299**, 1877-1881.
14. R. G. Freeman, K. C. Grabar, K. J. Allison, R. M. Bright, J. A. Davis, A. P. Guthrie, M. B. Hommer, M. A. Jackson, P. C. Smith, D. G. Walter and M. J. Natan, *Science*, 1995, **267**, 1629-1632.
15. K. C. Grabar, R. Griffith Freeman, M. B. Hommer and M. J. Natan, *Analytical Chemistry*, 1995, **67**, 735-743.
16. J. M. Pingarrón, P. Yáñez-Sedeño and A. González-Cortés, *Electrochimica Acta*, 2008, **53**, 5848-5866.
17. S. Zhang, N. Wang, Y. Niu and C. Sun, *Sensors and Actuators, B: Chemical*, 2005, **109**, 367-374.

18. F. Li, Z. Wang, C. Shan, J. Song, D. Han and L. Niu, *Biosensors and Bioelectronics*, 2009, **24**, 1765-1770.
19. D. Ragupathy, A. I. Gopalan and K. P. Lee, *Electrochemistry Communications*, 2009, **11**, 397-401.
20. M. Chirea, C. M. Pereira and F. Silva, *Journal of Physical Chemistry C*, 2007, **111**, 9255-9266.
21. J. R. Heath and M. A. Ratner, *Physics Today*, 2003, **56**, 43-49.
22. B. Y. Wu, S. H. Hou, F. Yin, J. Li, Z. X. Zhao, J. D. Huang and Q. Chen, *Biosensors and Bioelectronics*, 2007, **22**, 838-844.
23. X. B. Yan, X. J. Chen, B. K. Tay and K. A. Khor, *Electrochemistry Communications*, 2007, **9**, 1269-1275.
24. C. Deng, J. Chen, Z. Nie and S. Si, *Biosensors and Bioelectronics*, **26**, 213-219.
25. S. Komathi, A. I. Gopalan and K.-P. Lee, *Biosensors and Bioelectronics*, 2009, **24**, 3131-3134.
26. S. Zhang, W. Yang, Y. Niu and C. Sun, *Sensors and Actuators B: Chemical*, 2004, **101**, 387-393.
27. J. Wang, *Electroanalysis*, 2005, **17**, 7-14.
28. L. Agüí, P. Yáñez-Sedeño and J. M. Pingarrón, *Analytica Chimica Acta*, 2008, **622**, 11-47.
29. E. J. Calvo and A. Wolosiuk, *Journal of the American Chemical Society*, 2002, **124**, 8490-8497.
30. L. Guo, G. Chen and D. H. Kim, *Analytical Chemistry*, 2010.
31. R. G. Nuzzo, B. R. Zegarski and L. H. Dubois, *Journal of the American Chemical Society*, 1987, **109**, 733-740.
32. S. Kumar and S. Zou, *The Journal of Physical Chemistry B*, 2005, **109**, 15707-15713.
33. H. Ron and I. Rubinstein, *Langmuir*, 1994, **10**, 4566-4573.
34. T. Sagara, N. Kato and N. Nakashima, *The Journal of Physical Chemistry B*, 2002, **106**, 1205-1212.
35. N. Alexeyeva and K. Tammeveski, *Analytica Chimica Acta*, 2008, **618**, 140-146.
36. R. Ehret, W. Baumann, M. Brischwein, A. Schwinde, K. Stegbauer and B. Wolf, *Biosensors & Bioelectronics*, 1997, **12**, 29-41.
37. E. A. H. Hall, N. G. Skinner, C. Jung and S. Szunerits, *Electroanalysis*, 1995, **7**, 830-837.
38. F. Patolsky, M. Zayats, E. Katz and I. Willner, *Analytical Chemistry*, 1999, **71**, 3171-3180.
39. B. Y. Wu, S. H. Hou, F. Yin, J. Li, Z. X. Zhao, J. D. Huang and Q. Chen, *Biosensors & Bioelectronics*, 2007, **22**, 838-844.
40. B. Y. Wu, S. H. Hou, F. Yin, Z. X. Zhao, Y. Y. Wang, X. S. Wang and Q. Chen, *Biosensors & Bioelectronics*, 2007, **22**, 2854-2860.
41. S. X. Zhang, N. Wang, H. J. Yu, Y. M. Niu and C. Q. Sun, *Bioelectrochemistry*, 2005, **67**, 15-22.

42. H. Liu, Y. Tian and Z. Deng, *Langmuir*, 2007, **23**, 9487-9494.
43. C. Bourdillon, C. Demaille, J. Gueris, J. Moiroux and J. M. Saveant, *Journal of the American Chemical Society*, 1993, **115**, 12264-12269.
44. M. Yang, Y. Yang, H. Yang, G. Shen and R. Yu, *Biomaterials*, 2006, **27**, 246-255.
45. R. Kopelman, *Science*, 1988, **241**, 1620-1626.
46. W. Yang, J. Wang, S. Zhao, Y. Sun and C. Sun, *Electrochemistry Communications*, 2006, **8**, 665-672.
47. H. Lineweaver and D. Burk, *Journal of the American Chemical Society*, 1934, **56**, 658-666.
48. K. I. Ozoemena and T. Nyokong, *Electrochimica Acta*, 2006, **51**, 2669-2677.

Chapter 5-Hierarchically Structured One-Dimensional TiO_2 for Effective Enzyme Immobilization, Direct Electrochemistry and Mediatorless Glucose Sensing†

†Reproduced from [**P. Si,** S. Ding, J. Yuan, X. W. Lou and D. H. Kim, ***ACS Nano***, *2011, 5 (9), 7617-7626*] by permission from American Chemical Society. Copyright 2011

5.1. Introduction

Promoting direct electron transfer (DET) between an electrode and immobilized molecules is of scientific importance in the investigation of the fundamental mechanism of biological redox reactions[1-3] and of practical significance for the development of advanced bioelectronic devices such as highly sensitive enzymatic biosensors[4-6] and highly efficient biofuel cells.[7-9] However, the DET of proteins is rarely observed on bare electrodes because the redox center of the enzyme is deeply embedded in a thick insulating protein shell, and the spacing between the prosthetic group and the electrode surface generally exceeds the critical electron-tunneling distance.[10, 11] To facilitate the electron transfer, redox mediators (small diffusive molecules shuttling between the active center of the protein and the electrode surface) have been traditionally employed in the solution phase or immobilized on electrodes.[12-14]

Over the past decades, the exploration of nanomaterials designed to have high conductivity, good biocompatibility, suitable hydrophilicity, a large surface area and a uniform porosity has fueled research on the impregnation of biomolecules and the construction of biosensors.[15-18] Nanomaterials with tailored textures appear to facilitate electron transfer between the electrode and immobilized proteins because the unique chemical, physical and electrical properties of nanostructured materials may effectively shorten the electron-tunneling distance and provide an electron-mediating function.[19-22] Varied nanomaterials composed of carbon,[5, 23, 24] metal oxides[25-27] and

conducting polymers[28, 29] have demonstrated the capabilities of DET. However, significant challenges remain in the development of a nanomaterial that shows fast electron transfer, precise specificity, high sensitivity, and superior bioelectrocatalysis. Due to its superior photocatalytic capability and excellent electron transfer behavior, TiO_2 has been extensively investigated for use in a broad range of applications, including dye-sensitized solar cells,[30, 31] hydrolysis catalysts,[32, 33] electrochromic devices[34, 35] and lithium-ion batteries.[36, 37] Nanocrystalline TiO_2 films have recently been introduced to improve the catalytic activity of enzymes in the applications of gas sensors[38-40] and biosensors.[41-43] The electrochemical properties of TiO_2-based devices are not only influenced by the crystalline form of the TiO_2 but also likely affected by the textural properties of the TiO_2 such as dimension, geometry, porosity and surface area.[25, 44] In addition, the quantum confinement effect and electron transport properties are largely governed by the size and geometry of nanostructured TiO_2.[45, 46] A high surface area and a uniform pore distribution are especially beneficial for TiO_2-based bioelectronic devices because these properties promote the interaction between biomolecules and materials and allow for high accessibility of target molecules to the device surface. This high accessibility facilitates the reaction occurring at the medium/electrode interface.[44]

Template-assisted preparation methods have been used widely in nanoengineering due to their simplicity, cost-effectiveness and shape-control capabilities during synthesis. A variety of templates, including porous anodic alumina,[47, 48] polystyrene spheres,[49, 50] surfactants[51] and activated carbon,[52] have been employed to synthesize nanostructured materials with different morphologies, such as highly ordered nanowires,[53, 54] nanotube arrays,[55, 56] micro/nano hollow structures[57, 58] and mesoporous structures.[59-62] In the present work, a hierarchically structured one-dimensional TiO_2 was, for the first time, synthesized by a solvothermal method using multi-walled carbon nanotubes (MWCNTs) as a template. The synthesized material was characterized by a large surface area and a uniform distribution of pore

sizes. The synthesized TiO_2 showed great biocompatibility for biomolecule immobilization and allowed direct electrochemical reactions for the anchored redox protein. In addition, the glucose-sensing abilities of the electrodes modified with the synthesized TiO_2 were determined in the absence of mediators.

5.2 Enzyme Immobilization and Biosensor Fabrication

Enzyme immobilization was achieved by immersing 10 mg of the synthesized TiO_2 material in 1 mL of GOx solution (10 mg mL^{-1}) prepared in 0.1 M PBS (pH 7.4) under ambient conditions, followed by vigorously shaking of the solution for 0.5 h. The solution was then stored at 4 ℃ overnight to allow protein adsorption. The concentrations of GOx in the solution before and after protein adsorption were determined by UV-vis spectroscopy at 280 nm. The GOx loading on 1DHS TiO_2 was calculated by subtracting the amount of the remaining GOx in supernatant solution after adsorption from the initial amount of GOx. The bioconjugate obtained was later subjected to centrifugation, and the pellet was dispersed in 1 mL of protein-free PBS solution by continuously shaking the mixture for 0.5 h. A glassy carbon electrode (GCE, 3 mm in diameter) was polished to a mirror-like surface with 1.0, 0.3 and 0.05 μm alumina powder followed by sonication in acetone, ethanol and water for 3 min, respectively. Then the electrode was thoroughly rinsed with double-distilled water and dried using ultrapure nitrogen. Electrode modification was achieved by depositing 5 μL of the re-shaken bioconjugate dispersion on the center of the pre-cleaned GCE, which was left to dry at 4 ℃ overnight. Finally, 10 μL of 0.5 % Nafion was dropped on the whole electrode surface to fix the modifier on the electrode.

5.3. Results and Discussion

5.3.1. Material Characterizations

The surface morphology and microstructure of the synthesized TiO_2 were characterized by FESEM and TEM (Figure 5-1). Figure 5-1a shows the SEM image of the as-prepared CNT-TiO_2 nanocomposite synthesized *via* the solvothermal method. The composite displays one dimensional, rough and porous structure with diameter of

around 100 nm. The magnified SEM image (Inset of Figure 5-1a) reveals a hierarchically structured surface morphology of the composite material. The TEM image in Figure 5-1b shows that CNTs in the composite are homogeneously encapsulated by TiO_2 nanoclusters that consist of ultrathin nanosheet-like structures (inset of Figure 5-1b). The formation of TiO_2 nanosheets on the CNT surface could be mainly attributed to the dual function of diethylenetriamine (DETA): catalyzing the hydrolysis of titanium (IV) isopropoxide (TIP) to form TiO_2 nanosheets,[36] and assisting the formed TiO_2 nanostructures self-assemble on the surface of acid-treated CNT, possibly through electrostatic interactions.[37] Figure 5-1c shows the SEM image of TiO_2 obtained after calcining the CNT-TiO_2 composite at 550 ℃ for 2 h. The calcined TiO_2 maintains its one-dimensional (1D) structure after removing the CNT templates and displays more delicate surface textures (inset of Figure 5-1c). The TEM image of calcined TiO_2 (Figure 5-1d) reveals that the 1D TiO_2 has a hierarchical structure from which the CNT template has been completely removed. The diameter of the 1D hierarchically structured TiO_2 (1DHS TiO_2) is approximately 60~80 nm, much smaller than the CNT-TiO_2 composite, possibly because of the partial collapse of the hollowed TiO_2 structure during the annealing process.

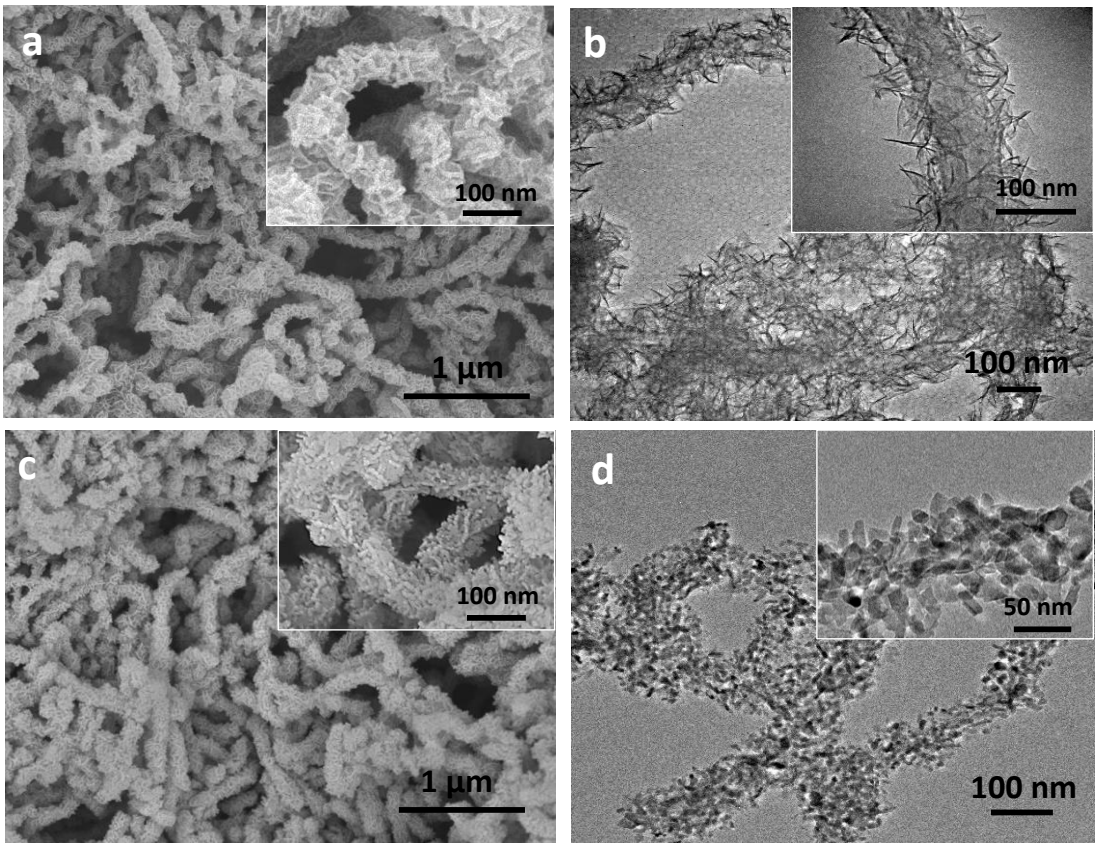

Figure 5-1. SEM (a, c) and TEM (b, d) images of the CNT-TiO_2 composite (a, b) and the 1DHS TiO_2 (c, d) obtained after calcining the composite at 550 ℃ for 2 h. Insets are the high-magnification SEM and TEM images.

The phase features of the synthesized TiO_2 were investigated by X-ray powder diffraction (XRD, Figure 5-2a). The pristine, uncalcined CNT-TiO_2 composite shows weak peak intensities (Figure 5-2a, pattern I), suggesting poor crystallinity of the uncalcined CNT-TiO_2. The two main peaks at 25 and 48 ℃ correspond to the anatase (101) and (200) diffractions (JCPDS card no: 21-1272), indicating that anatase TiO_2 formed on the surface of CNT during the solvothermal treatment. The intensities of the XRD peaks are significantly enhanced after sintering the composite at 550 ℃ for 2 h (Figure 5-2a, pattern II), reflecting the high crystallinity and high purity of the resultant TiO_2 material. The identified peaks matches perfectly with those of the standard XRD pattern of anatase TiO_2, with lattice constants of a_0=3.785 and c_0=9.513, respectively.

The nitrogen adsorption-desorption isotherms (Figure 5-2b) of the 1DHS TiO_2

shows a type-H3 hysteresis loop with an abrupt increase in the adsorption branch at a high relative pressure (P/P_0), implying the presence of mesoporous structures and a narrow distribution of pore sizes.[63] The inset of Figure 5-2b depicts the pore size distribution of 1DHS TiO_2, calculated by the Barrett-Joyner-Halenda method from the two branches of the isotherm. The 1DHS TiO_2 has a uniform distribution of pore diameters centered at 7 and 9 nm, roughly matching the dimension of GOx molecules (7.0 nm × 5.5 nm × 8.0 nm).[64] The 1DHS TiO_2 was also estimated to have a specific surface area as high as 218.4 m^2 g^{-1}, as analyzed by the Brunauer-Emmett-Teller (BET) method.

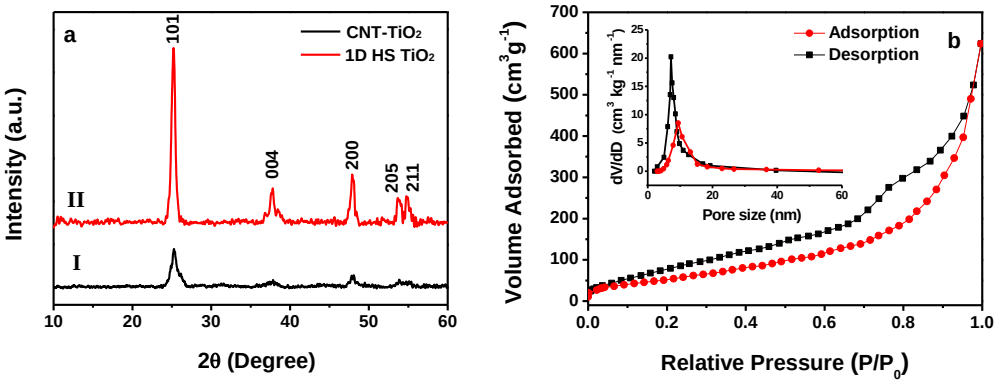

Figure 5-2. (a) XRD patterns for (I) the CNT-TiO_2 composite and (II) the 1DHS TiO_2 formed after calcination. (b) Nitrogen adsorption-desorption isotherms of the 1DHS TiO_2. Inset: Pore size distribution calculated from the adsorption branch and desorption branch of the isotherm by the Barrett-Joyner-Halenda method.

5.3.2. Immobilization of GOx on 1DHS TiO_2

To find the optimal immobilization concentration of GOx on 1DHS TiO_2, we investigated the nitrogen adsorption-desorption isotherms of 1DHS TiO_2 before GOx loading and after GOx loading with different initial concentrations of GOx. Since increases in the GOx concentration resulted in decreases in both the pore diameter and the pore volume (Table 5-1), we can infer that the GOx, when introduced, fills in the pores of the 1DHS TiO_2. As a result, the hysteresis loop shows that the amount of adsorbed nitrogen decreases as the GOx loading increases (Figure 5-3). The inset of Figure 5-3 depicts the relationship between the initial GOx concentration and the final

weight of GOx loaded on the TiO_2 material. Increases in the GOx concentration leads to increases in the amount of protein immobilized on the TiO_2, reaching a maximum loading of 42.7% at the GOx concentration of 10 mg mL^{-1}. Further increases in the GOx concentration does not result in increase in the protein loading, most likely due to the saturation of pore spaces in 1DHS TiO_2. A quantity of 10 mg mL^{-1} of GOx was therefore used for protein immobilization in the later experiment.

Table 5-1. Textural properties of 1DHS TiO_2 before and after GOx loading

GOx concentration (mg mL^{-1})	GOx loading (wt % TiO_2)	BET surface area (m^2 g^{-1})	Total pore volume (cm^3 kg^{-1})	Pore diameter (nm)
0	0	218.4	135.54	7.43
5	30.2 ±1.2	139.5	82.61	3.61
10	42.7 ±2.4	72.1	47.85	2.16
15	41.4 ±2.6	69.2	42.56	1.98
20	43.3 ±2.1	63.7	45.12	2.21

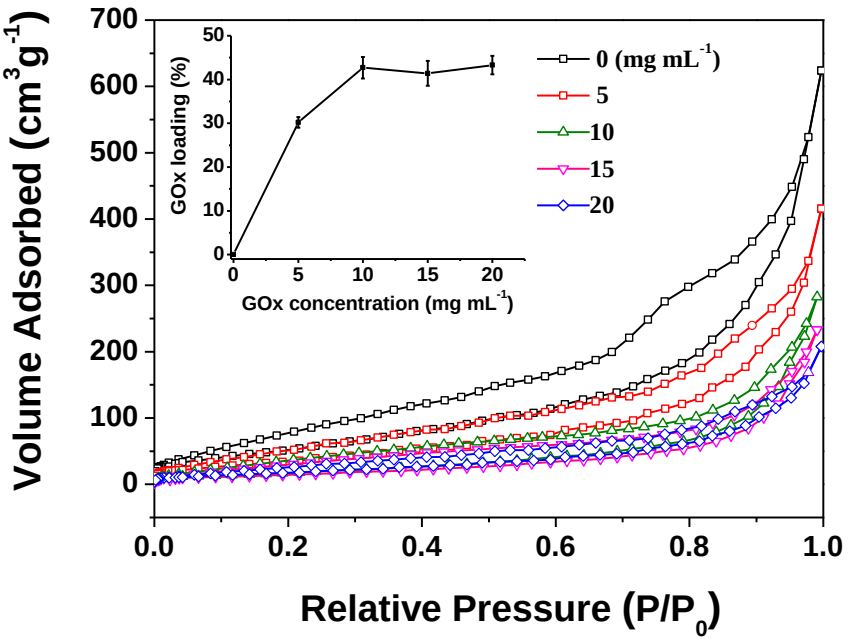

Figure 5-3. The nitrogen adsorption-desorption isotherms of 1DHS TiO_2 before and after loading with different GOx concentrations ranging from 0 to 20 mg mL^{-1}. Inset: The plot of the GOx loading ratio on 1DHS TiO_2 versus the GOx concentration.

The effectiveness of protein immobilization on 1DHS TiO_2 was investigated by IR spectroscopy (Figure 5-4) to detect the conformational changes of the secondary structure of the proteins. The spectrum of pure GOx molecules exhibits two characteristic peaks at 1658 and 1545 cm^{-1}, corresponding to the typical amide I and amide II adsorption bands of proteins.[23] The signal peaking at 1103 cm^{-1} is attributed to the C-O bond stretching vibration of GOx.[29] The 1DHS TiO_2 has bands at 1635 and 1040 cm^{-1}, which are ascribed to the deformational vibration of the H-O-H bond from absorbed water and the stretching vibration of the Ti-O-C bond from the hydrolysis of TIP, respectively.[25] The amide adsorption peaks are generally used as an indication of protein denaturation and conformational change upon immobilization. The presence of both amide I and amide II adsorption peaks in the spectrum of GOx-loaded 1DHS TiO_2 indicates that the enzyme retained its secondary structure after being adsorbed on the surface of TiO_2. The biocompatible nature of 1DHS TiO_2 may allow GOx to maintain its native structure, thus preventing denaturation of GOx. The amide adsorption peaks are downshifted slightly to 1647 and 1533 cm^{-1}, possibly due to the strong electrostatic interaction between the anchored enzyme and the TiO_2 (GOx is negatively charged at neutral pH (isoelectric point (pI)=4.2),[65] while TiO_2 is positively charged at neutral pH due to its relatively high pI.[66] In addition, a downshift of the Ti-O-C adsorption peak is observed in the spectrum of GOx-loaded 1DHS TiO_2, further corroborating the electrostatic interaction between the negatively charged GOx and the positively charged TiO_2. The surface density of GOx on the electrode is calculated to be 83.4 % by electrochemical impedance spectroscopy (EIS), which is an efficient method to investigate the surface properties of biomolecule-modified electrodes (Figure 5-5).

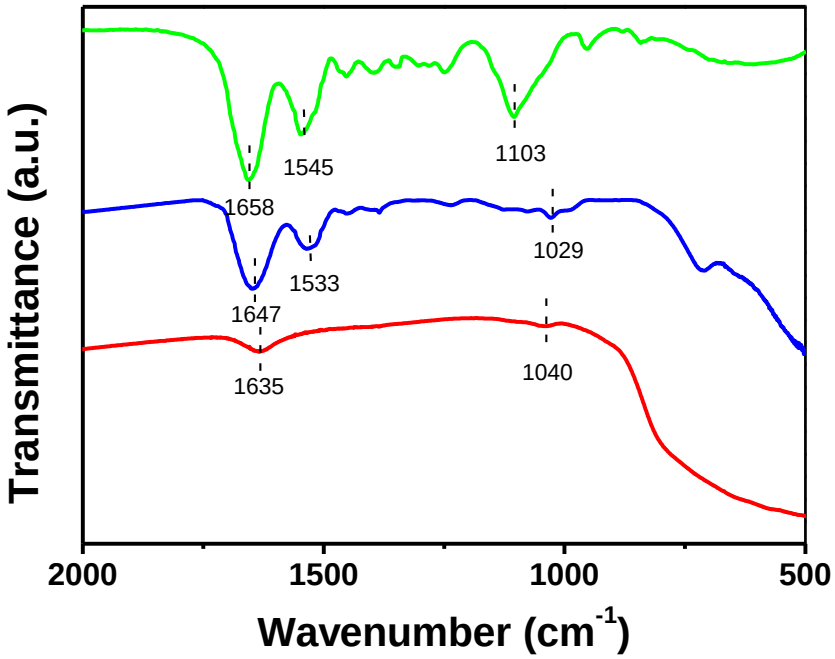

Figure 5-4. IR spectra of 1DHS TiO_2 (red), pure GOx (green) and GOx-loaded TiO_2 (blue).

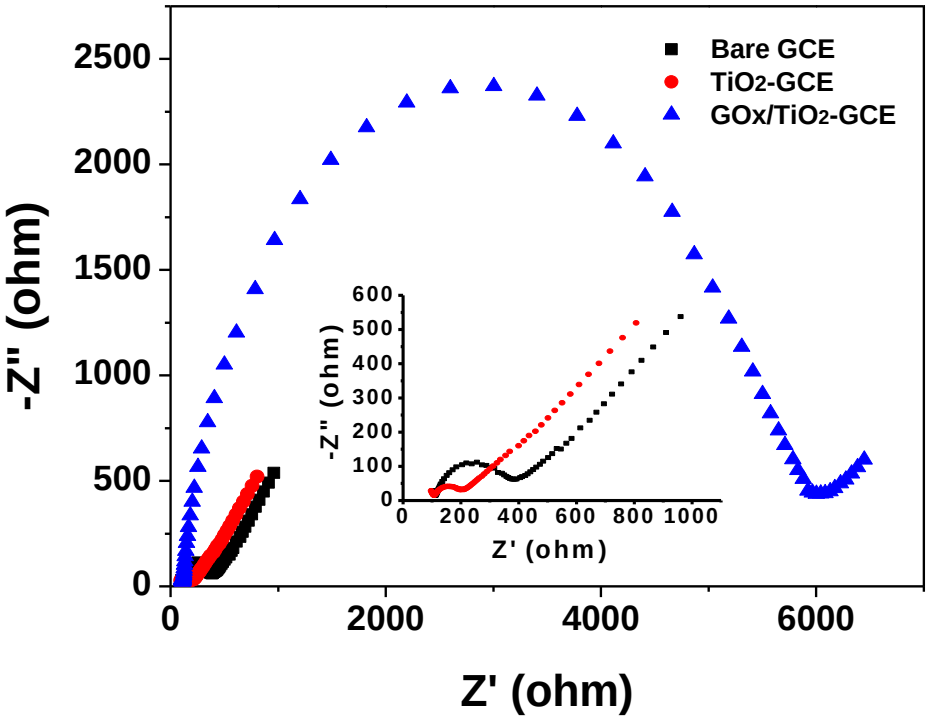

Figure 5-5. Nyquist plots of a bare GCE, a 1DHS TiO_2-modified GCE and a GOx/1DHS TiO_2-modified GCE measured in 1.0 M KCl solution containing 10 mM $Fe(CN)_6^{3-/4}$.

5.3.3. Direct Electrochemistry of GOx Immobilized on 1DHS TiO_2

To study the direct electron transfer of GOx immobilized on 1DHS TiO_2, cyclic voltammetry (CV) measurements were performed using 1DHS TiO_2/Nafion-, GOx/Nafion- and GOx/1DHS TiO_2/Nafion-modified GCEs in 0.1 M nitrogen-saturated PBS solution (pH 7.4) at a scan rate of 100 mV s^{-1}. A high scanning rate in CV measurement is used to achieve reversibility of an electrochemical reaction.[25] As shown in Figure 5-6, TiO_2/Nafion- and GOx/Nafion-modified electrodes exhibited only typical square-shaped CV curves as a result of double-layer capacitance in the applied potential window, indicating that both the 1DHS TiO_2 and GOx are electrochemically inactive over this potential range. In contrast, two well-defined redox peaks are observed in the CV of the GOx/1DHS TiO_2/Nafion-modified GCE, with a cathodic peak potential (E_{pc}) of -0.481 V and an anodic peak potential (E_{pa}) of -0.443 V. The formal potential (E^0) of 0.462 V in our study conforms well to the standard electrode potential of FAD/$FADH_2$ in solution at a neutral pH,[25, 29] indicating that the redox center of GOx immobilized on the 1DHS TiO_2 undergoes a quasi-reversible reaction on the electrode during the CV cycle:

$$\mathrm{GOx\ (FAD)} + 2\mathrm{H^+} + 2\mathrm{e^-} \rightarrow \mathrm{GOx\ (FADH_2)} \qquad (5-1)$$

$$\mathrm{GOx(FADH_2)} - 2\mathrm{e^-} \rightarrow \mathrm{GOx\ (FAD)} + 2\mathrm{H^+} \qquad (5-2)$$

where FAD and $FADH_2$ are the oxidized and reduced forms of the GOx redox center, respectively. This result illustrates that the 1DHS TiO_2 is apparently capable of mediating protein DET on the electrode. The heterogeneous electron transfer rate constant k_s of GOx immobilized on 1DHS TiO_2 is calculated to be 7.8 s^{-1} according to Laviron's model,[67] a value that is substantially greater than that of GOx immobilized on other materials, *e.g.*, porous TiO_2 (3.96 s^{-1}),[25] NiO (3.12 s^{-1}),[29] MWCNTs (1.53 s^{-1})[68] and SWCNTs (0.3 s^{-1}).[69] This remarkably improved electrochemical response of GOx on 1DHS TiO_2 could be attributed to several factors. First, the GOx could enter the pores in the 1DHS TiO_2 due to the similarity in their sizes, providing omnidirectional contacts to the TiO_2 surface and significantly

shortening the electron tunneling distance between the enzyme's active center and the material's conductive site. Secondly, the strong electrostatic interaction between GOx and TiO_2 could further narrow the spacing between the material and the adsorbed protein, thereby facilitating electron transfer between the electrode and immobilized GOx molecules. Finally, the high conductivity and low charge transfer resistance of 1DHS TiO_2 could provide an electron transfer conduction pathway, which is also favorable for the direct electrochemical reaction of immobilized proteins.

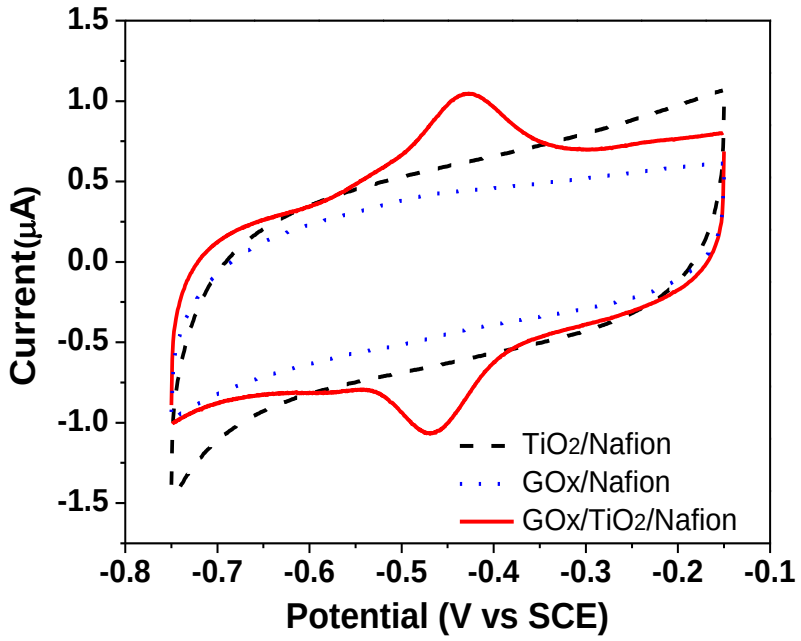

Figure 5-6. CVs of 1DHS TiO_2/Nafion-, GOx/Nafion- and GOx/1DHS TiO_2/Nafion-modified GCEs measured in 0.1 M pH 7.4 nitrogen-saturated PBS solution at scan rate of 100 mV s^{-1}.

The electroactive protein density (Γ, mol cm^{-2}) of the GOx/1DHS TiO_2/Nafion-modified electrode could be estimated from the integration of the reduction peak at 100 mV s^{-1} by the following equation:

$$Q = nFA\Gamma \qquad (5-3)$$

Where Q is the total charge passing through the electrode, n is the number of electrons being transferred, F is Faraday's constant, and A is the geometric area of the electrode's surface. The surface coverage of electroactive GOx is calculated to be 6.86 $\times$ 10^{-10} mol cm^{-2}, a value that is much greater than that observed for GOx

immobilized on porous TiO_2 (2.57×10^{-10} mol cm^{-2}),[25] PEDOT-NiO NS (1.56×10^{-10} mol cm^{-2}),[29] AuNPs (9.8×10^{-12} mol cm^{-2})[70] and CdS (1.54×10^{-11} mol cm^{-2}).[71] The measured GOx loading of 42.7% and the surface GOx coverage of 83.4% can be converted to a unit surface adsorption density of 1.82×10^{-9} mol cm^{-2} by taking account of the dimension of GOx (7.0 nm × 5.5 nm × 8.0 nm) and specific surface area of 1DHS TiO_2 (218.4 m^2 g^{-1}). We can infer that approximately 37.7 % of the enzyme immobilized on the 1DHS TiO_2 retains its electroactivity and achieves direct electrochemistry on the modified electrode surface. The results further corroborates that the 1DHS TiO_2 material has great biocompatibility that could well maintain the native structure of absorbed GOx, as confirmed by the FTIR results.

The electrochemical response of GOx immobilized on the 1DHS TiO_2 also displays strong dependence on the scanning rate (Figure 5-7) and solution pH (Figure 5-8), showing that the redox reaction of $FAD/FADH_2$ in the active center of GOx is surface-confined reaction and two-electron coupled electrochemical process. The proposed mechanisms are specifically described as follows.

Figure 5-7 displays the effect of the scan rate on the electrochemical response of GOx tethered to 1DHS TiO_2. The anodic and cathodic peak currents increase linearly with increases in the scan rate from 25 to 600 mV s^{-1}, indicating that the redox reaction of $FAD/FADH_2$ occurring in the active center of GOx is a surface-confined electrochemical process. The peak-to-peak separation (ΔE_p) is also observed to increase slightly with increases in the scan rate, possibly resulting from the internal resistance of the modified electrode.

The electrochemical response of GOx on 1DHS TiO_2 also demonstrates strong dependence on the pH of the testing environment, as shown in Figure 5-8. Both anodic and cathodic peak potentials shift negatively with increases in the solution pH (Figure 5-8a), indicating that protons are involved in the quasi-reversible reaction of $FAD/FADH_2$. The formal potential (E^0) exhibits a linear relationship with the pH over the range of 5.1~8.0, and the slope is calculated to be 57.6 mV pH^{-1} (inset of

Figure 5-8b), which is close to the theoretical value of 59.0 mV pH^{-1} obtained from the following equation: [25]

$$E = E^0 + \frac{2.3RT}{nF}\log\left[\frac{C_{GOx(FAD)} \times (C_{H^+})^2}{C_{GOx(FAD)}}\right] \quad (5\text{-}4)$$

The concentrations (C) of GOx(FAD) and GOx($FADH_2$) are constants in the electrochemical process, so the above equation could be simplified as:

$$E = E^0 - \frac{2.3RT \times 2}{nF}\mathrm{pH} \quad (5\text{-}5)$$

$$E^{0'} = E^0 - 0.059\mathrm{pH} \quad (5\text{-}6)$$

where n, R, T and F are the number of transferred electrons, the gas constant, the temperature and the Faraday constant, respectively. Because a value of 0.059 is obtained when n=2, the DET of GOx on 1DHS TiO_2 is a two-proton coupled redox reaction involving a two-electron transfer process (shown by *eqns.* 5-1 and 5-2). The pH also affects the peak current, which increases with increases in the pH until a maximum value is reached at pH of 7.4 (Figure 5-8b). Further increases in the pH, however, leads to a reduction in the peak current intensity, possibly because the GOx immobilized on 1DHS TiO_2 has the highest bioactivity at a neutral pH. Further experiments were conducted in PBS solutions at pH 7.4.

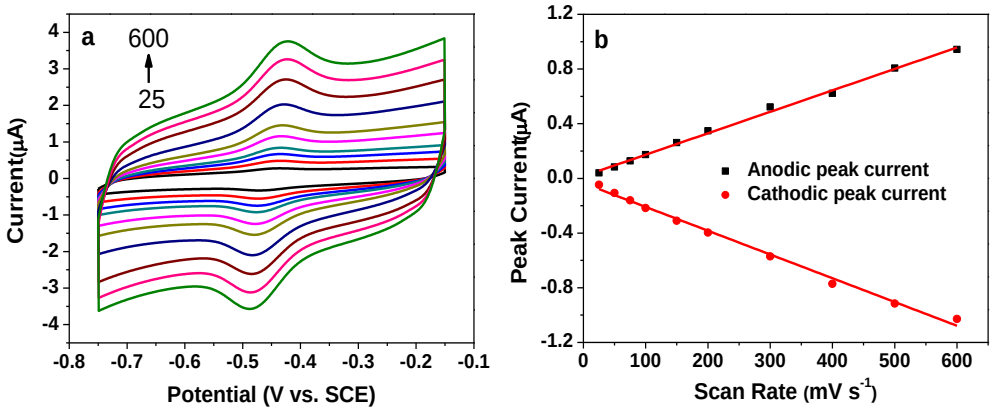

Figure 5-7. a) CVs of a GOx/1DHS TiO_2/Nafion-modified GCE in 0.1 M pH 7.4 nitrogen-saturated PBS solution at different scan rates (from 25 to 600 mV s^{-1}, inside to outside). b) Plots of peak current versus scan rate.

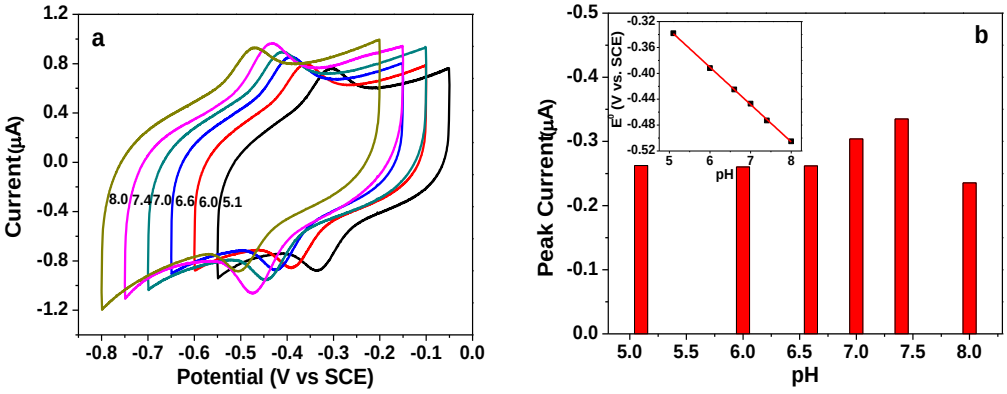

Figure 5-8. a) CVs of a GOx/1DHS TiO_2/Nafion-modified GCE in 0.1 M nitrogen-saturated PBS solution at different pHs at 100 mVs^{-1}. b) Plot of peak currents versus pH. Inset of (b): Plot of formal potential versus pH.

5.3.4. Glucose Oxidation and Oxygen Reduction on GOx/1DHS TiO_2

To study glucose oxidation through the direct electrochemical reaction of GOx on 1DHS TiO_2, CV measurements of the GOx/1DHS TiO_2/Nafion-modified electrode were carried out in nitrogen-saturated PBS solution containing different concentrations of glucose (0, 1, 2, 5, 10, 20 and 50 mM glucose) (Figure 5-9a). A pair of well-defined redox peaks is observed in the absence of glucose due to the reversible reaction of FAD/$FADH_2$. With increases in the glucose concentration, both the anodic and cathodic peak currents decrease, which could be explained by the following reaction:

$$\text{glucose} + \text{GOx(FAD)} \rightarrow \text{gluconic acid} + \text{GOx}(FADH_2) \qquad (5-7)$$

The equation indicates that FAD at the redox center of GOx is directly involved in the glucose oxidation reaction. As glucose concentration increases, GOx(FAD) is increasingly converted into GOx($FADH_2$), leading to a continuous decrease in the cathodic and corresponding anodic peak currents. Figure 5-9b depicts the cathodic branches of the background-subtracted CV curves in Figure 5-9a (Figure 5-9a was converted to the current increase by subtracting the background CV curve (0 mM glucose) from other CV curves (1~50 mM glucose)). The cathodic current increases linearly with increases in the glucose concentration until the saturation current reaches

10 mM glucose (inset of Figure 5-9b). This result indicates that the direct electrochemical reaction of protein achieved on the electrode could be effectively employed for glucose sensing without any mediator. The sensing mechanism in our system is different from those of both first-generation glucose sensors, in which glucose oxidation is based on oxygen reduction, and second-generation glucose sensors, which require a mediator to transfer the electrons between GOx and electrode.[11]

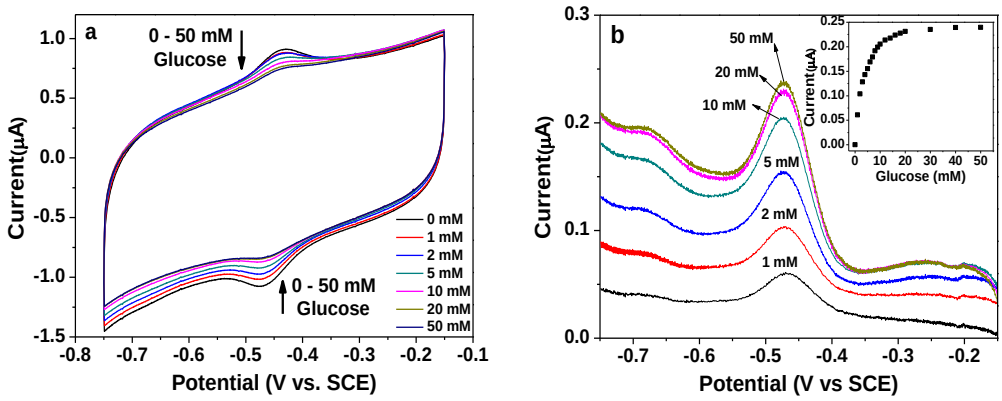

Figure 5-9. a) CVs of a GOx/1DHS TiO_2/Nafion-modified GCE in 0.1 M pH 7.4 nitrogen-saturated PBS solution with different glucose concentrations (some data not shown for clarity). b) Cathodic branches of the background-subtracted CV curves in (a). Inset of (b) is the calibration curve. Scan rate: 100 mV s^{-1}.

Similar CV measurements were conducted in air-saturated PBS solution containing different glucose concentrations on the GOx/1DHS TiO_2/Nafion-modified electrode. In contrast to the curves obtained in nitrogen-saturated PBS, a huge cathodic current is observed in the CV cycle at a potential of less than -0.4 V in the absence of glucose (Figure 5-10a), arising from the electrocatalytic reduction of the dissolved oxygen by the GOx/1DHS TiO_2/Nafion-modified electrode.[29, 70] However, the reductive current at the FAD redox potential gradually decreases with increases in the glucose concentration, exhibiting a linear relationship with the glucose concentration in the range of 0.2 to 1.0 mM. The current starts to saturate at 1.0 mM glucose and quickly reaches a maximum at 2.0 mM (Figure 5-10b). The relatively smaller linear range, however, is compensated by the remarkably enhanced sensitivity, which is nearly 40

times higher than the corresponding value measured in nitrogen-saturated PBS, possibly due to the integral effect of FAD reduction by glucose (*eqn.* 5-7) and competitive oxygen consumption by both glucose and $FADH_2$ (*eqns.* 5-8 and 5-9).[29]

$$\text{glucose} + O_2 \rightarrow \text{gluconic acid} + H_2O_2 \qquad (5-8)$$

$$GOx(FADH_2) + O_2 \rightarrow GOx(FAD) + H_2O_2 \qquad (5-9)$$

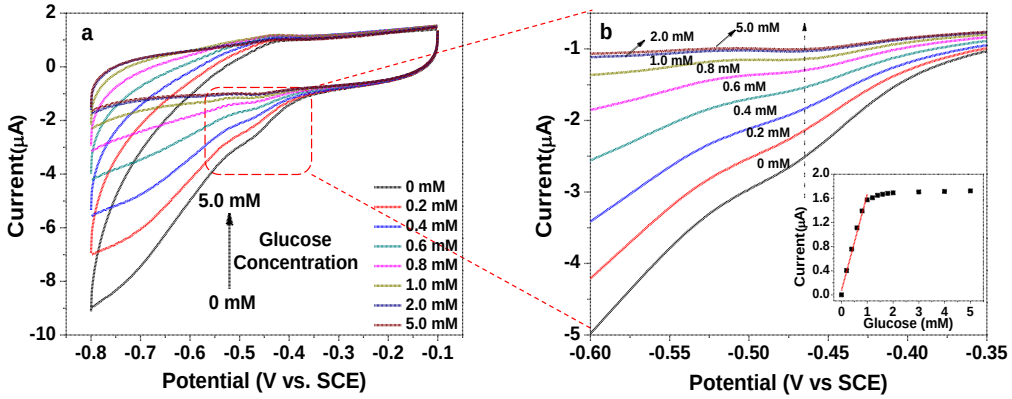

Figure 5-10. a) CVs of a GOx/1DHS TiO_2/Nafion-modified GCE in 0.1 M pH 7.4 air-saturated PBS solution with different glucose concentrations (some data not shown for clarity). b) Enlarged graph showing the rectangular region marked in (a). Inset of (b): The calibration plot of the cathodic current versus the glucose concentration at -0.462 V. Scan rate: 100 mV s^{-1}.

5.3.5. Glucose Sensing Performance of the GOx/1DHS TiO_2/Nafion-Modified Electrode

The glucose sensing performance of the GOx/1DHS TiO_2/Nafion-modified electrode was evaluated by amperometric measurements in air-saturated PBS at a fixed potential of -0.45 V, where a decrease in the voltammetric currents is observed with the repeated addition of glucose. Figure 5-11a shows the typical amperogram obtained by successive additions of 0.15 mM (2.25 μmol) glucose into homogeneously stirred 0.1 M PBS (pH 7.4) with a time interval of 50 s. Each injection of 0.15 mM glucose results in a decrease of 120 nA in the cathodic current for the first ten steps, which gives rise to a sensitivity of 9.90 μA mM^{-1} cm^{-2}. In addition, 95 % of the steady-state current could be reached within 5 s upon the addition of glucose, reflecting the fast response of our glucose sensor. Both the sensitivity and the response time of our sensor are greatly superior to those of other

metal-oxide-based glucose biosensors, which are listed in Table 5-2. Figure 5-11b depicts the calibration curve of the modified electrode obtained from the current-time plot, showing a well-defined typical behavior of an enzymatic reaction with a linear range up to 1.5 mM. A current plateau is observed when the glucose concentration is higher than 1.5 mM. A linear regression equation of $\mathrm{I\,(\mu A)} = 0.80\ (\mu A\ mM^{-1}) \times \mathrm{C\ (mM)}, (\mathrm{n} = 3, \mathrm{R} = 0.994)$ is thus derived from the calibration curve, revealing that the glucose sensor has a detection limit as low as 1.29 μM (S/N = 3). The apparent Michaelis-Menten constant $\mathrm{K_M^{app}}$ is calculated using the electrochemical version of the Lineweaver-Burk equation: [72]

$$\frac{1}{i_{ss}} = \frac{K_m^{app}}{i_{max}} \frac{1}{C} + \frac{1}{i_{max}} \qquad (5-10)$$

where i_{ss} is the steady-state current, i_{max} is the saturation current, and C is the glucose concentration. K_m^{app} is determined to be 1.54 mM from the intercept and slope of the Lineweaver-Burk plot (Figure 5-11b), a value that is much lower than the value of 8.5 mM for GOx immobilized on carbon nanohorns[73] and 6.08 mM for GOx immobilized on redox polymers.[74] The smaller $\mathrm{K_M^{app}}$ indicates that the GOx/1DHS TiO_2-modified electrode has superior enzymatic activity and higher affinity for the glucose substrate.[29]

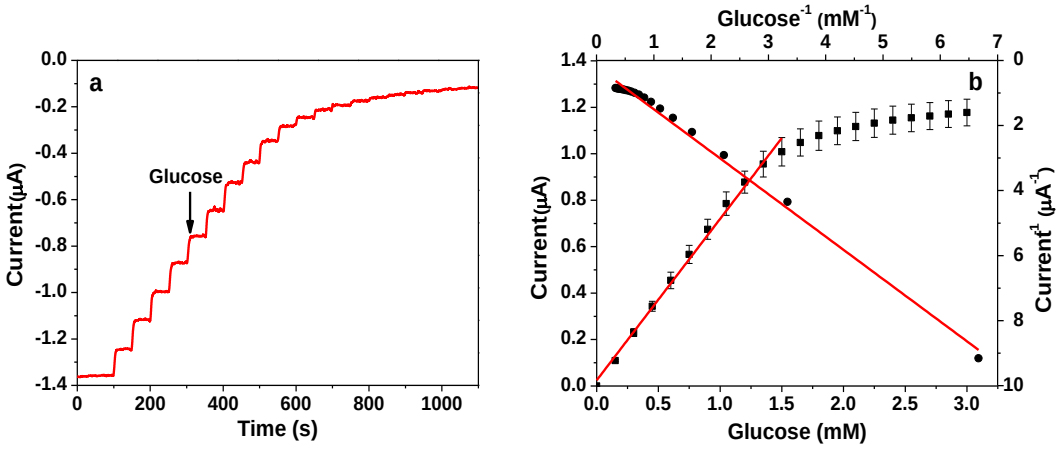

Figure 5-11. a) Current-time curve of a GOx/1DHS TiO_2/Nafion-modified GCE for successive addition of 0.15 mM glucose aliquots to stirred 0.1 M pH 7.4 air-saturated PBS at -0.45 V. b) The calibration curve (current versus glucose concentration) and the Lineweaver-Burk plot (current^{-1} versus concentration^{-1}) obtained from the amperometric response in (a).

Table 5-2. Comparison of the analytical performance of metal-oxide-based glucose sensors

Electrode material	Sensitivity (μA mM^{-1} cm^{-2})	Response time (s)	Reference
GOx/1DHS TiO_2	9.9	< 5	This work
GOx/Mesoporous TiO_2	3.9	< 10	[25]
GOx/Nanocrystalline TiO_2	4.6	< 30	[75]
GOx/TiO_2-copolymer	2.3	< 20	[76]
GOx/Porous carbon-silica	1.8	~ 4	[23]
GOx/NiO hollow spheres	3.4	~ 8	[77]

The GOx/1DHS TiO_2-modified electrode also exhibits excellent selectivity for glucose detection. As shown in Figure 5-12a, the addition of interferents, *e.g.*, 0.3 mM ascorbic acid (AA), 0.2 mM dopamine (DA) and 0.5 mM uric acid (UA), in 0.1 M PBS containing 0.6 mM glucose gives rise to negligible current changes, while a significant current response is observed for the subsequent addition of 0.45 mM glucose. To assess its stability, the GOx/1DHS TiO_2-modified electrode was stored at 4 ℃ after use and used to measure the current response for 0.3 mM glucose every three days. The GOx/1DHS TiO_2/Nafion-modified electrode retains 91.2 % of its original current response over a storage period of 2 weeks (Figure 5-12b), indicating a good shelf lifetime for the modified electrode. In addition, upon repeated scanning of the GOx/1DHS TiO_2-modified electrode in 0.1 M PBS containing 0.3 mM glucose at 100 mV s^{-1}, the voltammetric current response was observed to decrease very slowly, i.e., a peak current drop of 4.5 %, even after continuous sweeping for 5 h. Moreover, UV-Vis spectroscopy reveals no desorbed GOx detectable in the CV measurement solution, possibly due to the protein-leaching barrier formed by the Nafion membrane on the electrode. The superior sensing performance and long-term storage stability of the GOx/1DHS TiO_2-modified electrode may be attributable to the unique structure and great biocompatibility of 1DHS TiO_2 and to the strong electrostatic interaction between GOx and the synthesized TiO_2 material.

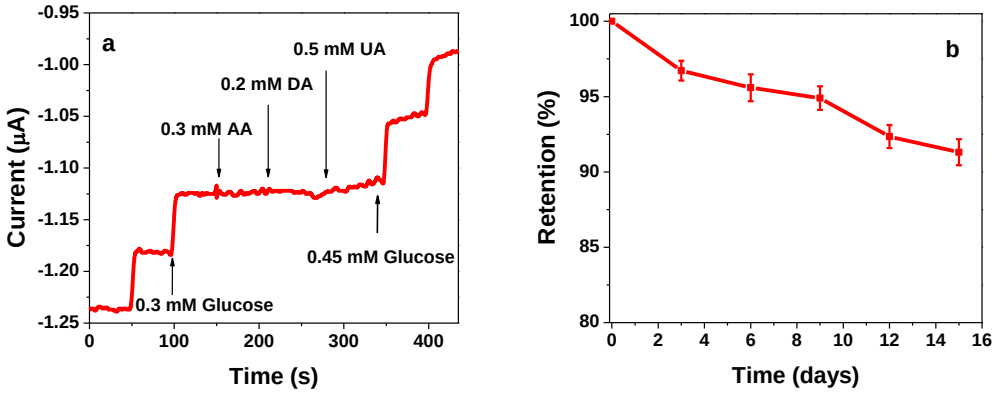

Figure 5-12. a) Amperogram showing the effect of interfering compounds (0.3 mM AA, 0.2 mM DA and 0.5 mM UA) on the detection of glucose. b) The stability of the GOx/1DHS TiO_2/Nafion-modified electrode over a two-week storage period.

5.4. Conclusion

In the present work, a novel material, 1DHS TiO_2, was synthesized, characterized and used for the immobilization of GOx for direct electrochemical reactions and mediator-free glucose sensing. The 1DHS TiO_2 was easily synthesized by a solvothermal method using MWCNT as a template with a large surface area and a uniform pore distribution. The protein immobilization was characterized by BET, FTIR and EIS, revealing that GOx immobilized on 1DHS TiO_2 maintained its original conformation well and that the maximum protein loading on 1DHS TiO_2 was achieved at a GOx concentration of 10 mg mL^{-1}. The great biocompatibility of 1DHS TiO_2 and the electrostatic interaction between GOx and 1DHS TiO_2 may contribute to the high bioactivity of the immobilized proteins. The electrochemical properties of GOx immobilized on 1DHS TiO_2 were studied systematically. These electrochemical properties included fast direct electrochemical reactions, surface-confined electron transfer behavior and strong pH dependence. The sensing mechanism of protein DET on 1DHS TiO_2 was demonstrated by cyclic voltammetry in both nitrogen-saturated PBS and air-saturated PBS, revealing that the integral effect of glucose oxidation by FAD and oxygen reduction by both glucose and $FADH_2$ resulted in a significant decrease in the cathodic current and allowed for a high sensitivity for glucose

detection. The analytical performance of the GOx/1DHS TiO_2/Nafion-modified electrode was investigated by the amperometric response, showing a fast response time, good specificity and long-lifetime stability. Our study not only demonstrates a unique structured and biocompatible TiO_2 nanomaterial suitable for protein immobilization, direct electrochemical reactions and the construction of third-generation biosensors but also provides fundamental insight leading to the understanding of the mechanism of protein DET on nanomaterials, especially the direct electrochemical reaction of GOx for glucose sensing.

Reference

1. M. K. Beissenhirtz, F. W. Scheller, W. F. M. Stocklein, D. G. Kurth, H. Mohwald and F. Lisdat, *Angewandte Chemie-International Edition*, 2004, **43**, 4357-4360.
2. A. El Kasmi, J. M. Wallace, E. F. Bowden, S. M. Binet and R. J. Linderman, *Journal of the American Chemical Society*, 1998, **120**, 225-226.
3. J. J. Wei, H. Y. Liu, A. R. Dick, H. Yamamoto, Y. F. He and D. H. Waldeck, *Journal of the American Chemical Society*, 2002, **124**, 9591-9599.
4. S. Y. Deng, G. Q. Jian, J. P. Lei, Z. Hu and H. X. Ju, *Biosensors & Bioelectronics*, 2009, **25**, 373-377.
5. C. S. Shan, H. F. Yang, J. F. Song, D. X. Han, A. Ivaska and L. Niu, *Analytical Chemistry*, 2009, **81**, 2378-2382.
6. Y. Xiao, F. Patolsky, E. Katz, J. F. Hainfeld and I. Willner, *Science*, 2003, **299**, 1877-1881.
7. S. K. Chaudhuri and D. R. Lovley, *Nature Biotechnology*, 2003, **21**, 1229-1232.
8. D. Ivnitski, B. Branch, P. Atanassov and C. Apblett, *Electrochemistry Communications*, 2006, **8**, 1204-1210.
9. Y. M. Yan, W. Zheng, L. Su and L. Q. Mao, *Advanced Materials*, 2006, **18**, 2639-2643.
10. A. Riklin, E. Katz, I. Willner, A. Stocker and A. F. Buckmann, *Nature*, 1995, **376**, 672-675.
11. N. J. Ronkainen, H. B. Halsall and W. R. Heineman, *Chemical Society Reviews*, 2010, **39**, 1747-1763.
12. J. Wang, *Electroanalysis*, 2001, **13**, 983-988.
13. J. Wang, *Chemical Reviews*, 2008, **108**, 814-825.
14. P. Si, P. Kannan, L. Guo, H. Son and D.-H. Kim, *Biosensors and Bioelectronics*, 2011, **26**, 3845-3851.
15. V. B. Kandimalla, V. S. Tripathi and H. X. Ju, *Biomaterials*, 2006, **27**, 1167-1174.
16. D. Ivnitski, K. Artyushkova, R. A. Rincon, P. Atanassov, H. R. Luckarift and G. R. Johnson, *Small*, 2008, **4**, 357-364.
17. L. Guo, A. R. Ferhan, K. Lee and D.-H. Kim, *Analytical Chemistry*, 2011, **83**,

2605-2612.
18. S. Z. Qiao, L. Zhang, W. C. Geng, H. J. Zheng, G. Q. Lu and Z. F. Yan, *ACS Applied Materials & Interfaces*, 2010, **2**, 2767-2772.
19. A. Liu, M. Wei, I. Honma and H. Zhou, *Analytical Chemistry*, 2005, **77**, 8068-8074.
20. K. J. McKenzie and F. Marken, *Langmuir*, 2003, **19**, 4327-4331.
21. G. Z. Liu, M. N. Paddon-Row and J. J. Gooding, *Electrochemistry Communications*, 2007, **9**, 2218-2223.
22. J. Zhang, M. Feng and H. Tachikawa, *Biosensors & Bioelectronics*, 2007, **22**, 3036-3041.
23. S. Wu, H. X. Ju and Y. Liu, *Advanced Functional Materials*, 2007, **17**, 585-592.
24. J. J. Gooding, R. Wibowo, J. Q. Liu, W. R. Yang, D. Losic, S. Orbons, F. J. Mearns, J. G. Shapter and D. B. Hibbert, *Journal of the American Chemical Society*, 2003, **125**, 9006-9007.
25. S. J. Bao, C. M. Li, J. F. Zang, X. Q. Cui, Y. Qiao and J. Guo, *Advanced Functional Materials*, 2008, **18**, 591-599.
26. H. P. Peng, R. P. Liang and J. D. Qiu, *Biosensors & Bioelectronics*, 2011, **26**, 3005-3011.
27. Z. H. Zhu, L. N. Qu, Q. J. Niu, Y. Zeng, W. Sun and X. T. Huang, *Biosensors & Bioelectronics*, 2011, **26**, 2119-2124.
28. Z. Y. Wang, S. N. Liu, P. Wu and C. X. Cai, *Analytical Chemistry*, 2009, **81**, 1638-1645.
29. C. X. Guo and C. M. Li, *Physical Chemistry Chemical Physics*, 2010, **12**, 12153-12159.
30. U. Bach, D. Lupo, P. Comte, J. E. Moser, F. Weissortel, J. Salbeck, H. Spreitzer and M. Gratzel, *Nature*, 1998, **395**, 583-585.
31. B. Oregan and M. Gratzel, *Nature*, 1991, **353**, 737-740.
32. A. Fujishima and K. Honda, *Nature*, 1972, **238**, 37-38.
33. G. K. Mor, K. Shankar, M. Paulose, O. K. Varghese and C. A. Grimes, *Nano Letters*, 2005, **5**, 191-195.
34. M. Gratzel, *Nature*, 2001, **409**, 575-576.
35. A. Hagfeldt and M. Gratzel, *Chemical Reviews*, 1995, **95**, 49-68.
36. J. S. Chen, Y. L. Tan, C. M. Li, Y. L. Cheah, D. Luan, S. Madhavi, F. Y. C. Boey, L. A. Archer and X. W. Lou, *Journal of the American Chemical Society*, 2010, **132**, 6124-6130.
37. S. J. Ding, J. S. Chen, D. Y. Luan, F. Y. C. Boey, S. Madhavi and X. W. Lou, *Chemical Communications*, 2011, **47**, 5780-5782.
38. O. K. Varghese, D. W. Gong, M. Paulose, K. G. Ong, E. C. Dickey and C. A. Grimes, *Advanced Materials*, 2003, **15**, 624-627.
39. C. A. Grimes, K. G. Ong, O. K. Varghese, X. P. Yang, G. Mor, M. Paulose, E. C. Dickey, C. M. Ruan, M. V. Pishko, J. W. Kendig and A. J. Mason, *Sensors*, 2003, **3**, 69-82.

40. H. Miyazaki, T. Hyodo, Y. Shimizu and M. Egashira, *Sensors and Actuators B-Chemical*, 2005, **108**, 467-472.
41. S. Q. Liu and A. C. Chen, *Langmuir*, 2005, **21**, 8409-8413.
42. E. Topoglidis, C. J. Campbell, A. E. G. Cass and J. R. Durrant, *Langmuir*, 2001, **17**, 7899-7906.
43. H. M. Cao, Y. H. Zhu, L. H. Tang, X. L. Yang and C. Z. Li, *Electroanalysis*, 2008, **20**, 2223-2228.
44. X. Chen and S. S. Mao, *Chemical Reviews*, 2007, **107**, 2891-2959.
45. C. Burda, X. B. Chen, R. Narayanan and M. A. El-Sayed, *Chemical Reviews*, 2005, **105**, 1025-1102.
46. C. B. Murray, C. R. Kagan and M. G. Bawendi, *Annual Review of Materials Science*, 2000, **30**, 545-610.
47. W. R. Hendren, A. Murphy, P. Evans, D. O'Connor, G. A. Wurtz, A. V. Zayats, R. Atkinson and R. J. Pollard, *Journal of Physics-Condensed Matter*, 2008, **20**, 362203.
48. H. O. Lee, E. M. Kim, H. Yu, J. S. Jung and W. S. Chae, *Nanotechnology*, 2009, **20**, 325604.
49. I. Yamaguchi, M. Watanabe, T. Shinagawa, M. Chigane, M. Inaba, A. Tasaka and M. Izaki, *ACS Applied Materials & Interfaces*, 2009, **1**, 1070-1075.
50. X. H. Xia, J. P. Tu, J. Zhang, J. Y. Xiang, X. L. Wang and X. B. Zhao, *ACS Applied Materials & Interfaces*, 2009, **2**, 186-192.
51. T. Y. Peng, A. Hasegawa, J. R. Qiu and K. Hirao, *Chemistry of Materials*, 2003, **15**, 2011-2016.
52. H. Fan, Q. Xu, Y. Guo and Y. Cao, *Industrial & Engineering Chemistry Research*, 2006, **45**, 5009-5012.
53. Y. Lei, L. D. Zhang and J. C. Fan, *Chemical Physics Letters*, 2001, **338**, 231-236.
54. S. Q. Liu and K. L. Huang, *Solar Energy Materials and Solar Cells*, 2005, **85**, 125-131.
55. T. S. Kang, A. P. Smith, B. E. Taylor and M. F. Durstock, *Nano Letters*, 2009, **9**, 601-606.
56. M. Lai, J. H. Lim, S. Mubeen, Y. Rheem, A. Mulchandani, M. A. Deshusses and N. V. Myung, *Nanotechnology*, 2009, **20**, 185602.
57. X. W. Lou, L. A. Archer and Z. Yang, *Advanced Materials*, 2008, **20**, 3987-4019.
58. S. Ding, J. S. Chen, G. Qi, X. Duan, Z. Wang, E. P. Giannelis, L. A. Archer and X. W. Lou, *Journal of the American Chemical Society*, 2010, **133**, 21-23.
59. P. D. Yang, D. Y. Zhao, D. I. Margolese, B. F. Chmelka and G. D. Stucky, *Nature*, 1998, **396**, 152-155.
60. J. Lee, S. Yoon, S. M. Oh, C. H. Shin and T. Hyeon, *Advanced Materials*, 2000, **12**, 359-362.
61. G. S. Attard, J. C. Glyde and C. G. Goltner, *Nature*, 1995, **378**, 366-368.
62. D. Y. Zhao, J. L. Feng, Q. S. Huo, N. Melosh, G. H. Fredrickson, B. F. Chmelka and G. D. Stucky, *Science*, 1998, **279**, 548-552.
63. M. Kruk and M. Jaroniec, *Chemistry of Materials*, 2001, **13**, 3169-3183.

64. M. Hartmann, *Chemistry of Materials*, 2005, **17**, 4577-4593.
65. J. H. Pazur and K. Kleppe, *Biochemistry*, 1964, **3**, 578-583.
66. A. K. V. V. A. P. R. Solanki and B. D. Malhotra, *NPG Asia Materials*, 2011, 17-24.
67. E. Laviron, *Journal of Electroanalytical Chemistry*, 1979, **101**, 19-28.
68. C. X. Cai and J. Chen, *Analytical Biochemistry*, 2004, **332**, 75-83.
69. J. Q. Liu, A. Chou, W. Rahmat, M. N. Paddon-Row and J. J. Gooding, *Electroanalysis*, 2005, **17**, 38-46.
70. S. Q. Liu and H. X. Ju, *Biosensors & Bioelectronics*, 2003, **19**, 177-183.
71. Y. X. Huang, W. J. Zhang, H. Xiao and G. X. Li, *Biosensors & Bioelectronics*, 2005, **21**, 817-821.
72. H. Lineweaver and D. Burk, *Journal of the American Chemical Society*, 1934, **56**, 658-666.
73. G. B. Xu, X. Q. Liu, L. H. Shi, W. X. Niu and H. J. Li, *Biosensors & Bioelectronics*, 2008, **23**, 1887-1890.
74. B. A. Gregg and A. Heller, *Analytical Chemistry*, 1990, **62**, 258-263.
75. Q. W. Li, G. A. Luo, J. Feng, Q. Zhou, L. Zhang and Y. F. Zhu, *Electroanalysis*, 2001, **13**, 413-416.
76. X. Chen and S. J. Dong, *Biosensors & Bioelectronics*, 2003, **18**, 999-1004.
77. T. H. Wang, C. C. Li, Y. L. Liu, L. M. Li, Z. F. Du, S. J. Xu, M. Zhang and X. M. Yin, *Talanta*, 2008, **77**, 455-459.

Chapter 6-Electrodeposition of Hierarchical MnO_2 Spheres for Interfacing with Redox Enzyme and Glucose Biosensing†

†Reproduced from [**P. Si,** P. Chen and D. H. Kim, ***Journal of Materials Chemistry-B***, 2013, 1, 2696-2700] by permission from The Royal Society of Chemistry. Copyright 2013.

6.1. Introduction

Manganese dioxide (MnO_2) is one of the most attractive transition metal oxides that have been extensively studied in the applications of mild oxidizing catalysis,[1] water treatment,[2] supercapacitors,[3] lithium-ion batteries,[4] and biosensors.[5, 6] Since the catalytic, magnetic and electronic properties of MnO_2 are known to be strongly influenced by their architecture and crystallinity, the design and synthesis of MnO_2 with ordered structures have drawn considerable research attention from chemists and material scientists. For example, one dimensional (1D) MnO_2 nanostructures including nanowires,[7] nanorods,[8] and nanotubes[9] have been synthesized by hydrothermal- and so-gel methods. Three dimensional (3D) MnO_2 such as MnO_2 helices,[10] urchin-like α-MnO_2 core-shells,[11] mesoporous γ-MnO_2 hollow spheres[12] and ε-MnO_2 dendritic structures[13] have been reported by Suib's and Xie's groups. MnO_2 with 3D hierarchical architectures are preferable for various applications because they produce more reaction-active sites than 1D- and 2D structured materials and exhibit attractive optical, electrical and magnetic properties. [14, 15]

The formation of hierarchically structures is generally a self-assembly process, in which the ordered superstructures are packaged by small building blocks, i.e., 0D nanoparticles, 1D nanorod or nanowires, and 2D nanoflakes. In literatures, hierarchically structured materials have been usually fabricated by physically constrained crystal growth with the assistance of templates[16, 17] which need to be completely removed after synthesis. Template-free methods, including chemical

vapour deposition,[18] thermal vapour transport and condensation,[19] laser-assisted catalytic growth,[20] and electrochemical deposition,[21] have also been explored to synthesize hierarchically structured materials. Among them, the electrochemical method received much attention because it is a low-cost and room-temperature technique, which offers abundant control parameters and can be used for microelectrode modification. Although a variety of 1D and 2D MnO_2 architectures have been successfully prepared by electrodeposition,[22-25] it is still a great challenge to directly grow 3D hierarchical MnO_2 through electrochemical process. In this work, we report that hierarchically structured MnO_2 spheres composed of nanorods can grow on indium tin oxide (ITO) substrate by electrodeoposition without any templates, to the best of our knowledge, which has never been reported.

Direct electron transfer (DET) of redox proteins is of great significance in improving the energy conversion efficiency of biofuel cells and fabricating third-generation biosensors.[26] Inorganic nanomaterials are of great interest because they not only provide a suitable microenvironment for protein immobilization, but their chemical inertness, mechanical strength, and good biocompatibility also improve the stability and bioactivity of immobilized enzymes.[27] Recently, we reported one dimensional hierarchically structured TiO_2 (1DHS TiO_2), which allowed fast DET of immobilized GOx and mediatorless glucose sensing.[28] In this work, hierarchical MnO_2 spheres were synthesized as a new electrode material to demonstrate effective immobilization of GOx and mediatorless detection of glucose.

6.2. Protein Immobilization and Electrode Preparation

The enzyme immobilization was performed by mixing 10 mg MnO_2 with 1 mL PBS solution (pH 7.4) containing 10 mg GOx. The mixture was vigorously shaken at room temperature for 30 min, following by storage at 4 ℃ overnight to allow the adsorption of GOx on MnO_2. The bioconjugate was then collected by centrifugation, and washed by enzyme-free PBS for three times. Finally, the composite material was resuspended in PBS solution by continuously staking for 20 min.

The GOx activity was measured at 420 nm by a standard enzymatic assay with 2,2′-azino-di-[3-ethylbenzthiazoline-6-sulfonate] diammonium salt (ABTS) as chromogenic substrate. Assays were performed under oxygen saturation in 0.1 M sodium acetate buffer, pH 6, at 25 ℃ with 0.1 M glucose as substrate.[29] One unit of GOx is defined as the amount of enzyme that catalyzes the oxidation of 1 μmol of glucose to gluconolactone and H_2O_2 in 1 min at 25 ℃.

Glassy carbon electrodes (GCE, 3 mm in diameter) were polished to mirror-like surfaces with alumina powder followed by sonication with acetone, ethanol and water respectively. The electrode surface was then washed with double distilled water and dried with ultrapure nitrogen. After that, 5 μL GOx/MnO_2 was dropped on center of GCE, which was allowed to dry at 4℃ for 24 h. Finally, 10 μL Nafion was casted on the entire electrode surface to fix the modified layer.

6.3. Results and Discussion

6.3.1. Characterization of Synthesized Material

Figure 6-1a shows the surface morphology of as-synthesized MnO_2 hierarchical spheres, which are uniformly distributed spherical architectures on the surface of ITO substrate. A close observation reveals that surface of MnO_2 is composed of randomly oriented nanorod-like structure (Figure 6-1b). The TEM image in Figure 6-1c shows that MnO_2 has a mesoporous inner structure. The particle size of the mesoporous MnO_2 spheres is in the range of 100 nm ~ 500 nm. Figure 6-1d shows the nitrogen adsorption/desorption isotherm of MnO_2 powder scraped from ITO substrates. The presence of hysteresis loop at high relative pressure (P/P_0) region further corroborates the presence of mesopore inside MnO_2. The pore size is estimated by Barrett-Joyner-Halenda (BJH) method to be 5~12 nm (inset of Figure 6-1d), which gives rise a high specific surface are of 128.5 m^2 g^{-1}.

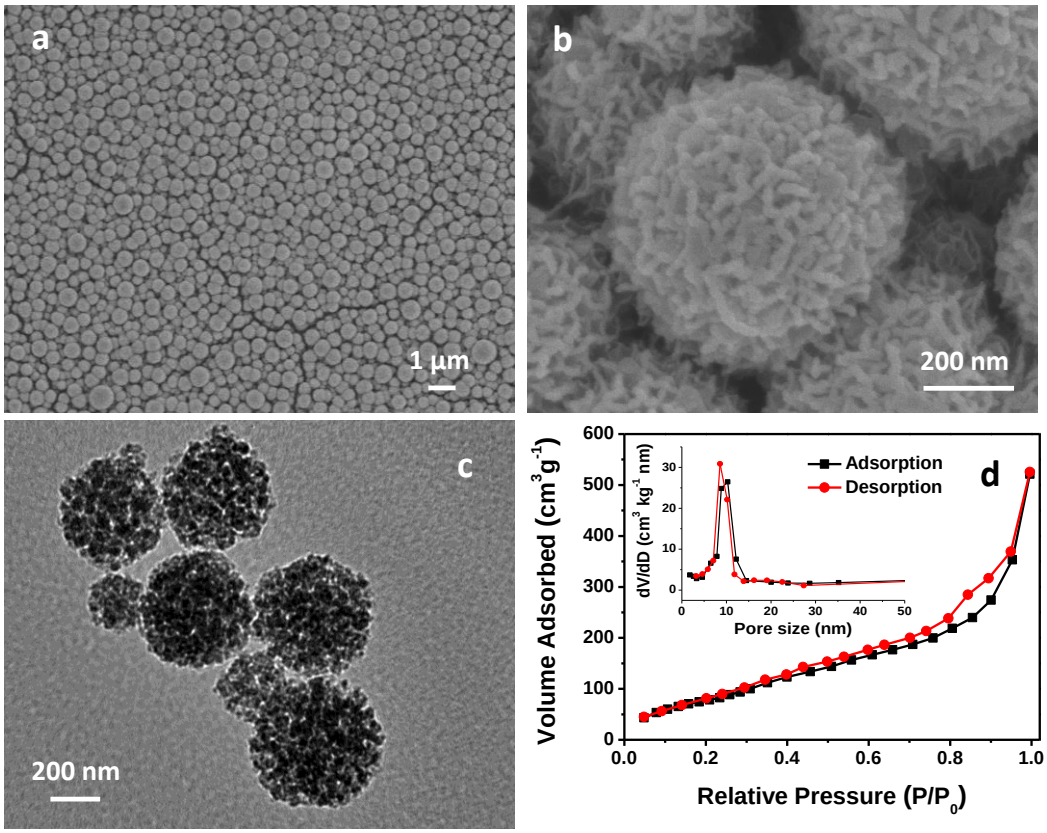

Figure 6-1. (a) Low and (b) high magnification SEM images of MnO_2. (c) TEM image of MnO_2. (d) Nitrogen adsorption-desorption isotherm and pore size distribution (inset) of MnO_2.

6.3.2. Studies of Structural Evolution and Growth Mechanism

The structural evolution of MnO_2 on ITO was observed by adjusting the electrodeposition potential, as shown in Figure 6-2. Three distinct nanostructures of MnO_2 were obtained under different deposition conditions. The surface morphology of MnO_2 are nanosheets (Figure 6-2a), nanorods (Figure 6-2b) and hierarchical spheres (Figure 6-2c and 6-2d) at the deposition potentials of 0.5, 0.8 V and 1.2 ~ 1.5 V, respectively. The diversity of MnO_2 architectures formed at different deposition potentials can be explained by the reaction kinetics. Kinetic manipulation is a versatile approach to control the morphology and shape of nanostructures. It can potentially generate novel nanostructures with unusual shapes or morphologies.[30] We believe that the nucleation and growth of MnO_2 nanostructures are highly sensitive to the rate at which the precursor is oxidized and the MnO_2 nanoparticles are deposited to the surface of growing seeds. The rate can be manipulated by tuning the deposition

potential. Larger deposition potential leads to faster oxidation rate of the manganese acetate precursors, which would generate a large amount of MnO_2 nanoparticles at any moment. At nucleation stage, a large number of MnO_2 nanoparticles are deposited on the ITO surface as reactive growth sites. The subsequently deposited precursors is preferably oxidized on these sites, rather than forming new sites on ITO surfaces due to the relatively large lattice mismatch between MnO_2 and ITO. Larger deposition potential also results in faster deposition rate of the precursors, which facilitates the formation of hollow and hierarchical structures.

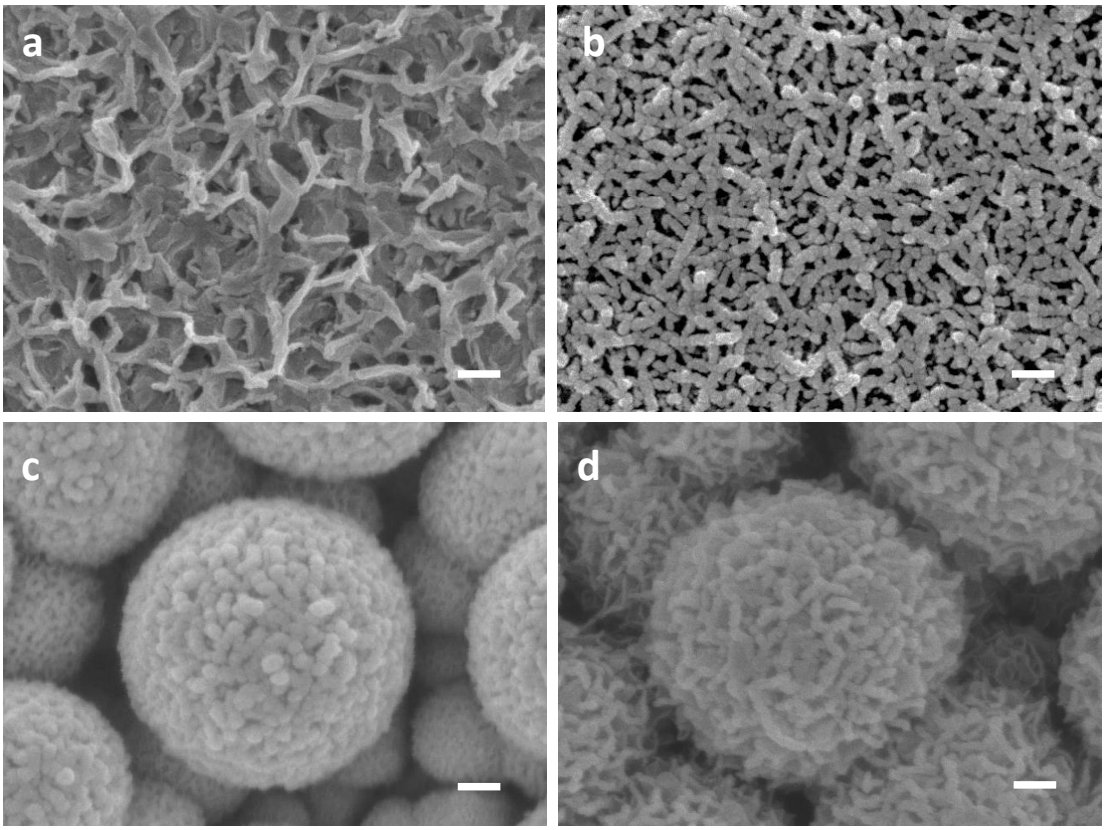

Figure 6-2. SEM images showing the architecture evolution of MnO_2 synthesized in the solution of 10 mM manganese acetate with different applied deposition potentials: (a) 0.5 V, (b) 0.8 V, (c) 1.2 V and (d) 1.5 V. The growth time is 300 s. The scale bar represents 100 nm.

To study the growth mechanism of hierarchical MnO_2 spheres on ITO, we observed the surface morphology of MnO_2 at different deposition time at 1.5 V. As shown in Figure 6-3, after 50 s of deposition, the surface of ITO was covered with small MnO_2 nanoparticles (Figure 6-3a). When the deposition time was elongated to 150 s, MnO_2 hierarchical structures composed of nanorods were observed (Figure

6-3b). Hierarchical MnO_2 spheres with uniform distribution on the ITO surface were obtained at the deposition time of longer than 300 s (Figure 6-3c). The cross-section SEM image again reveals that MnO_2 possessed a porous and interconnected inner structure (Figure 6-3d). We believe that the formation of MnO_2 on ITO is an epitaxial growth process. The growth mechanism is proposed as shown in Figure 6-3e. (1) At the initial stage of deposition, MnO_2 nanoparticles (0D) are nucleated on the ITO surface to serve as the reactive sites for the subsequent growth of complex MnO_2 nanostructure. (2) In the second stage the deposited precursors absorb on the reactive growth sites rather than bare ITO surface and the nanoparticles continue to grow into nanorods (1D). (3) Due to fast deposition rate arising from the large potential, the formed MnO_2 nanorods rapidly accumulate onto the ITO substrate and pack into porous and hierarchical structures (3D). (4) The deposited MnO_2 undergoes surface growth to form sphere-like structures. The phase purity and element composition of the as-deposited MnO_2 was characterized by energy-dispersive X-ray spectroscopy (EDX), which showed strong Mn and O signals (Figure 6-4). The formation of MnO_2 on the anodic electrode surface from the solution of manganese acetate can be explained by the following reaction:[3]

$$Mn^{2+} + 2H_2O \rightarrow MnO_2 + 4H^+ + 2e^- \qquad (6\text{-}1)$$

in which Mn (II) species in the electrolyte is electro-oxidized to Mn (IV) on the anode when a positive potential is applied. However, no obvious diffraction peaks could be observed on the XRD spectrum, possibly due to the low crystallinity of the as synthesized MnO_2 material.

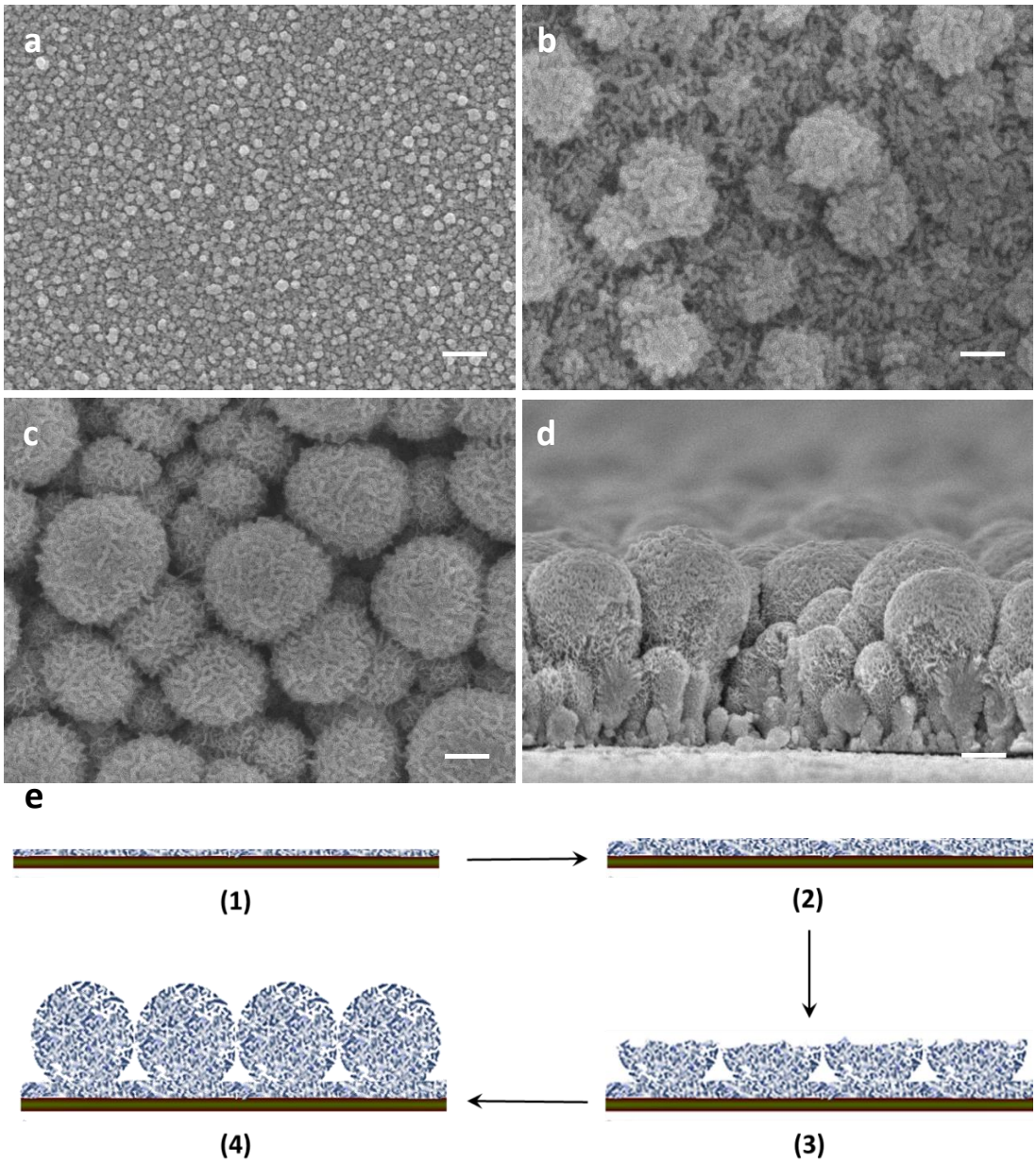

Figure 6-3. (a)~(c): SEM images showing the structural evolution of MnO_2 deposited at 1.5 V for 50 s, 150 s and 300 s respectively in 10 mM manganese acetate solution. (d): Cross-section SEM image of the MnO_2 film. The scale bars in (a) ~ (d) are 200 nm. (e): Schematic illustration of the growth process of MnO_2 hierarchical spheres on ITO substrate.

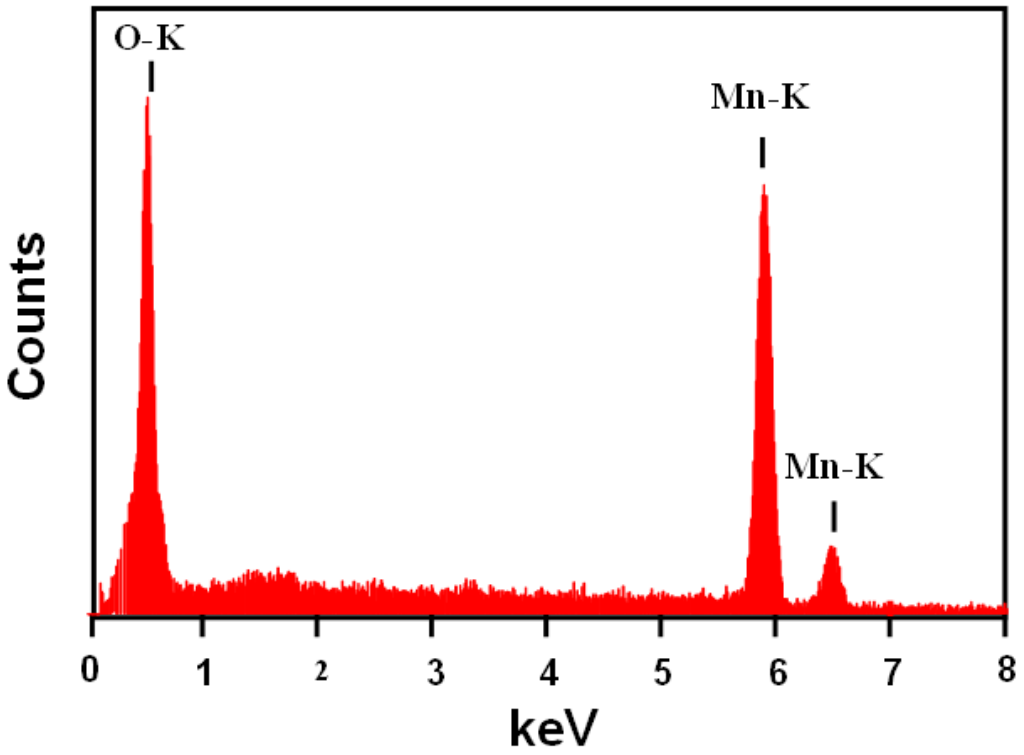

Figure 6-4. EDX spectrum of the as synthesized MnO_2 hierarchical spheres.

6.3.3. Immobilization of Protein on Hierarchically Structured MnO_2

To take advantage of its unique pore size and large surface area, the hierarchical MnO_2 spheres were used for enzyme immobilization. The pore size of MnO_2 is a good match to the dimension of GOx (7.0 nm × 5.5 nm × 8.0 nm). The immobilization of GOx on MnO_2 was examined by FTIR (Figure 6-5). The presence of amid I and amide II characteristic bands of GOx on the FTIR spectrum of GOx/MnO_2 composite indicates the enzyme well maintains its activity post immobilization.[31] The activity of GOx was also measured by the enzymatic assay. The enzyme activity before and after immobilization was determined to be 215 U mg^{-1} and 173 U mg^{-1} respectively, indicating GOx could still remain over 80 % of its original catalytic activity upon immobilization. We infer that the size of mesopores in MnO_2 (5 ~12 nm) is favourable for the accommodation of GOx molecules and preventing the enzyme from denaturation during and after immobilization. The surface protein density of GOx/MnO_2-modified GCE was studied by electrochemical impedance

spectroscopy (EIS) (Figure 6-6). The charge transfer resistance of MnO_2 -GCE (R_{ct}) and GOx/MnO_2-GCE (R_{ct}^{GOx}) are 48.6 Ω and 2917.5 Ω, respectively. The surface coverage of GOx (θ) on the electrode surface is calculated to be 98.3 % from the equation $\theta = (1- R_{ct}/R_{ct}^{GOx}) \times 100$ %.[32] Such high surface protein coverage could be contributed to the large surface area and mesoporous structure of MnO_2.

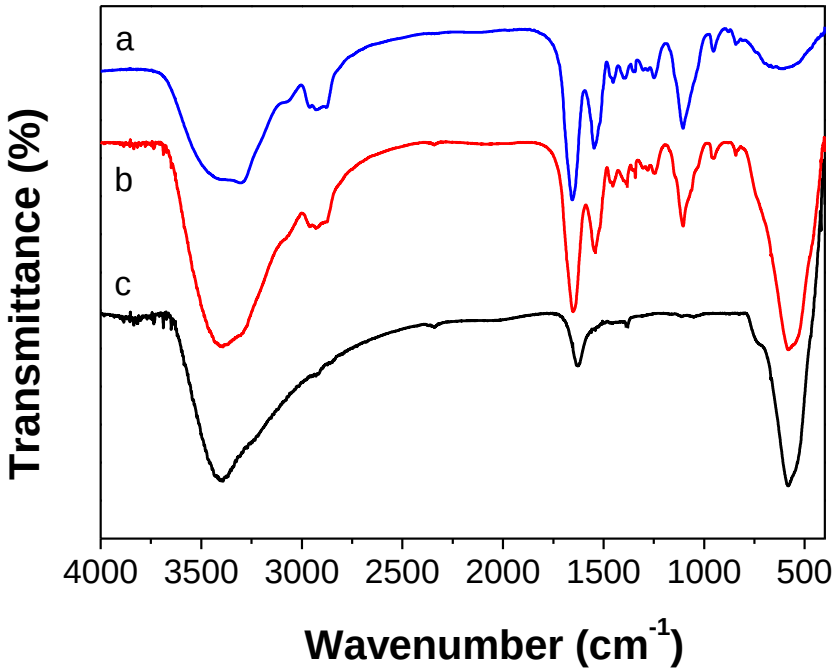

Figure 6-5. FTIR spectra of (a) pure GOx, (b) GOx/MnO_2 composite and (c) hierarchical MnO_2 spheres.

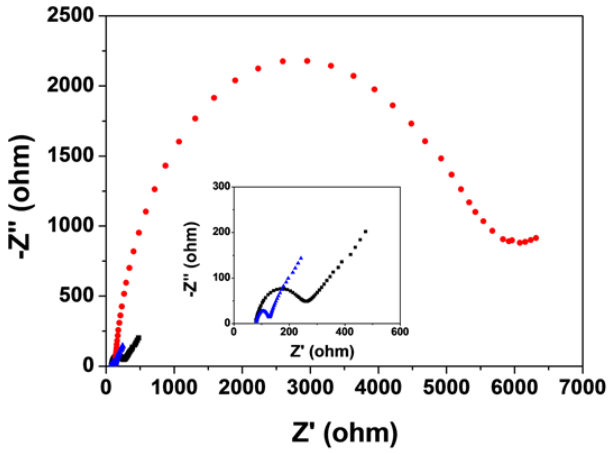

Figure 6-6. Nyquist plots of a bare GCE (black), MnO_2 NRHS-modified GCE (blue) and GOx/MnO_2 NRHS-modified GCE (red) measured in 0.1 M KCl solution containing 10 mM $Fe(CN)_6^{3-/4}$.

6.3.4. Electron Transfer Behavior of Immobilized Protein

The electron transfer behaviour of immobilized GOx was studied by cyclic voltammetry (CV), which was conducted on GOx/Nafion-, MnO_2/Nafion- and GOx/MnO_2/Nafion-modified GCE in N_2 saturated 0.1 M PBS. As shown in Figure 6-7a, both GOx/Nafion- and MnO_2/Nafion-modified electrodes exhibit square-shaped CV, resulting from the capacitive response of an electrical double layer. This result implies that both GOx and MnO_2 are electro-inactive on bare electrode surfaces. On the CV of GOx/MnO_2-GCE, a pair of well-defined redox peaks are observed at the potentials of -0.441 V (E_{pa}) and -0.465 V (E_{pc}), respectively. The peak potentials are close to the standard potential of flavin adenine dinucleotide (FAD, E^0 = -0.45 V),[33] could be attributed to a number of factors as follows. First, the MnO_2 possesses a high specific surface area (128 m^2 g^{-1}), which is favourable for the adsorption of a large amount of GOx. Second, the similarity in size of GOx and mesopores of MnO_2 greatly shortens the electron tunnelling distance between the prosthetic group and electrode, facilitating the direct electron transfer. Finally, the MnO_2 could provide a conduction pathway that further expedites the electron transfer kinetics between the immobilized protein and the electrode surface.

The effect of scan rate on the electrochemical response of GOx/MnO_2/Nafion-modified electrode is shown in Figure 6-7b. The anodic and cathodic peak currents increased proportionally with the scan rate from 25 to 500 mV s^{-1}, indicating the redox reaction on GOx/MnO_2/Nafion-GCE is surface-confined electrochemical process. The peak-to-peak separation is less than 34 mV until the scan rate reaches 500 mV s^{-1}, giving rise to a large electron transfer rate constant (k_s) of 11.6 ± 1.2 s, determined by Laviron's equation.[34] The k_s obtained in this study is substantially greater than that of GOx immobilized on other electrode materials, such as PEDOT-NiO(6.5 s^{-1}),[31] TiO_2 (3.96 s^{-1}),[35] MWCNT (1.12 s^{-1}),[36] SWCNT (0.3 s^{-1})[37] and Au nanoparticles (2.2 s^{-1}).[38] The electrochemical response of GOx immobilized

on MnO_2 also exhibits strong pH dependence (Figure 6-7c). The electrode formal potential (E^0) decreases linearly with the increase in the solution pH (inset of Figure 6-7d), revealing the protons in the external solution involves the redox reaction of $FAD/FADH_2$. The slope of E^0 *versus* pH in the range of 5.0 ~ 8.2 is 62 mV pH^{-1} is analogous to the theoretical value of 59 mV pH^{-1}, suggesting that the electrochemical reaction involves two-proton coupled with two-electron transfer process. As shown in Figure 6-7d, GOx/MnO_2 /Nafion-modified electrode has the largest peak current at pH of 7.4, showing the highest bioactivity of GOx on MnO_2 could be achieved at the physiological pH value.

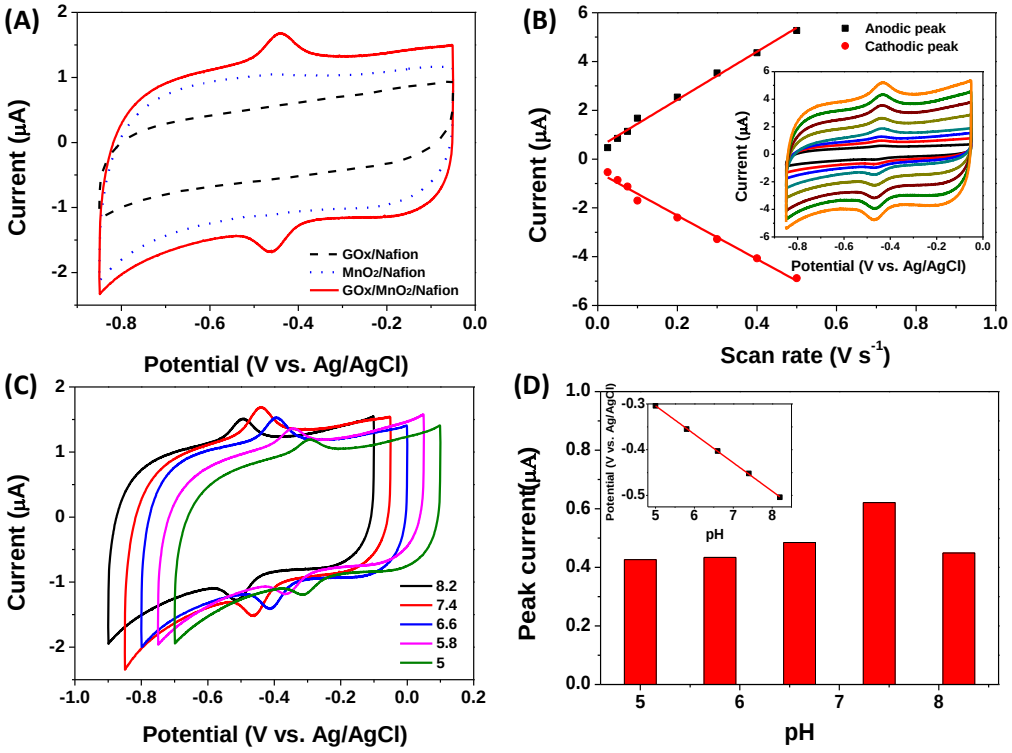

Figure 6-7. (a) CVs of GOx/Nafion-, MnO_2/Nafion- and GOx/MnO_2 /Nafion-modified GCE measured in N_2 saturated 0.1 M PBS. Scan rate: 100 mV s^{-1}. (b) Plots of scan rate *versus* peak current. Inset shows the CVs of GOx/MnO_2/Nafion-GCE at different scan rates (from inside to outside): 25, 50, 75, 100, 200, 300, 400, and 500 mV s^{-1}. (c) CVs of GOx/MnO_2/Nafion-GCE measured in N_2 saturated 0.1 M PBS with different pH. (d) Plot of peak current *versus* pH. Inset: plot of formal potential versus pH.

6.3.5. Biosensing Performance

The biosensing performance of the GOx/MnO_2/Nafion-modified electrode was

studied by amperometry in air-saturated 0.1 M PBS (pH 7.4) at a fixed potential of -0.45 V, at which decreased voltammetric currents were obtained by successive addition of glucose (Figure 6-8). This could be explained by the following reaction:

$$\text{Glucose} + \text{GOx (FAD)} \rightarrow \text{Gluconic acid} + \text{GOx (FADH}_2\text{)} \qquad (6\text{-}2)$$

which implies that glucose could be directly oxidized by FAD at its redox potential. Figure 6-9a shows the time-current curve of GOx/MnO_2 /Nafion-GCE upon repeated injection of 0.15 mM (2.25 μM) glucose every 50 s. A current response of 0.3 μA is observed for each injection at the initial 1000 s, with 95% of the steady-state current achieved within 3 s. The current response starts to decrease after 20 times of injection, and eventually becomes saturated at the glucose concentration of 4 mM, reflecting the typical feature of Michaelis-Menten kinetics. The proposed biosensor shows negligible current response to the injection of common interferential electroactive species that co-exist with glucose in the blood, including ascorbic acid (AA), uric acid (UA), and acetaminophen (AP) (inset of Figure 6-9a), indicating good specificity of the biosensor. The calibration curve is plotted in Figure 6-9b. MnO_2 /GOx/Nafion-GCE shows a high sensitivity of 31.6 μA mM cm^{-2}, with a linear range up to 3.15 mM and a detection limit of 0.35 μM (3σ). The sensitivity of present electrode is 3 times higher than 1DHS TiO_2-based third generation glucose sensor[28] and 1.5 times higher than MWCNT/AuNPs nanocomposite based second-generation glucose sensor.[39] The performance of present biosensor also outperforms other third-generation glucose sensors based on nanomaterials, as shown in Table 6-1. The improved sensitivity could contribute to the enhanced electron transfer kinetics, and the enlarged linear range may result from increased concentration of dissolved oxygen around the immobilized GOx due to the large surface area of MnO_2. The apparent Michaelis-Menten constant K_m^{app} of MnO_2 based glucose sensor is determined to be 0.42 mM by the Lineweaver-Burk curve (Figure 6-9b), which is smaller than that of GOx on MWCNT (5.15 mM)[40], Au nanoparticles (4.3 mM),[41] NiO (2.7 mM)[42] and

TiO_2 (1.54 mM)[28]. The smaller K_m^{app} reflects the electrode has a better affinity for glucose.

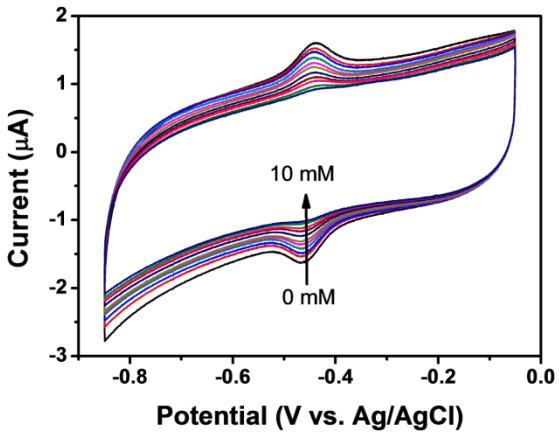

Figure 6-8. CVs of GOx/MnO_2 NRHS/Nafion-GCE measured in N_2-saturated 0.1 M PBS with different glucose concentrations: (from outside to inside) 0, 1, 2, 3, 4, 5, 6, 7, 8, 9, 10 mM.

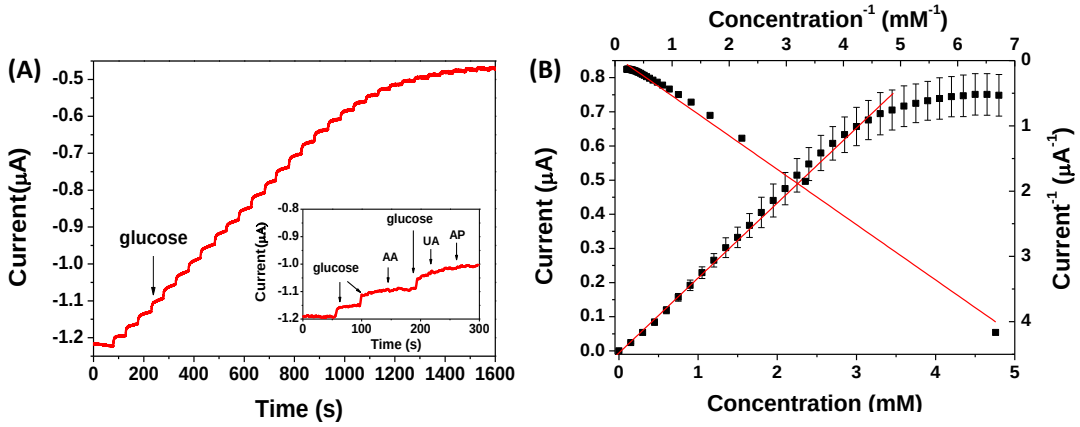

Figure 6-9. (a) Amprometric response of GOx/MnO_2/Nafion-GCE to the successive addition of 150 μM glucose at a fixed potential of -0.45 V in 0.1 M PBS solution. Inset shows the current response of GOx/MnO_2/Nafion-GCE for 0.3 mM glucose, 0.3 mM AA, 0.5 mM UA and 0.5 mM AP. (b) The calibration curve (current versus glucose concentration) and the Lineweaver-Burk plot (current^{-1} versus concentration^{-1}) of the biosensor obtained from amperometric response.

Table 6-1. Comparison of the analytical performance of MnO_2/GOx/Nafion-GCE with other nanomaterials based third-generation glucose biosensors.

Electrode materials	Sensitivity	Linear range	Response time (s)	Ref
GOx/MnO_2	31.6	Up to 3.15 mM	< 3	This work
GOx/PEDOT-NiO HS	16.9	Up to 1.5 mM	< 10	[31]
GOx/NiO hollow spheres	3.4	1.5 ~ 7 mM	~ 8	[43]
GOx/N_2-doped CNTs	13.0	Up to 1.02 mM	-	[44]
GOx/1DHS TiO_2	9.9	0.05~1.5 mM	< 5	[28]
GOx/Nanocrystal TiO_2	4.6	0 ~ 3 mM	< 30	[45]
GOx/Mesoporous TiO_2	3.9	0.15 ~ 1.2	< 10	[35]

6.4. Conclusion

In summary, a facile electrodeposition method is described for the growth of hierarchically structured MnO_2 spheres on ITO. We systematically studied the structural evolution and growth mechanism of hierarchical MnO_2 spheres. In addition, the MnO_2 powder was successfully employed for immobilization of enzyme and mediatorless sensing of glucose. The synthesized MnO_2 possessed a high specific surface area and uniform pore size distribution. GOx immobilized on the hierarchical MnO_2 showed excellent bioactivity and direct electrochemistry. The GOx/MnO_2 based third generation glucose sensor exhibited a high sensitivity of 31.6 μA mM cm^{-2}, a large linear range up to 3.15 mM and a low detection limit of 0.35 μM. The sensitivity of present glucose biosensor is much superior to other third-generation ones based on nanomaterials. Our study demonstrates that electrodeposition could serve as a convenient and versatile pathway for the synthesis of novel nanomaterials with hierarchical structures for new applications.

Reference

1. S. Liang, F. Teng, G. Bulgan, R. Zong and Y. Zhu, *The Journal of Physical Chemistry C*, 2008, **112**, 5307-5315.
2. H. Chen and J. He, *The Journal of Physical Chemistry C*, 2008, **112**, 17540-17545.
3. W. Wei, X. Cui, W. Chen and D. G. Ivey, *Chemical Society Reviews*, 2011, **40**, 1697-1721.
4. B. Ammundsen and J. Paulsen, *Advanced Materials*, 2001, **13**, 943-+.
5. Y. H. Bai, Y. Du, J. J. Xu and H. Y. Chen, *Electrochemistry Communications*, 2007, **9**, 2611-2616.
6. Z. Zhu, L. Qu, Q. Niu, Y. Zeng, W. Sun and X. Huang, *Biosensors and Bioelectronics*, 2011, **26**, 2119-2124.

7. X. Wang and Y. D. Li, *Journal of the American Chemical Society*, 2002, **124**, 2880-2881.
8. H. R. Chen, X. P. Dong, J. L. Shi, J. J. Zhao, Z. L. Hua, J. H. Gao, M. L. Ruan and D. S. Yan, *Journal of Materials Chemistry*, 2007, **17**, 855-860.
9. D. S. Zheng, S. X. Sun, W. L. Fan, H. Y. Yu, C. H. Fan, G. X. Cao, Z. L. Yin and X. Y. Song, *Journal of Physical Chemistry B*, 2005, **109**, 16439-16443.
10. O. Giraldo, S. L. Brock, M. Marquez, S. L. Suib, H. Hillhouse and M. Tsapatsis, *Nature*, 2000, **405**, 38-38.
11. Z. Q. Li, Y. Ding, Y. J. Xiong, Q. Yang and Y. Xie, *Chemical Communications*, 2005, 918-920.
12. J. Yuan, K. Laubernds, Q. Zhang and S. L. Suib, *Journal of the American Chemical Society*, 2003, **125**, 4966-4967.
13. Y. S. Ding, X. F. Shen, S. Gomez, H. Luo, M. Aindow and S. L. Suib, *Advanced Functional Materials*, 2006, **16**, 549-555.
14. D. L. Wang and C. M. Lieber, *Nature Materials*, 2003, **2**, 355-356.
15. L. Manna, D. J. Milliron, A. Meisel, E. C. Scher and A. P. Alivisatos, *Nature Materials*, 2003, **2**, 382-385.
16. Z. Y. Zhong, Y. D. Yin, B. Gates and Y. N. Xia, *Advanced Materials*, 2000, **12**, 206-+.
17. Y. Lu, Y. D. Yin and Y. N. Xia, *Advanced Materials*, 2001, **13**, 271-+.
18. Z. W. Pan, Z. R. Dai and Z. L. Wang, *Science*, 2001, **291**, 1947-1949.
19. D. Banerjee, J. Y. Lao, D. Z. Wang, J. Y. Huang, D. Steeves, B. Kimball and Z. F. Ren, *Nanotechnology*, 2004, **15**, 404-409.
20. X. F. Duan and C. M. Lieber, *Advanced Materials*, 2000, **12**, 298-302.
21. Z. L. Xiao, C. Y. Han, W. K. Kwok, H. W. Wang, U. Welp, J. Wang and G. W. Crabtree, *Journal of the American Chemical Society*, 2004, **126**, 2316-2317.
22. M. S. Wu, *Applied Physics Letters*, 2005, **87**.
23. B. Babakhani and D. G. Ivey, *Journal of Power Sources*, 2010, **195**, 2110-2117.
24. S. L. Chou, F. Y. Cheng and J. Chen, *Journal of Power Sources*, 2006, **162**, 727-734.
25. H. Xia, J. K. Feng, H. L. Wang, M. O. Lai and L. Lu, *Journal of Power Sources*, 2010, **195**, 4410-4413.
26. X. Zhang, H. Ju and J. Wang, *Electrochemical sensors, biosensors and their biomedical applications*, Academic Pr, 2007.
27. M. Hartmann, *Chemistry of Materials*, 2005, **17**, 4577-4593.
28. P. Si, S. Ding, J. Yuan, X. W. Lou and D.-H. Kim, *ACS Nano*, 2011, **5**, 7617-7626.
29. H. M. Kalisz, J. Hendle and R. D. Schmid, *Journal of Chromatography*, 1990, **521**, 245-250.
30. Y. Xia, Y. Xiong, B. Lim and S. E. Skrabalak, *Angewandte Chemie International Edition*, 2009, **48**, 60-103.
31. C. X. Guo and C. M. Li, *Physical Chemistry Chemical Physics*, 2010, **12**, 12153-12159.

32. H. Q. Liu, Y. Tian and Z. F. Deng, *Langmuir*, 2007, **23**, 9487-9494.
33. Y. Xiao, F. Patolsky, E. Katz, J. F. Hainfeld and I. Willner, *Science*, 2003, **299**, 1877.
34. E. Laviron, *Journal of Electroanalytical Chemistry*, 1979, **101**, 19-28.
35. S. J. Bao, C. M. Li, J. F. Zang, X. Q. Cui, Y. Qiao and J. Guo, *Advanced Functional Materials*, 2008, **18**, 591-599.
36. M. V. Jose, S. Marx, H. Murata, R. R. Koepsel and A. J. Russell, *Carbon*, 2012, **50**, 4010-4020.
37. J. Q. Liu, A. Chou, W. Rahmat, M. N. Paddon-Row and J. J. Gooding, *Electroanalysis*, 2005, **17**, 38-46.
38. H. F. Zhang, Z. C. Meng, Q. Wang and J. B. Zheng, *Sensors and Actuators B-Chemical*, 2011, **158**, 23-27.
39. P. Si, P. Kannan, L. H. Guo, H. S. Son and D. H. Kim, *Biosensors & Bioelectronics*, 2011, **26**, 3845-3851.
40. X. B. Yan, X. J. Chen, B. K. Tay and K. A. Khor, *Electrochemistry Communications*, 2007, **9**, 1269-1275.
41. S. Zhang, N. Wang, H. Yu, Y. Niu and C. Sun, *Bioelectrochemistry*, 2005, **67**, 15-22.
42. A. Salimi, E. Sharifi, A. Noorbakhsh and S. Soltanian, *Biosensors and Bioelectronics*, 2007, **22**, 3146-3153.
43. C. C. Li, Y. L. Liu, L. M. Li, Z. F. Du, S. J. Xu, M. Zhang, X. M. Yin and T. H. Wang, *Talanta*, 2008, **77**, 455-459.
44. S. Y. Deng, G. Q. Jian, J. P. Lei, Z. Hu and H. X. Ju, *Biosensors & Bioelectronics*, 2009, **25**, 373-377.
45. Q. W. Li, G. A. Luo, J. Feng, Q. Zhou, L. Zhang and Y. F. Zhu, *Electroanalysis*, 2001, **13**, 413-416.

Chapter 7-Carbon Nanocages as Unique Electrode Materials for Enzyme Immobilization, Fast Direct Electrochemistry and High-Performance Glucose Biosensing

7.1. Introduction

To achieve direct electron transfer (DET) between a redox protein and electrode is not only of scientific significance in illuminating the rodox mechanisms behind the complex biological systems,[1-3] but is also of great importance in improving the performance of bioelectronic devices such as biosensors and biofuel cells.[4-6] Unfortunately, the prosthetic groups or electroactive centers of most redox proteins are deeply embedded in thick and electrically insulating protein shell, rendering the direct electrical communication between protein and electrode extremely difficult due to the long electron tunneling distance and prohibitively slow electron transfer rate.[7, 8] Traditionally, small artificial redox mediators are employed as electron shuttles to overcome the electron transfer barrier between the redox center of protein and electrode surface in the application of bioelectronic devices.[9-12] However, mediator-based biosensors suffer from the shortages such as potential toxicity, limited stability and relatively poor specificity.[13] Therefore, the development of DET-based mediatorless biosensors which is promising to offer ultrahigh sensitivity and superior selectivity has attracted tremendous research interest and intensive research effort in the recent years.

Several strategies have been developed up to date to facilitate the direct electrical communication between enzyme and electrode for the application of biosensors. For example, the ‘enzyme plugging’ method developed by Willner[5, 14, 15]allows for protein DET by covalently attaching the prosthetic group or cofactor on the surface of highly conductive nanomaterials, followed by reassembling the apo-protein on cofactor to recover the function of a whole enzyme. The conductive nanomaterials can be gold

nanoparticles or carbon nanotubes, which are electrically linked to the electrode surface. Gooding[16] and Rusling[17] reported the direct electrochemistry of redox proteins based on ‘molecular wires’ by covalent binding the biomolecules to the end of aligned carbon nanotubes ‘forests’ that were modified on electrode surfaces. The recently reported genetic modification strategy allows the enzyme to display a free thiol group near its active site.[18] By attaching a maleimide-modified gold nanoparticle to the genetically modified protein via the thiol-maleimide reaction, the electron tunneling distance was greatly shortened and DET between enzyme and electrode could be achieved. Another popular approach is entrapping the redox protein in mesoporous nanomateirals. This method has received considerable attention in recent years due to its simplicity, stability and low-cost. In addition, the biosensors based on mesoporous electrode materials generally exhibit very high sensitivity by taking the advantages of their high specific surface area, large pore volumes and high mesoporosity.[19-21] Until now, several different types of molecular sieves, including mesoporous silicates,[22-24] metal oxides[20, 25, 26] and carbon nanomaterials[27-29] have been developed and explored to for protein immobilization. Their microstructure,[24, 25] pore size distribution,[30] chemical composition and surface properties[23, 31] were well tailored and designed in order to promote DET and improve the biosensor performance. Our previous works have demonstrated that hierarchically structured TiO_2[26] and MnO_2[32] with suitable mesopore dimensions were effective in facilitating the direct electrochemistry of immobilized redox proteins by shortening the direct electron tunneling distance. However, it is still great challenge to develop novel mesoporous nanomaterials which could offer larger surface area, higher conductivity and better biocompatibility for super bioelectroanalysis.

Among the variety of mesoporous structured nanomateirals, mesoporous carbon is an ideal electrode material for biosensor fabrication due to its high conductivity, low cost and good biocompatibility.[33, 34] Immobilization of biomolecules in mesoporous carbon materials for the construction of enzymatic biosensors has attracted increasing

research interest in recent years. For example, bicontinuous gyroidal carbon[35] has been developed for the immobilization of myoglobin; Feng *et al*[36] reported the immobilization of hemoglobin with whiskerlike mesoporous carbon material; porous carbon aerogel was studied by Tsujimura[37] to immobilize multicopper oxidases; and ordered mesoporous carbon was employed by You and colleagues[38] for the immobilization of glucose oxidase (GOx). In spite of the great research effort, there are very few reports focusing on the electrochemical biosensing application with the mesoporous carbon as electrode materials, possibly due to their limited pore diameters which are usually less than 5 nm[34, 39] and poor graphitic property which results in low conductivity.[40, 41] Mesoporous carbon with larger pore diameter which is close to the dimension of protein (7~9 nm) is very important for the immobilization of biomolecules; while good conductivity of an electrode material is essential to achieve a high biosensing performance.[42, 43] Therefore, mesoporous carbon materials with suitable pore size distribution and well developed graphitic structure are highly desirable for biosensing application.

In this work, we report the development of carbon nanocages (CNCs) with distinguished hollow interiors, large specific surface area, suitable pore diameters and well-developed graphitic structure. The CNCs were investigated for the immobilization of GOx, which exhibited fast DET on the electrode surface. The Nafion/GOx/CNCs-modified electrode was successfully employed as a mediatorless glucose sensor, which achieved a high and reproducible sensitivity, fast response and wide linear dynamic range for the measurement of glucose concentration in human serum.

7.2. Enzyme Immobilizaition and Electrode Modification

The immobilization of GOx on CNCs was achieved by mixing 10 mg CNCs with the PBS buffer containing different concentrations of GOx. The mixture was vigorously shaken for 30 min before it was placed quiesently at 4 ℃ for 12 h for protein adsorption. The GOx/CNCs bioconjugate was collected by centrifugation,

followed by rinsing with PBS buffer for 3 times. The attained product was then dried in vaccume and analyzed by FTIR (Bruker EQUINOX 55 DuroscopeTM). For biosensor fabrication, a glassy carbon electrode (GCE, 3 mm in diameter) was polished sequencingly with 1.0, 0.3 and 0.05 μm alumina powder to a mirror-like surface followed by ultrasonication in acetone, ethanol and water each for 3 min, respectively. After that, the electrode surface was cleaned and dried with ultrapure nitrogen flow. The obtained GOx/CNCs composite was re-dispersed in 1 mL of protein-free PBS buffer by continuously shaking for 15 min. Then 5 μL of the composite dispersion was drop-casted on the center of electrode surface, which was allowed to dry at 4 ℃ overnight. Finally, 10 μL Nafion (0.5 % in water) was coated on the sensor surface to prevent the electrode materials from detaching during electrochemical test.

7.3. Results and Discussion

7.3.1. Material Characterizations

The surface morphology of as synthesized CNCs was characterized by scanning electron microscopy (SEM), which shows that the nanocages have polygonal particle-like structure with uniform size of 20~30 nm (Figure 7-1a). The transmission electron microscopic (TEM) images in Figure 7-1b clearly reveals that the CNCs consist of pronounced hollow interiors. The high resolution TEM images (insets of Figure 7-1b) illustrates that the nanocages have a thin shell structure with thickness of 2~ 3 nm. The shells of CNCs comprise a few layers of graphitic carbon with the lattice distance of 0.34 nm. The XRD pattern of CNCs in Figure 7-1c displays three distinct reflection peaks at 26 °, 44 ° and 54 °, respectively, which could be well assigned to the (002), (101) and (004) diffraction planes of the graphite carbon (JCPDS card no: 3-401).[44] The result suggests that the prepared CNCs have well-developed graphitic structure with high phase purity. The plotted nitrogen adsorption/desorption isotherm of CNCs (Figure 7-1d) exhibits a hysteresis loop at the relative pressure (P/P_0) of 0.5, indicating a mesoporous feature. The Brunauer–

Emmett–Teller (BET) specific surface area of CNCs was calculated to be as high as 1651 m^2 g^{-1}, which is significantly larger than those of CNTs[45] and CNCs[29, 46] reported previously. The major pore size distribution of CNCs is in the range of 5~20 nm (inset of Figure 7-1d), estimated from the desorption branch by Barrett–Joyner–Halenda (BJH) method. The presence of mesoporous structure could be mainly contribute to the defects induced by acid treatment and the unsealed feature of CNCs, which is favorable for the immobilization of redox protein and the rapid access of electrolyte ions and target molecules.

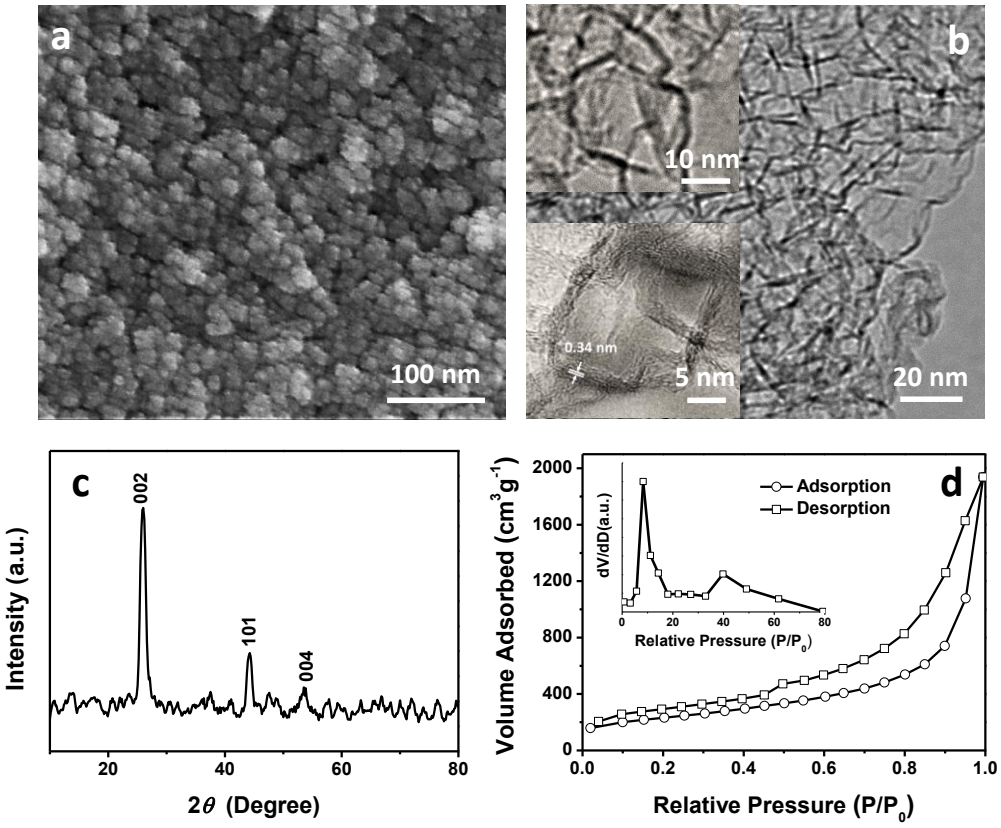

Figure 7-1. (a) SEM image, (b) TEM image, (c) XRD pattern and (d) Nitrogen adsorption-desorption isotherms of CNCs. Insets of (b) are the HR-TEM images of CNCs, showing a lattice distance of 0.34 nm. Inset of (d) shows the pore size distribution.

7.3.2. Investigation of Enzyme Immobilization on CNCs

The conformational change of the enzyme upon immobilization on CNCs was investigated by Fourier transform infrared spectroscopy (FTIR), showing GOx exhibits three characteristic peaks at 1100, 1541 and 1654 cm^{-1}, which are

corresponding to the amide I, amide II adsorption bands and C-O stretching vibration, respectively (Figure 7-2a). The two peaks at 1631 and 1398 cm^{-1} on the IR spectrum of CNCs could be attribute to the C=O stretching vibration of ketones and carboxyl functional groups (Figure 7-2b). After the enzyme was immobilized on CNCs, the three representative bands of GOx are still clearly observable on the spectrum of GOx/CNCs biocomposite (Figure 7-2c), indicating the protein well maintained its native secondary structure upon immobilization. The reservation of the enzyme secondary structure is an important feature that illustrates GOx is able to keep its high catalytic activity on CNCs.

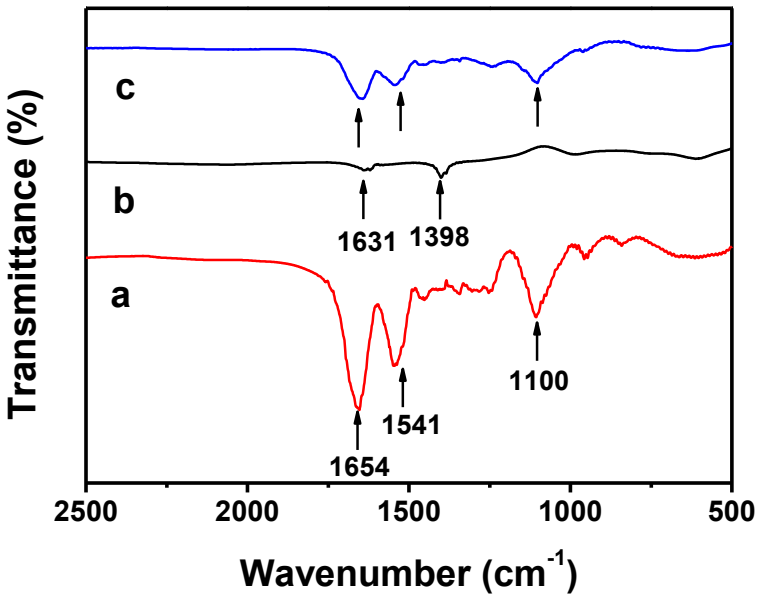

Figure 7-2. FTIR spectra of GOx (a), CNCs (b) and GOx/CNCs biocomposite (c).

7.3.3. Electrochemical Behavior of GOx Immobilized on CNCs

The electrochemical property of GOx immobilized on CNCs was studied by cyclic voltammetry (CV). As shown in Figure 7-3a, the CVs of pure CNCs- and GOx-modifed glassy carbon electrode (GCE) barely show any redox peaks, indicating the electrochemical inactivity of these two materials. However, CNCs-modified GCE shows a square-shaped CV curve with mcuh larger area than that of GOx-GCE, possibly due to the significantly augmented double-layer capacitance enabled by the

highly porous structure of CNCs. In contrast, a pair of well-defined and nearly reversible redox peaks could be observed on the CV curve of GOx/CNCs-modified GCE, clearly indicating the direct electrochemistry of GOx was achieved on CNCs-modified electrode. The anodic and cathodic peak potentials are -0.445 V and -0.481 V, respectively, which are consitent with the formal redox potential of FAD/$FADH_2$ at neural pH.[25, 38] The small peak-to-peak seperation (ΔE) of 36 mV suggests a fast electron transfer rate, which was calculated to be 8.2 s^{-1} by Laviron's equation.[47] The rate constant is apparently larger than those for GOx immobilzed on ordered mesoporous carbon (4.2 s^{-1}),[38] mesoporous TiO_2 (3.96 s^{-1}),[25] MWCNTs (1.53 s^{-1})[48] and SWCNTs (0.3 s^{-1}).[49] The CV peak currents incrased propotionally with the increase of scan rate (Figure 7-4), indicating the DET process was surface-confined electrochemical reaction. With the increase of solution pH, the redox peak potential shifts negatively, showing a linear response in the pH range of 5.1 ~ 8.0 (Figure 7-5). The slope value of 57.8 mV pH^{-1} is very close to the theoratical value of 59.0 mV pH^{-1} predicted for the redox reaction of FAD/$FADH_2$,[25] suggesting the DET between electrode and GOx immobilzied on CNCs underwent two-electron involved redox reaction coupling with two-proton transfer process. To study the catalytic activity of GOx immobilized on CNCs, the voltammetric response of GOx/CNCs-GCE toward the addition of glucose was examined in air-saturated PBS (Figure 7-3b). The CV of GOx/CNCs-modified electrode shows a large reduction peak at the potential of -0.6 V in the absence of glucose, which is corresponding to reduction of dissolved oxygen molecules in PBS. With the increase of added glucose concentraion, the reduction peak gradually decreases until completely disappears at a concentraiton of 12 mM, apparently indicating that GOx immobilzied on CNCs retained high catalytic activity for the oxidation of glucose. The phenomenon of DET was investigated for glucsoe detection in nitrogen-saturated PBS. Interestingly, with the increased glucose concentration from 1~10 mM, both anodic and cathodic peak currents are reduced (Figure 7-3c). Similar phenomenon was also observed in our previous study,[26]

suggesting glucose was oxidized directly by FAD without any mediators and the electrode could regenerate FAD by direct electrochemical oxidation of $FADH_2$ in GOx. The calibration curve of DET-based glucose detection could be obtained by substacting the background of CV curves (Figure 7-3d), showing a linear range up to 3 mM (inset of Figure 7-1d).

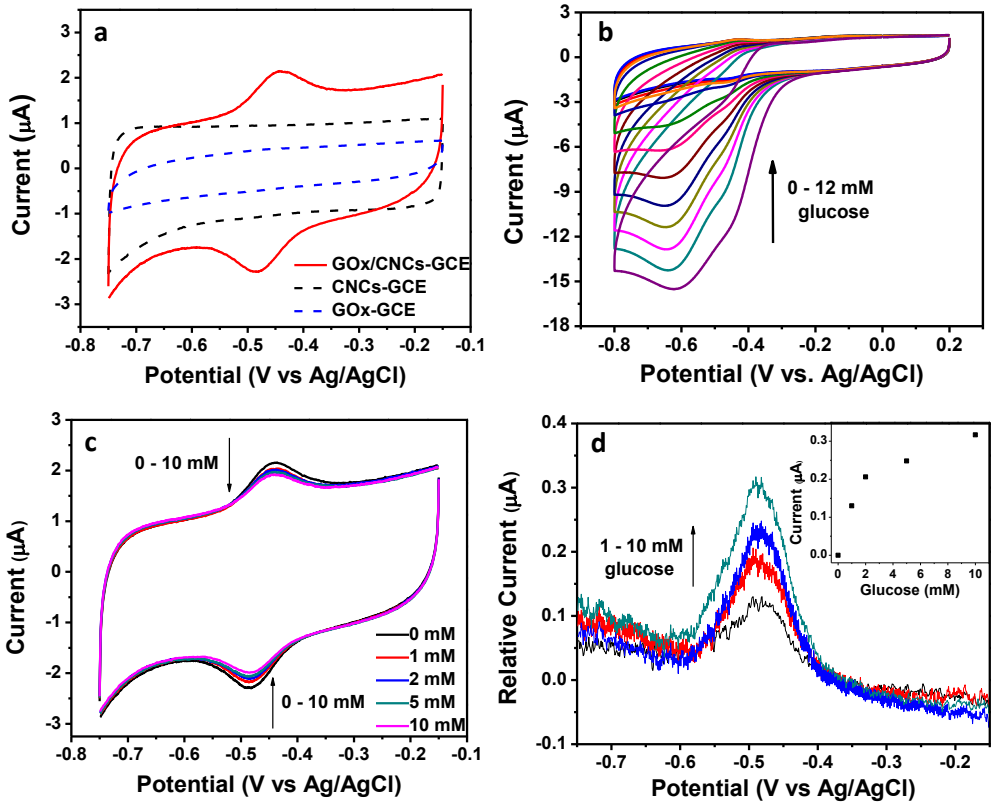

Figure 7-3. (a) CVs of GOx/CNCs-, CNCs- and GOx-modified GCE measured in N_2-saturated 0.1 M PBS. (b) CVs of GOx/CNCs-GCE in the presence of 0~12 mM glucose measured in air-saturated 0.1 M PBS. (c) CVs obtained for GOx/CNCs-GCE with different glucose concentrations from 0~10 mM in N_2-saturated 0.1 M PBS. (d) Background-subtracted CV curves from the cathodic branches of (c). Inset of (d) shows the calibration curve. Scan rate: 100 mV s^{-1}. PBS pH: 7.4.

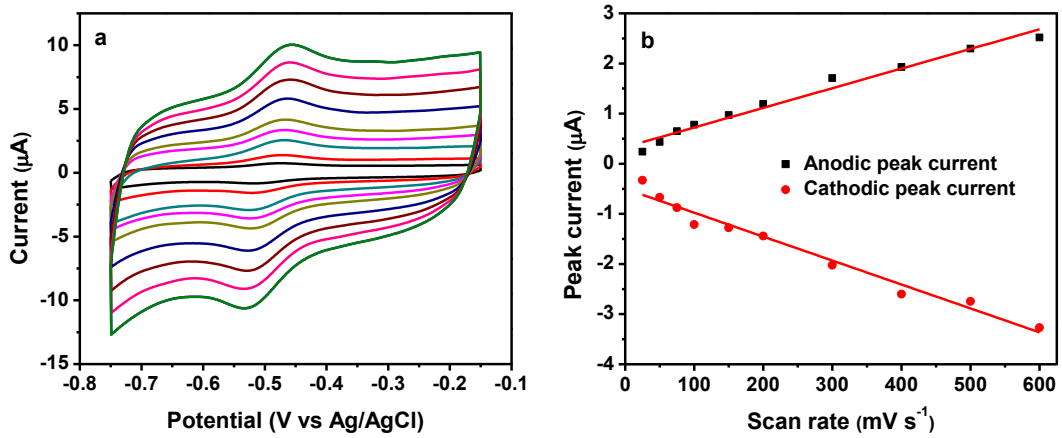

Figure 7-4. (a) CVs of GOx/CNCs-GCE measured in 0.1 M nitrogen-saturated PBS (pH 7.4) with the increase of scan rate from 25 to 600 mV s^{-1} (inside to outside). (b) Plots of peak current versus scan rate.

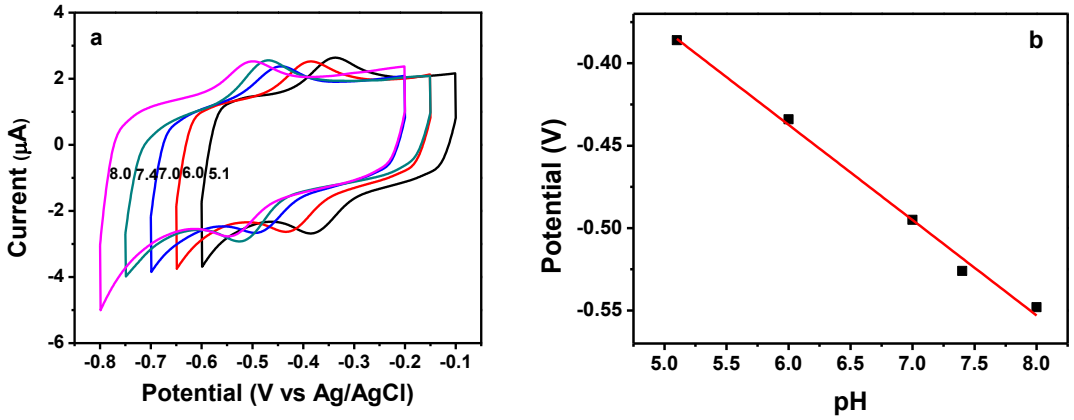

Figure 7-5. (a) CVs of GOx/CNCs-GCE measured in 0.1 M nitrogen-saturated PBS (pH 7.4) with different pH in the range of 5.1~8.0. Scan rate: 100 mV s^{-1}. (b) Plot of electrode formal potential versus pH.

7.3.4. Optimization of the Parameters for Amperometric Biosensing

The amperometric sensing performance of GOx/CNCs-modified electrode could be affected by a variety of factors, including the amount of enzyme loaded on the electrode material, the operating potential, pH of the buffer solution and the system temperature. These parameters were carefully optimized in the present work. The GOx concentration in PBS buffer could affect the amount of enzyme loaded on CNCs during the incubation procedure. As plotted in Figure 7-6a, the fabricated biosensor showed an enhanced current response for 2 mM glucose with the increase of

incubated GOx concentration, and achieved the maximum current density when the GOx concentration reached 8 mg mL^{-1}. Further increase of the GOx concentration results in a slight decrease of the amperometric response, possibly because the overloaded GOx blocked the channels in CNCs and impeded the free access of electrolyte and substrate molecules. In addition, the excess of GOx molecules may lead to the formation of an insulting protein layer on the electrode surface, which also disturbed the biosensing performance. Therefore, 8 mg mL^{-1} was used as the optimal GOx concentration for incubation with CNCs. The proper selection of operating potential is essential for an amperometric glucose sensor to achieve a high sensitivity and limit the interfering reactions. As is observed in Figure 7-6b, the response current did not show notable alternation at the detection potentials from -0.6 V to -0.5 V. However, the response of the electrode decreased significantly when the operation potential was more positive than -0.5 V, and completely vanished when the potential was increased to -0.2 V. Since an operating voltage close to the redox potential of FAD/$FADH_2$ could minimize the interferential responses of electroactive species in blood,[9] the detection potential of -0.5 V was selected for mediatorless glucose sensing. Further optimized experimental conditions include buffer pH and temperature. The largest current response of GOx/CNCs-GCE was obtained at the solution pH of 6.5 (Figure 7-6c), which is close to the most suitable pH reported for native GOx in solution.[50] The result further corroborates that GOx retained its native activity after the immobilization procedure. The influence of temperature on the electrochemical response of the biosensor toward glucose oxidation was investigated in the range of 25~50 ℃ (Figure 7-6d). The increase of temperature from 25 ℃ to 37 ℃ resulted in the improvement of responsive current until the maximum obtained at approximately 37 ℃. However, when the temperature was higher than 37 ℃, the current started to decrease probably due to the denaturation of enzyme.

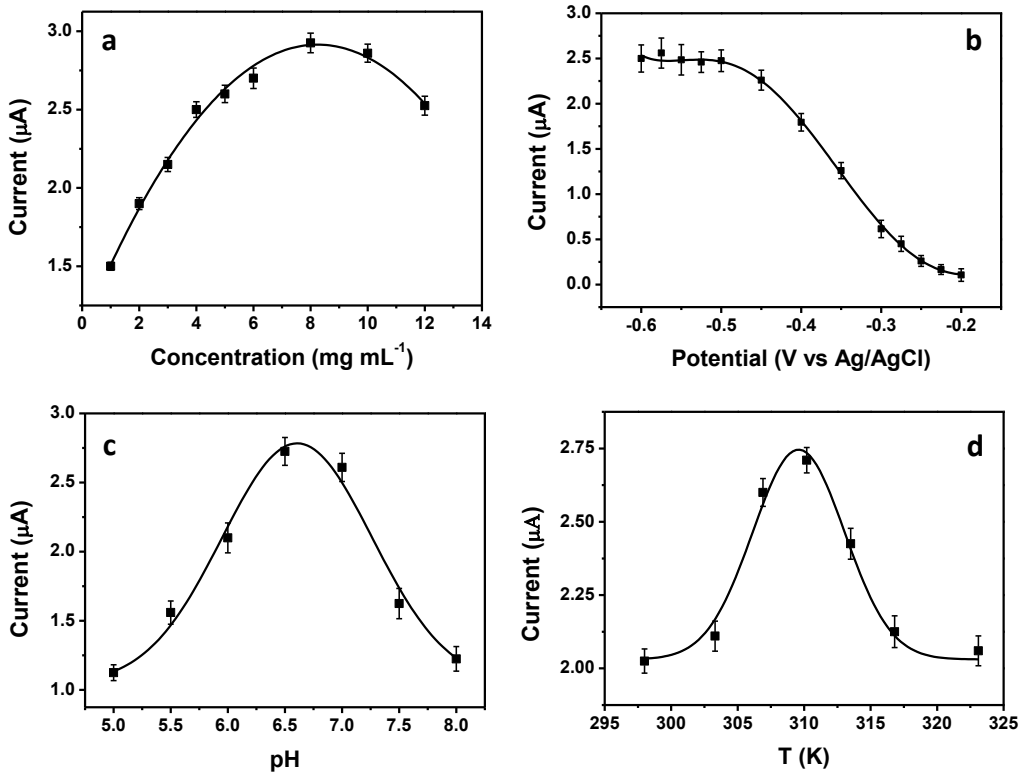

Figure 7-6. The current response of GOx/CNCs-GCE toward the addition of 2 mM glucose with the influence of different (a) incubated GOx concentration, (b) detection potential, (c) buffer pH and (d) temperature of the reaction system. The points were sketched with the average values of three independent measurements.

7.3.5. Analytical Performance of Fabricated Glucose Sensor

The amperometric measurement of glucose was conducted under the optimized experimental conditions without the presence of any mediator. The biosensor showed a swift and sensitive response toward the successive addition of either 1 mM or 0.1 mM glucose in each step, with 95 % of the steady-state current achieved within 3s (Figure 7-7a). The response time is comparable to that of GOx/porous MnO_2-modified electrode, but much shorter than other mesoporous materials based biosensors (Table 7-1). The rapid response could mainly contribute to the high catalytic activity of the immobilized GOx and the fast electron transfer rate between enzyme and electrode. The calibration curve plotted in Figure 7-7b shows that the biosensor has a linear response toward glucose in the low concentration range, while saturated currents could be observed at high glucose level, reflecting the typical

Michaelis-Menten enzyme kinetics. The apparent Michaelis-Menten constant (K_m^{app}) was calculated to be as small as 1.87±0.3 mM by the Lineweaver-Burk equation,[51] implying the electrode possesses high affinity to glucose. According to the calibration plot, the mediatorless biosensor exhibits a large linear range up to 14 mM with a correlation coefficient of 0.998. The linear range is significantly wider than other DET-based glucose sensors as compared in Table 7-1. The improved upper limit for glucose detection enables the electrode for practical measurement in blood samples, which normally contain glucose with a concentration range of 4.4~6.6 mM.[9] In addition, the biosensor offered a high sensitivity of 19.18 ± 0.3 μA mM cm^{-2}, with a detection estimated to be ~0.33 ± 0.1 μM at a signal to noise ratio (S/N) of 3, which is much lower than those obtained at other electrodes reported previously (Table 7-1). The selectivity of the present glucose sensor was evaluated by examining the response of electrode upon the addition of a variety of common interfering species in blood such as ascorbic acid (AA), dopamine (DA), acetaminophen (AP) and uric acid (UA). As shown in Figure 7-7c, the biosensor exhibits negligible current responses toward injection of 0.1 mM AA and UA into the buffer solution. However, significant current steps could be observed when 0.5 mM glucose was added. Figure 7-7d further demonstrates that even the concentrations of AA, AP, DA and UA are as high as 0.3 mM (more than 3 times higher than their physiological levels in blood), their influences on the electrode for glucose detection are very limited. The accuracy of the electrode for practical application was inspected by measuring the glucose concentration in human serum sample. The injection of 100 μL human serum to 900 μL PBS buffer produced a distinguished current response of 0.78±0.08 μA, which could be converted to a glucose concentration of 5.83±0.05 mM according to the calibration equation. The measured glucose concentration is nearly the same with value of 5.85 mM in the product information sheet provided by the manufacturer, indicating the biosensor is able provide high clinical accuracy for practical usage.

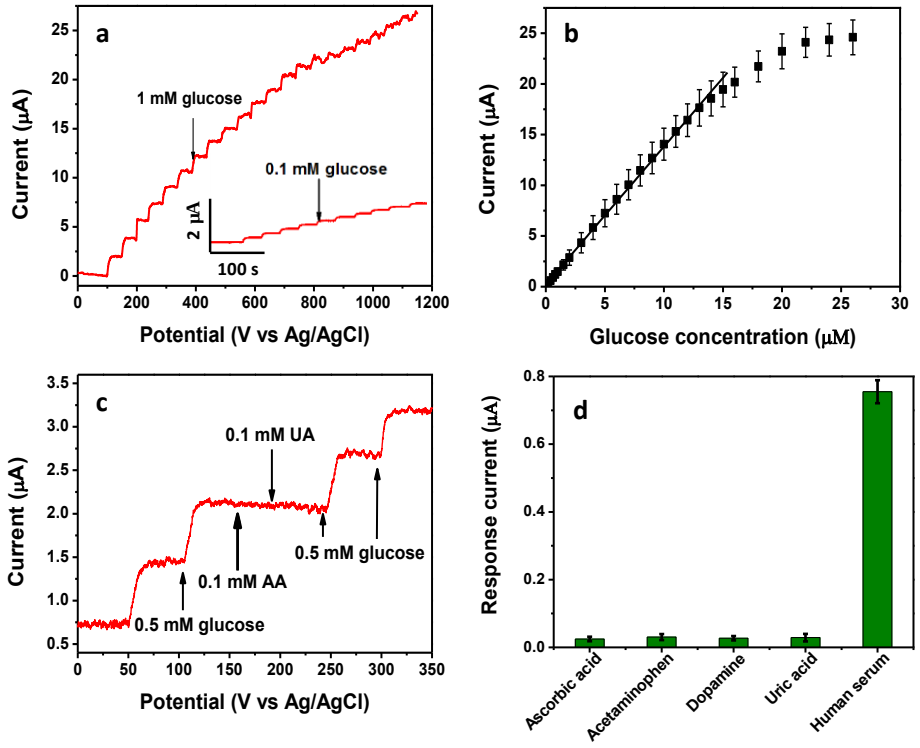

Figure 7-7. (a) Amperometric responses of Nafion/GOx/CNCs-GCE toward the successive addition of 1 mM and 0.1 mM (inset) glucose to stirred PBS buffer (0.1 M, pH 6.5) at an operating potential of -0.5 V. (b) The calibration curve plotted according to the amperometric current response of the mediatorless biosensor. (c) Amperometric responses of the electrode for 0.5 mM glucose and the addition of some interfering species (0.1 mM AA and 0.1 mM UA) to stirred 0.1 M PBS buffer (pH 6.5). (d) The current responses of fabricated biosensor toward the addition of 0.3 mM electrocative species in blood (AA, AP, DA and UA) and 100 μL human serum to 900 μL air-saturated PBS buffer (0.1 M, pH 6.5).

Table 7-1. Comparison of the analytical performance of mediator-free glucose biosensors based on mesoporous electrode materials enabled DET

Electrode materials	Response time [s]	Linear range [mM]	Sensitivity [μA mM cm^{-2}]	Detection limit [μM]	Ref
CNCs	<3	Up to 14	19.18	0.33	This work
Mesoporous carbon/silica foam	~4	0.05~5	1.8	34	[24]
Mesoporous TiO_2	<10	0.15~1.2	3.9	-	[25]
1DHS[a]porous TiO_2	<5	Up to 1.5	9.9	1.29	[26]
Mesoporous MnO_2	<3	Up to 3.15	31.6	0.35	[32]
Graphitic nanocage	<5	0.02~6.2	13.3	8	[29]
Ordered mesoporous carbon	-	Up to 9.9	1.16	10	[38]

[a] One-dimensional hierarchically structured TiO_2

7.4. Conclusion

In conclusion, a novel mesoporous material of CNCs was synthesized in this work and successfully employed for enzyme immobilization, DET facilitation, and mediatorless glucose measurement in human serum. The developed CNCs exhibit unique physiochemical properties including a large specific surface area, high and uniform mesoporosity, and pronounced graphitic crystallinity, which enable the immobilized GOx to retain a high catalytic activity and to achieve a fast electron transfer rate toward direct oxidation of glucose. The carefully optimized experimental conditions allow the fabricated amperometric biosensor based on Nafion/GOx/CNCs-GCE to achieve a fast response, wide linear range, high sensitivity and excellent selectivity for mediatorless glucose detection in human serum. The research in this work demonstrates that CNCs-based biocomposite materials could be novel promising platforms for the development of third-generation biosensors and other bioelectronic devices.

Reference

1. M. K. Beissenhirtz, F. W. Scheller, W. F. M. Stocklein, D. G. Kurth, H. Mohwald and F. Lisdat, *Angewandte Chemie-International Edition*, 2004, **43**, 4357-4360.
2. A. El Kasmi, J. M. Wallace, E. F. Bowden, S. M. Binet and R. J. Linderman, *Journal of the American Chemical Society*, 1998, **120**, 225-226.
3. J. J. Wei, H. Y. Liu, A. R. Dick, H. Yamamoto, Y. F. He and D. H. Waldeck, *Journal of the American Chemical Society*, 2002, **124**, 9591-9599.
4. C. S. Shan, H. F. Yang, J. F. Song, D. X. Han, A. Ivaska and L. Niu, *Analytical Chemistry*, 2009, **81**, 2378-2382.
5. Y. Xiao, F. Patolsky, E. Katz, J. F. Hainfeld and I. Willner, *Science*, 2003, **299**, 1877-1881.
6. S. K. Chaudhuri and D. R. Lovley, *Nature Biotechnology*, 2003, **21**, 1229-1232.
7. A. Riklin, E. Katz, I. Willner, A. Stocker and A. F. Buckmann, *Nature*, 1995, **376**, 672-675.
8. N. J. Ronkainen, H. B. Halsall and W. R. Heineman, *Chemical Society Reviews*, 2010, **39**, 1747-1763.
9. J. Wang, *Chemical Reviews*, 2008, **108**, 814-825.
10. J. Wang, *Electroanalysis*, 2001, **13**, 983-988.
11. A. Heller and B. Feldman, *Chemical Reviews*, 2008, **108**, 2482-2505.
12. P. Si, P. Kannan, L. H. Guo, H. S. Son and D. H. Kim, *Biosensors & Bioelectronics*, 2011, **26**, 3845-3851.

13. Y. Liu, Y. Du and C. M. Li, *Electroanalysis*, 2013, **25**, 815-831.
14. M. Zayats, E. Katz, R. Baron and I. Willner, *Journal of the American Chemical Society*, 2005, **127**, 12400-12406.
15. F. Patolsky, Y. Weizmann and I. Willner, *Angewandte Chemie-International Edition*, 2004, **43**, 2113-2117.
16. J. J. Gooding, R. Wibowo, J. Q. Liu, W. R. Yang, D. Losic, S. Orbons, F. J. Mearns, J. G. Shapter and D. B. Hibbert, *Journal of the American Chemical Society*, 2003, **125**, 9006-9007.
17. X. Yu, D. Chattopadhyay, I. Galeska, F. Papadimitrakopoulos and J. F. Rusling, *Electrochemistry Communications*, 2003, **5**, 408-411.
18. J. T. Holland, C. Lau, S. Brozik, P. Atanassov and S. Banta, *Journal of the American Chemical Society*, 2011, **133**, 19262-19265.
19. P. D. Yang, D. Y. Zhao, D. I. Margolese, B. F. Chmelka and G. D. Stucky, *Nature*, 1998, **396**, 152-155.
20. X. Xu, B. Z. Tian, J. L. Kong, S. Zhang, B. H. Liu and D. Y. Zhao, *Advanced Materials*, 2003, **15**, 1932-+.
21. H. G. Zhu, E. W. Stein, Z. H. Lu, Y. M. Lvov and M. J. McShane, *Chemistry of Materials*, 2005, **17**, 2323-2328.
22. J. F. Diaz and K. J. Balkus, *Journal of Molecular Catalysis B-Enzymatic*, 1996, **2**, 115-126.
23. Y. Han, S. S. Lee and J. Y. Ying, *Chemistry of Materials*, 2006, **18**, 643-649.
24. S. Wu, H. X. Ju and Y. Liu, *Advanced Functional Materials*, 2007, **17**, 585-592.
25. S. J. Bao, C. M. Li, J. F. Zang, X. Q. Cui, Y. Qiao and J. Guo, *Advanced Functional Materials*, 2008, **18**, 591-599.
26. P. Si, S. J. Ding, J. Yuan, X. W. Lou and D. H. Kim, *ACS Nano*, 2011, **5**, 7617-7626.
27. M. Hartmann, A. Vinu and G. Chandrasekar, *Chemistry of Materials*, 2005, **17**, 829-833.
28. A. Vinu, M. Miyahara and K. Ariga, *Journal of Physical Chemistry B*, 2005, **109**, 6436-6441.
29. C. X. Guo, Z. M. Sheng, Y. Q. Shen, Z. L. Dong and C. M. Li, *ACS Applied Materials & Interfaces*, 2010, **2**, 2481-2484.
30. J. Deere, E. Magner, J. G. Wall and B. K. Hodnett, *Catalysis Letters*, 2003, **85**, 19-23.
31. H. Takahashi, B. Li, T. Sasaki, C. Miyazaki, T. Kajino and S. Inagaki, *Chemistry of Materials*, 2000, **12**, 3301-3305.
32. P. Si, P. Chen and D. H. Kim, *Journal of Materials Chemistry B*, 2013, **1**, 2696-2700.
33. D. Lee, J. Lee, J. Kim, J. Kim, H. B. Na, B. Kim, C. H. Shin, J. H. Kwak, A. Dohnalkova, J. W. Grate, T. Hyeon and H. S. Kim, *Advanced Materials*, 2005, **17**, 2828-+.
34. A. Vinu, C. Streb, V. Murugesan and M. Hartmann, *Journal of Physical Chemistry*

B, 2003, **107**, 8297-8299.
35. C. P. You, X. W. Yan, J. L. Kong, D. Y. Zhao and B. H. Liu, *Electrochemistry Communications*, 2008, **10**, 1864-1867.
36. J. J. Feng, J. J. Xu and H. Y. Chen, *Biosensors & Bioelectronics*, 2007, **22**, 1618-1624.
37. S. Tsujimura, Y. Kamitaka and K. Kano, *Fuel Cells*, 2007, **7**, 463-469.
38. C. P. You, X. Xu, B. Z. Tian, J. L. Kong, D. Y. Zhao and B. H. Liu, *Talanta*, 2009, **78**, 705-710.
39. L. F. Wang, Y. Zhao, K. F. Lin, X. J. Zhao, Z. C. Shan, Y. Di, Z. H. Sun, X. J. Cao, Y. C. Zou, D. Z. Jiang, L. Jiang and F. S. Xiao, *Carbon*, 2006, **44**, 1336-1339.
40. Z. M. Sheng and J. N. Wang, *Advanced Materials*, 2008, **20**, 1071-+.
41. J. N. Wang, L. Zhang, J. J. Niu, F. Yu, Z. M. Sheng, Y. Z. Zhao, H. Chang and C. Pak, *Chemistry of Materials*, 2007, **19**, 453-459.
42. J. P. Liu, C. X. Guo, C. M. Li, Y. Y. Li, Q. B. Chi, X. T. Huang, L. Liao and T. Yu, *Electrochemistry Communications*, 2009, **11**, 202-205.
43. W. Sun, C. X. Guo, Z. H. Zhu and C. M. Li, *Electrochemistry Communications*, 2009, **11**, 2105-2108.
44. C. D. Liang, Z. J. Li and S. Dai, *Angewandte Chemie-International Edition*, 2008, **47**, 3696-3717.
45. D. Tasis, N. Tagmatarchis, A. Bianco and M. Prato, *Chemical Reviews*, 2006, **106**, 1105-1136.
46. Y. M. Tan, C. F. Xu, G. X. Chen, Z. H. Liu, M. Ma, Q. J. Xie, N. F. Zheng and S. Z. Yao, *ACS Applied Materials & Interfaces*, 2013, **5**, 2241-2248.
47. E. Laviron, *Journal of Electroanalytical Chemistry and Interfacial Electrochemistry*, 1979, **101**, 19-28.
48. C. Cai and J. Chen, *Analytical Biochemistry*, 2004, **332**, 75-83.
49. J. Liu, A. Chou, W. Rahmat, M. N. Paddon-Row and J. J. Gooding, *Electroanalysis*, 2005, **17**, 38-46.
50. H. J. Bright and M. Appleby, *Journal of Biological Chemistry*, 1969, **244**, 3625-&.
51. H. Lineweaver and D. Burk, *Journal of the American Chemical Society*, 1934, **56**, 658-666.

Chapter 8-Hierarchically Structured Nanocomposite of Three-Dimensional Graphene-Mn_3O_4 as Flexible Electrode for Nonenzymatic Glucose Biosensing†

†Adapted from [**P. Si**, X.C. Dong, P. Chen and D.H. Kim, ***Journal of Materials Chemistry-B***, 2013, 1, 110-115] by permission from The Royal Society of Chemistry. Copyright 2013

8.1. Introduction

The glucose level in blood is commonly used for medical diagnosis of diabetes mellitus, which is a worldwide health problem resulting from insulin dependency and hyperglymia.[1] Consequently, sensitive and reliable monitoring of glucose is of paramount importance in clinical, food and environmental analysis. Currently, most glucose sensors rely on enzyme-based electrodes which employ glucose oxidase or glucose dehydrogenase as a catalyst.[2-5] Although the enzyme-based approaches provide an additional capability of selective measurement to the sensors, several drawbacks has hindered its widespread use. Due to intrinsic nature of protein, the enzymatic sensor is of poor stability which prevents it from long-term and reproducible usage. In addition, the enzyme-based detection is susceptible to the environment, such as pH, temperature, and humidity. Furthermore, the incorporation of enzyme also increases the manufacturing cost and complexity, and the insulating property of enzyme greatly compromises the sensitivity of biosensors. To address these issues, great effort has been dedicated in recent years to the development of enzymeless electrodes using metals[6], metallic nanoparticles,[7, 8] alloys [9, 10] and oxides [11, 12] as an electrocatalyst. However, some of the electrodes may display poor sensitivity and selectivity due to the severe surface fouling by absorbing intermediates and chloride.[10, 13] Hence, there is a great demand for the development of nonenzymatic glucose biosensors with high sensitivity and good selectivity at low cost for the efficient determination of glucose.

Graphene has been integrated with other functional nanomaterials to fabricate composite materials. The attained synergistic effects of graphene composite provide vast opportunities that lead to advances in energy harvesting/storage devices,[14-18] transparent conductors[19-21] and chemical/bio-sensors.[22-24] Recently, highly conductive and seamless three-dimensional graphene foam (3DGF) with microscopic network structure has been synthesized by template-directed chemical vapor deposition (CVD),[25] enabling the production of graphene with both high quality and relatively large quantity. The mechanical strength and flexibility of 3DGF allows it to be used as a freestanding electrode, where charge carriers could move along the continuous graphene skeleton with a small resistance. In addition, the three dimensional architecture of 3DGF provides a large surface area which allows for the construction of graphene-based nanocomposites without agglomeration. Recently, we reported a composite material of Co_3O_4/3DGF for the nonenzymatic biosensing of glucose.[26] Despite of extraordinarly high sensitivity it achieved, the Co_3O_4/3DGF biosensor offers relatively small linear resposne range (up to 80 μM) due to the thick coating layer of Co_3O_4. Moreover, Co_3O_4/3DGF could not be used for the detection of H_2O_2. In the present work, we synthesized a novel composite material of hierarchically structured Mn_3O_4/3DGF for the development of a highly sensitive and enzymeless sensor for detection of both glucose and H_2O_2. Due to the excellent electrocatalytic acitivy of nanostructured Mn_3O_4, good conductivity of graphene, great abundance of catalytic sites and high specific surface area of the composite material, the Mn_3O_4/3DGF-based glucose sensor achieved a large lienar detection range of 0.1~8 mM, which is 2 orders of magnitude larger than that of 3DGF/Co_3O_4. In addition, the material also showed the capability of highly sensitive and selective detection of H_2O_2. Moreover, thanks to the good stiffness of 3DGF, the composite material can be fabricated as a flexible and freestanding biosensor.

8.2. Fabrication of the Flexible Electrode

The nanocomposite material of hierarchically structured Mn_3O_4/3DGF was

synthesized by CVD growth of 3DGF followed by electrochemical deposition of Mn_3O_4, which was described previously in Chapter 3, Section 3.16 and Section 3.17. The composite was then affixed to a flexible polyethylene terephthalate (PET) substrate by silicon rubber to use as a freestanding electrode and flexible biosensor.

8.3. Results and Discussion

8.3.1. Material Characterizations

Figure 8-1a shows the SEM image of 3DGF grown by ethanol-CVD method using nickel foam as a sacrificial template. The 3DGF reveals macroporous network structure that replicate the nickel foam, hence exhibiting continuous and smooth graphene skeleton without observable cracks or breaks, indicating that graphene sheets well maintain its original structure after removal of Ni template without collapse. The width of graphene skeleton is around 100 μm. In Figure 8-1b, the observed wrinkles and ripples on the surface of 3DGF skeleton results from difference in the thermal expansion coefficients of nickel and graphene.[27] Similar to the effect of winkles of chemically derived graphene,[28] these ripples on 3DGF skeleton could contribute to the large surface area and the good mechanical strength of 3DGF. The surface morphology of Mn_3O_4/3DGF is shown in Figure 8-1c and Figure 8-1d, displaying good uniformity of Mn_3O_4 nanostructures on the graphene surface. The magnified SEM image (Figure 8-1e) shows the highly porous and nanomesh-like structure of the Mn_3O_4, which is uniformly covered on the entire surface of 3DGF. The TEM image (Figure 8-1f) shows that the microstructure of Mn_3O_4 grown on graphene is composed of ultrathin nanoflaklets with the dimension of 100~200 nm. With uniform distribution, hierarchical structure at nanometer scale, the Mn_3O_4 nanomesh offers abundant catalytic sites, which contributes to the high electrocatalytic activity of the composite material. The nanoporous Mn_3O_4 network, together with the macroporous structure of 3DGF provides a large specific surface area which allows for the rapid access of electrolyte ions and facilitates fast electron transport between the active materials and the electroactive analytes. Taking advantage of the flexibility

and robustness of 3DGF, the composite material was fabricated as a flexible biosensor and used as a monolithic electrode for the measurement of analytes of interest (Figure 8-2).

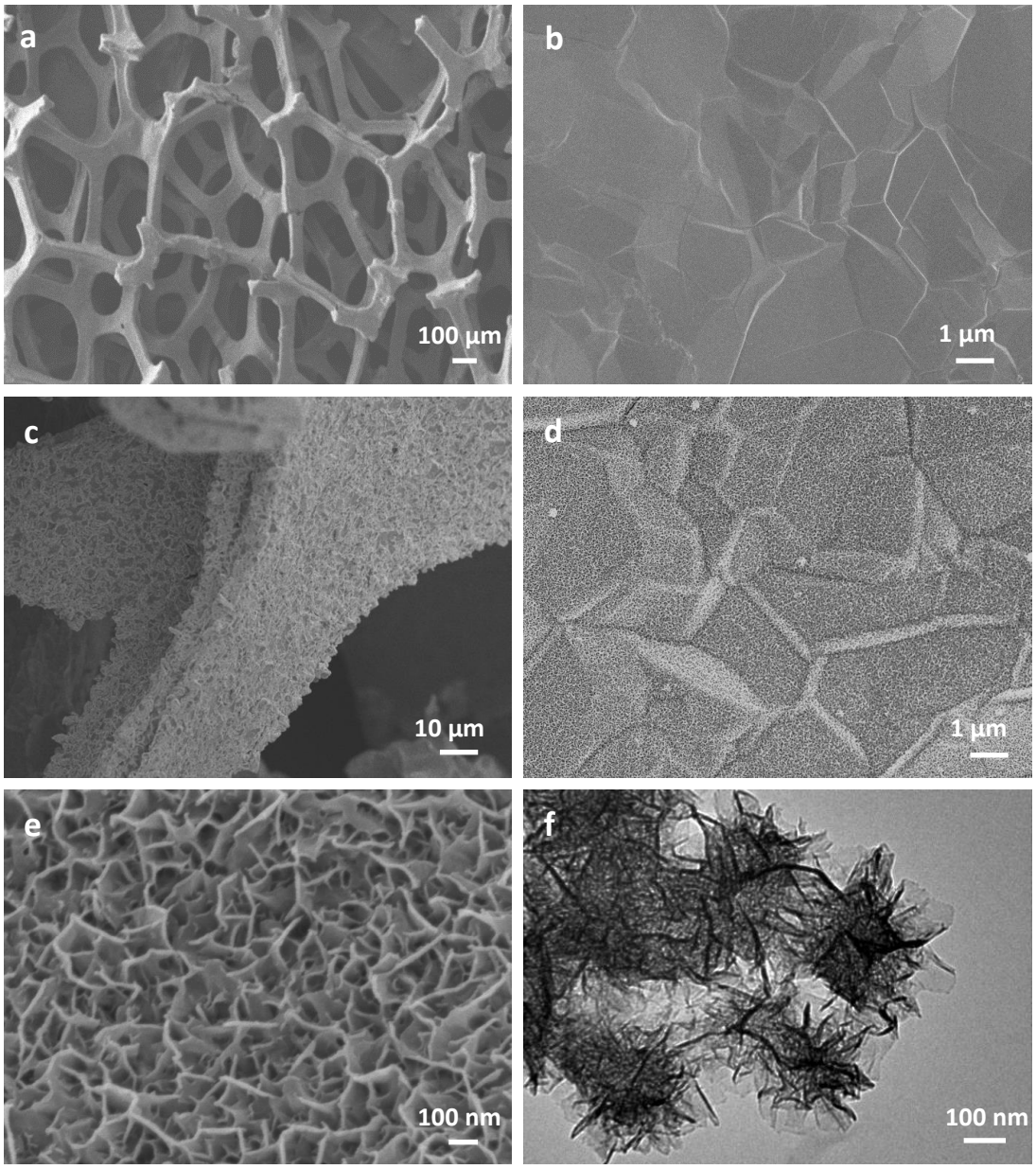

Figure 8-1. (a, b) Low- and high-magnification SEM images of the CVD-grown 3DGF. (c, d) Low- and high-magnification SEM images of the Mn_3O_4/3DGF composite. (e, f) SEM and TEM images of the hierarchically structured Mn_3O_4 nanomesh grown on the surface of 3DGF skeleton.

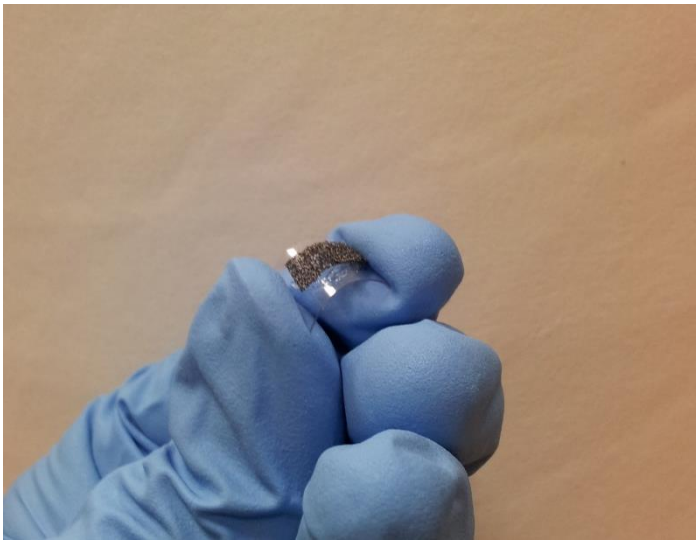

Figure 8-2. Photograph of the Flexible biosensor based on Mn_3O_4/3DGF freestanding electrode.

The phase purity of Mn_3O_4/3DGF composite was analyzed by XRD. As shown in Figure 8-3a, the XRD spectrum of 3DGF shows two notable diffraction peaks at 2θ = 26.5 ° and 54.6 ° corresponding to the (002) and (004) reflection of graphitic carbon, respectively (JCPDS 75-1621). On the XRD spectrum of Mn_3O_4/3DGF composite, except for the characteristic peaks of graphene which are labeled by asterisk, all other peaks can be well indexed to the tetragonal phase of Mn_3O_4 (a=5.762 Å, c=9.469 Å, JCPDS card no. 24-0734), indicating that no impurity phase exists in the Mn_3O_4/3DGF composite. The phase purity of the Mn_3O_4/3DGF composite was also confirmed by Energy-dispersive X-ray spectroscopy (EDX) (Figure 8-4), showing strong peak signals of only C, Mn, and O, components of Mn_3O_4/3DGF composite. In further analysis by Raman spectroscopy (Figure 8-3b), 3DGF shows distinct peaks at 1581 cm^{-1} and 2725 cm^{-1}, which are attributed to the G and 2D bands of single- to a few layers of graphene.[29, 30] It is worth mentioning that D band (~1350 cm^{-1}) cannot be discerned on the 3DGF spectrum, suggesting the CVD-grown graphene foam possesses high quality since the D band is an indication of defects and distorted carbon.[31, 32] On the Raman spectrum of Mn_3O_4/3DGF, the peaks observed at 314, 360, 480 and 650 cm^{-1} are ascribed to the characteristic A_{1g}, $F_{2g}(1)$, $F_{2g}(2)$ and E_g modes of

crystalline Mn_3O_4, respectively.[33, 34] Both XRD and Raman results corroborate successful integration of the Mn_3O_4 with the 3DGF. The content of Mn_3O_4 in the composite was measured by thermogravimetric analysis (TGA) (Figure 8-5). The large weight loss appeared at ~600 ℃ for both 3DGF and Mn_3O_4/3DGF result from the decomposition of 3DGF carbon, which combust completely at 800 ℃. The total weight loss of Mn_3O_4/3DGF is 55.84 wt%, we can thus estimate the amount of Mn_3O_4 present in the composite is 44.16 wt%.

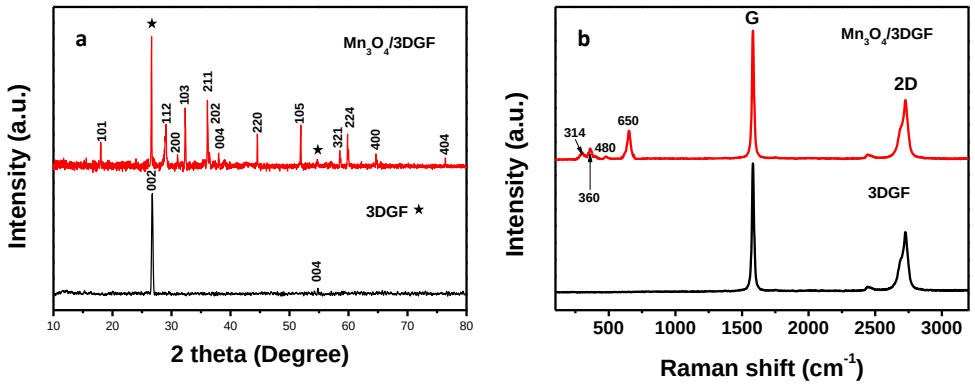

Figure 8-3. XRD (a) and Raman (b) spectra of 3DGF (black) and Mn_3O_4/3DGF composite (red).

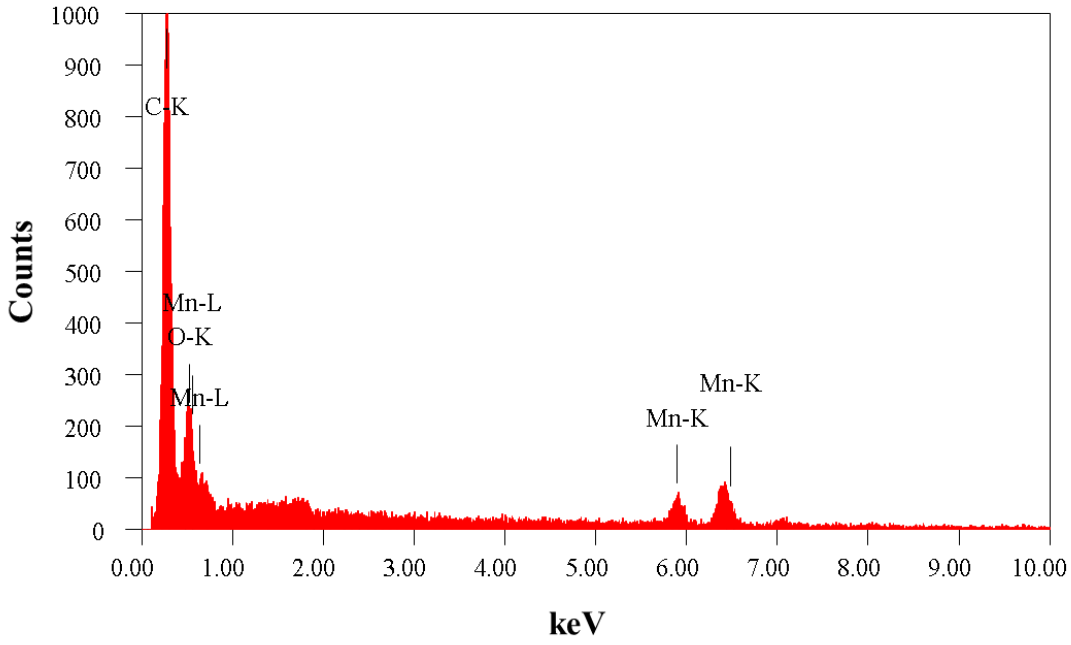

Figure 8-4. Energy-dispersive X-ray (EDX) spectrum of the Mn_3O_4/3DGF composite material.

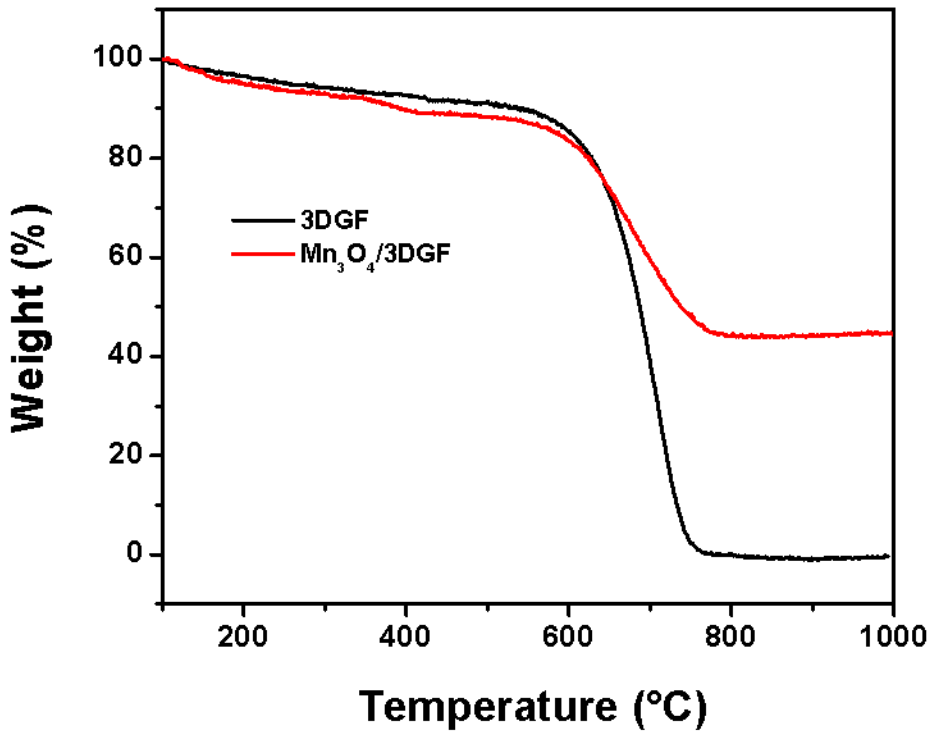

Figure 8-5. TGA curve of 3DGF and the Mn_3O_4/3DGF composite.

8.3.2. Electrocatalytic Behavior of the Electrode

The electrocatalytic behavior of Mn_3O_4 toward the oxidation of glucose was studied by cyclic voltammetry (CV) in 0.1 M NaOH solution. Figure 8-6a shows the CVs of Mn_3O_4/3DGF measured at different scan rates. At the scan rate of 5 mV s^{-1}, two pairs of redox peaks are observed at the potentials of 0.16 V/0.03 V (I/II) and 0.26 V/0.18 V (III/IV), which may attribute to the reversible transition between Mn_3O_4/MnOOH and MnOOH/MnO_2, respectively. With an increase of the scan rate, both the anodic- and cathodic peak currents increase. The intensities of redox currents exhibit good linearity against the scan rate (inset of Figure 8-6a), indicating a surface-confined electrochemical process. Upon the introduction of glucose, notable current increase at anodic peak (III) is observed on the CV curve at scan rate of 20 mV/s, while the cathodic peak currents remain constant (Figure 8-6b). The result suggests that the electrooxidation of glucose could be catalyzed by MnO_2 presumably due to the following reaction:

$$2MnO_2 + C_6H_{12}O_6\,(\text{glucose}) \rightarrow 2MnOOH + C_6H_{10}O_6 \qquad (8\text{-}1)$$

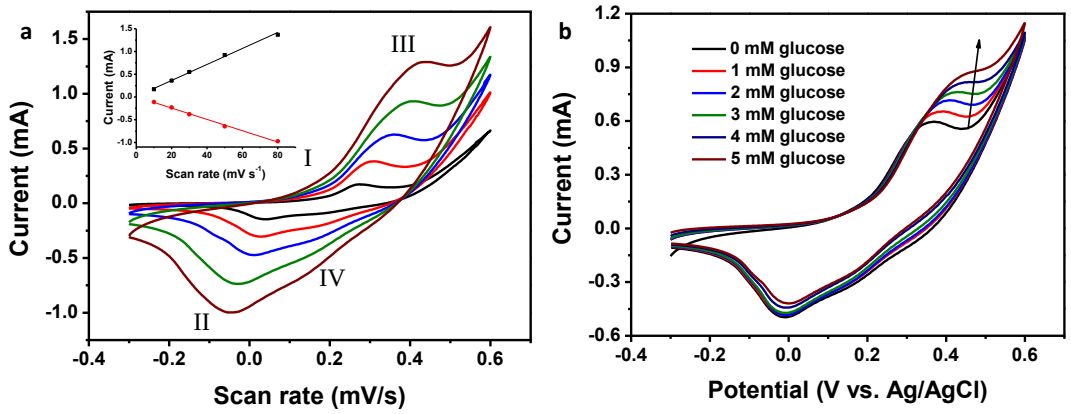

Figure 8-6. (a) CV curves of the Mn_3O_4/3DGF composite electrode recorded at different scan rates (from inside to outside: 10, 20, 30, 50 and 80 mV/s) in 0.1 M NaOH solution. Inset: Plots of scan rate *versus* peak current. (c) CVs of the composite electrode recorded at 20 mV/s with the presence of different concentrations of glucose (from inside to outside: 0, 1, 2, 3, 4, and 5 mM).

8.3.3. Performance of the Non-enzymatic Glucose Sensor

Next, real-time and enzymeless detection of glucose was studied by addition of various concentrations of glucose to a homogeneously stirred 0.1 M NaOH solution at a fixed potential of 0.4 V, where the increase of voltammetric current was observed. Figure 8-7a shows the amperometric responses of the Mn_3O_4/3DGF monolithic electrode to successive addition of 1 mM and 100 μM glucose. A remarkable increase and fast response of amperometric current is observed by the Mn_3O_4/3DGF, which reaches 95% of the steady state current within 5s upon the addition of glucose. The calibration curve of the Mn_3O_4/3DGF is plotted in Figure 8-7b, showing a high sensitivity of 360 μA mM cm^{-2} and a large linear range of 0.1 mM ~ 8 mM. The sensitivity of Mn_3O_4/3DGF is much superior to those enzymatic or enzymeless glucose sensors based on chemically derived graphene,[9, 35-43] most of which are in the range of 1~50 μA mM cm^{-2}. Furthermore, in contrast to the small linear range of Co_3O_4-based enzymeless glucose sensors,[11, 26] the Mn_3O_4/3DGF in the present study fully satisfies the demand for *in-situ* determination of sugar level in human blood, which is 4.4~6.6 mM.[1] As shown by the inset of Figure 8-7b, Mn_3O_4/3DGF also

exhibits a limit of detection as low as 10 μM (S/N=5.5). The performance of our glucose sensor is compared with other nonenzymatic glucose sensor in Table 8-1. The Mn_3O_4/3DGF shows both high sensitivity and large linear range toward glucose detection. Good selectivity of our glucose biosensor was demonstrated by negligible current response to the addition of 0.1 mM uric acid (UA), ascorbic acid (AA) and acetaminophen (AP), common electroactive species coexisting in blood (Figure 7). Additionally, the practicability of the glucose sensor was examined by adding glucose-free and glucose-containing serum to the electrolyte (Figure 8-8). The Mn_3O_4/3DGF showed insensitivity to glucose-free serum sample, which contains a large quantity of various proteins and interferential molecules. Upon the addition of serum supplemented with 0.1 mM glucose, the Mn_3O_4/3DGF showed comparable response to 0.1 mM glucose in serum-free solution. The above results demonstrate that the Mn_3O_4/3DGF-based glucose sensor has excellent selectivity and great potential for *in-situ* determination of blood glucose level.

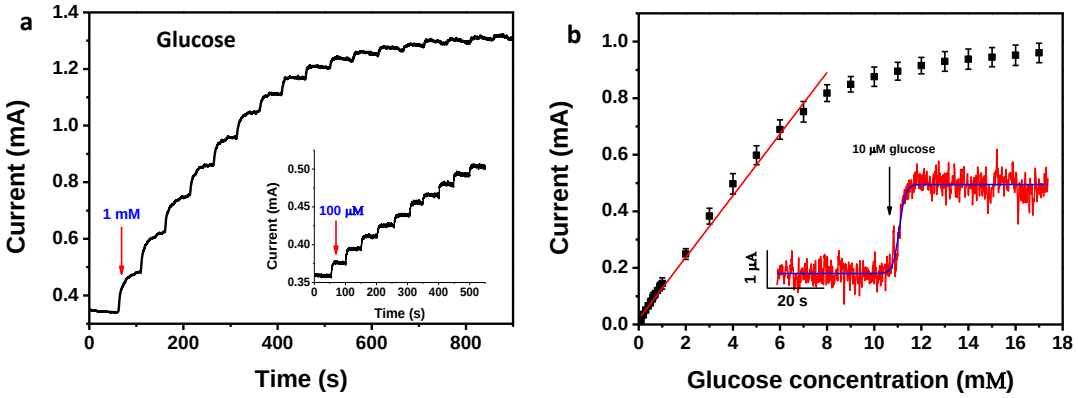

Figure 8-7. (a) Amperometric response of the Mn_3O_4/3DGF composite electrode at 0.4 V upon the successive addition of 1 mM and 100 μM glucose (inset). (b) Calibration curve of composite material-based glucose sensor. Inset shows the current response of the composite electrode toward the addition of 10 μM glucose.

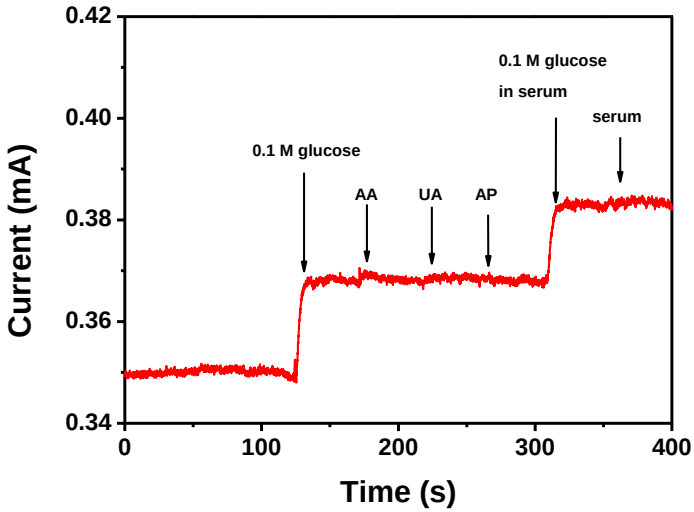

Figure 8-8. Amperometric responses of the Mn_3O_4/3DGF composite electrode toward the addition of glucose and different interferential compounds.

Table 8-1. Comparison of the analytical performance of various nonenzymatic glucose biosensors

Sensing material	Sensitivity ($\mu A\ mM\ cm^{-2}$)	Detection limit (μM)	Linear range	Reference
Co_3O_4 nanofiber	36.25	0.97	up to 2.04 mM	[44]
Co_3O_4/3DGF	3390	0.025	up to 80 μM	[26]
NiO/MWCNT	436	160	up to 12 mM	[45]
MWCNT	4.36	1	2 μM ~ 11 mM	[46]
Porous Au	11.8	5	2 ~ 10 mM	[47]
Mesoporous Pt	9.6	-	0 ~ 10 mM	[48]
Pd/SWCNT	160	0.2±0.05	0.5 ~ 17 mM	[49]
Pt-Pb alloy/MWCNT	17.8	1.8	up to 11 mM	[50]
Pt-Ni alloy/graphene	20.42	10	up to 35 mM	[51]
Mn_3O_4/3DGF	360	10	0.1 ~ 8 mM	This work

MWCNT: multi-walled carbon nanotubes

8.4. Conclusion

To conclude, we synthesized a novel composite material of hierarchical Mn_3O_4/3DGF and evaluated it for enzyme-free detection of glucose. The composite showed good flexibility and mechanical strength which enabled it to be used as a flexible and freestanding biosensor. In addition, the macro- and nanoporous structure of the composite was highly accessible to the medium that greatly facilitated the diffusion of electrolyte ions, resulting in extremely high sensitivity, large linear range, and low detection limit for the detection of glucose. Such high sensing performance of the biosensor could be attributed to the synergistic effect of the two nanomaterials, i.e., the electrocatalytic property of nanostructured Mn_3O_4 and the large surface area of 3DGF. We believe that the uniquely structured Mn_3O_4/3DGF composite with well-defined crystallinity and high electrochemical activity could be beneficial to other applications, such as lithium-ion batteries and supercapacitors.

Reference

1. J. Wang, *Chemical Reviews*, 2008, **108**, 814-825.
2. C. Guo, F. Hu, C. M. Li and P. K. Shen, *Biosensors and Bioelectronics*, 2008, **24**, 819-824.
3. J. Liu, C. Guo, C. M. Li, Y. Li, Q. Chi, X. Huang, L. Liao and T. Yu, *Electrochemistry Communications*, 2009, **11**, 202-205.
4. P. Si, S. Ding, J. Yuan, X. W. Lou and D.-H. Kim, *ACS Nano*, 2011, **5**, 7617-7626.
5. P. Si, P. Kannan, L. Guo, H. Son and D.-H. Kim, *Biosensors and Bioelectronics*, 2011, **26**, 3845-3851.
6. K. E. Toghill, L. Xiao, M. A. Phillips and R. G. Compton, *Sensors and Actuators B-Chemical*, 2010, **147**, 642-652.
7. J. Lu, I. Do, L. T. Drzal, R. M. Worden and I. Lee, *ACS Nano*, 2008, **2**, 1825-1832.
8. F. Xiao, Y. Q. Li, X. L. Zan, K. Liao, R. Xu and H. W. Duan, *Advanced Functional Materials*, 2012, **22**, 2487-2494.
9. H. Gao, F. Xiao, C. B. Ching and H. Duan, *ACS Applied Materials & Interfaces*, 2011, **3**, 3049-3057.
10. Y. Sun, H. Buck and T. E. Mallouk, *Analytical Chemistry*, 2001, **73**, 1599-1604.
11. C.-W. Kung, C.-Y. Lin, Y.-H. Lai, R. Vittal and K.-C. Ho, *Biosensors and Bioelectronics*, 2011, **27**, 125-131.
12. J. Chen, W.-D. Zhang and J.-S. Ye, *Electrochemistry Communications*, 2008, **10**, 1268-1271.
13. J. Wang, D. F. Thomas and A. Chen, *Analytical Chemistry*, 2008, **80**, 997-1004.

14. D. Yu, K. Park, M. Durstock and L. Dai, *The Journal of Physical Chemistry Letters*, 2011, **2**, 1113-1118.
15. Q. Wu, Y. Xu, Z. Yao, A. Liu and G. Shi, *ACS Nano*, 2010, **4**, 1963-1970.
16. C. X. Guo, H. B. Yang, Z. M. Sheng, Z. S. Lu, Q. L. Song and C. M. Li, *Angewandte Chemie International Edition*, 2010, **49**, 3014-3017.
17. Y. Zhu, S. Murali, M. D. Stoller, K. J. Ganesh, W. Cai, P. J. Ferreira, A. Pirkle, R. M. Wallace, K. A. Cychosz, M. Thommes, D. Su, E. A. Stach and R. S. Ruoff, *Science*, 2011.
18. S. Ding, J. S. Chen, D. Luan, F. Y. C. Boey, S. Madhavi and X. W. Lou, *Chemical Communications*, 2011, **47**, 5780-5782.
19. S. Bae, H. Kim, Y. Lee, X. Xu, J.-S. Park, Y. Zheng, J. Balakrishnan, T. Lei, H. Ri Kim, Y. I. Song, Y.-J. Kim, K. S. Kim, B. Ozyilmaz, J.-H. Ahn, B. H. Hong and S. Iijima, *Nat Nano*, 2010, **5**, 574-578.
20. K. S. Kim, Y. Zhao, H. Jang, S. Y. Lee, J. M. Kim, K. S. Kim, J.-H. Ahn, P. Kim, J.-Y. Choi and B. H. Hong, *Nature*, 2009, **457**, 706-710.
21. A. Kasry, M. A. Kuroda, G. J. Martyna, G. S. Tulevski and A. A. Bol, *ACS Nano*, 2010, **4**, 3839-3844.
22. J. D. Fowler, M. J. Allen, V. C. Tung, Y. Yang, R. B. Kaner and B. H. Weiller, *ACS Nano*, 2009, **3**, 301-306.
23. X. C. Dong, Y. M. Shi, W. Huang, P. Chen and L. J. Li, *Advanced Materials*, 2010, **22**, 1649 -1653.
24. Y. Liu, X. Dong and P. Chen, *Chemical Society Reviews*, 2012, **41**, 2283-2307.
25. Z. Chen, W. Ren, L. Gao, B. Liu, S. Pei and H.-M. Cheng, *Nature Materials*, 2011, **10**, 424-428.
26. X.-C. Dong, H. Xu, X.-W. Wang, Y.-X. Huang, M. B. Chan-Park, H. Zhang, L.-H. Wang, W. Huang and P. Chen, *ACS Nano*, 2012, **6**, 3206-3213.
27. S. J. Chae, F. Gunes, K. K. Kim, E. S. Kim, G. H. Han, S. M. Kim, H. J. Shin, S. M. Yoon, J. Y. Choi, M. H. Park, C. W. Yang, D. Pribat and Y. H. Lee, *Advanced Materials*, 2009, **21**, 2328-+.
28. T. Ramanathan, A. A. Abdala, S. Stankovich, D. A. Dikin, M. Herrera-Alonso, R. D. Piner, D. H. Adamson, H. C. Schniepp, X. Chen, R. S. Ruoff, S. T. Nguyen, I. A. Aksay, R. K. Prud'homme and L. C. Brinson, *Nature Nanotechnology*, 2008, **3**, 327-331.
29. A. C. Ferrari, J. C. Meyer, V. Scardaci, C. Casiraghi, M. Lazzeri, F. Mauri, S. Piscanec, D. Jiang, K. S. Novoselov, S. Roth and A. K. Geim, *Physical Review Letters*, 2006, **97**.
30. X. C. Dong, Y. M. Shi, Y. Zhao, D. M. Chen, J. Ye, Y. G. Yao, F. Gao, Z. H. Ni, T. Yu, Z. X. Shen, Y. X. Huang, P. Chen and L. J. Li, *Physical Review Letters*, 2009, **102**.
31. M. S. Dresselhaus, A. Jorio, M. Hofmann, G. Dresselhaus and R. Saito, *Nano Letters*, 2010, **10**, 751-758.
32. X. C. Dong, D. L. Fu, W. J. Fang, Y. M. Shi, P. Chen and L. J. Li, *Small*, 2009, **5**, 1422-1426.

33. C. M. Julien and M. Massot, *Journal of Physics: Condensed Matter*, 2003, **15**, 3151.
34. D. P. Dubal, D. S. Dhawale, R. R. Salunkhe and C. D. Lokhande, *Journal of Alloys and Compounds*, 2010, **496**, 370-375.
35. X. Kang, J. Wang, H. Wu, I. A. Aksay, J. Liu and Y. Lin, *Biosensors and Bioelectronics*, 2009, **25**, 901-905.
36. T. T. Baby, S. S. J. Aravind, T. Arockiadoss, R. B. Rakhi and S. Ramaprabhu, *Sensors and Actuators B-Chemical*, 2010, **145**, 71-77.
37. S. J. Guo, D. Wen, Y. M. Zhai, S. J. Dong and E. K. Wang, *ACS Nano*, 2010, **4**, 3959-3968.
38. M. Pumera, A. Ambrosi, A. Bonanni, E. L. K. Chng and H. L. Poh, *Trac-Trends in Analytical Chemistry*, 2010, **29**, 954-965.
39. C. S. Shan, H. F. Yang, D. X. Han, Q. X. Zhang, A. Ivaska and L. Niu, *Biosensors & Bioelectronics*, 2010, **25**, 1070-1074.
40. C. S. Shan, H. F. Yang, J. F. Song, D. X. Han, A. Ivaska and L. Niu, *Analytical Chemistry*, 2009, **81**, 2378-2382.
41. H. Wu, J. Wang, X. H. Kang, C. M. Wang, D. H. Wang, J. Liu, I. A. Aksay and Y. H. Lin, *Talanta*, 2009, **80**, 403-406.
42. L. M. Lu, H. B. Li, F. L. Qu, X. B. Zhang, G. L. Shen and R. Q. Yu, *Biosensors & Bioelectronics*, 2011, **26**, 3500-3504.
43. C. Z. Zhu, Y. X. Fang, D. Wen and S. J. Dong, *Journal of Materials Chemistry*, 2011, **21**, 16911-16917.
44. Y. Ding, Y. Wang, L. A. Su, M. Bellagamba, H. Zhang and Y. Lei, *Biosensors & Bioelectronics*, 2010, **26**, 542-548.
45. M. Shamsipur, M. Najafi and M.-R. M. Hosseini, *Bioelectrochemistry*, 2010, **77**, 120-124.
46. J. S. Ye, Y. Wen, W. D. Zhang, L. M. Gan, G. Q. Xu and F. S. Sheu, *Electrochemistry Communications*, 2004, **6**, 66-70.
47. Y. Li, Y. Y. Song, C. Yang and X. H. Xia, *Electrochemistry Communications*, 2007, **9**, 981-988.
48. S. Park, T. D. Chung and H. C. Kim, *Analytical Chemistry*, 2003, **75**, 3046-3049.
49. L. Meng, J. Jin, G. X. Yang, T. H. Lu, H. Zhang and C. X. Cai, *Analytical Chemistry*, 2009, **81**, 7271-7280.
50. H. F. Cui, J. S. Ye, W. D. Zhang, C. M. Li, J. H. T. Luong and F. S. Sheu, *Analytica Chimica Acta*, 2007, **594**, 175-183.
51. H. C. Gao, F. Xiao, C. B. Ching and H. W. Duan, *ACS Applied Materials & Interfaces*, 2011, **3**, 3049-3057.

Chapter 9-Conclusions and Outlook

9.1. Conclusions

The thesis work focused on the development of novel nanostructured electrode materials with large surface areas, high conductivity, good biocompatibility, and outstanding electrocatalytic activity for the fabrication of high-performance glucose biosensors with high sensitivity, excellent selectivity, wide linear dynamic range, low interferences and long storage time. Five types of uniquely structured nanomaterials have been synthesized and employed to modify the electrode surface, immobilize the enzyme or used directly as an electrode material. These materials were well characterized and they exhibited unique physical and chemical properties. The fabricated biosensors based on these electrode materials generally showed excellent performance toward the oxidation of glucose and measurement of glucose concentrations in human serum. Specifically:

1) A second-generation glucose biosensor was developed by modification of the Au electrode surface with multi-layered nanohybrid material of MWCNT/AuNPs followed by the adsorption of GOx. By functionalization of MWCNTs with MPTS, the end and side walls of MWCNTs were decorated with a high density of AuNPs, which allowed for the immobilization of a high quantity of GOx on the electrode surface. The fabricated biosensor therefore exhibited a high sensitivity of 19.27 μA mM^{-1} cm^{-2}, a wide linear range of 20 μM to 10 mM with a low detection limit of 2.3 μM (S/N=3) for the detection of glucose in serum.

2) A third-generation glucose biosensor based on DET of GOx was fabricated by modification of GCE with a mesoporous nanomaterial of 1DHS TiO_2, which was immobilized with a large amount of GOx in its uniformly distributed mesopores. The mesoporous structured 1DHS TiO_2 was synthesized by CVD method with MWCNT as a sacrificing template. The resulting Nafion/GOx/1DHS TiO_2-modified electrode was successfully employed as a mediatorless glucose sensor, achieving a high

sensitivity of 9.90 μA mM^{-1} cm^{-2}, a linear range of up to 1.5 mM and a low detection limit of 1.29 μM. In addition, the biosensor exhibited a long storage time of up to 2 weeks and excellent anti-interference performance.

3) Next, a third-generation glucose biosensor was constructed by immobilizing GOx on hierarchically structured MnO_2 spheres, which were thereafter modified on GCE. The electrodeposited MnO_2 hierarchical spheres exhibited a mesoporous structure with a large specific surface of 128.5 m^2 g^{-1} and a narrow pore size distribution of 5~12 nm. GOx immobilized in the mesopores of MnO_2 presented fast DET and the biosensor based on GOx/MnO_2-GCE exhibited an enhanced sensitivity of 31.6 μA mM cm^{-2}, an improved linear range up to 3.15 mM and a low detection limit of 0.35 μM for mediatorless detection of glucose.

4) Furthermore, a mediatorless third-generation glucose biosensor was designed by immobilizing GOx on CNCs followed by modification of GCE with the GOx/CNCs biocomposite. The uniquely structured CNCs with a large specific surface area of 1651 m^2 g^{-1} narrow distribution of pore size in the range of 5~20 nm, well developed graphitic structure was synthesized by MgO template-assisted CVD method. The constructed biosensor displayed a significantly enlarged linear range of up to 14 mM, with a sensitivity of 19.18 μA mM cm^{-2} and a low detection limit of 0.33 μM

5) Finally, a flexible non-enzymatic glucose biosensor was fabricated by a nanocomposite material of hierarchically structured Mn_3O_4/3DGF, which was synthesized by CVD growth of 3DGF followed by electrodeposition of Mn_3O_4. The nanocomposite-based electrode exhibited a remarkable electrocatalytic activity toward the direct oxidation of glucose, and offered an ultrahigh sensitivity of 360 μA mM cm^{-2}, a satisfied linear range of 0.1 ~ 8 mM and a low detection limit of 10 μM for glucose detection.

Table 9-1 compares the electrode materials and analytical performances of the five different types of glucose biosensors developed in this thesis work. The detection mechanisms, advantages and limitations of these glucose sensors based on different

nanostructured electrode materials are summarized in Table 9-2. The key features of the developed glucose sensors are also compared with commercial glucose sensors and literature reported studies in Table 9-3.

Table 9-1. Comparison of the electrode materials and analytical performances of glucose biosensors developed in this thesis work

Electrode material	Analytical performance		
	Sensitivity (μA mM cm^{-2})	**Detection limit (μM)**	**Linear range (mM)**
GOx/$(AuNPs/MWCNT)_5$/Au electrode	19.27	2.3	0.02~10
GOx/1DHS TiO_2/ GCE	9.9	1.29	Up to 1.5
GOx/MnO_2/ GCE	31.6	0.35	Up to 3.15
GOx/CNCs/GCE	19.18	0.33	Up to 14
Mn_3O_4/3DGF	360	10	0.1 ~ 8

Table 9-2. Summary of the detection mechanisms, advantages and limitations of different types of glucose biosensors developed in this thesis work

Electrode	Detection mechanism	Advantages	Limitations
GOx/$(AuNPs/MWCNT)_5$/Au electrode	GOx-catalysed glucose oxidation reaction; Ferrocene-mediated electron transfer between enzyme and electrode	The enzyme immobilized on the electrode surface is very stable; The sensor has long-term stability	Surface modification of the electrode is time-consuming; The sensor is not suitable for glucose detection *in-vivo* due to the soluble and toxic nature of mediator
GOx/1DHS	GOx-catalysed	The electrode material	Blood glucose

TiO_2/ GCE	glucose oxidation reaction; Direct electron transfer between enzyme and electrode	is easy and cheap to be fabricated; The sensor could be used for *in-vivo* detection	detection requires dilution due to the small linear range of this sensor
GOx/MnO_2/ GCE	GOx-catalysed glucose oxidation reaction; Direct electron transfer between enzyme and electrode	Facile electrode fabrication process; Low detection limit and very high sensitivity	The electrode material peels off from the sensor surface after long-term usage; Blood glucose detection requires dilution
GOx/CNCs/GCE	GOx-catalysed glucose oxidation reaction; Direct electron transfer between enzyme and electrode	Large linear range and low detection limit; The sensor is capable for blood glucose detection without dilution	It is difficult to scale up the production of electrode material CNCs; Enzyme immobilization on CNCs is not very stable
Mn_3O_4/3DGF	Electrocatalyst Mn_3O_4-catalyzed glucose oxidation reaction; Enzyme-free glucose detection	Extremely high sensitivity; Stable for glucose detection under harsh conditions such as high temperature, high humidity and extreme pH; Low cost	Not available for glucose detection in neutral pH buffer; Susceptible to many interferences; Long response time

Table 9-3. Comparison of the key features of commercial and literature reported glucose sensors and with the sensors developed in this thesis work.

Manufacturer	**Brand**	**Classification**	**Enzyme**	**Mediator**	**Test time (s)**
Abbott	FreeStyle Freedom Lite	Second-generation	GDH-PQQ	Osmium	−5
Arkray	Glucocard X-meter	Second-generation	GDH	Ferrocene	5
Bayer	Ascensia Contour	Second generation	GDH-FAD	Ferrocene	5
Bionime	Rightest GM300	Second-generation	GOx	Ferrocene	8
Diabestic Supply of Suncoast	Advocate Redi-Code	Second-generation	GOx	Ferricyanide	7
Diagnostic Devices	Prodigy Autocode	Second-generation	GOx	Ferricyanide	6
LifeScan	OneTouch UltraLink	Second-generation	GOx	Ferricyanide	5
Nova Biomedical	Nova Max	Second generation	GOx	Ferrocene	5
Roche	Accu-Chek Aviva	Second generation	GDH-PQQ	Ferricyanide	5
Electrode	**Literature**	**Classification**	**Enzyme**	**Mediator**	**Test time (s)**
Mesoporous TiO_2	1	Third-generation	GOx	NA	10
Nanocrystalline	2	Third-generation	GOx	NA	30

TiO_2					
TiO_2-copolymer	3	Third-generation	GOx	NA	20
NiO hollow spheres	4	Third-generation	GOx	NA	8
PEDOT-NiO HS	5	Third-generation	GOx	NA	10
Graphitic nanocage	6	Third-generation	GOx	NA	5
AuNPs/MWCNT)5	This work	Second-generation	GOx	Ferrocene	3
GOx/1DHS TiO_2/ GCE	This work	Third-generation	GOx	NA	<5
MnO_2 spheres	This work	Third-generation	GOx	NA	<3
CNCs	This work	Third-generation	GOx	NA	<3
Mn_3O_4/3DGF	This work	Non-enzymatic	NA	NA	5

9.2. Outlook

Although the thesis work has dedicated to improve the performance glucose sensors with novel nanostructured electrode materials, there are still many challenges ahead toward the commercialization of third-generation glucose biosensors and non-enzymatic glucose biosensors for clinical applications. For third-generation glucose biosensor, further efforts are expected in the future to solve the following problems:

1) Further improvement of the biosensor linear range is needed. Although the present thesis work has enlarged the linear range of the third-generation glucose sensor to up to 14 mM with the unique electrode material of CNCs, the commercial glucose sensors usually have a linear dynamic range up to 30 mM, since the blood glucose levels of diabetic patients are generally much higher than 11 mM. A further improved upper limit of the linear range will ensure most diabetic patients will have accurate readings of their blood glucose levels, rather than just knowing whether their glucose concentrations exceed the normal range qualitatively.

2) Further electrode modification is required to prevent the surface fouling effect. The third-generation glucose biosensor is ideal for implantation and *in-vivo* measurement of glucose concentrations in a real-time manner, since it eliminates the use of artificial redox mediators, which are considered to be toxic to the human body. However, the fouling of the sensor surface with various proteins in blood or interstitial fluid of the subcutaneous tissue could deteriorate the performance of implanted electrode over a long term. Therefore, it is highly desirable to functionalize the sensor surface with anti-fouling materials which effectively prevent the electrode from fouling of proteins and in the same time do not compromise the sensitivity of the biosensor.

3) Better strategies are needed for the development of non-invasive third generation glucose biosensors. Non-invasive glucose detection is the ultimate goal of glucose sensor development, since it will alleviate the problems associated with point-of-care and implantable glucose sensors such as patient discomfort, risk of infection, inflammatory response and surface fouling effects. However, current non-invasive glucose sensors are still based on the scheme of first-generation biosensor, which is lacking in accuracy and reliability. The integration of non-invasive detection methods with third-generation glucose biosensors will provide many exciting opportunities since such biosensors could offer unprecedented advantages such as high sensitivity, high accuracy, non-invasiveness and real-time glucose monitoring. Nevertheless, integration of non-invasive and third-generation glucose biosensors requires delicate design of the sensing system, which should minimize the warm-up time, calibration frequency, avoid irritation and other side-effect to the human body.

The challenges and future development of non-enzymatic glucose biosensors toward practical usage and commercialization are considered as follows:

1) The major obstacle that prevents many non-enzymatic glucose biosensors from clinical application is that they are not able to catalyse the glucose oxidation under physiological conditions. This is especially the case for Ni, Cu, metal oxide and

carbon nanomaterials based electrodes, in spite of their extraordinarily high sensitivity. This problem is attempting to be solved by development of nanostructured noble metal based electrode materials, which are capable of catalysing glucose oxidation in neutral pH buffer.

2) Another concern of non-enzymatic electrodes toward commercialization would be the fabrication cost. Since the electrode materials of many non-enzymatic glucose sensors are based on nanostructured noble metals such as Au, Pt, Pd or Rb or their alloys, it is essential to reduce the geometric surface area of sensing electrode in order to lower the fabrication cost. Development of microelectrode-based non-enzymatic glucose sensors should be an ideal option since it can offer additional advantages such as minimally invasive glucose detection, which greatly reduces the pain of diabetic patients.

3) In addition to blood glucose sensing, nanomaterials based non-enzymatic glucose sensors may also find extensive applications in bioindustrial process monitoring due to their sterilization compatibility. Besides oxygen and pH, we might also be able to monitor the glucose level in a fermentation plant or bioreactor in a real time manner. Furthermore, although some non-enzymatic glucose catalysts are not applicable for blood glucose monitoring, they are well suited for application in glucose fuel cells which do not require physiological condition. In contrast to enzymatic systems that merely oxidize glucose to glucolactone, many nanostructured non-enzymatic electrocatalysts are capable of oxidizing glucose completely to CO_2 and H_2O at low potentials, which could significantly enhance the energy conversion efficiency.

Reference

1. S. J. Bao, C. M. Li, J. F. Zang, X. Q. Cui, Y. Qiao and J. Guo, *Advanced Functional Materials*, 2008, **18**, 591-599

2. Q. W. Li, G. A. Luo, J. Feng, Q. Zhou, L. Zhang and Y. F. Zhu, *Electroanalysis*, 2001, **13**, 413-416.

3. X. Chen and S. J. Dong, *Biosensors & Bioelectronics*, 2003, **18**, 999-1004.

4. T. H. Wang, C. C. Li, Y. L. Liu, L. M. Li, Z. F. Du, S. J. Xu, M. Zhang and X. M. Yin, *Talanta*, 2008, **77**, 455-459.
5. 31. C. X. Guo and C. M. Li, *Physical Chemistry Chemical Physics*, 2010, **12**, 12153-12159
6. S. Wu, H. X. Ju and Y. Liu, *Advanced Functional Materials*, 2007, **17**, 585-592.

Appendix A: List of Publications

1. **P. Si,** S. Ding, J. Yuan, X. W. Lou and D. H. Kim, "Hierarchically Structured One-Dimensional TiO_2 for Protein Immobilization, Direct Electrochemistry and Mediator-Free Glucose Sensing", ***ACS Nano***, 2011, 5 (9), 7617-7626 *(Impact factor: 12.062, citations: 23*)

2. **P. Si,** P. Kannan, L. Guo, H. Son and D. H. Kim, "Highly Stable and Sensitive Glucose Biosensor Based on Covalently Assembled High Density Au Nanostructures", ***Biosensors and Bioelectronics***, 2011, 26 (9), 3845-3851 *(Impact factor: 5.437, citations: 24*)

3. **P. Si,** H. Chen, P. Kannan and D. H. Kim, "Selective and Sensitive Determination of Dopamine by Composites of Polypyrrole and Graphene Modified Electrodes", ***Analyst,*** 2011, 136 (24), 5134-5138 *(Impact factor: 4.23, citations: 16*)

4. **P. Si,** S. Ding, X. W. Lou and D. H. Kim, "An Electrochemically Formed Three-Dimensional Structure of Polypyrrole/Graphene Nanoplatelets for High-Performance Supercapacitors", ***RSC Advances,*** *2011, 1 (7), 1271-1278 (Impact factor: 2.562, Citations: 9*)

5. **P. Si**, X.C. Dong, P. Chen and D.H. Kim, "A Hierarchically Structured Composite of Mn_3O_4/3D Graphene Foam for flexible Nonenzymatic Biosensors", ***Journal of Materials Chemistry-B***, 2013, 1, 110-115

6. **P. Si,** P. Chen and D. H. Kim, "Electrodeposition of hierarchical MnO_2 spheres for enzyme immobilization and glucose biosensing", ***Journal of Materials Chemistry-B***, 2013, 1, 2696-2700

7. Z. Bai, R. Chen, **P. Si,** Y. Huang, H. Sun and D. H. Kim, "Fluorescent pH sensor based on Ag@SiO2 core-shell nanoparticle", ***ACS Applied Materials & Interfaces***, *accepted*. DOI: 10.1021/am401528w

8. **P. Si**, "A 'Nano' Era for Blood Glucose Sensing", ***Asia Pacific Biotech News,*** 2012, 16 (8) special issue on 'Singapore's Next-Gen Researchers**',** 48-50

9. **P. Si,** X. Wang, P. Chen and D. H. Kim, “Carbon Nanocages as Unique Electrode Materials for Efficient Enzyme Immobilization, Fast Direct Electrochemistry and High-Performance Glucose Biosensing”, *submitted*

10. **P. Si** and D. H. Kim, “Direct Electron Transfer at Enzyme-Nanomaterials Interface for Glucose Biosensors: A Review”, *submitted*

11. H. Chen, **P. Si**, S. Chen, W. Pei and D. H. Kim, “Template-Free, Organic Solvent Based Synthesis of Nanostructured PEDOT to Interface Neurons”, *Submitted.*

12. Y. Huang, **P. Si** and D. H. Kim, “Au-Pd Core-Shell Superstructures with Closely Packed Ultra-Small Pd Nanorods as Shells: Mediator-Free H_2O_2 Sensing and Surface-Enhanced Raman Scattering Properties”, *Submitted*

Appendix B: List of Abbreviations

AA: ascorbic acid

Ab: antibody

Ag: antigen

AuNP: gold nanoparticle

BET: Brunauer-Emmett-Teller

BJH: Barrett-Joyner-Halenda

BSA: bovine serum albumin

BSA: bovine serum albumin

CGMS: continuous glucose monitoring system

CNC: carbon nanocage

CNT: carbon nanotube

CTAB: cetyltrimethylammonium bromide

CV: cyclic voltammetry

DA: dopamine

DET: direct electron transfer

DPV: differential pulse voltammetry

EDX: energy-dispersive X-ray spectroscopy

EIS: electrochemical impedance spectroscopy

FAD: flavin adenine dinucleotide

FE-SEM: field-emission scanning electron microscopy

FTIR: Fourier transform infrared spectroscopy

GCE: glassy carbon electrode

GDH: glucose dehydrogenase

GOx: glucose oxidase

HRP: horseradish peroxidase

HR-TEM: high-resolution transmission electron microscopy

ITO: indium tin oxide

LBL: Layer-by-layer

LOD: limit of detection

MgO: magnesium oxide

MnO_2: manganese dioxide

MPTS: (3-Mercaptopropyl)triethoxysilane

MWCNT: multi-walled carbon nanotube

NAD: nicotinamide adenine dinucleotide

NIR: near infrared

OCT: optical coherence tomography

PBS: phosphate buffered saline

PEDOT: 3,4-ethylenedioxythiophene

PPy: polypyrrole

PQQ: pyrroloquinoline quinone

SCE: saturated calomel electrode

SEM: scanning electron microscopy

SPR: surface plasmon resonance

SWCNT: single-walled carbon nanotube

TEM: transmission electron microscopy

TGA: thermogravimetric analysis

UA: uric acid

WHO: World Health Organization

XRD: X-ray diffraction

1DHS TiO_2: one-dimensional hierarchically structured titanium dioxide

3DGF: three-dimensional graphene foam

Appendix C: List of Figures

Inset: CVs of bare Au electrode (dashed) and GOx/(AuNPs/MWCNT)$_5$/Au electrode (solid) in 0.1 M PBS containing 0.1 mM ferrocenemethanol. (B) The current response for 20 mM glucose on Au electrode modified with 1~10 layers of AuNPs/MWCNT and GOx.

Figure 4-6. (A) CVs obtained for the GOx/(AuNPs/MWNCNT)$_5$/Au electrode in 0.1 M PBS (pH 7.4) containing 0.1 mM ferrocenemethanol at different scan rates. From inside to outside: 20, 40, 60, 80, 100, 150, 200, 250, 300 mV/s. (B) The relationship of the anodic and cationic peak current vs. the square root of the scan rate.

Figure 4-7. (A) Amperometric response of the GOx/(AuNPs/MWNCNT)$_5$/Au electrode to successive addition of different concentrations of glucose at applied potential of 0.3 V (vs. SCE) in PBS containing 0.1 mM ferrocenemethanol. (B) Amperometric response of the above electrode to successive addition of 1 mM glucose at applied potential of 0.3 V (vs. SCE) in PBS containing 0.1 mM ferrocenemethanol.. (C) The calibration curve of present glucose biosensor obtained from (A) and (B). (D) Lineweaver-Burk plot of the above glucose biosensor for the determination of K_m^{app}.

Figure 4-8. Amperometric response of 0.5 mM AA, 0.5 mM AP, 1 mM UA and 0.5 mM glucose on the GOx/(AuNPs/MWCNT)$_5$/Au electrode recorded at 0.3V vs. SCE in 0.1 M PBS containing 0.1 mM ferrocenemethanol.

Figure 5-1. SEM (a, c) and TEM (b, d) images of the CNT-TiO_2 composite (a, b) and the 1DHS TiO_2 (c, d) obtained after calcining the composite at 550 ℃ for 2 h. Insets are the high-magnification SEM and TEM images.

Figure 5-2. (a) XRD patterns for (I) the CNT-TiO_2 composite and (II) the 1DHS TiO_2 formed after calcination. (b) Nitrogen adsorption-desorption isotherms of the 1DHS TiO_2. Inset: Pore size distribution calculated from the adsorption branch and desorption branch of the isotherm by the Barrett-Joyner-Halenda method.

Figure 5-3. The nitrogen adsorption-desorption isotherms of 1DHS TiO_2 before and after loading with different GOx concentrations ranging from 0 to 20 mg mL^{-1}. Inset:

The plot of the GOx loading ratio on 1DHS TiO_2 versus the GOx concentration.

Figure 5-4. IR spectra of 1DHS TiO_2 (red), pure GOx (green) and GOx-loaded TiO_2 (blue).

Figure 5-5. Nyquist plots of a bare GCE, a 1DHS TiO_2-modified GCE and a GOx/1DHS TiO_2-modified GCE measured in 1.0 M KCl solution containing 10 mM $Fe(CN)_6^{3-/4}$.

Figure 5-6. CVs of 1DHS TiO_2/Nafion-, GOx/Nafion- and GOx/1DHS TiO_2/Nafion-modified GCEs measured in 0.1 M pH 7.4 nitrogen-saturated PBS solution at scan rate of 100 mV s^{-1}.

Figure 5-7. a) CVs of a GOx/1DHS TiO_2/Nafion-modified GCE in 0.1 M pH 7.4 nitrogen-saturated PBS solution at different scan rates (from 25 to 600 mV s^{-1}, inside to outside). b) Plots of peak current versus scan rate.

Figure 5-8. a) CVs of a GOx/1DHS TiO_2/Nafion-modified GCE in 0.1 M nitrogen-saturated PBS solution at different pHs at 100 mVs^{-1}. b) Plot of peak currents versus pH. Inset of (b): Plot of formal potential versus pH.

Figure 5-9. a) CVs of a GOx/1DHS TiO_2/Nafion-modified GCE in 0.1 M pH 7.4 nitrogen-saturated PBS solution with different glucose concentrations (some data not shown for clarity). b) Cathodic branches of the background-subtracted CV curves in (a). Inset of (b) is the calibration curve. Scan rate: 100 mV s^{-1}.

Figure 5-10. a) CVs of a GOx/1DHS TiO_2/Nafion-modified GCE in 0.1 M pH 7.4 air-saturated PBS solution with different glucose concentrations (some data not shown for clarity). b) Enlarged graph showing the rectangular region marked in (a). Inset of (b): The calibration plot of the cathodic current versus the glucose concentration at -0.462 V. Scan rate: 100 mV s^{-1}.

Figure 5-11. a) Current-time curve of a GOx/1DHS TiO_2/Nafion-modified GCE for successive addition of 0.15 mM glucose aliquots to stirred 0.1 M pH 7.4 air-saturated PBS at -0.45 V. b) The calibration curve (current versus glucose concentration) and the Lineweaver-Burk plot ($current^{-1}$ versus $concentration^{-1}$) obtained from the

amperometric response in (a).

Figure 5-12. a) Amperogram showing the effect of interfering compounds (0.3 mM AA, 0.2 mM DA and 0.5 mM UA) on the detection of glucose. b) The stability of the GOx/1DHS TiO_2/Nafion-modified electrode over a two-week storage period.

Figure 6-1. (a) Low and (b) high magnification SEM images of MnO_2. (c) TEM image of MnO_2. (d) Nitrogen adsorption-desorption isotherm and pore size distribution (inset) of MnO_2.

Figure 6-2. SEM images showing the architecture evolution of MnO_2 synthesized in the solution of 10 mM manganese acetate with different applied deposition potentials: (a) 0.5 V, (b) 0.8 V, (c) 1.2 V and (d) 1.5 V. The growth time is 300 s. The scale bar represents 100 nm.

Figure 6-3. (a)~(c): SEM images showing the structural evolution of MnO_2 deposited at 1.5 V for 50 s, 150 s and 300 s respectively in 10 mM manganese acetate solution. (d): Cross-section SEM image of the MnO_2 film. The scale bars in (a) ~ (d) are 200 nm. (e): Schematic illustration of the growth process of MnO_2 hierarchical spheres on ITO substrate.

Figure 6-4. EDX spectrum of the as synthesized MnO_2 hierarchical spheres.

Figure 6-5. FTIR spectra of (a) pure GOx, (b) GOx/MnO_2 composite and (c) hierarchical MnO_2 spheres.

Figure 6-6. Nyquist plots of a bare GCE (black), MnO_2 NRHS-modified GCE (blue) and GOx/MnO_2 NRHS-modified GCE (red) measured in 0.1 M KCl solution containing 10 mM $Fe(CN)_6^{3-/4}$.

Figure 6-7. (a) CVs of GOx/Nafion-, MnO_2/Nafion- and GOx/MnO_2 /Nafion-modified GCE measured in N_2 saturated 0.1 M PBS. Scan rate: 100 mV s^{-1}. (b) Plots of scan rate *versus* peak current. Inset shows the CVs of GOx/MnO_2/Nafion-GCE at different scan rates (from inside to outside): 25, 50, 75, 100, 200, 300, 400, and 500 mV s^{-1}. (c) CVs of GOx/MnO_2/Nafion-GCE measured in N_2 saturated 0.1 M PBS with different pH. (d) Plot of peak current *versus* pH. Inset:

glucose with the influence of different (a) incubated GOx concentration, (b) detection potential, (c) buffer pH and (d) temperature of the reaction system. The points were sketched with the average values of three independent measurements.

Figure 7-7. (a) Amperometric responses of Nafion/GOx/CNCs-GCE toward the successive addition of 1 mM and 0.1 mM (inset) glucose to stirred PBS buffer (0.1 M, pH 6.5) at an operating potential of -0.5 V. (b) The calibration curve plotted according to the amperometric current response of the mediatorless biosensor. (c) Amperometric responses of the electrode for 0.5 mM glucose and the addition of some interfering species (0.1 mM AA and 0.1 mM UA) to stirred 0.1 M PBS buffer (pH 6.5). (d) The current responses of fabricated biosensor toward the addition of 0.3 mM electrocative species in blood (AA, AP, DA and UA) and 100 μL human serum to 900 μL air-saturated PBS buffer (0.1 M, pH 6.5).

Figure 8-1. (a, b) Low- and high-magnification SEM images of the CVD-grown 3DGF. (c, d) Low- and high-magnification SEM images of the Mn_3O_4/3DGF composite. (e, f) SEM and TEM images of the hierarchically structured Mn_3O_4 nanomesh grown on the surface of 3DGF skeleton.

Figure 8-2. Photograph of the Flexible biosensor based on Mn_3O_4/3DGF freestanding electrode.

Figure 8-3. XRD (a) and Raman (b) spectra of 3DGF (black) and Mn_3O_4/3DGF composite (red).

Figure 8-4. Energy-dispersive X-ray (EDX) spectrum of the Mn_3O_4/3DGF composite material.

Figure 8-5. TGA curve of 3DGF and the Mn_3O_4/3DGF composite.

Figure 8-6. (a) CV curves of the Mn_3O_4/3DGF composite electrode recorded at different scan rates (from inside to outside: 10, 20, 30, 50 and 80 mV/s) in 0.1 M NaOH solution. Inset: Plots of scan rate *versus* peak current. (c) CVs of the composite electrode recorded at 20 mV/s with the presence of different concentrations of glucose (from inside to outside: 0, 1, 2, 3, 4, and 5 mM).

Figure 8-7. (a) Amperometric response of the Mn_3O_4/3DGF composite electrode at 0.4 V upon the successive addition of 1 mM and 100 μM glucose (inset). (b) Calibration curve of composite material-based glucose sensor. Inset shows the current response of the composite electrode toward the addition of 10 μM glucose.

Figure 8-8. Amperometric responses of the Mn_3O_4/3DGF composite electrode toward the addition of glucose and different interferential compounds.

Appendix D: List of Tables